

Molecular Imaging of Opioid Receptors and
Butyrylcholinesterase with Selective, Tailored Probes
Using Positron Emission Tomography and
Fluorescence Microscopy

Dissertation

zur Erlangung des naturwissenschaftlichen Doktorgrades
der Julius-Maximilians-Universität Würzburg



vorgelegt von
Christian Gentsch
aus Mitwitz

Würzburg, 2021



Dedicated to my Parents

„Es wird ja fleißig gearbeitet und viel mikroskopiert, aber es müßte mal wieder einer einen gescheiten Gedanken haben.“

Rudolf Virchow (1821 - 1902)

Eingereicht bei der Fakultät für Chemie und Pharmazie am

Gutachter der Dissertation

1. Gutachter: _____

2. Gutachter: _____

Prüfer des öffentlichen Promotionskolloquiums

1. Prüfer: _____

2. Prüfer: _____

3. Prüfer: _____

Datum des öffentlichen Promotionskolloquiums

Doktorurkunde ausgehändigt am

The scientific work described in the present thesis was carried out under the supervision of Prof. Dr. Michael Decker at the Chair of Pharmaceutical and Medicinal Chemistry (Institute of Pharmacy and Food Chemistry) of the Julius-Maximilian-University of Würzburg between March 2017 and January 2021.

Contents

Abbreviations.....	I
List of Publications.....	IV
Other Scientific Contributions	V
Copyrights	VI
Declaration of Authorship	VII
1. Introduction – Opioid Receptors	1
1.1. The Opioid System.....	1
1.2. Homo- and Heteromerization of Opioid Receptors.....	3
1.3. Fluorescent Ligands for Opioid Receptors	7
1.4. Selective and Wash-Resistant Fluorescent Dihydrocodeinone Derivatives Allow Single-Molecule Imaging of μ -Opioid Receptor Dimerization (published research work) ^[56]	12
1.4.1. Aim of the Study	13
1.4.2. Design of Fluorescent Ligands	14
1.4.3. Synthesis of Fluorescent Ligands.....	16
1.4.4. Binding Affinity, Selectivity and Intrinsic Activity of Fluorescent Ligands	18
1.4.5. Wash Resistance of Fluorescent Ligands	21
1.4.6. Single-Molecule Microscopy with Fluorescent Ligands	22
1.4.7. Experimental Procedures	27
1.5. Non-fluorescent Opioid Ligands selectively targeting Opioid Receptor Heterodimers (unpublished research work)	42
1.5.1. Aim of the Work.....	42
1.5.2. Synthesis of Unlabeled, Heterodimer-selective Opioid Ligands	43
1.5.3. Binding Affinity and Intrinsic Activity of Heterodimer-selective Opioid Ligands	45
1.5.4. Experimental Procedures	49

2. Imaging of Butyrylcholinesterase Activity by Positron Emission Tomography with ¹⁸ F-Radiotracers	63
2.1. Synthesis and Initial Characterization of a Reversible, Selective ¹⁸ F-Labeled Radiotracer for Human Butyrylcholinesterase (published research work) ^[179]	67
2.1.1. Aim of the Study	68
2.1.2. Design and Synthesis	68
2.1.3. Inhibitory Potency and Binding Kinetics.....	71
2.1.4. ¹⁸ F-Radiolabeling and preliminary <i>ex vivo</i> and <i>in vivo</i> Characterization ..	73
2.1.5. Experimental Procedures	76
2.2. Synthesis and Initial Characterization of a Pseudo-irreversible, Selective Inhibitor of Human Butyrylcholinesterase as PET Tracer (published research work) ^[194]	88
2.2.1. Aim of the Study	88
2.2.2. Design and Synthesis	89
2.2.3. Inhibitory Potency and Binding Kinetics.....	93
2.2.4. ¹⁸ F-Radiolabeling and preliminary <i>ex vivo</i> and <i>in vivo</i> Characterization ..	95
2.2.5. Experimental Procedures	98
3. Summary	115
4. Zusammenfassung	118
References	122
Appendix I.....	132
Appendix II.....	139
Appendix III.....	150
Acknowledgements	161
Eidesstattliche Erklärung	163

Abbreviations

A β	amyloid- β
AChE	acetylcholinesterase
AD	Alzheimer's disease
ar	aryl
ATCI	acetylthiocholine iodide
β -arr	β -arrestin
BBB	blood-brain barrier
BChE	butyrylcholinesterase
β -FNA	β -funaltrexamine
Boc	<i>tert</i> -butyloxycarbonyl
Boc ₂ O	di- <i>tert</i> -butyl dicarbonate
BODIPY	boron dipyrromethene difluoride
BRET	bioluminescence resonance energy transfer
BTCl	butyrylthiocholine iodide
Bz	benzyl
CACO	14 β -(<i>p</i> -nitrocinnamoylamino)-7,8-dihydrocodeinone
cAMP	cyclic adenosine monophosphate
Cav2.2	N-type calcium channel
CB1	cannabinoid receptor 1
Cbz	<i>N</i> -carboxybenzyl
CCP	clathrin-coated pit
cDNA	complementary deoxyribonucleic acid
cf	compare
CHO	chinese hamster ovary
CNS	central nervous system
Cy	cyanine
cycloprop	cyclopropyl
DADLE	[d-Ala ² , d-Leu ⁵]-enkephalin
DAMGO	[d-Ala ² , N-MePhe ⁴ , Gly-ol]-enkephalin
DAST	diethylaminosulfur trifluoride
DCM	dichloromethane
DIPEA	<i>N,N</i> -diisopropylethylamine
DMEM	Dulbecco's modified Eagle's medium
DMF	<i>N,N</i> -dimethylformamide
DMSO	dimethylsulfoxide
DOP	δ -opioid receptor
DPDPE	[d-Pen ^{2,5}]-enkephalin
DTNB	5,5'-dithiobis-(2-nitrobenzoic acid)
EA	ethyl acetate
e.g.	for example
ERK	extracellular signal regulated kinase
ESI	electrospray ionization
FBS	fetal bovine serum
FCS	fetal calf serum
Fig	figure

FRET	fluorescence resonance energy transfer
FT	Fourier transformation
GASP1	G-protein coupled receptor-associated sorting protein 1
GEC1	GABA type A receptor associated protein like 1
GFP	green fluorescent protein
G _{i/o}	inhibitory G-protein for adenylyl cyclase
6'-GNTI	6'-guanidinonaltrindole
GPCR	G-protein coupled receptor
GRK	G-protein coupled receptor kinase
GTP	Guanosine triphosphate
<i>h</i>	human
HBTU	(2-(1 <i>H</i> -benzotriazol-1-yl)-1,1,3,3-tetramethyluronium hexafluorophosphate
HEK	Human embryonic kidney
HTRF	homogenous time resolved FRET
i.c.v.	intracerebroventricular
INTA	<i>N</i> -2'-indolylnaltrexamine
IP1	inositol monophosphate
i.t.	intrathecal
Kir3	inwardly rectifying potassium channel
KOP	κ-opioid receptor
LC/MS	liquid chromatography / mass spectrometry
MAPK	mitogen-activated protein kinase
MOM	methoxymethyl
MOP	μ-opioid receptor
m.p.	melting point
<i>m</i>	murine
naph	naphtyl
NHS	<i>N</i> -hydroxysuccinimide
NMR	nuclear magnetic resonance
NNTA	<i>N</i> -naphthoyl-β-naltrexamine
NOP	nociceptin opioid peptide receptor
nor-BNI	Nor-binaltorphimine
OR	opioid receptor
ORL-1	opioid receptor like-1
p	primary
PE	petroleum ether
PET	positron emission tomography
PK1	pyruvate kinase 1
q	quaternary
RT	room temperature
RTF4	receptor transport factor 4
s	secondary
SAR	structure-activity relationship
SD	standard deviation
S.E.M.	standard error of the mean
SMM	single-molecule microscopy
SPECT	single photon emission computed tomography
t	tertiary
TAMSD	time-averaged mean square displacement

TBDMS	<i>tert</i> -butyldimethylsilyl
TEA	triethylamine
THF	tetrahydrofuran
TIRF	total internal reflection fluorescence
TLC	thin layer chromatography
TMS	trimethylsilyl
unsat	ungesättigt

List of Publications

- **Gentzsch, C.**; Seier, K.; Drakopoulos, A.; Jobin, M.-L.; Lanoiselée, Y.; Koszegi, Z.; Maurel, D.; Sounier, R.; Hübner, H.; Gmeiner, P.; Granier, S.; Calebiro, D.; Decker, M. Selective and Wash-Resistant Fluorescent Dihydrocodeinone Derivatives Allow Single-Molecule Imaging of μ -Opioid Receptor Dimerization. *Angew. Chem. Int. Ed.* **2020**, *59*, 5958–5964. *Angew. Chem.* **2020**, *132*, 6014–6020.
→ Ranked as “highly important” and selected for inside back cover picture
- **Gentzsch, C.**; Chen, X.; Spatz, P.; Košak, U.; Knez, D.; Nose, N.; Gobec, S.; Higuchi, T.; Decker, M. Synthesis and Initial Characterization of a Reversible, Selective ^{18}F -Labeled Radiotracer for Human Butyrylcholinesterase. *Mol. Imaging Biol.* **2021**, <https://doi.org/10.1007/s11307-021-01584-2>.
- **Gentzsch, C.**; Hofmann, M.; Ohshima, Y.; Nose, N.; Chen, X.; Higuchi, T.; Decker, M. Synthesis and Initial Characterization of a Selective, Pseudoirreversible Inhibitor of Human Butyrylcholinesterase as PET Tracer. *ChemMedChem* **2021**, *16*, 1427–1437.
→ This article also appears in “[Hot Topic: Fluorine Chemistry](#)”

Other Scientific Contributions

- **Gentsch, C.**; Seier, K.; Drakopoulos, A.; Jobin, M.-L.; Maurel, D.; Sounier, R.; Granier, S.; Calebiro, D.; Decker, M. Synthesis of fluorescent ligands to investigate μ -opioid receptor dimerization, 3rd Working Group Meeting of MuTaLig COST Action, Paris (France), February 23rd – 24th, 2019. (Poster Presentation).

Copyrights

Parts of this work have been published previously and are reproduced, adapted, and/or modified with permission from:

Gentzsch, C.; Seier, K.; Drakopoulos, A.; Jobin, M.-L.; Lanoiselée, Y.; Koszegi, Z.; Maurel, D.; Sounier, R.; Hübner, H.; Gmeiner, P.; Granier, S.; Calebiro, D.; Decker, M. Selective and Wash-Resistant Fluorescent Dihydrocodeinone Derivatives Allow Single-Molecule Imaging of μ -Opioid Receptor Dimerization. *Angew. Chem. Int. Ed.* **2020**, *59*, 5958–5964. *Angew. Chem.* **2020**, *132*, 6014–6020.

Copyright © 2019, The Authors. Published by Wiley-VCH Verlag GmbH & Co. KGaA, Weinheim. This is an open access article distributed under the terms of the [Creative Commons CC BY license](#).

<https://doi.org/10.1002/anie.201912683>

Gentzsch, C.; Chen, X.; Spatz, P.; Košak, U.; Knez, D.; Nose, N.; Gobec, S.; Higuchi, T.; Decker, M. Synthesis and Initial Characterization of a Reversible, Selective ¹⁸F-Labeled Radiotracer for Human Butyrylcholinesterase. *Mol. Imaging Biol.* **2021**, *in press*.

Copyright © 2021, The Authors. Published by Springer Nature AG & Co. KGaA, Berlin. This is an open access article distributed under the terms of the [Creative Commons CC BY license](#).

<https://doi.org/10.1007/s11307-021-01584-2>

Gentzsch, C.; Hofmann, M.; Ohshima, Y.; Nose, N.; Chen, X.; Higuchi, T.; Decker, M. Synthesis and Initial Characterization of a Selective, Pseudoirreversible Inhibitor of Human Butyrylcholinesterase as PET Tracer. *ChemMedChem* **2021**, *16*, 1427–1437.

Copyright © 2021, The Authors. Published by Wiley-VCH Verlag GmbH & Co. KGaA, Weinheim. This is an open access article distributed under the terms of the [Creative Commons CC BY license](#).

<https://doi.org/10.1002/cmdc.202000942>

Declaration of Authorship

Gentzsch, C.; Seier, K.; Drakopoulos, A.; Jobin, M.-L.; Lanoiselée, Y.; Koszegi, Z.; Maurel, D.; Sounier, R.; Hübner, H.; Gmeiner, P.; Granier, S.; Calebiro, D.; Decker, M. Selective and Wash-Resistant Fluorescent Dihydrocodeinone Derivatives Allow Single-Molecule Imaging of μ -Opioid Receptor Dimerization. *Angew. Chem. Int. Ed.* **2020**, *59*, 5958–5964. *Angew. Chem.* **2020**, *132*, 6014–6020.

Detaillierte Darstellung der Anteile an der Veröffentlichung (in %)

Angabe Autoren/innen (ggf. Haupt- / Ko- / korrespondierende/r Autor/in) mit Vorname
Nachname (Initialen)

C. Gentzsch (CG), K. Seier (KS), A. Drakopoulos (AD), M.-L. Jobin (MLJ), Y. Lanoiselée (YL), Z. Koszegi (ZK), D. Maurel (DM), R. Sounier (RS), H. Hübner (HH), P. Gmeiner (PG), S. Granier (SG), D. Calebiro (DC), M. Decker (MD)

Autor	CG	KS	AD	MLJ	YL	ZK	DM	RS	HH	PG	SG	DC	MD	Σ (%)
Design & Synthese der Zielverbindungen	15%		2%											17%
Analytik der Zielverbindungen	8,5%													8,5%
HTRF assay (Selektivität)							3%	3%			3%			9%
Bindungskurven (Affinität)		4%												4%
Funktionelle Aktivität									2%	2%				4%
Auswasch – Assay		2,5%												2,5%
Diffusionsverhalten		7%		2%	2%	2%								13%
Dimerisierungs – Assays		10%		2%	2%	2%								16%
Verfassen der Veröffentlichung	5%	5%	2%									3%	3%	18%
Betreuung der Doktoranden												4%	4%	8%
Summe	28,5%	28,5%	4%	4%	4%	4%	3%	3%	2%	2%	3%	7%	7%	100%

Gentzsch, C.; Chen, X.; Spatz, P.; Košak, U.; Knez, D.; Nose, N.; Gobec, S.; Higuchi, T.; Decker, M. Synthesis and Initial Characterization of a Reversible, Selective ¹⁸F-Labeled Radiotracer for Human Butyrylcholinesterase. *Mol. Imaging Biol.* **2021**, *in press*.

Detaillierte Darstellung der Anteile an der Veröffentlichung (in %)

Angabe Autoren/innen (ggf. Haupt- / Ko- / korrespondierende/r Autor/in) mit Vorname
Nachname (Initialen)

C. Gentzsch (CG), X. Chen (XC), P. Spatz (PS), U. Košak (UK), D. Knez (DK), N. Nose (NN), S. Gobec (SG), T. Higuchi (TH), M. Decker (MD)

Autor	CG	XC	PS	UK	DK	NN	SG	TH	MD	Σ (%)
Synthese der kalten Referenzverbindung	10%			1%	1%		0,75%			12,75%
Synthese des Precursors	11%			1%	1%		0,75%			13,75%
<i>In vitro</i> Bindungsstudien	1,5%		3%	6%	6%		3%			19,5%
Radiolabeling		4%								4%
<i>Ex vivo</i> Autoradiographie		4%				2%				6%
<i>In vivo</i> microPET		6%				3%				9%
Verfassen der Veröffentlichung	8%	2%		1,5%	1,5%		2%	4%	4%	23%
Betreuung der Doktoranden								6%	6%	12%
Summe	30,5%	16%	3%	9,5%	9,5%	5%	6,5%	10%	10%	100%

Gentzsch, C.; Hoffmann, M.; Ohshima, Y.; Nose, N.; Chen, X.; Higuchi, T.; Decker, M. Synthesis and Initial Characterization of a Selective, Pseudoirreversible Inhibitor of Human Butyrylcholinesterase as PET Tracer. *ChemMedChem* **2021**, *16*, 1427–1437.

Detaillierte Darstellung der Anteile an der Veröffentlichung (in %)

Angabe Autoren/innen (ggf. Haupt- / Ko- / korrespondierende/r Autor/in) mit Vorname Nachname (Initialen)

C. Gentzsch (CG), M. Hoffmann (MH), Y. Ohshima (YO), N. Nose (NN), X. Chen (XC), T. Higuchi (TH), M. Decker (MD)

Autor	CG	MH	YO	NN	XC	TH	MD	Σ (%)
Synthese der kalten Referenzverbindung	8%	10%						18%
Synthese des Precursors	11%	13%						24%
<i>In vitro</i> Bindungsstudien		4%	5%					9%
Radiolabeling				1%	4%			5%
<i>Ex vivo</i> Autoradiographie				2%	3%			5%
<i>In vivo</i> microPET				2%	4%			6%
Verfassen der Veröffentlichung	10%	2%			3%	3%	3%	21%
Betreuung der Doktoranden						6%	6%	12%
Summe	29%	29%	5%	5%	14%	9%	9%	100%

1. Introduction – Opioid Receptors

1.1. The Opioid System

The endogenous opioid system is known to play important roles in processes like nociception, reward and motivation, cognition and neuroendocrine physiology. Additionally, it contributes to the regulation of emotional responses and some autonomic functions (e.g. gastric motility or peristaltic in the colon).^[1-2] It consists of several types of endogenous peptides and three respective receptors occurring in the nervous system. Endorphins, endomorphins and morphiceptin mainly address the μ -opioid receptor (MOP), enkephalins the δ -opioid receptor (DOP) and dynorphins the κ -opioid receptor (KOP).^[3-4] Signaling of these typical G-protein coupled receptors (GPCRs) is primarily mediated by their interaction with the inhibitory G-protein for adenylyl cyclase ($G_{i/o}$).^[5] A doubtful case of a fourth opioid receptor (OR) was discovered much later and is known as nociceptin opioid peptide receptor (NOP) or opioid receptor like-1 (ORL-1). The endogenous nociceptin/orphanin FQ neuropeptide binds selectively to this GPCR, which shares high sequence identity with the other subtypes, but does not bind typical opioid ligands with a comparable high affinity.^[6-8] ORs remain the target of the most widely used clinical analgesics, despite their distinct potential to mediate severe side effects, among which are tolerance and dependence with withdrawal symptoms, respiratory depression, constipation and nausea.^[9] Furthermore, activation of MOP and DOP causes euphoria, while KOP stimulation contrarily leads to dysphoria.^[1, 10] For these reasons the biochemical signal transduction mediated by ORs has been intensively investigated over decades. In general, OR activation inhibits neurons, which themselves block pain transmission in the spinal cord.^[11-12] Thus, the perception of pain is decreased. Upon OR activation by an (endo- or exogenous) agonist, $G\alpha$ and $G\beta\gamma$ subunits dissociate and consequently stimulate diverse intracellular effector pathways (Fig. 1).^[13-15] Exemplarily, GTPase activity is affected as a consequence of agonistic binding and the production of cyclic adenosine monophosphate (cAMP) is inhibited, which is the case for many other typical GPCRs as well.^[16-17] Importantly, calcium and potassium channels are subsequently modulated. The $G\alpha$ protein subunit interacts with the G-protein gated inwardly rectifying potassium channel (Kir3), whose subsequent deactivation is GTP-dependent and causes cellular hyperpolarization and therefore an inhibition of

1.1. The Opioid System

neuronal excitability.^[18-22] Calcium ion channels can be inhibited by binding of the $G\beta\gamma$ subunit. Thus, activation of channel pore opening by voltage is decreased. It could be shown that calcium ion currents sensitive to P/Q-, N- and L-type channel blockers are reduced upon activation of all OR subtypes. Furthermore, cAMP dependent calcium ion influx is also down-regulated, due to the inhibition of adenylyl cyclase activity after agonistic stimulation of all ORs.^[23-25] Numerous studies in cells and model systems proved, that ORs open Kir3-, while closing calcium channels. However, other pathways of signal transduction are also influenced in a slower, yet intense manner.

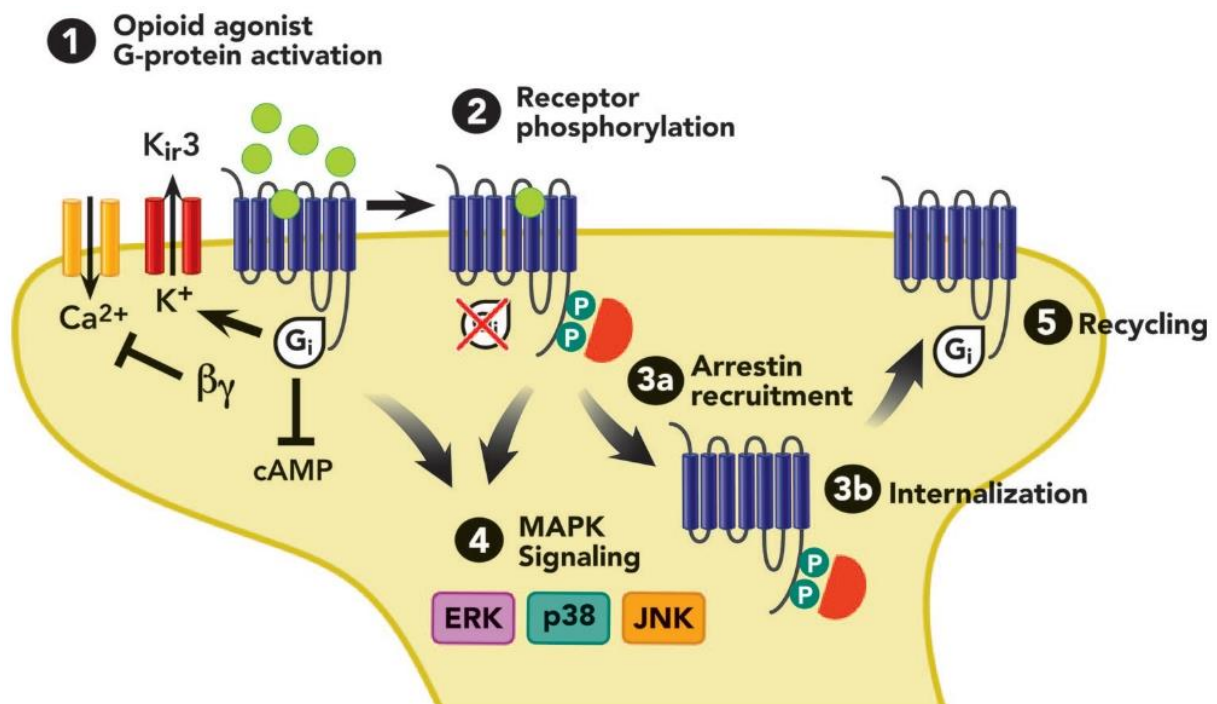


Fig. 1. Pathways of OR signaling and trafficking for all three subtypes (and NOP). Arrows depict an activation event, while *T* lines present blocking or inhibition. $\beta\gamma$ = subunit of G protein, ERK = extracellular signal regulated kinase, JNK = c-jun N-terminal kinase, MAPK = mitogen-activated protein kinase, P = phosphorylation. (Adapted with permission from Wolters Kluwer Health, Inc.: Al-Hasani, R.; Bruchas, M. R. Molecular Mechanisms of Opioid Receptor-dependent Signaling and Behavior. *Anesthesiology* 2011, 115 (6), 1363–1381.)^[13]

Activation of β -arrestin (β -arr) signaling was associated with some severe side effects of opioids in clinical use. Subsequently, biased ligands of ORs were developed, that provide functional selectivity by precisely controlling the biological output of ORs.^[26-27] If these ligands favor G_i protein activation over β -arr signaling, they display a clinically more useful pharmacological profile and provide access to efficient pain treatment with reduced side effects, such as respiratory depression.^[28] A prominent example is the G-protein biased MOP agonist oliceridine, which is approved for the treatment of moderate to severe pain in adults.^[27] β -arr recruitment occurs as a consequence of

phosphorylation of the activated receptor. For the MOP this takes place at the long C-terminal tail and is induced by GPCR kinase (GRK).^[29-31] To some extent, this enzyme is recruited by the decoupled $G\beta\gamma$ subunit.^[32-34] Arrestin-coupling leads to desensitization and activation of certain downstream effector proteins like MAPKs, furthermore the receptor can be subsequently internalized into endosomes, where it is degraded or alternatively recycled to the plasma membrane (Fig. 1).^[35] Non-biased agonists in complex with the MOP do not inhibit subsequent β -arr recruitment by the phosphorylated C-tail, which forms strong polar interactions. Biased agonists cause a conformational change of MOP preventing β -arr-2 from forming these polar anchors. Receptor desensitization and internalization is subsequently diminished (Fig. 1).^[13, 31, 36-38] Nevertheless, studies with knock-in mice expressing MOP with a series of mutations causing a disability to recruit β -arr revealed that indeed tolerance was significantly diminished, while analgesia was increased, however, respiratory depression, constipation and opioid withdrawal signs were unexpectedly not altered.^[37] This suggests, that other mechanisms apart from β -arr signaling are involved in the formation of these adverse effects.

1.2. Homo- and Heteromerization of Opioid Receptors

Even though GPCRs were considered as solely monomeric species for a long time, evidence over the past decades arose, that they form homo – and heteromers in living cells.^[39-42] The term homomer correlates to two (dimer) or more (oligomer) receptors of the same species, while heteromer refers to different receptors interacting with each other (Fig. 2).^[13] Nowadays, it is most widely accepted for class C GPCRs, that they exist and exclusively function as homo- or heteromers.^[43-45] In the case of class A (rhodopsin-like) GPCRs, this question is still controversially debated. Nevertheless, studies of some prototypical class A GPCRs (e.g. MOP, β_2 adrenergic- and rhodopsin receptor) clearly revealed, that they are capable of G protein activation in the monomeric state.^[46-49] However, this finding does not exclude the presence or transient forming of homo- and heteromers of class A GPCRs. Moreover, they offer a suitable possibility to explain the diversity of effects, e.g. for ORs. Binding-, signaling- and trafficking properties of homo- or heteromeric receptor species can be altered as compared to the respective monomer. Therefore GPCR oligomers might represent promising new targets in drug discovery and development.^[50]

1.2. Homo- and Heteromerization of Opioid Receptors

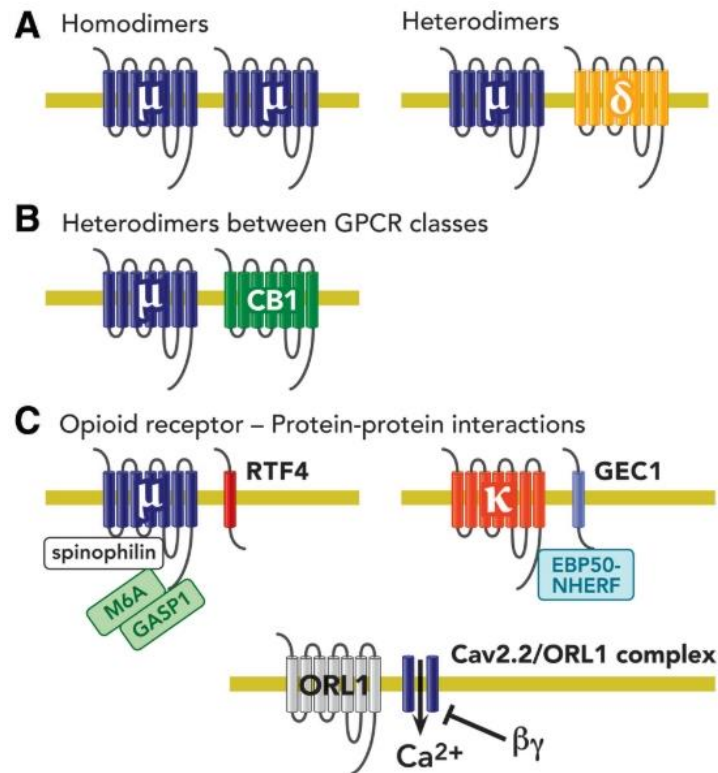


Fig. 2. Illustration of **A**) Homodimerization (Interaction of two receptors of the same species) of MOPs and Heterodimerization (Interaction of two receptors of different subtypes) of MOP and DOP, **B**) Heterodimerization between MOP and cannabinoid receptor 1 (CB1) as different class A GPCR type. **C**) Interactions between proteins of OR signal transduction. GASP1 = G-protein coupled receptor-associated sorting protein 1, M6A = Neural glycoprotein, GEC1 = GABA type A receptor associated protein like 1, Cav2.2 = N-type calcium channel. (Adapted with permission from Wolters Kluwer Health, Inc.: Al-Hasani, R.; Bruchas, M. R. Molecular Mechanisms of Opioid Receptor-dependent Signaling and Behavior. *Anesthesiology* 2011, 115 (6), 1363–1381.)^[13]

At the beginning, homodimerization was reported for the DOP and interestingly it was found, that the extent of homodimers depended on agonist treatment, with increasing agonist concentrations reducing the dimer level. A correlation between agonist-promoted internalization and the degree of dimerization was suggested.^[51] Shortly afterwards KOP dimers were found, which turned out to be present in majority, independent of applied crosslinkers, detergents or extraction conditions.^[52] Finally, MOP oligomers that influenced trafficking properties were discovered, however, for oligomerization wild-type MOP was used in combination with a mutant, chimeric variant.^[53] Much later, the MOP was crystallized in complex with the irreversible, morphinan-based antagonist β -funaltrexamine (β -FNA) and X-ray analysis revealed a two-fold, symmetrical dimeric structure. Even though this might be a result of conditions applied during receptor crystallization, this paved the way to enable structure-based design of optimized MOP analgesics.^[54] Very recently, transient and agonist-dependent homodimer-formation of MOP could be shown independently in two studies using single-molecule microscopy (SMM) to track receptors on the surface of living

1.2. Homo- and Heteromerization of Opioid Receptors

CHO cells. In one study, receptors were fused with a SNAP-tag at their N-terminus and labeled with a fluorescent dye (SNAP-Surface 549).^[55] In the second study, which is part of this thesis, a pair of selective, fluorescent MOP ligands differing only marginally in their fluorophore-part were used.^[56] Thus, unmodified, wild-type receptors could be applied in fluorescence microscopy experiments.

Concerning heteromerization of ORs, the MOP/DOP dimer is the best investigated pair up to now. Initially, co-immunoprecipitation studies with tagged receptors in co-transfected cells and spinal cord membranes of wild-type mice revealed an interaction of both ORs. Bioluminescence resonance energy transfer (BRET) assays displayed close proximity of MOP and DOP in live cells, potentially allowing dimer formation.^[57-59] Interestingly, binding affinity of selective agonists to each monomer was decreased for the dimer but increased in the presence of agonists and antagonists selective for the respective other monomeric receptor, which happened due to allosteric modulation.^[57-60] Moreover, intracellular signaling was affected through dimer formation, e.g. binding to one of the receptors in the dimer enhanced signaling mediated by the unoccupied protomer. It could be shown, that the dimer itself might be coupled to pertussis-toxin insensitive G proteins like Gz, while the monomers are associated with $G_{\alpha_{i/o}}$.^[57, 59, 61-62] Additionally, studies suggested that internalization and endocytosis (Fig. 1) of the partaking receptors is also influenced by dimer formation and depends on agonist treatment.^[61, 63-64] Finally, maturation and expression on cell surface could be altered by dimerization, since the dimer requires a chaperone (RTF4 = Receptor transport factor 4, Fig. 2) to protect it from degradation by the ubiquitin-proteasome system during folding and maturation.^[65] Subsequently, first MOP/DOP heteromer-selective ligands provided initial *in vivo* indications for the possibility to achieve an improved pharmacological profile concerning pronounced analgesia with less side effects.^[66-70]

The first OR heteromer to be reported was the DOP/KOP pair. At first, co-immunoprecipitation studies with cells co-expressing both receptors revealed the presence of an interacting complex and later another study using BRET assays with live cells demonstrated that the two receptors are close enough to potentially interact.^[52, 71] Binding affinities of DOP and KOP agonists were decreased at the heteromer compared to the respective homomers, but simultaneous treatment of a mixture of DOP and KOP agonists or antagonists increased binding affinities. For the agonist mixture, enhanced intracellular signaling was observed.^[52] Taken together,

1.2. Homo- and Heteromerization of Opioid Receptors

these results indicated allosteric interactions of both receptors, as described similarly for the MOP/DOP heteromer. Furthermore, it could be shown, that DOP/KOP heteromerization influences trafficking properties of DOP. While cells singly expressing DOP internalized the receptor upon treatment with etorphine (a non-selective OR agonist), cells expressing the heteromer did not exhibit receptor internalization of DOP.^[52] Concerning the potential role of the heteromer *in vivo*, selective ligands and antibodies have been developed to address this question. It could be shown, that a heteromer selective antibody can enhance the effect of [d-Pen^{2,5}]-enkephalin (DPDPE, a DOP agonist) in a behavioral rat model of thermal allodynia. Heteromers were detected in rat peripheral sensory neurons by co-immunoprecipitation. In the same study, KOP selective antagonists (nor-binaltorphimine = nor-BNI and 5'-guanidinonaltrindole = 5'-GNTI) were found to differentially alter the effect of DOP agonists like DPDPE, [d-Ala²,d-Leu⁵]-enkephalin (DADLE) or 4-[(*R*)-[(2*S*,5*R*)-4-allyl-2,5-dimethylpiperazin-1-yl](3-methoxyphenyl)-methyl]-*N,N*-diethylbenzamide (SNC80) in the rat model. Interestingly, the DOP/KOP heterodimer-selective agonist 6'-guanidinonaltrindole (6'-GNTI) could inhibit stimulated thermal allodynia.^[72] 6'-GNTI was found to produce approximately 50 times more potent antinociception than the KOP selective agonist U50488H after intrathecal (i.t.), but not after intracerebroventricular (i.c.v.) administration, suggesting a tissue-specific role of DOP/KOP heterodimers in the spinal cord, but not in the brain.^[73] However, 6'-GNTI was also described to act as extreme G-protein biased partial agonist on KOPs alone, while inhibiting the recruitment of β -arr.^[74] Nevertheless, this finding does not rule out a role of DOP/KOP heteromerization. Altogether, these results again not only suggest the presence of KOP/DOP heteromers but are additionally indicative of allosteric receptor interactions, as described before.

Heteromerization between MOP and KOP subtypes was investigated initially in co-immunoprecipitation studies with antibodies to epitope-tagged receptors but interacting complexes could not be detected in heterologous cells.^[52] Later, it was possible to detect heteromerization by using antibodies to endogenous receptors in spinal cord membrane preparation of female rats. Interestingly, it was observed, that levels of heteromerization were dependent on the stage of the estrous cycle, suggesting a possible influence of sex hormones.^[75] Further hints were provided by BRET assays, that demonstrated sufficient proximity of both receptors to interact.^[76] Thus, MOP/KOP heteromerization could depend on detergent conditions, utilized

tissue and/or physiological conditions. Binding affinities of MOP agonists (DAMGO and endomorphin-1) were shown to be decreased in cells co-expressing both receptor subtypes, but KOP agonists (U69593 and U50488H) did not display a difference in radioligand binding- and [³⁵S]GTP γ S assays.^[76] Concerning MOP/KOP heteromer-selective ligands, *N*-naphthoyl- β -naltrexamine (NNTA) has to be mentioned, since this compound produced a 50 times more potent antinociceptive effect than morphine. The effect was more pronounced after i.t. injection, compared to i.c.v. administration. This was not observed in MOP knock-out mice, suggesting a potential role of heteromerization in the spinal cord. Moreover, NNTA did not produce physical dependence at all, tolerance was low after chronic i.c.v. administration or not present upon chronic i.t. treatment.^[77] Altogether, these facts also point out MOP/KOP heteromers as promising targets for improved analgesics and imaging tool-compounds to gain deeper insights into their pharmacology.

1.3. Fluorescent Ligands for Opioid Receptors

Fluorescent ligands represent versatile tools, not only to investigate GPCR homo- and heteromerization, but also to elucidate thermodynamics of ligand-receptor interactions or to identify potential new therapeutic targets and to develop novel high-throughput screening approaches. Importantly, these ligands can be applied in living cells and native tissues and can be a beneficial alternative to radioactive binding assays with regard to expenses and dangers.^[78] Fluorescence resonance energy transfer (FRET)-based approaches gained importance in the study of GPCR oligomerization. FRET is based on the nonradiative energy transfer from a donor-chromophore in an excited state to an acceptor-chromophore.^[79-80] Consequently, donor emission is decreased at the same amount that acceptor emission is increased. This phenomenon is highly distance-dependent, as the efficiency is inversely proportional to the sixth power of the distance between donor and acceptor. Other influencing variables are the orientation between donor and acceptor, the overlap between donor and acceptor spectra, the quantum yield of the donor and the absorption coefficient of the acceptor.^[80-81] In practice FRET occurs, if a suitable pair of fluorophores gets closer to each other than approximately 10 nm and the dipole-moments are not oriented perpendicularly. Dynamic FRET is usually measured by monitoring the intensity ratio of acceptor/donor emission. Nonspecific FRET, which can occur by random collision of partaking

1.3. Fluorescent Ligands for Opioid Receptors

chromophores, should be avoided by thoroughly controlling donor-/acceptor densities.^[82] Consequently, selective ligands that exhibit high affinity to a receptor of choice can be chemically labeled with two fluorophores acting as FRET pair and employed as imaging tools for oligomerization events. A FRET signal will be measurable, when two receptors with bound ligands interact to form a dimer or higher order oligomer (Fig. 3). If the structure of the fluorescent ligands differs exclusively in their fluorophore part, they are suitable to investigate homodimerization events. However, it is also possible to apply different pharmacophore parts, e.g., selective ligands for different receptor subtypes, to study heteromerization events.^[78]

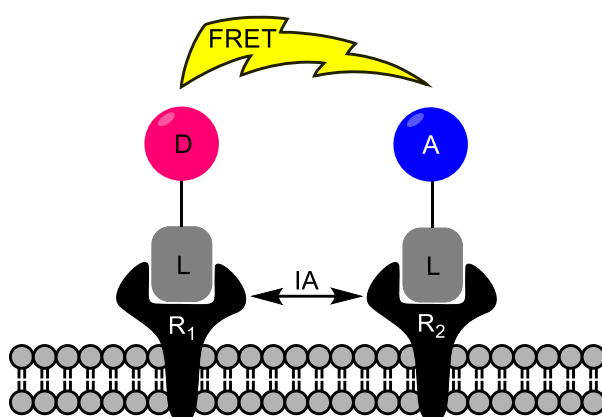


Fig. 3. Depiction of a FRET event between two receptors of the same type (R₁ / R₂) with bound ligands (L) undergoing an interaction (IA). One ligand carries the donor chromophore (D) and the other the acceptor (A).

These described approaches imply the important advantage, that native receptors can be studied. Nevertheless, it is also possible to use receptors bearing fluorescent tags coupled to their *N*-terminus, which requires ectopic expression of the labeled receptor construct. Additionally, specific fluorescent antibodies to the receptors can be applied.^[78] Requirements for the fluorophore part of a fluorescent ligand arise from:

- Low molecular weight, since binding affinity of small-molecule ligands can be influenced by increased steric demand
- Coupling in straightforward conjugation reactions of high yield
- High chemical and photostability
- Easily tunable fluorescence signaling to match requirements of instrumental readout
- Broad compatibility (e.g. a donor can be used in combination with several acceptors)^[78, 83-84]

It has to be mentioned, that recent developments focused on dyes emitting in the

1.3. Fluorescent Ligands for Opioid Receptors

infrared region, which results in a decreased background and good compatibility in experiments with cells and tissues, even though these dyes typically exhibit lower stability.^[84-85] Concerning ORs, there is already a variety of fluorescent ligands, which were developed aiming at their desired applicability in fluorescence-based assays and/or fluorescence imaging (for a review cf. A. Drakopoulos, M. Decker 2020^[86]). A representative example is naltrexone^{dy647} (red-naltrexone, Fig. 4), which was used in a time-resolved- (TR) FRET assay with SNAP tagged MOP, KOP and DOP receptors fused to Lumi4-Tb as donor chromophore.^[87] Naltrexone acts as antagonist with high affinity on all OR subtypes, which was desired in this study, since subtype-selectivity was not required.

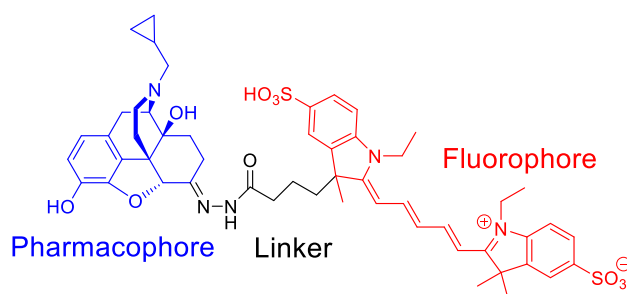


Fig. 4. Naltrexone, a high affinity antagonist on MOP, KOP and DOP, coupled to cyanine5 (Cy5) as fluorophore via a small alkylene linker (red-naltrexone).

This fluorescent probe displayed good affinity on all OR subtypes, thus providing stable homogenous, time-resolved FRET- (HTRF) signals ($K_d = 1.3 \pm 0.4$ nM for MOP, $K_d = 5.4 \pm 1.8$ nM for DOP, $K_d = 2.8 \pm 0.6$ nM for KOP). Competition binding assays, in which naltrexone-red was incubated with increasing concentrations of the antagonists naloxone and naltrindole resulted in K_i values in good agreement with literature data. Thereby first evidence was provided, that fluorescence-based technology (Tag-lite[®]) represents a promising alternative for radioligand-binding assays.^[87]

More recently, two fluorescent derivatives of morphine were developed and evaluated for their applicability in cell-based assays and live cell imaging.^[88] Morphine is one of the most prominent active ingredients of opium from the plant *Papaver somniferum* and is prevalently used for the treatment of pain, despite exhibiting typical opioid side effects. It mediates its effects by acting as agonist on the MOP but displays significant affinity to the other subtypes as well. Cy5 as fluorophore was coupled to the morphine scaffold via the C6-Hydroxy group as ester or ether and a linker was incorporated respectively (Fig. 5).^[88] The C6 position was chosen as linking point, since modifications there are known to be most widely tolerated in terms of activity.^[89]

1.3. Fluorescent Ligands for Opioid Receptors

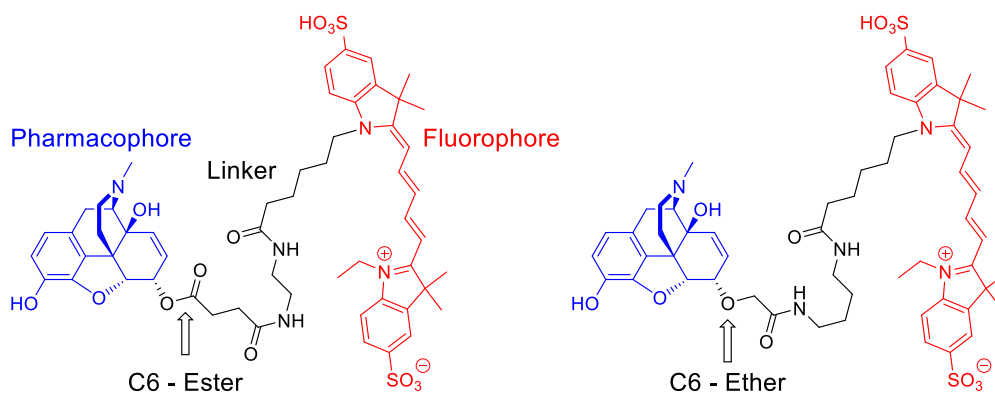


Fig. 5. Fluorescent derivatives of morphine. Cy5 as fluorophore was introduced on the C6-hydroxy group via a linker as ester (left) or ether (right).^[88]

Cy5 was attached as fluorophore due to its reduced potential to increase nonspecific binding to the cell membrane.^[90] Functional assays revealed, that both compounds could activate MOP with potencies in the nM range, however, efficacy was significantly decreased in comparison to morphine. The ether derivative acted as partial agonist, when compared with DAMGO. Both compounds were investigated for their applicability in confocal microscopy experiments with SNAP-tagged, labeled human (*h*)MOP. However, only the ether derivative showed specific binding to MOP on the surface of HEK293 cells. Some weak intracellular signals were observed, consistent with the minor ability of morphine to induce internalization. Importantly, the fluorescent probe was not wash-resistant and hence removed from cell-surface receptors by washing steps.^[88]

Few years earlier, buprenorphine-based, antagonistic fluorescent probes were designed by Schembri et al.^[90] Buprenorphine itself acts as partial agonist on MOP and NOP and as antagonist on DOP and KOP. It was chosen as pharmacologically active part due to its high binding affinity to ORs.^[91] Subsequently, four different small organic fluorophores were attached to the scaffold via an amidoalkylamine linker: Cy5, boron dipyrromethene difluoride (BODIPY 630/650), 4-((6-methoxy-1,2,4,5-tetrazin-3-yl)oxy)butanoic acid (tetrazine), and 3-(6-amino-1,3-dioxo-1H-benzo[de]isoquinolin-2(3H)-yl)-propanoic acid (naphthalimide). The Cy5 derivative (Fig. 6) turned out to be the most suitable candidate for imaging studies (e.g. receptor localization) or for *in vitro* binding assays, while all four probes showed high affinity and pronounced selectivity for MOP.^[90] After recording single-time point images of HEK cells stably expressing MOP with green fluorescent protein (GFP) attached at its C terminus, co-localization of probe- and GFP fluorescence revealed, that the BODIPY derivative could be used

1.3. Fluorescent Ligands for Opioid Receptors

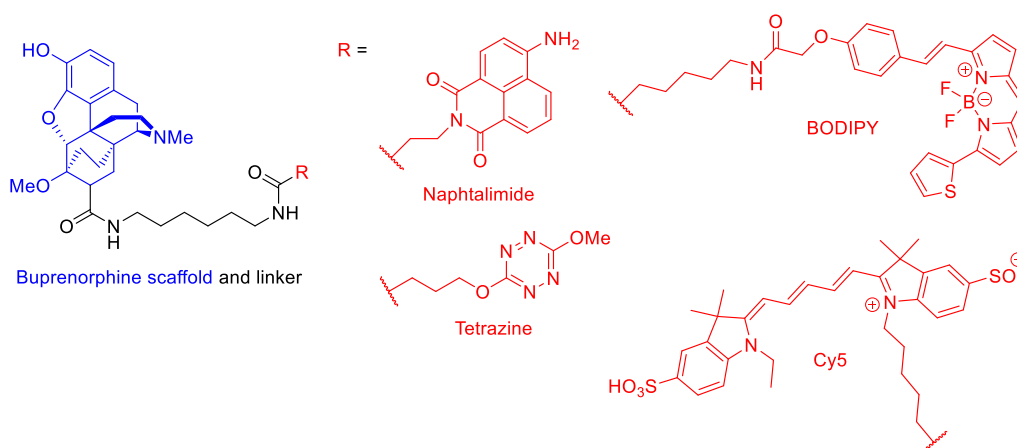


Fig. 6. Structures of fluorescent antagonistic buprenorphine derivatives. Four different fluorophores (right, in red) were attached to the pharmacologically active scaffold (left, in blue) via an amidoalkylamine linker (black).

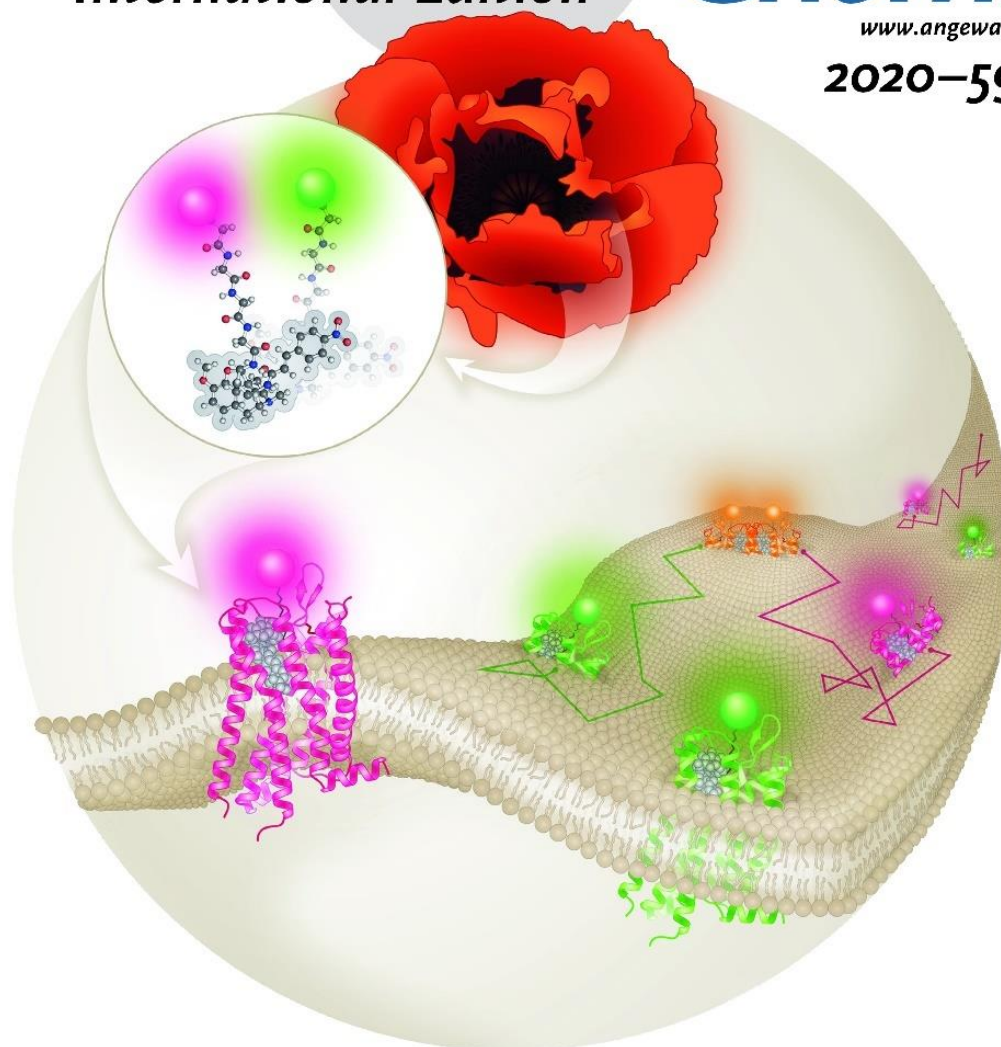
to image MOP with high specificity. However, even though displacement with a large excess of naloxone resulted in a significant decrease of fluorescence, not all signal was lost, which suggests some non-specific binding to the cell membrane.^[90] The required concentration for MOP imaging was higher for the Cy5 derivative, consistent with its lower affinity, but binding was more specific since it could be almost completely displaced by excess naloxone. Interestingly, no washing steps were performed, but fluorescence intensity was decreased upon displacement of the ligand due to the aqueous environment.^[90] Finally, the Cy5 derivative exhibited promising properties in a fluorescence-based competition assay, like short required incubation times, negligible non-specific binding and fast dissociation kinetics. Subsequently, it was possible to reproduce affinity data known from literature for several unlabeled antagonists, but not for the agonists DAMGO and dermorphine, whose pK_i values were generally lower. It was assumed, that this was due to uncomparable assay conditions.^[90]

Altogether, the described studies suggest, that promising operative fluorescent probes can be obtained by coupling fluorophores to morphinan-based pharmacophores. Selectivity, sufficient binding affinity and/or agonistic properties can be retained, even though this can hardly be predicted. Incorporated linkers can strongly influence suitability of the probes. Fluorophores of the sulfo-cyanine type displayed the most promising optical and pharmacological attributes, e.g. minor non-specific binding, good signal-to-noise ratio and strong fluorescence. There is also a variety of peptide-based and other non-morphinan fluorescent probes for ORs, as well as selective probes for DOP and KOP, which are beyond the scope of the present thesis (for a detailed review, see Drakopoulos et al., 2020^[86]).

1.4. Selective and Wash-Resistant Fluorescent Dihydrocodeinone Derivatives Allow Single-Molecule Imaging of μ -Opioid Receptor Dimerization (published research work)^[56]



A Journal of the German Chemical Society
Angewandte
GDCh
International Edition **Chemie**
www.angewandte.org
2020–59/15



Highly selective fluorescent ligands ...

... derived from the opium poppy were developed by D. Calebiro, M. Decker et al. in their Research Article on page 5958 to investigate whether μ -opioid receptors (μ -ORs) can form dimers on the plasma membrane. These compounds exhibit long residence time and high affinity. Applying these chemical tools, single-molecule microscopy allowed detection of a small fraction of short-lived homodimers.

WILEY-VCH

1.4. Selective and Wash-Resistant Fluorescent Dihydrocodeinone Derivatives Allow Single-Molecule Imaging of μ -Opioid Receptor Dimerization

The content of this chapter has been published^[56] (Gentzsch, C.; Seier, K.; Drakopoulos, A.; Jobin, M.-L.; Lanoiselée, Y.; Koszegi, Z.; Maurel, D.; Sounier, R.; Hübner, H.; Gmeiner, P.; Granier, S.; Calebiro, D.; Decker, M. *Angew. Chem. Int. Ed.* **2020**, *59*, 5958–5964, DOI: 10.1002/anie.201912683) and is adapted with permission from the respective authors.

Author contributions:

- C. Gentzsch performed the synthesis and analytical characterization of the fluorescent ligands. Design of target compounds and a synthetic approach were developed by A. Drakopoulos and C. Gentzsch under the supervision of M. Decker
- K. Seier performed fluorescence microscopy studies (TIRF- and SM microscopy) and their evaluation with the assistance of M.-L. Jobin, Y. Lanoiselée and Z. Koszegi under the supervision of D. Calebiro
- H. Hübner from the working group of P. Gmeiner performed functional activity assays (IP1 accumulation- and β -arr-2 recruitment assay)
- D. Maurel, R. Sounier and S. Granier performed the HTRF assay to characterize selectivity of the ligands

1.4.1. Aim of the Study

The presented work focused on the design and synthesis of a fluorescent, selective pair of ligands targeting the MOP with preferable high affinity and long residence time on the receptor. The ligands should be suitable for fluorescence microscopy experiments, particularly total internal reflection fluorescence (TIRF) microscopy and SMM, to visualize wild-type MOP on the surface of living cells. Thus, the dynamics of natural receptor diffusion behavior within the plasma membrane should be investigated. Finally, the pair of ligands of different color should be employed in SMM experiments to characterize MOP homomerization. Additionally, these ligands could also represent initial, novel tools to study heteromerization of MOP (e.g. with other OR subtypes or other GPCRs). On condition that they match the established requirements, these ligands should represent optimized tools to study MOP pharmacology, as compared to the fluorescent ligands described before (cf. chapter 1.3.).

1.4. Selective and Wash-Resistant Fluorescent Dihydrocodeinone Derivatives Allow Single-Molecule Imaging of μ -Opioid Receptor Dimerization

1.4.2. Design of Fluorescent Ligands

The fluorescent ligands were designed by Christian Gentsch and Dr. Antonios Drakopoulos under the supervision of Prof. Dr. Michael Decker (Institute of Pharmacy and Food Chemistry, Julius Maximilian University of Würzburg) with respect to the following requirements:

- Pronounced selectivity and affinity of the pharmacophore part
- Preferably uncomplicated synthetic access
- Wash resistance of the fluorescent ligands
- Preferably photostable, small fluorescent dye with suitable photophysical properties (e.g., high quantum yield)
- Fluorophore part should not increase non-specific binding and therefore signal-to-noise ratio in microscopy experiments

Concerning the pharmacological active part of the fluorescent ligands, 14 β -(*p*-nitrocinnamoylamino)-7,8-dihydrocodeinone (CACO) was chosen as promising candidate. This ligand exhibited high affinity and selectivity in competition binding assays using bovine striatal membranes (Table 1).^[92]

Table 1. IC₅₀ values of unlabeled CACO as determined in a competition binding assay (³H]DAMGO for MOP, [³H]pCI-DPDPE for DOP, [³H]U69,593 for KOP).^[92]

Ligand	IC ₅₀ (nM, \pm S.E.M.) MOP	IC ₅₀ (nM, \pm S.E.M.) DOP	IC ₅₀ (nM, \pm S.E.M.) KOP
CACO	0.46 \pm 0.003 ^[92]	4.2 \pm 1.3 ^[92]	19 \pm 2.8 ^[92]

Additionally, the unlabeled ligand displayed wash-resistant, concentration-dependent inhibition of [³H]DAMGO binding, likely due to the capability of the 14 β -(*p*-nitrocinnamoylamino)-side chain to form a covalent bond within the receptor binding site.^[92] This is advantageous, since it enables the implementation of several washing steps to remove non-specifically bound ligand and receptor-internalization studies can be performed. CACO acted as short-term agonist as demonstrated in *in vivo* studies with mice. The ligand produced dose-dependent antinociception after i.c.v. administration, as determined in a warm water tail-flick assay. Antinociception lasted up to 2 h and was inhibited by the MOP-selective antagonist β -FNA, but not DOP- or KOP selective antagonists. Additionally, CACO produced long-term antagonism of morphine-induced antinociception in mice, which was time- and dose dependent and

1.4. Selective and Wash-Resistant Fluorescent Dihydrocodeinone Derivatives Allow Single-Molecule Imaging of μ -Opioid Receptor Dimerization

lasted up to 48 h. Antinociception induced by DOP- and KOP selective agonists DPDPE and U50,488 was not inhibited by CACO.^[92] These findings particularly represented CACO as attractive candidate for a fluorescent probe.

An important decision in the design of fluorescent ligands is the coupling position of the fluorophore at the pharmacologically active scaffold since this can strongly influence binding properties and/or selectivity. As described above (cf. chapter 1.3.), the C6 of the morphinan scaffold of CACO represented the most promising position (Fig. 7). Importantly, previous studies with a BODIPY derivative of CACO had confirmed this notion.^[93]

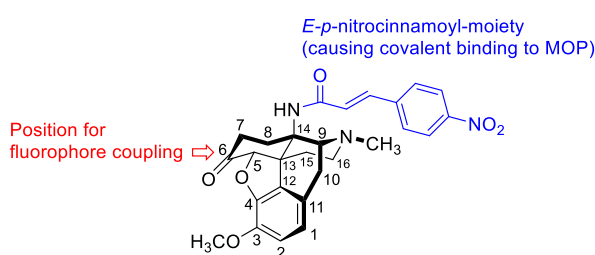


Fig. 7. Structure and numbering of morphinan-C-scaffold of 14 β -(*p*-nitrocinnamoylamino)-7,8-dihydrocodeinone (CACO) with depicted position for fluorophore coupling (C6) and *E-p*-nitrocinnamoyl-moiety causing covalent bonding (in blue).

In that study, the C6-BODIPY derivative of CACO retained high affinity and selectivity ($EC_{50} = 24.4 \pm 3.9$ nM for MOP vs. >1000 nM for DOP/KOP), as investigated in radioligand binding studies on preparations of rhesus monkey brains, which contain all OR subtypes.^[93]

Regarding the fluorophore part of the fluorescent ligands, the sulfo-cyanine dyes Cy3 and Cy5 (Fig. 8) were chosen as most suitable candidates due to their advantageous properties like emission in the red and near infrared spectral regions, high absorption coefficients and quantum yields, good photostability and minor potential to induce non-specific binding (cf. chapter 1.3.).^[94] The pair of dyes is commercially available as

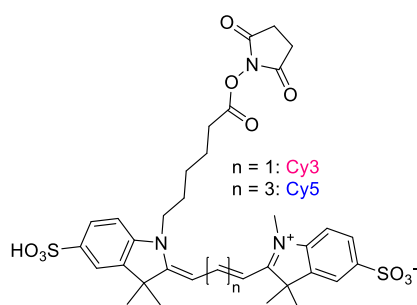


Fig. 8. Structure of commercially available NHS-activated sulfo-cyanine dyes Cy3 and Cy5 for reliable coupling with primary amines.

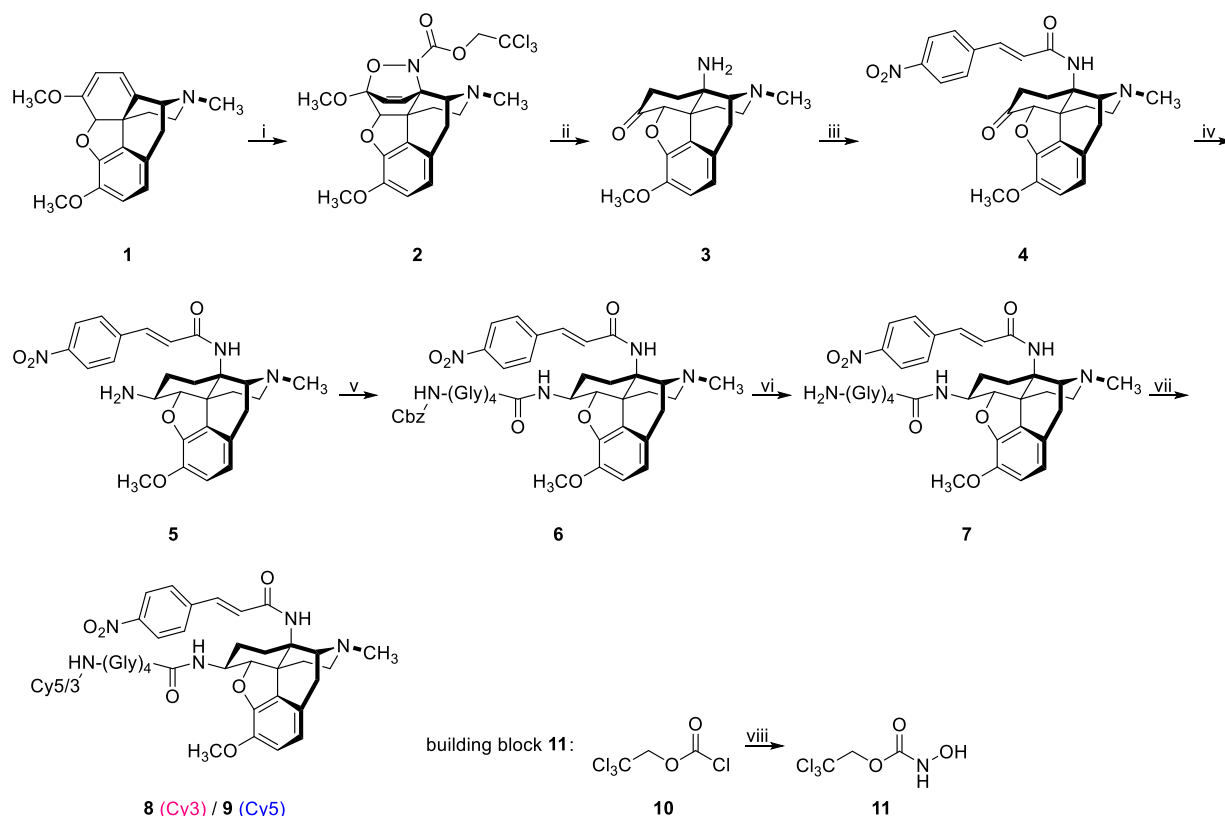
1.4. Selective and Wash-Resistant Fluorescent Dihydrocodeinone Derivatives Allow Single-Molecule Imaging of μ -Opioid Receptor Dimerization

activated *N*-hydroxysuccinimide (NHS) esters, enabling a reliable coupling with primary amine groups. The structural difference of Cy3 and Cy5 is minor (Fig. 8). Importantly, the labeled ligands can be engaged in two-color fluorescence microscopy experiments and the dyes can act as FRET pair. The pentylene linker, which separates fluorophore part and NHS coupling group provides distance between dye and pharmacologically active part after coupling, however, a first generation of fluorescent ligands, which were synthesized via direct coupling of the respective fluorophore to the CACO scaffold, exhibited inconvenient signal-to-noise ratios and high background in SMM experiments due to non-specific binding to the glass coverslip.^[95] Thus, an additional tetraglycine linker moiety was attached at the C6 position of CACO prior to dye coupling, since studies with fluorescent ligands and incorporated small peptide linkers demonstrated improved results.^[96-98]

1.4.3. Synthesis of Fluorescent Ligands

The fluorescent CACO derivatives were synthesized by Christian Gentsch under the supervision of Prof. Dr. Michael Decker (Institute of Pharmacy and Food Chemistry, Julius-Maximilian-University of Würzburg). Starting point was thebaine (**1**), a naturally occurring alkaloid from the milky juice of *papaver bracteatum* and a common synthetic starting point for several opioids with morphinan scaffold (Scheme 1).^[99] The diene moiety was reacted in a hetero-Diels Alder reaction with 2,2,2-trichloroethyl-*N*-hydroxycarbamate (**11**), which was intermediately oxidized by sodium periodate to the respective nitroso derivative comprising the required double bond.^[100] Hydroxycarbamate **11** could be obtained from 2,2,2-trichloroethyl chloroformate (**10**) by reaction with hydroxylamine hydrochloride in basic, aqueous media.^[100] The lipophilic target compound can be easily extracted using unpolar solvents like dichloromethane or diethylether. Cycloadduct **2** was reduced by catalytic hydrogenation at 1 atm using 10% palladium on activated charcoal.^[101] However, this procedure leads to the formation of several byproducts complicating the isolation of amine **3**. Even though this reaction just gave moderate yields and purification of the target compound was demanding, a more complicated procedure of three steps to generate amine **3** from cycloadduct **2** could be avoided this way.^[102] Subsequently, the C14 primary amine group was coupled to *E*-*p*-nitrocinnamic acid using (2-(1*H*-benzotriazol-1-yl)-1,1,3,3-tetramethyluronium hexafluorophosphate (HBTU) as

1.4. Selective and Wash-Resistant Fluorescent Dihydrocodeinone Derivatives Allow Single-Molecule Imaging of μ -Opioid Receptor Dimerization



Scheme 1. Synthesis of fluorescent, MOP selective CACO derivatives **8** and **9**. Reagents and conditions: i) **11**, NaOAc, NaIO₄, EtOAc/H₂O, 0°C, 1 h, 97%; ii) H₂, Pd/C, MeOH / 5% AcOH, RT, 2.5 h, 57%; iii) *E*-*p*-nitrocinnamic acid, HBTU, DIPEA, DMF (anhydrous), RT, 18 h, 87%; iv) NH₄OAc, NaCNBH₃, MeOH/THF, RT, 24 h, 84%; v) *N*-Cbz-Gly₄-COOH, HBTU, DIPEA, DMF (anhydrous), RT, 18 h, 91%; vi) HBr in AcOH, 0°C, 20 min, quant.; vii) Cy3-NHS or Cy5-NHS, TEA, DMF (anhydrous), RT, 48 h, 38% for **8**, 26% for **9**; viii) H₂N-OH · HCl, NaOH, H₂O, 0°C-RT, 1 h, 66%.^[56]

reagent to generate the activated ester of the deprotonated acid.^[103] This step gave CACO **4** as intermediate, which was favorable for comparison with the labeled target compounds. CACO **4** was subjected to a stereoselective, reductive amination yielding the 6 β -primary amine **5** in very good to excellent yields.^[93] The β -position of the amine group was verified in the ¹H-NMR spectrum by the coupling constant of the C6 proton. Afterwards, amine **5** was coupled to *N*-carboxybenzyl (Cbz) protected tetraglycine with the HBTU method in excellent yields.^[103] Subsequent Cbz deprotection was achieved using hydrobromic acid in acetic acid at 0°C for 20 min, after which time the reaction must be stopped to avoid bromination reactions and decomposition. It is also possible to slowly drip the deprotection reagent to a pre-cooled solution of the starting material in dichloromethane, which simplifies the procedure regarding reaction control and workup. Deprotection proceeded quantitatively with this method. Notably, Cbz removal cannot be achieved by catalytic hydrogenation, which is the standard method to deprotect benzyl groups, since starting material **6** comprises hydrogenation-sensitive

1.4. Selective and Wash-Resistant Fluorescent Dihydrocodeinone Derivatives Allow Single-Molecule Imaging of μ -Opioid Receptor Dimerization

functional groups (e.g., nitro-group and double bond of cinnamoyl moiety). Finally, the deprotected amine **7** was coupled to the NHS-activated esters of the dyes Cy3 and Cy5 using dry conditions and triethylamine as base. Yields of the purified product were low, which is likely due to hydrolysis of the NHS ester to the corresponding acid, as indicated by LC/MS. Notably, the acid could be reactivated to increase yields during reaction (e.g. by adding HBTU).^[88] Crude target compounds were purified either by flash chromatography or by semi-preparative HPLC, each on a reversed phase column.

1.4.4. Binding Affinity, Selectivity and Intrinsic Activity of Fluorescent Ligands

To investigate if the fluorescent ligands **8** and **9** (Scheme 1) retained sufficient selectivity over the other OR subtypes, a HTRF assay was performed by Dr. Damien Maurel, Dr. Rémy Sounier and Dr. Sébastien Granier (Institut de Génomique Fonctionnelle, Université de Montpellier) (cf. chapter 1.3.). HEK293 cells transiently expressing SNAP-tagged ORs labeled with Lumi4-Tb were used. Thereby terbium cryptate of the modified receptors served as donor and the red, fluorescent ligand acted as acceptor. The cells were incubated with increasing concentrations of ligand **9** (Scheme 1) in presence and absence of an excess of naloxone to control for non-specific binding. HTRF signal detection was carried out at 665 nm (acceptor) and 620 nm (donor) and the HTRF ratio (acceptor- / donor signal) was plotted against the ligand concentration to obtain saturation binding curves, demonstrating the pronounced selectivity of **9** for the MOP (Fig. 9).

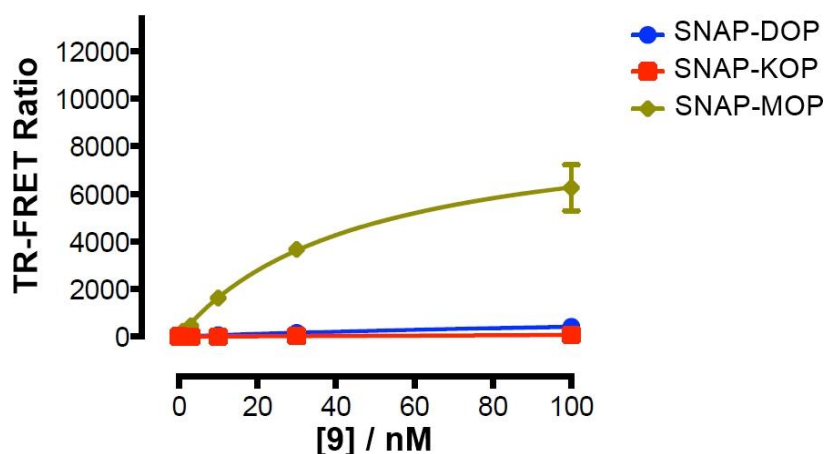


Fig. 9. Saturation binding curves obtained for Cy5 labeled CACO derivative **9** on ORs fused to Lumi4-Tb via SNAP-tag. HEK293 cells were transiently transfected to express SNAP-ORs. The cells were incubated with increasing concentrations of ligand **9**. Data is presented as means \pm standard deviation (SD) for triplicates of a representative experiment.^[56]

1.4. Selective and Wash-Resistant Fluorescent Dihydrocodeinone Derivatives Allow Single-Molecule Imaging of μ -Opioid Receptor Dimerization

The respective K_d value was 45 ± 9 nM for SNAP-MOP, while no affinity to the other OR subtypes was detectable. This met our expectations and is in good agreement with previous studies using the BODIPY derivative of CACO (cf. chapter 1.4.2.).^[93] Additionally, both fluorescent CACO derivatives **8** and **9** were tested on wild type MOP expressed in CHO cells via TIRF microscopy by Dr. Kerstin Seier under the supervision of Prof. Dr. Davide Calebiro (Institute of Pharmacology and Toxicology, Julius Maximilian University of Würzburg) to see a potential influence of epitope tagged receptors on binding affinity. This cell line was used for this assay due to some advantageous attributes for microscopy, e.g. very good adhesion to glass-coverslips. CHO cells not expressing MOPs served as control for unspecific binding. Concentration-binding curves were obtained by incubating the cells with increasing concentrations of the respective ligand and measuring fluorescence intensities of at least 40 cells per condition (Fig. 10a). Non-specific binding at the cell surface or the

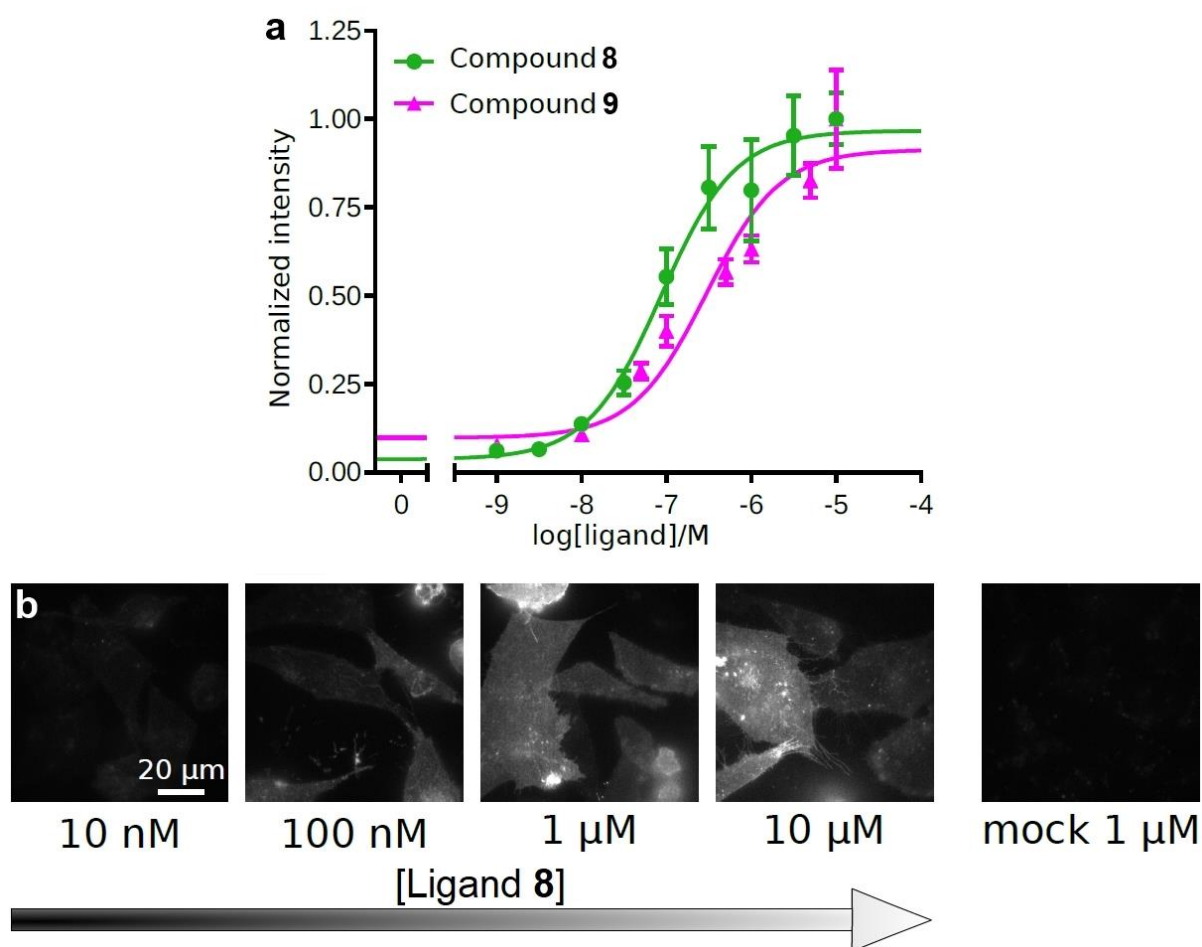


Fig. 10. a) Concentration-binding curves obtained for compounds **8** and **9**. Data is presented as means \pm S.E.M. for triplicates of a representative experiment. The mean intensities of 32–86 cells per data point were averaged.

b) Representative TIRF images of CHO cells transiently transfected with wild-type MOP or mock transfected and incubated with increasing concentrations of fluorescent ligand **8**.^[56]

1.4. Selective and Wash-Resistant Fluorescent Dihydrocodeinone Derivatives Allow Single-Molecule Imaging of μ -Opioid Receptor Dimerization

glass coverslip was negligible as can be seen in TIRF microscopy images of the incubated CHO cells (Fig. 10b). The binding affinities in this assay were determined for both derivatives (**8**: $K_d = 87 \pm 49$ nM, **9**: $K_d = 295 \pm 141$ nM). While binding affinity of the Cy3 derivative **8** is in the range of the K_d value determined in the HTRF assay with ligand **9** on SNAP-tagged MOPs (Fig. 9, $K_d = 45 \pm 9$ nM), the Cy5 derivative shows an approximately three-fold increase in binding affinity. Since the structural difference between **8** and **9** is marginal, this could likely be a result of varying fluorescence intensity due to photobleaching during illumination in microscopy experiments or upon storage and transport of the ligand. It is known, that Cy5 is more sensitive to photobleaching than Cy3.^[104] The relatively high standard error could also be a result of this. Nevertheless, both ligands retained sufficient two- and three-digit nM binding affinities in combination with high specificity, which made them suitable for further TIRF- and SM microscopy experiments.

Since CACO was reported to act as short-time agonist, the intrinsic activity of Cy3 derivative **8** was also determined by Dr. Harald Hübner from the working group of Prof. Dr. Peter Gmeiner (Department of Chemistry and Pharmacy, Friedrich-Alexander University of Erlangen-Nuremberg). G-protein mediated signaling was investigated in an inositol monophosphate (IP₁) accumulation assay on HEK-293T cells transiently co-transfected with the cDNA of *hMOP* and of the hybrid G-protein $G_{\alpha_{qi}}$ (Fig. 11a). Ligand **8** acted as partial agonist to morphine with an EC₅₀ value of 190 nM ($E_{max} = 57\%$ of maximal response to morphine). Interestingly, the ligand was not capable of inducing β -arr-2 binding, as determined in a β -arr-2 recruitment assay on HEK-293

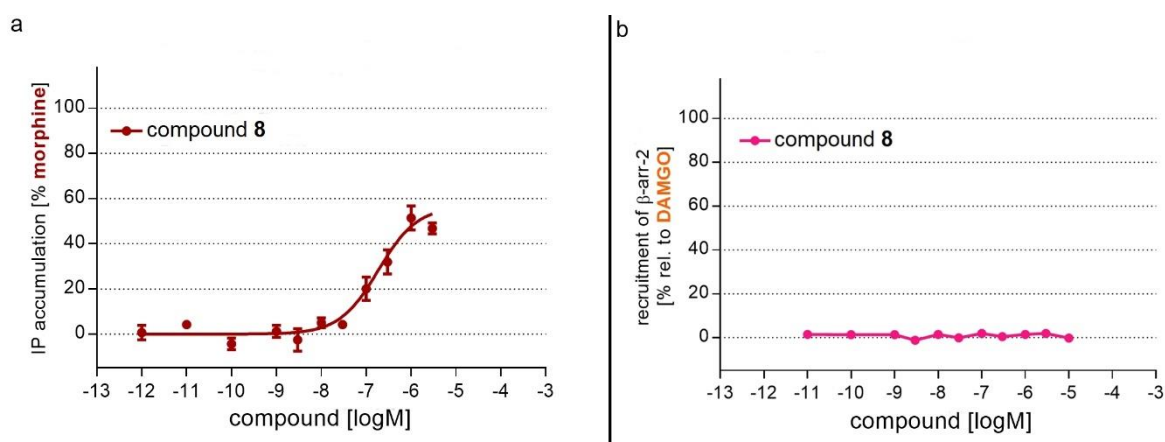


Fig. 11. a) Intrinsic activity of fluorescent CACO derivative **8** determined in an inositol monophosphate (IP₁) accumulation assay for G-protein mediated signaling. IP₁ accumulation in percentage of morphine was plotted against the logarithmic ligand concentration (range from 0.1 pM up to 10 μ M). Data is presented as means \pm S.E.M. for duplicates of the respective experiments. **b)** β -arr-2 recruitment assay with Cy3 labeled CACO derivative **8**. Recruitment of β -arr-2 in percentage relative to DAMGO was plotted against the logarithmic ligand concentration (range from 1 pM to 10 μ M).^[56]

1.4. Selective and Wash-Resistant Fluorescent Dihydrocodeinone Derivatives Allow Single-Molecule Imaging of μ -Opioid Receptor Dimerization

cells stably expressing the enzyme acceptor tagged β -arr-2 fusion protein and transiently transfected with the ProLink tagged MOP-PK1 construct (Fig. 11b).

1.4.5. Wash Resistance of Fluorescent Ligands

As mentioned above (cf. chapter 1.4.2.), an important consideration in the design of the fluorescent ligands was wash-resistance, since fluorescence microscopy experiments and assays can require washing steps and a preferably long residence time of the ligands on the receptor is beneficial for SMM, because this enables precise particle tracking. Previous studies with unlabeled CACO demonstrated a concentration-dependent, wash resistant inhibition of [3 H]DAMGO binding. Inhibition of 50% binding of 0.25 nM [3 H]DAMGO were caused by 11 ± 1 nM of CACO.^[92] Additionally, it was shown that this inhibition of binding to the MOP happens due to a reduction of binding sites and not by altering the affinity. Thus, it was suggested, that the MOP is alkylated through the irreversible formation of a covalent bond.^[92] This is likely due to the nitrocinnamoylamino-side chain acting as Michael acceptor (Fig. 12).

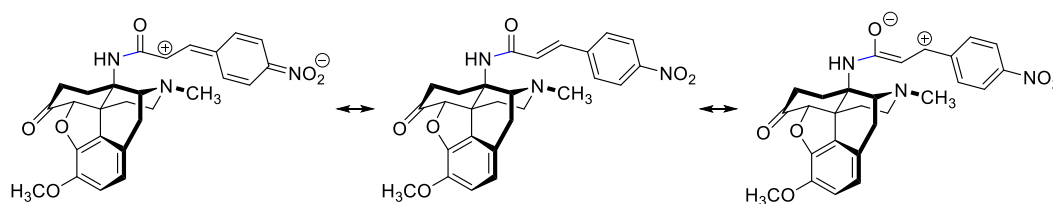


Fig. 12. Mesomeric structures of CACO showing potential electrophilic sites to be attacked by nucleophiles, e.g. in amino acid side chains.

Thus, both fluorescent ligands **8** and **9** were examined for their retained wash resistance in wash-out experiments performed by Dr. Kerstin Seier (Institute of Pharmacology and Toxicology, Julius Maximilian University of Würzburg) (Fig. 13).

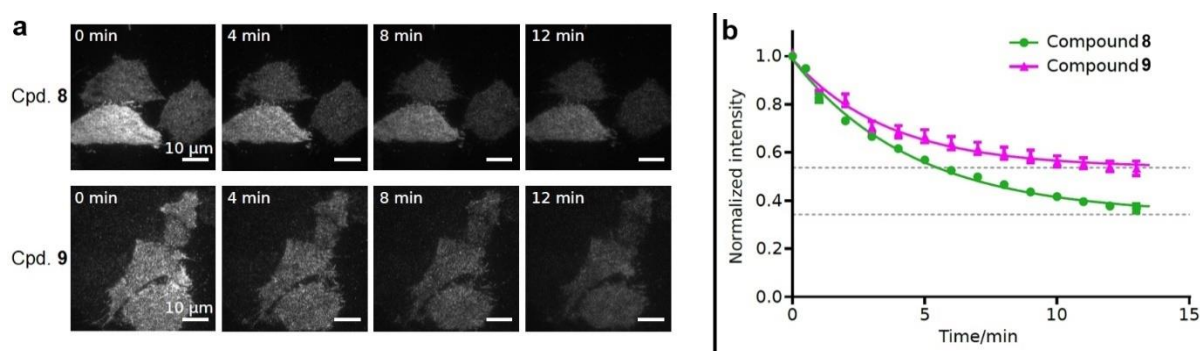


Fig. 13. a) TIRF microscopy images of CHO cells transiently transfected with wild-type MOP and incubated with 1 μ M of compound **8** (Top) or **9** (bottom) for 20 min. Images were taken every minute after washing.

b) Time-dependent dissociation of **8** and **9** from the MOP (analyzed from TIRF microscopy images as presented in **a**). Normalized intensity of 13 and 15 cells per time-point was measured in four independent experiments. The mean \pm S.E.M. is presented.^[56]

1.4. Selective and Wash-Resistant Fluorescent Dihydrocodeinone Derivatives Allow Single-Molecule Imaging of μ -Opioid Receptor Dimerization

CHO cells were treated with the compounds for 20 min and subsequently imaged by TIRF microscopy (Fig 13a). Washing steps led to an initial, slow decrease of fluorescence intensity. The curve approached a plateau at 33% for compound **8** and 53% for compound **9** (Fig. 13b). Thus, wash resistance was proven and both fluorescent ligands exhibited a long residence time on the receptor.

1.4.6. Single-Molecule Microscopy with Fluorescent Ligands

The experiments described in this chapter were carried out by Dr. Kerstin Seier with the assistance of Dr. Marie-Lise Jobin (Institute of Pharmacology and Toxicology, Julius-Maximilian-University of Würzburg), Dr. Yann Lanoiselée and Dr. Zsombor Koszegi (Institute of Metabolism and Systems Research & Centre of Membrane Proteins and Receptors, University of Birmingham) under the supervision of Prof. Dr. Davide Calebiro. Both fluorescent ligands were suitable for SMM due to their favorable photophysical properties. Consequently, fluorescent spots in TIRF images could easily be detected, giving occasion to characterize the diffusion behavior of individual MOPs on the cell surface. The Cy3 labeled derivative of CACO (compound **8**, cf. Scheme 1) was used for this purpose due to its slower photobleaching compared to Cy5 derivative **9**, as described above (cf. chapter 1.4.4.).^[104] For the diffusion study CHO cells transiently expressing wild-type MOP at a low receptor density were used (~ 0.8 receptors / μm^2). These cells were incubated with a saturating concentration of **8** (1 μM) and subsequently imaged by TIRF microscopy. Ligand-bound receptors were detected and tracked by an automated algorithm, which identified the positions and trajectories of individual MOPs on the cell surface (Fig. 14).^[105-107] The diffusion

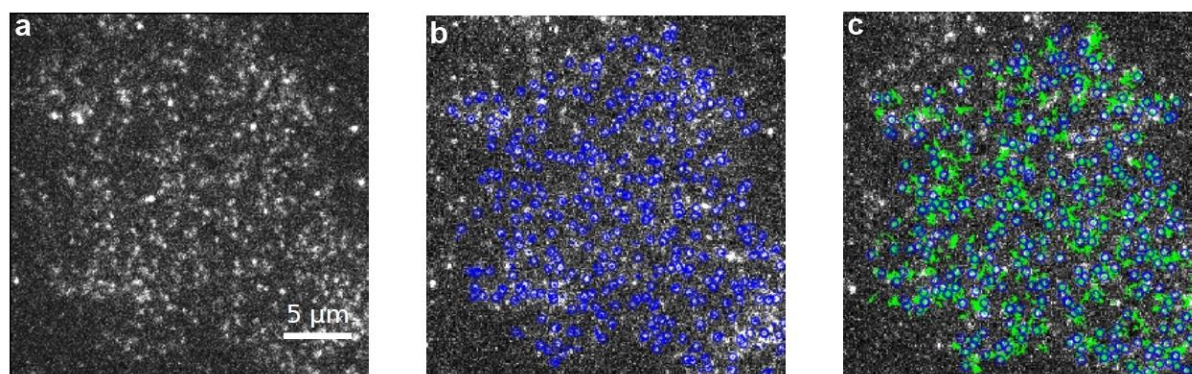


Fig. 14. Single-molecule microscopy of wild-type MOP on the CHO cell surface, labeled with ligand **8** (Cy3 derivative of CACO). **a)** Frame of a TIRF image sequence (white spots are ligand-bound receptors). **b)** Result of automated single-particle-detection (blue circles depict the position of individual receptors). **c)** Result of the automated tracking algorithm (trajectories in green represent movement sequences of individual receptors).^[56]

1.4. Selective and Wash-Resistant Fluorescent Dihydrocodeinone Derivatives Allow Single-Molecule Imaging of μ -Opioid Receptor Dimerization

behavior of the receptors in the plasma membrane was subsequently investigated by a time-averaged mean square displacement (TAMSD) analysis, which represents the extent of volume passed by a particle like a labeled receptor through random movement. The diffusion behavior of receptors was heterogenous, meaning that individual receptors underwent different types and velocities of motion. Basically four categories of receptor motion were observed and the percentage of receptors performing each kind of diffusion was analyzed (Fig. 15).^[106] An amount of $22 \pm 2\%$ of receptors were immobile, which means they did not perform any movement in an evaluable manner. This could happen, when receptors interact with rigid membrane components or enter nanodomains, where they are trapped. Sub-diffusive movement was performed by $34 \pm 1\%$ of the receptors, which indicates hampered, decelerated motion, possibly in a crowded environment or after transient trapping in a nanodomain.^[106, 108] A percentage of $34 \pm 1\%$ of receptor particles were diffusing normally according to Brownian particle motion and the remaining $10 \pm 1\%$ of receptors performed super-diffusion, meaning their motion had a directional character. Interestingly, this diffusion profile is in good agreement with other GPCRs (e.g. α_{2A} - and β_2 - adrenergic receptor).^[106]

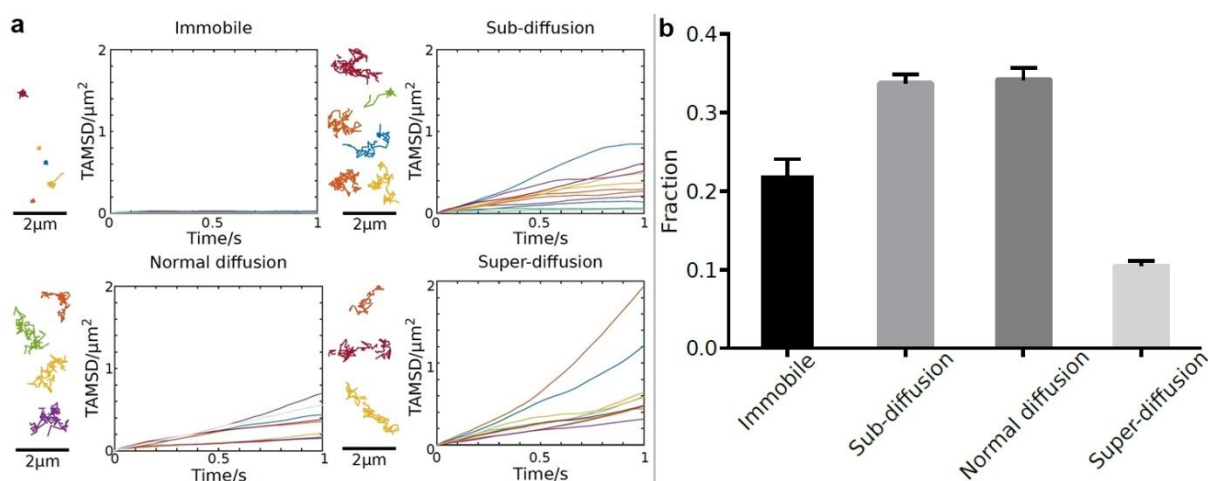


Fig. 15. a) Results of time-averaged mean square displacement analysis of MOP diffusion behavior. Categorization was conducted in (virtually) immobile (top, left), sub-diffusion (top, right), normal (Brownian) diffusion (bottom, left) and super-diffusion (bottom, right). Examples of trajectories of individual receptors of each category are presented left to the respective TAMSD-curves. **b)** Rates of MOPs in the four diffusion categories as revealed by TAMSD analysis of their respective trajectories. Data is presented as means \pm S.E.M. for 29 individual cells corresponding to 2,225 trajectories.^[56]

Finally, the pair of fluorescent ligands was used for two-color SMM experiments to study homomerization of wild-type MOP on the surface of living CHO cells. Thus, the cells were transiently transfected to yield a low, physiological receptor density of

1.4. Selective and Wash-Resistant Fluorescent Dihydrocodeinone Derivatives Allow Single-Molecule Imaging of μ -Opioid Receptor Dimerization

approximately 1.7 particles / μm^2 . Labeling was carried out simultaneously with both ligands (**8**: 1 μM , **9**: 0.5 μM), whereas the choice of concentrations was a compromise between labeling as many receptors as possible (~80%) and minimizing non-specific binding of the ligands to the glass-coverslip. Subsequently, rapid two-color TIRF microscopy was performed and co-localizations between two receptors carrying each ligand were analyzed using automated algorithms.^[106] Since co-localization of two receptors can happen randomly by collision, a control experiment was performed in an identical manner, apart from utilizing CD86 labeled with Alexa Fluor 647 by a SNAP-tagged *N*-terminus instead of Cy5 derivative **9**.^[105] Since CD86 is a protein known to not interact with MOP, this approach enabled controlling for random co-localizations without real interactions. Subsequent analysis by deconvolution of the co-localization times revealed, that more than 95% of MOPs exist as monomers, while a minority interacted to form a short-lived dimer with a lifetime of approximately 1-2 seconds. At any time 4-5% of receptors were interacting to dimerize and stopped diffusing during this time (Fig. 16). Deconvolution of the distribution of co-localization times of MOPs

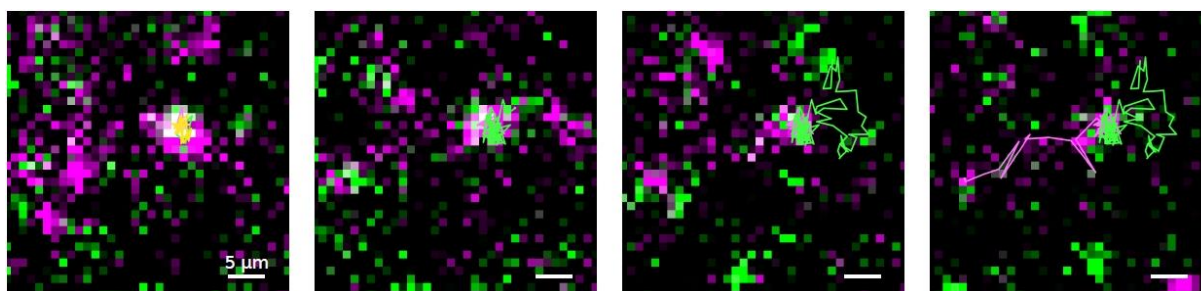


Fig. 16. Imaging of MOP dimerization via two-color SMM. The images present an example of a co-localization event (yellow, left image) between two receptors labeled with each ligand. One MOP labeled with Cy3 derivative **8** (and its respective trajectory) is presented in green, the other receptor carrying Cy5 derivative **9** is presented in magenta. Both receptors stopped their motion during the interaction.^[56]

labeled with each ligand and MOP with CD86 enabled an estimation of the duration and frequency of interactions (Fig. 17).^[106] The relaxation plot of interacting MOPs against co-localization time resulted in an exponential decay, corresponding to a time constant $\tau = 1.797 \pm 0.487$ s and the respective dissociation rate constant $k_{\text{off}} = 0.557 \pm 0.207$ s^{-1} . The two-dimensional association rate k_{on} , which describes dimer-formation, was estimated as 0.020 ± 0.004 $\mu\text{m}^2 / \text{molecule} \cdot \text{s}$. Thus, the dissociation equilibrium constant, defined by k_{off} and k_{on} was determined as $K_d = 27.43 \pm 11.75$ molecules / μm^2 . It must be noted, that the small percental fraction of homodimers is similar to the rate of active receptors in complex with G-proteins, suggesting a possible

1.4. Selective and Wash-Resistant Fluorescent Dihydrocodeinone Derivatives Allow Single-Molecule Imaging of μ -Opioid Receptor Dimerization

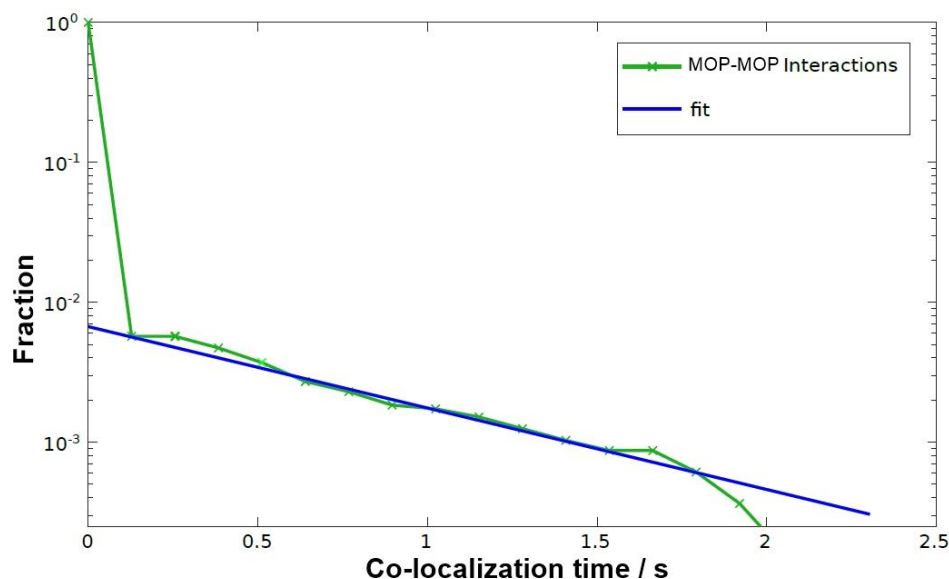


Fig. 17. Estimated duration and frequency of MOP-MOP interactions achieved by deconvolution of co-localization times of MOP-MOP and MOP-CD86 (no expected interactions). 51832 co-localizations of 25 individual cells were analyzed for MOP-MOP and 61259 co-localizations for MOP-CD86.^[56]

biological relevance.^[106] However, this experimental setup cannot preclude the presence of smaller fractions of higher order oligomers, even though the intensities and bleaching behavior of most receptors point towards monomers and dimers. Interestingly, the estimated time constant and dissociation rate are similar to previous results for other class A GPCRs.^[105-106, 109-110] Moreover, the dissociation equilibrium constant K_d admits an estimation of the mono- and dimeric MOP fraction in relation to the receptor density on the plasma membrane. Thus, a density of approximately 27 receptor particles per μm^2 would produce a dimer-fraction of ~50%, while the density of receptors expressed by the transfected CHO cells was only 1.7 particles / μm^2 . These required receptor densities of the MOP can be achieved at synapses,^[111-113] meaning a pronounced fraction of dimers could exist *in vivo*.^[114]

Due to the results of the TAMSD analysis revealing a relevant fraction of virtually immobile or sub-diffusive particles (Fig. 15) and the investigated dimers, which interrupted their motion during interaction, it was necessary to control if co-localization happens when two receptor particles enter the same clathrin-coated pit (CCP) before internalization. This would mean, that co-localization is forced and a real interaction of dimerization does not necessarily have to occur. Thus, the same general experiment was performed again, but cells were transiently co-transfected with green fluorescent protein (GFP)-tagged clathrin and wild-type MOP. Then the cells were incubated with both ligands **8** and **9**, as described above. After imaging by fast two-color TIRF

1.4. Selective and Wash-Resistant Fluorescent Dihydrocodeinone Derivatives Allow Single-Molecule Imaging of μ -Opioid Receptor Dimerization

microscopy and acquisition of a CCP image, computational analysis was performed. As a result, interactions of MOPs mainly occurred outside CCPs, while just a minor fraction of receptors were co-localized within or near CCPs (Fig. 18). In detail, the analysis revealed that $77 \pm 9\%$ of receptor particles interacted apart from CCPs, while $23 \pm 9\%$ were co-localized directly within or in close proximity to CCPs. Consequently, it can be concluded that co-localization is not exclusively driven by CCP recruitment and other mechanisms must be involved to move the receptors towards interaction.

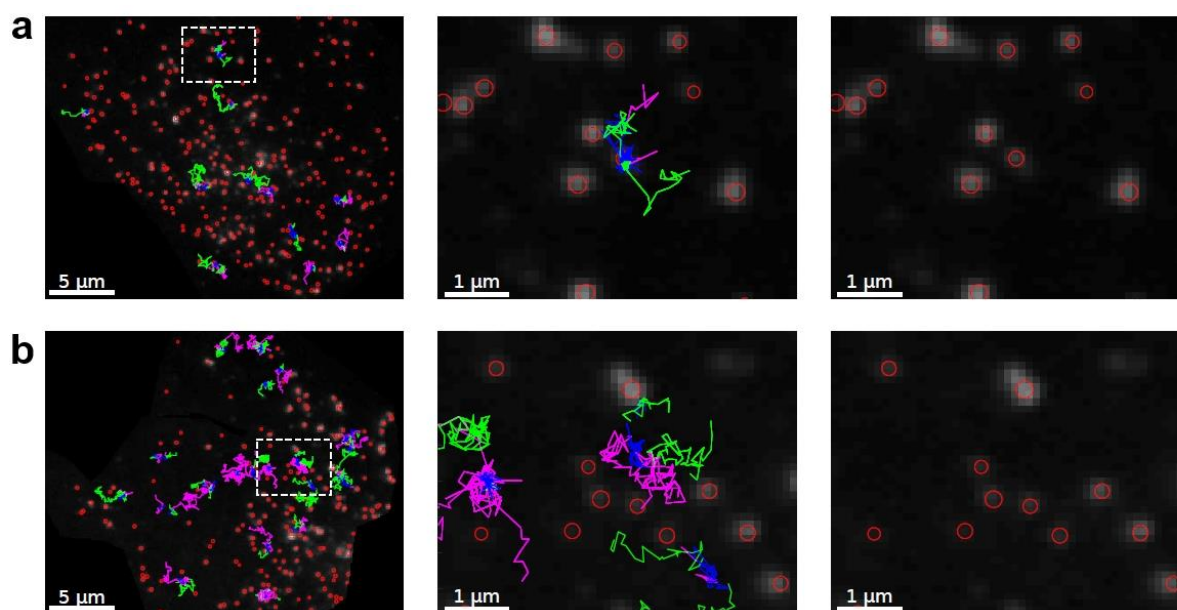


Fig. 18. Representative images of two CHO cells transiently co-transfected with wild-type MOP and GFP-tagged clathrin (grey spots marked with red circles). Cells were incubated with Cy3 ligand **8** (1 μ M, green trajectories) and Cy5 ligand **9** (0.5 μ M, magenta trajectories). Interactions of two MOPs are presented in blue. **a)** The left image shows the whole cell with a representative interaction of MOPs within or near a CCP marked in the dashed box. The image in the middle is the enlarged view of the respective area. The right image depicts the same area without particle trajectories. **b)** The left image shows another CHO cell with an area marked by the dashed, white box, where three MOP-MOP interactions occur outside CCPs. The middle image is the enlarged view of this area. The right image represents the same area without trajectories.^[56]

Altogether, the pair of fluorescent ligands accomplished the established design criteria (cf. chapter 1.4.2.) and turned out to be a suitable tool to investigate wild-type MOP on the surface of living cells via TIRF- and SM microscopy. A small fraction of homodimers of MOP was discovered, however, it must be noted that dimer formation could be agonist-driven, which is also suggested by later studies.^[55, 115] Nevertheless, these ligands are currently the subject of ongoing studies to investigate the MOP in living neurons and nervous tissue. Additionally, an application of these ligands to investigate MOP heteromerization in combination with other fluorescent, subtype selective agonists or antagonists is conceivable.

1.4. Selective and Wash-Resistant Fluorescent Dihydrocodeinone Derivatives Allow Single-Molecule Imaging of μ -Opioid Receptor Dimerization

1.4.7. Experimental Procedures

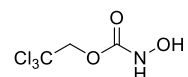
The following section describes detailed procedures for all performed experiments in the published research work of chapter 1.4.^[56] These experimental details were published separately as [Supporting Information](#).

Common reagents and methods for chemical synthesis

Common reagents and solvents were obtained from commercial suppliers (Sigma-Aldrich, Steinheim, Germany; Merck, Darmstadt, Germany; Cy3 and Cy5 NHS esters: Click Chemistry Tools, Scottsdale, USA; *N*-Cbz-Gly₄: Bachem, Bubendorf, Switzerland) and were used without any further purification, unless stated otherwise. The thin layer chromatography (TLC) for reaction control was performed on precoated plates (Silica Gel 60 F254, Macherey-Nagel GmbH & Co. KG, Düren, Germany). The substances were either visualized by their fluorescence, when irradiated with UV-light (254 nm), by spray-reagents (Dragendorff's reagent) or by their discoloration in an iodine chamber. Silica gels with grain sizes of 0.063 - 0.2 mm (company Merck, Darmstadt, Germany) were used for manual column chromatography. The columns were packed wet. The composition of the eluents is indicated in percentage by volume. NMR spectra were recorded at room temperature on a Bruker AV 400 FT-NMR Spectrometer (company Bruker Biospin, Karlsruhe, Germany) (¹H: 400 MHz, ¹³C: 100 MHz). The residual protons and the ¹³C-resonance signals of the deuterated solvents were used as internal standards. The chemical shifts δ are indicated in [ppm] and the coupling constants in [Hz]. The signal multiplicities are abbreviated as follows: s = singlet, d = doublet, t = triplet, q = quartet, dd = doublet of doublets, m = multiplet. Analytical HPLC was performed on a Shimadzu LC20AB system equipped with a DGU-20A3R controller, and a SPD-20A UV/Vis detector. The stationary phase was a Synergi 4u Fusion-RP (150x4.6 mm) column. A MeOH/water gradient + 0.1% formic acid (phase A/ phase B) was used as mobile phase. For analytical HPLC a flow rate of 1 mL/min was used. For semi-preparative HPLC, a Synergi 4u Fusion-RP 80A (250x10.0 mm) column was used as stationary phase and the flow rate was 2.5 mL/min. ESI-MS spectral data were acquired on a Shimadzu LCMS-2020 single quadrupole LC/MS (Shimadzu Europe, Duisburg, Germany).

1.4. Selective and Wash-Resistant Fluorescent Dihydrocodeinone Derivatives Allow Single-Molecule Imaging of μ -Opioid Receptor Dimerization

Synthesis of 2,2,2-trichloroethyl-*N*-hydroxycarbamate (**11**)



1.13 g (28.3 mmol, 6.00 eq) of sodium hydroxide were dissolved in water, while vigorous stirring and cooling with ice (0°C) and 1.64 g (23.6 mmol, 5.00 eq) of hydroxylamine hydrochloride were added to the solution. Then 0.65 mL (4.72 mmol, 1.00 eq, 1.00 g, 1.54 g/mL) of 2,2,2-trichloroethyl chloroformate were cautiously dripped into the reaction mixture, which was subsequently allowed to warm up to room temperature and stirred for 1 h. After that, the aqueous phase was extracted with six small portions of dichloromethane and the combined organic layers were washed with three small amounts of brine. After drying over sodium sulphate, the crude product was purified by column chromatography (eluent = PE : EA = 2 : 1) to yield a white, crystalline solid.

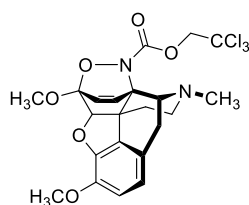
Yield: 646.4 mg, 3.10 mmol, 66%.

$^1\text{H-NMR}$ (400 MHz, DMSO- d_6) δ [ppm]: 4.82 (s, 2H, $-\text{CH}_2-$), 9.04 (brs, 1H, $-\text{OH}$), 10.26 (brs, 1H, $-\text{NH}-$).

$^{13}\text{C-NMR}$ (100 MHz, DMSO- d_6) δ [ppm]: 73.28 ($-\text{CH}_2-$), 96.11 ($\text{Cl}_3\text{C}-$), 155.69 ($\text{C}=\text{O}$).

m.p.: 89°C

Synthesis of cycloadduct **2**



427 mg (2.05 mmol, 1.50 eq) of 2,2,2-trichloroethyl-*N*-hydroxycarbamate (**11**) were slowly added to a solution of 426.58 mg (1.37 mmol, 1.00 eq) thebaine (**1**) in 43 mL ethyl acetate and 438.47 mg (2.05 mmol, 1.50 eq) sodium periodate in 21.33 mL of a 0.5 M sodium acetate solution. The reaction mixture was cooled with ice and the pH-value was adjusted to 6 by addition of a few drops of aqueous hydrochloric acid (2 M). The reaction was stirred for one hour at 0°C, before saturated, aqueous sodium hydrogen carbonate solution was added to produce alkaline conditions. The ethyl acetate layer was washed with saturated, aqueous sodium thiosulphate and brine,

1.4. Selective and Wash-Resistant Fluorescent Dihydrocodeinone Derivatives Allow Single-Molecule Imaging of μ -Opioid Receptor Dimerization

dried over sodium sulphate and evaporated. The crude product was purified by column chromatography (eluent = PE : EA = 3 : 1 \rightarrow 2 : 1 \rightarrow 1 : 1) to yield a white, crystalline solid.

Yield: 686 mg, 1.325 mmol, 97%.

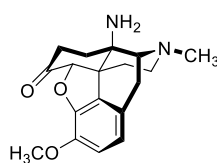
$^1\text{H-NMR}$ (400 MHz, CDCl_3) δ [ppm]: 1.16 - 2.04 (m, 2H, H-15), 2.36 - 2.72 (m, 4H, H-10 / H-16), 2.49 (s, 3H, N- CH_3), 3.42 (d, $^3\text{J} = 18.5$ Hz, 1H, H-9), 3.63 (s, 3H, OCH_3 -6), 3.81 (s, 3H, OCH_3 -3), 4.59 (s, 1H, H-5), 4.91 (brs, 2H, O- CH_2), 6.06 and 6.14 (ABq, $^3\text{J} = 8.9$ Hz, 2H, H-7 / H-8), 6.58 and 6.68 (ABq, $^3\text{J}_1 = 8.18$ Hz, $^3\text{J}_2 = 8.19$ Hz, 2H, H-1 / H-2).

$^{13}\text{C-NMR}$ (100 MHz, CDCl_3) δ [ppm]: 23.79 (C-10), 33.45 (C-15), 43.23 (N- CH_3), 45.28 (C-16), 53.42 (OCH_3 -6), 56.84 (OCH_3 -3), 58.64 (C-9), 75.59 (OCH_2), 87.52 (CCl_3), 90.45 (C-5), 104.90 (C-11), 114.95 (C-2), 119.95 (C-1), 123.05 (C-7 / C-8), 142.50 (C-3), 148.25 (C-4).

ESI-MS: 517.05 m/z [$\text{M}+\text{H}$] $^+$, calculated 517.07 m/z (100%).

m.p.: 181°C

Synthesis of 14 β -amino-7,8-dihydrocodeinone (**3**)



351 mg (0.678 mmol, 1.00 eq) of cycloadduct **2** were dissolved in 13.5 mL of distilled methanol and 13.5 mL of 5% aqueous acetic acid were added. Then 35.1 mg (10 wt-%) of palladium on activated charcoal (10% Pd) were added carefully under an argon-atmosphere. This suspension was hydrogenated (1 atm) at room temperature for 2.5 h while vigorous stirring. A balloon was used to keep an atmosphere of hydrogen. After that, the reaction mixture was filtered through a small pad of celite and the filtrate was evaporated. The crude product was purified by column-chromatography (eluent = CH_2Cl_2 : MeOH = 9.5 : 0.5 \rightarrow 9 : 1 + 0.1% NH_3) to yield a colorless, viscid solid.

Yield: 122.4 mg, 0.389 mmol, 57%.

1.4. Selective and Wash-Resistant Fluorescent Dihydrocodeinone Derivatives Allow Single-Molecule Imaging of μ -Opioid Receptor Dimerization

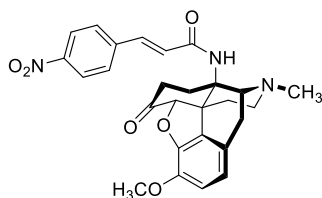
$^1\text{H-NMR}$ (400 MHz, CDCl_3) δ [ppm]: 2.38 (s, 3H, N- CH_3), 3.03 - 3.17 (m, 3H, H-9 / H-10), 3.89 (s, 3H, O CH_3), 4.64 (s, 1H, H-5), 6.65 (q, $^3J_1 = 8.2$ Hz, $^3J_2 = 25.2$ Hz, 2H, H-1 / H-2).

$^{13}\text{C-NMR}$ (100 MHz, CDCl_3) δ [ppm]: 21.78 (C-10), 29.98 (C-15), 32.40 (C-8), 36.66 (C-7), 43.28 (N- CH_3), 45.91 (C-16), 57.03 (O CH_3), 66.67 (C-9), 90.35 (C-5), 114.85 (C-2), 119.52 (C-1), 208.91 (C-6).

ESI-MS: 315.15 m/z $[\text{M}+\text{H}]^+$, calculated 315.17 m/z (100%).

m.p.: 98°C

Synthesis of 14 β -[(*p*-nitrocinnamoyl)amino]-7,8-dihydrocodeinone CACO (4)



26.3 mg (0.136 mmol, 1.05 eq) of *E-p*-nitrocinnamic acid were dissolved in dry DMF and 54.1 mg (0.143 mmol, 1.10 eq) HBTU and 33.2 μL (0.195 mmol, 1.50 eq) of dry DIPEA were added to the solution. Then 40.8 mg (0.130 mmol, 1.00 eq) of amine **3** were transferred to the reaction mixture in dry DMF ($V = 5$ mL) and the solution was stirred for 18 h at room temperature. Then ethyl acetate was added and the organic phase was washed with each two portions of saturated, aqueous sodium carbonate solution, water and brine. The organic phase was dried over sodium sulphate and the crude product was purified by manual column chromatography (normal phase, eluent = CH_2Cl_2 : MeOH = 99 : 1 + 0.1% NH_3) to yield a pale yellow solid.

Yield: 55.3 mg, 0.113 mmol, 87%.

$^1\text{H-NMR}$ (400 MHz, CDCl_3) δ [ppm]: 2.45 (s, 3H, N- CH_3), 2.92 - 3.02 (m, 1H, H-10), 3.10 (d, $J = 7.3$ Hz, 1H, H-9), 3.25 (d, $J = 18.6$ Hz, 1H, H-10), 3.89 (s, 3H, O CH_3), 4.96 (s, 1H, H-5), 6.68 - 6.78 (m, 3H, H-1 / H-2 / H-2'), 7.22 (s, 1H, NH), 7.69 - 7.73 (m, 3H, H-3' / H-5' / H-9'), 8.26 (d, $^3J = 8.8$ Hz, 2H, H-6' / H-8').

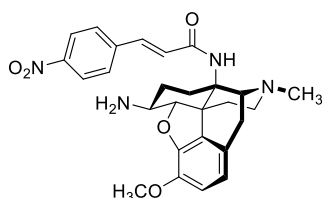
1.4. Selective and Wash-Resistant Fluorescent Dihydrocodeinone Derivatives Allow Single-Molecule Imaging of μ -Opioid Receptor Dimerization

^{13}C -NMR (100 MHz, CDCl_3) δ [ppm]: 20.92 (CH_2), 30.50 (CH_2), 36.94 (C-7), 43.28 (N- CH_3), 48.02, 56.60 (C-13), 57.00 (OCH_3), 63.58 (C-9), 89.78 (C-5), 115.36 (C-2), 119.34 (C-1 / C-2'), 124.30 (C-6' / C-8'), 125.36 (C-11), 128.65 (C-5' / C-9'), 139.08 (C-4'), 165.77 (C-1').

ESI-MS: 490.15 m/z $[\text{M}+\text{H}]^+$, calculated 490.20 m/z (100%).

m.p.: 270°C

Synthesis of 14 β -[(*p*-nitrocinnamoyl)amino]-7,8-dihydrocodein-6 β -amine (**5**)



16.8 mg (0.034 mmol, 1.00 eq) of 14 β -[(*p*-nitrocinnamoyl)amino]-7,8-dihydrocodeinone (**4**) were dissolved in 2 mL of methanol and 0.5 mL of tetrahydrofuran. Then 40.5 mg (0.525 mmol, 15.3 eq) of ammonium acetate and 6.7 mg (0.107 mmol, 3.12 eq) of sodium cyanoborohydride were given to the solution and the pH was adjusted to 6 by adding some drops of aqueous hydrochloric acid (2 M). The reaction mixture was stirred for 24 h at room temperature. After that, the solvents were evaporated and the crude product was taken up in chloroform. The organic phase was washed with each two portions of saturated, aqueous sodium hydrogen carbonate and water. After drying over sodium sulphate and removal of the solvent under reduced pressure, the crude product was purified by manual column chromatography (normal phase, eluent = CH_2Cl_2 : MeOH = 9.5 : 0.5 + 0.1% NH_3) to give a pale yellow solid.

Yield: 14.2 mg, 0.029 mmol, 84%.

^1H -NMR (400 MHz, CDCl_3) δ [ppm]: 2.34 (s, 3H, N- CH_3), 3.15 (d, $^3J = 18.2$ Hz, 1H, H-6), 3.86 (s, 3H, O- CH_3), 4.71 (d, $^3J = 6.9$ Hz, 1H, H-5), 6.69 (dd, $^3J_1 = 8.2$ Hz, $^3J_2 = 33.4$ Hz, 2H, H-1' / H-2'), 6.84 (d, $^3J = 15.6$ Hz, 1H, H-2'), 6.98 (s, 1H, N-H), 7.59 (d, $^3J = 15.6$ Hz, 1H, H-3'), 7.65 (d, $^3J = 8.6$ Hz, 2H, H-5' / H-9'), 8.21 (d, $^3J = 8.7$ Hz, 2H, H-6' / H-8').

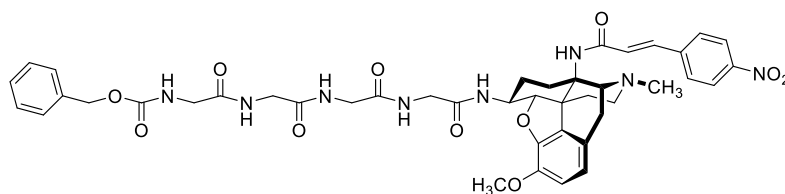
1.4. Selective and Wash-Resistant Fluorescent Dihydrocodeinone Derivatives Allow Single-Molecule Imaging of μ -Opioid Receptor Dimerization

^{13}C -NMR (100 MHz, CDCl_3) δ [ppm]: 27.20 (CH_2), 29.47 (CH_2), 29.81 (CH_2), 32.04 (CH_2), 43.08 (N- CH_3), 46.25 (C-16), 56.57 (O- CH_3), 67.14 (C-9), 68.07 (C-5), 114.16 (C-2), 118.81 (C-1), 124.21 (C-6' / C-8'), 128.46 (C-5' / C-9'), 144.02 (C-3'), 172.95 (C-1').

ESI-MS: 491.20 m/z $[\text{M}+\text{H}]^+$, calculated 491.23 m/z (100%).

m.p.: Decomposition > 165°C

Synthesis of 14 β -[(*p*-nitrocinnamoyl)amino]-7,8-dihydrocodein-6 β -tetraglycylcarboxybenzylamide (**6**)



20.4 mg (53.6 μmol , 1.05 eq) of *N*-Cbz-protected tetraglycine were dissolved in 5 mL of dry DMF under an argon atmosphere. Then 13.01 μL (76.5 μmol , 1.50 eq) of DIPEA and 21.3 mg (56.1 μmol , 1.10 eq) of HBTU were given to the solution. After that, 25 mg (51 μmol , 1.00 eq) of 14 β -[(*p*-nitrocinnamoyl)amino]-7,8-dihydrocodein-6 β -amine (**5**) were transferred to the reaction mixture in another 5 mL of dry DMF. The solution was subsequently stirred for 18 h at room temperature, before ethyl acetate was added and the organic phase was washed with each two portions of aqueous, saturated sodium carbonate, water and brine. After drying over sodium sulphate, the solvent was removed under reduced pressure and the crude product was purified by manual column chromatography (normal phase, eluent = CH_2Cl_2 : MeOH = 9 : 1). The product was obtained as a white solid after final purification.

Yield: 39.7 mg, 46.6 μmol , 91%.

^1H -NMR (400 MHz, CD_3OD) δ [ppm]: 2.31 (t, $^4J = 7.4$ Hz, 5H, N- CH_3 / H-16), 3.60 (s, 2H, Gly- CH_2), 3.65 (s, 6H, Gly- CH_2), 3.85 (s, 3H, O- CH_3), 5.08 (s, 2H, Cbz- CH_2), 6.85 (d, $^3J = 8.7$ Hz, 1H, H-2), 6.91 (d, $^3J = 16.5$ Hz, 1H, H-2'), 6.95 (d, $^3J = 4.8$ Hz, 1H, H-1), 7.32 (d, $^3J = 6.4$ Hz, 4H, Cbz-ArH), 7.66 (d, $^3J = 15.8$ Hz,

1.4. Selective and Wash-Resistant Fluorescent Dihydrocodeinone Derivatives Allow Single-Molecule Imaging of μ -Opioid Receptor Dimerization

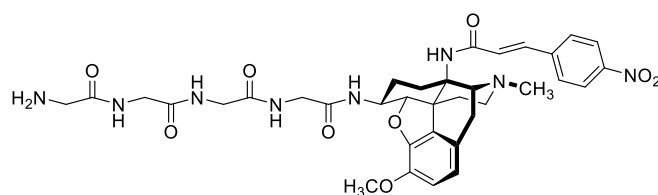
1H, H-3'), 7.84 (d, $^3J = 8.7$ Hz, 2H, H-5' / H-9'),
8.28 (d, $^3J = 8.6$ Hz, 2H, H-6' / H-8').

^{13}C -NMR (100 MHz, DMSO- d_6) δ [ppm]: 22.13 (CH_2), 24.46 (CH_2), 26.60 (CH_2),
29.06 (CH_2), 43.71 (CH_2), 43.80 (N- CH_3),
51.22 (CH_2), 54.94 (O CH_3), 79.22 (O- CH),
91.60 (CH_2), 109.82 (CH_{ar}), 122.85 (CH_{ar}),
127.78 (CH_{ar}), 127.86 (C_{ar}), 128.40 (CH_{ar}),
130.83 (CH_{ar}), 141.58 (C_{ar}), 143.86 (CH_{unsat}),
148.34 (C_{ar}), 148.53 (C_{ar}), 152.32 ($\text{C}=\text{O}$),
159.63 ($\text{C}=\text{O}$), 174.04 ($\text{C}=\text{O}$).

ESI-MS: 853.35 m/z $[\text{M}+\text{H}]^+$, calculated 853.35 m/z (100%).

m.p.: 167°C

Synthesis of 14 β -[(p-nitrocinnamoyl)amino]-7,8-dihydrocodein-6 β -tetraglycylamide (**7**)



Alternative 1: 26.3 mg (30.8 μmol , 1.00 eq) of 14 β -[(p-nitrocinnamoyl)amino]-7,8-dihydrocodein-6 β -tetraglycylcarboxybenzylamide (**6**) were dissolved in 3 mL of an ice-cold solution of hydrobromic acid in acetic acid (33 wt.-%). The reaction mixture was stirred for 20 min at 0°C, then the solvent was removed under reduced pressure and the product was obtained as a slight orange solid (HBr salt). It was dried in the desiccator and used without further purification.

Alternative 2: 18.4 mg (21.6 μmol , 1.00 eq) of 14 β -[(p-nitrocinnamoyl)amino]-7,8-dihydrocodein-6 β -tetraglycylcarboxybenzylamide (**6**) were dissolved in dichloromethane at room temperature, while stirring. The solution was cooled to 0°C by an ice bath, before an ice-cold solution of hydrobromic acid in acetic acid (33 wt.-%) was added dropwise, until the color changed to an intense yellow. The reaction mixture was stirred for 20 min at 0°C. After that, the solvent was evaporated and the crude product was purified by flash column chromatography on a reversed phase (C18) column (eluent: MeOH / H₂O + 0.1% formic acid). Optionally, the crude product in the dichloromethane phase can be washed with a saturated, aqueous sodium hydrogen

1.4. Selective and Wash-Resistant Fluorescent Dihydrocodeinone Derivatives Allow Single-Molecule Imaging of μ -Opioid Receptor Dimerization

carbonate solution to obtain the free base. After drying over sodium sulphate, the solvent can be evaporated and the crude product can be purified by flash column chromatography, as described above.

Yield 1: 24.6 mg, 30.8 μ mol, quant.

Yield 2: 6.3 mg, 8.77 μ mol, 41%.

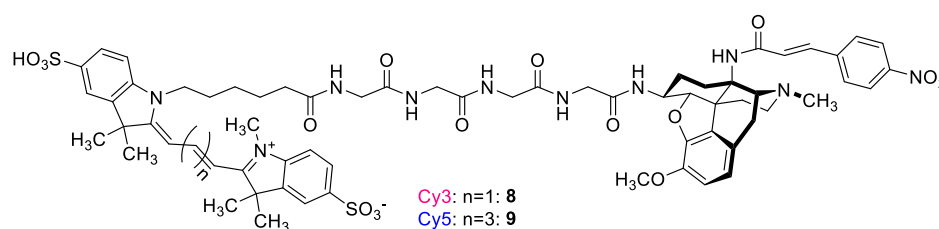
$^1\text{H-NMR}$ (400 MHz, DMSO- d_6) δ [ppm]: 2.26-2.33 (m, 5H, N- CH_3 / H-16), 3.57 (s, 6H, Gly- CH_2), 3.77 (s, 2H, Gly- CH_2), 3.78 (s, 3H, O- CH_3), 6.83 (d, $^3J = 7.1$ Hz, 1H, H-2'), 6.94 (m, 2H, H-1 / H-2), 7.83 (d, $^3J = 8.8$ Hz, 1H, H-3'), 7.89 (d, $^3J = 8.7$ Hz, 2H, H-5' / H-9'), 8.18 (d, $^3J = 8.7$ Hz, 2H, H-6' / H-8').

$^{13}\text{C-NMR}$ (100 MHz, DMSO- d_6) δ [ppm]: 19.2 (CH_2), 23.08 (CH_2), 27.1 (CH_2), 29.89 (CH_2), 42.40 (CH_2), 42.77 (N- CH_3), 45.25 (CH_2), 45.42 (CH_2), 57.99 (O- CH_3), 61.12 (CH), 63.08 (C_q), 70.34 (CH), 81.39 (CH), 108.97 (CH_{ar}), 125.48 (CH_{ar}), 131.61 (CH_{ar}), 145.71 (CH_{unsat}), 152.52 ($\text{C}=\text{O}$), 158.47 ($\text{C}=\text{O}$), 175.52 ($\text{C}=\text{O}$).

ESI-MS: 360.30 m/z [$\text{M}+2\text{H}$] $^{2+}$, 719.30 m/z [$\text{M}+\text{H}$] $^+$, calculated 719.31 m/z (100%).

m.p.: Decomposition > 205°C

Procedure for the labeling with sulfo-Cyanine 3/5 giving fluorescent ligands 8/9



8.90 mg (12.1 μ mol, 0.60 eq) of *N*-hydroxysuccinimide activated cyanine 3 or 8.95 mg (12.1 μ mol, 0.60 eq) of the respective cyanine 5 derivative were dissolved in 0.50 mL of dry DMF at room temperature under an argon atmosphere, while vigorous stirring. Then 14.5 mg (20.2 μ mol, 1.00 eq) of 14 β -[(*p*-nitrocinnamoyl)amino]-7,8-dihydrocodein-6 β -tetraglycylamide (**7**) in 1.00 mL of dry DMF were transferred to the solution containing the respective dye. The reaction mixture was stirred for 48 h at

1.4. Selective and Wash-Resistant Fluorescent Dihydrocodeinone Derivatives Allow Single-Molecule Imaging of μ -Opioid Receptor Dimerization

room temperature and the progress was carefully monitored by TLC and LC/MS. Then the solvent was evaporated and the crude product was directly purified by semi-preparative HPLC (reversed phase, eluent: MeOH/H₂O + 0.1% formic acid) to give the target compounds **8** and **9** in purities of >95%.

When starting material **7** was used as bromide-salt, the reaction was carried out in the presence of a small excess of triethylamine (1.2 eq) or *N,N*-diisopropylethylamine (1.2 eq). When the crude product was already over ~70% pure (as indicated by LC/MS analysis), purification to over 95% purity was accomplished by flash column chromatography (reversed phase, eluent: MeOH/H₂O + 0.1% NH₃).

Yield: Cpd. **8**: 6.00 mg, 4.55 μ mol, 38% (Cy3-labeling).

Cpd. **9**: 4.30 mg, 3.20 μ mol, 26% (Cy5-labeling).

ESI-MS: Cpd. **8**: 659.50 m/z [M+2H]²⁺, 1318.15 m/z [M+H]⁺, calculated 1317.50 m/z (100%).

Cpd. **9**: 672.50 m/z [M+2H]²⁺, 1344.45 m/z [M+H]⁺, calculated 1343.51 m/z (100%).

Cell culture

For the binding curves and the single-molecule experiments, Chinese Hamster Ovary (CHO) K1 (Leibniz-Institute DSMZ-German Collection of Microorganisms and Cell Cultures) cells were used. Cells were cultured in phenol red-free Dulbecco's modified Eagle's medium (DMEM)/F12 supplemented with 5% (v/v) FCS, 100 U/mL penicillin and 0.1 mg/mL streptomycin at 37°C and 5% CO₂. The cell lines were routinely passaged every two to three days.

Transfection

CHO-K1 cells were seeded the day before transfection at a density of 1.8 x 10⁵ cells per well on ultraclean 24-mm glass coverslips in 6-well culture plates. Transfection was performed with Lipofectamine 2000 (Thermo Fisher Scientific) according to the manufacturer's protocol. For each well, 2 μ g of wild-type MOP and 6 μ L of Lipofectamine 2000 were used.

*Binding analysis of fluorescent ligands **8** and **9** by TIRF*

The experiments were performed 24 h after transfection. Before imaging, each coverslip was incubated for 20 min with the indicated concentrations of either

1.4. Selective and Wash-Resistant Fluorescent Dihydrocodeinone Derivatives Allow Single-Molecule Imaging of μ -Opioid Receptor Dimerization

compound **8** or **9** dissolved in complete medium at 37°C, rapidly washed once with 1 ml of medium and immediately imaged in a microscopy chamber filled with 400 μ l of complete medium. TIRF imaging was performed on a customized Nikon Eclipse Ti TIRF microscope using a 60x oil-immersion objective (CFI Apochromat TIRF 60x oil NA 1.49). The sample and objective were kept at 20°C via a water-cooling system. Cells were searched and focused using a low laser power (3%) to avoid photo bleaching. Images acquired using 10% power of a 561 nm diode laser for compound **9** and 20% power of a 638 nm diode laser for compound **8** (both lasers from Coherent), were analyzed using FIJI. At least 50 cells per condition from three independent experiments were used. Intensity values were normalized to those obtained with the highest concentration (10 μ M). Data were fitted to a one site ligand binding model with Hill slope of 1 in GraphPad Prism (GraphPad Software, Inc., San Diego, CA).

Selectivity

Fluorescent ligand binding was monitored by HTRF (Homogeneous Time-Resolved FRET). The SNAP opioid receptors expressed at the surface of HEK293 cells were labeled with non-permanent SNAP-tag substrates derivatized with Lumi4-Tb (SNAPLumi4-Tb). Upon binding of the red fluorescent ligands on SNAP-ORs, the HTRF signal from the sensitized acceptor can be detected. Dulbecco's Modified Eagle's Medium (DMEM) and fetal bovine serum (FBS) were obtained from Life Technologies (Grand Island, NY, USA). SNAP-OR plasmids and BG-Lumi4-Tb were commercialized by CisBio bioassays and provided by Dr. S. Granier. HEK293 cells (from ATCC) were grown in DMEM supplemented with 10% FBS (without antibiotics) at 37°C, 5% CO₂. Transient transfection was performed using electroporation in a volume of 200 μ l with 1 μ g SNAP-OR plasmids and 10 millions of HEK293 cells in electroporation buffer (50mM K₂HPO₄, 20 mM CH₃COOK and 20 mM KOH, pH 7.4). After electroporation (250 V, 500 μ F, Bio-Rad Gene Pulser electroporator; Bio-Rad Laboratories, Hercules, CA), cells were resuspended in 10 ml DMEM supplemented with 10% fetal bovine serum and seeded for 24h in a white 96-well plate (pretreated with Poly-L-Ornithine 1X) at a density of 100,000 cells per well. 24 hours after transfection, SNAP-ORs were labeled with 100 nM of BG-Tb (benzylguanine-Terbium cryptate) for 1 h at 37°C in Tag-Lite buffer (commercialized by CisBio bioassays). After four washing steps with PBS, the fluorescence signal from BG-Lumi4-Tb was measured on a SPARK20M plate reader (TECAN) with an excitation at 337 nm and an

1.4. Selective and Wash-Resistant Fluorescent Dihydrocodeinone Derivatives Allow Single-Molecule Imaging of μ -Opioid Receptor Dimerization

emission at 620 nm. HEK293 cells expressing SNAP-ORs and labeled with Lumi4-Tb were incubated with increasing concentrations of fluorescent ligands for 1 h at room temperature (from 0.1 nM to 100 nM) +/- an excess of naloxone (100 μ M). HTRF signal detection was performed on a SPARK20M (TECAN). The signal was collected both at 665 nm and 620 nm. HTRF ratios were obtained by dividing the acceptor signal at 665 nm by the donor signal at 620 nm and multiplying obtained ratios by 10,000. Data were then analyzed using GraphPad Prism (GraphPad Software, Inc., San Diego, CA). K_d values of the fluorescent ligands were obtained from saturation curves of the specific binding.

Intrinsic activity

Accumulation of inositol monophosphate (IP1): HEK-293T cells were grown to a confluence of approximately 70% and transiently co-transfected with the cDNA of the human MOP (gift from Ernest Gallo Clinic and Research Center, UCSF, CA) and of the hybrid G-protein $G_{\alpha_{qi}}$ (G_{α_q} protein with the last five amino acids at the C-terminus replaced by the corresponding sequence of G_{α_i} ; gift from The J. David Gladstone Institutes, San Francisco, CA) applying the Mirus TransIT-293 transfection reagent (PepLab, Erlangen, Germany). After one day cells were detached from the culture dish with Versene (Life Technologies, Darmstadt, Germany), seeded into black 384-well plates (10,000 cells/well) (Greiner Bio-One, Frickenhausen, Germany) and maintained for 24 h at 37°C. Agonist properties were determined by incubating compound **8** (final range of concentration from 0.1 pM up to 10 μ M) in duplicates for 180 min at 37°C. Incubation was stopped by addition of the detection reagents (IP1-d2 conjugate and Anti-IP1 cryptate TB conjugate each dissolved in lysis buffer) for further 60 min at room temperature. Homogenous time resolved fluorescence resonance energy transfer (HTRF) was measured using the Clariostar plate reader (BMG, Ortenberg, Germany). Data analysis was performed by nonlinear regression using the algorithms for log(agonist) vs. response of PRISM 6.0 (GraphPad, San Diego, CA) and normalization of the raw data to basal (0%) and the maximum effect of morphine on MOP, 100%).

Recruitment of β -arrestin-2: HEK-293 cells stably expressing the enzyme acceptor (EA) tagged β -arrestin-2 fusion protein were transiently transfected with the ProLink tagged MOP-PK1, employing the Mirus TransIT-293 transfection reagent. After 24 h cells were transferred into white clear bottom 384-well plates (5000 cells/well) (Greiner Bio-One) and maintained for further 24 h at 37°C, 5% CO₂. To start receptor stimulated

1.4. Selective and Wash-Resistant Fluorescent Dihydrocodeinone Derivatives Allow Single-Molecule Imaging of μ -Opioid Receptor Dimerization

arrestin recruitment, compound **8** was added to the cells to get a final concentration range of 1 pM to 10 μ M. Incubation was continued for 90 min at 37°C. Stimulation was stopped by addition of the detection mix and further incubation for 60 min at room temperature. Chemiluminescence was determined using a Clariostar plate reader. Data analysis was done by nonlinear regression using the algorithms for log(agonist) vs. response of PRISM 6.0 (GraphPad, San Diego, CA) and normalization of the raw data to basal (0%) and the maximum effect of DAMGO (100%).

Washing experiments

Washing experiments were performed 24 h after transfection. Before imaging, each coverslip was incubated for 20 minutes at 37°C with the indicated concentration of either compound **8** or **9** dissolved in complete medium. After incubation, the coverslips were rapidly washed and immediately imaged in a microscopy chamber filled with 400 μ L of complete medium. Imaging was performed on the same customized Nikon Eclipse Ti TIRF microscope used for the analysis of fluorescent ligand binding. Images were acquired every minute, upon excitation with 15% power of either the 561 nm (compound **8**) or the 638 nm (compound **9**) diode laser, respectively. The obtained image sequences were analyzed using FIJI. For each cell, a region of interest (ROI) comprising the cell was manually defined and its background-subtracted average intensity was measured. The intensity values were then normalized to corresponding ones obtained at the beginning of the image sequence. Data were plotted and fitted to a one-phase exponential decay in PRISM 6.0 (GraphPad, San Diego, CA). Photo bleaching during image acquisition was negligible, as verified by control experiments in which the same number of frames were acquired very rapidly (within 600 ms) showing less than 2% reduction of the fluorescent signal at the end of the acquisition for Cy3. For the compound bound to Cy5 the bleaching was significantly higher with 21%. Therefore, the washing data for Cy5 were corrected for the bleaching.

Single-molecule microscopy experiments

Five hours after transfection, the cells were incubated for 20 minutes with 1 μ M of compound **9** dissolved in complete medium. After incubation, the coverslips were rapidly washed and immediately imaged in a microscopy chamber filled with 400 μ L of complete medium. Imaging was performed on the same customized Nikon Eclipse Ti TIRF microscope used for the analysis of fluorescent ligand binding, but this time with

1.4. Selective and Wash-Resistant Fluorescent Dihydrocodeinone Derivatives Allow Single-Molecule Imaging of μ -Opioid Receptor Dimerization

a 100x oil-immersion objective (CFI Apo TIRF 100x, NA 1.49). The sample was searched and focused using low laser power (3%) of a 561 nm diode laser. Movies of 200 frames were recorded with 15% laser power in crop mode with an acquisition rate of one image every 28.4 ms, resulting in 35 frames per second. The acquisition of movies was performed only in the first four to five minutes after mounting. These conditions result in less than 40% dissociation of either ligand from the receptor, as estimated by the washing experiments.

For the two-color single-molecule experiments, the cells were incubated for 20 minutes with a mixture of 1 μ M compound **8** (Cy3) and 0.5 μ M compound **9** (Cy5) in order to obtain similar labeling efficiencies. As a negative control, cells were co-transfected with wild type MOP and CD86 with an *N*-terminal SNAP-tag. After 5 hours of transfection, cells were incubated with 1 μ M of Cy3 derivative **8** and 1 μ M SNAP Alexa Fluorophore 647 (NEB). The settings for data acquisition were the same as above. To check if co-localizations happen at clathrin-coated pits, control experiments were performed by co-expression of Clathrin-GFP. Movies of MOP/MOP co-localizations with compound **8** and **9** were acquired as mentioned above. Immediately after, a movie of 200 frames of Clathrin-GFP was obtained using 30% power of a 488 nm laser (Coherent).

Analysis of single-molecule experiments

Single-molecule movies were selected for low receptor density with an average of 0.85 receptors per μm^2 , and a mask corresponding to the cell shape was applied to perform automated single-particle detection and tracking in Matlab using u-track software as described by Metzler et al.^[116-117] Single-particles were located by fitting 2D Gaussian functions to the diffraction-limited spots taking into account the point spread function of the microscope. Next, the detected particles were linked in consecutive frames. Therefore, costs were assigned for every potential event like blinking, merging, splitting and leaving out the focal plane. The overall tracking with the lowest costs was thus selected. The obtained single trajectories were then analyzed for their time-averaged mean square displacement (TAMSD), which was used to categorize the particles into four classes of motion: virtually immobile, sub-diffusive, diffusive or super-diffusive motion.^[117-119] The four classes were separated based on D , their diffusion coefficient and α , the anomalous diffusion coefficient, whereas virtually immobile was classified as $D < 0.01 \mu\text{m}^2 \text{s}^{-1}$, sub-diffusion as $\alpha < 0.75$, normal diffusion as $0.75 \leq \alpha \leq 1.25$ and super-diffusion as $\alpha > 1.25$. The two-color experiments were corrected for distortion

1.4. Selective and Wash-Resistant Fluorescent Dihydrocodeinone Derivatives Allow Single-Molecule Imaging of μ -Opioid Receptor Dimerization

and misalignment of the detectors using fluorescent beads. Both channels were analyzed as described above to obtain single-particle trajectories. As a control for random co-localization, movies with labeled CD86 and MOP were analyzed in the same way as the movies with MOP labeled with compound **9** and **8**. The obtained trajectories for the two colors were further analyzed for co-localizations. A search radius $R_0 = 265$ nm was defined and each particle in channel two, falling into this R_0 for a particle in channel 1 was registered as a co-localization. This was done for each frame and thus co-localization could be linked analogous to the single-particle tracking. Overall a starting and terminating frame was obtained for each co-localization thus the probability density function of co-localization times could be computed. Those interaction times were further analyzed comparing those from the MOP/MOP interactions with those from MOP/CD86. In order to isolate the true interaction times from the co-localization times that consist in the true interaction durations plus random ones, a deconvolution was applied using the Lucy-Richardson algorithm.^[120] The co-localizations observed between CD86 and MOP were considered as a control for random co-localizations. By deconvolving the MOP/MOP co-localization times with the co-localization times from MOP/CD86, the proportion of “true” interactions (F_{true}) was deduced (for more details, see Supplementary Methods of Sungkaworn et al. **2017**^[106]). The deconvolved data was normalized and the fraction of surviving interactions after time t , noted $F_r(t)$, was fitted to an exponential decay function:

$$F_r(t) = F_{true} e^{-(k_{off} + k_{loss})t}$$

The quantity k_{loss} accounts for premature termination due to photobleaching or particle loss from errors in detection and tracking. This was obtained previously from control experiments. Thus the dissociation rate k_{off} was derived from the deconvolved co-localization data. The quantity k_{on} was calculated from F_{true} and the rate of new co-localizations per unit of area $d[D]_{\rho}/dt$ with the following equation:

$$\frac{d[D]_{\rho}}{dt} \cdot F_{true} = k_{on} \cdot [\mu_1]_{\rho} [\mu_2]_{\rho}$$

whereas $[\mu_1]_{\rho}$ and $[\mu_2]_{\rho}$ are the densities of monomers in each channel estimated as the difference between the measured densities $[\mu_1]_{\rho}$ and $[\mu_2]_{\rho}$ in channel 1 and 2 and the estimated concentration of dimers such that $[\mu_1]_{\rho} = [Ch1]_{\rho} - [D]_{\rho}$ and $[\mu_2]_{\rho} = [Ch2]_{\rho} - [D]_{\rho}$. The density of dimers $[D]_{\rho}$ was deduced owing to the equality between association- and dissociation rate through the formula

1.4. Selective and Wash-Resistant Fluorescent Dihydrocodeinone Derivatives Allow Single-Molecule Imaging of μ -Opioid Receptor Dimerization

$$[D]_{\rho} = \frac{1}{k_{off}} \frac{d[D]_{\rho}}{dt} \cdot F_{true}$$

such that k_{on} could be expressed as a function of measurable quantities

$$k_{on} = \frac{\frac{d[D]_{\rho}}{dt} \cdot F_{true}}{([Ch1]_{\rho} - \frac{1}{k_{off}} \frac{d[D]_{\rho}}{dt} \cdot F_{true})([Ch2]_{\rho} - \frac{1}{k_{off}} \frac{d[D]_{\rho}}{dt} \cdot F_{true})}$$

An estimation of k_{on} has been done between each successive frame and the presented k_{on} was obtained by averaging the obtained k_{on} over time. The obtained interactions were further analyzed for co-localization with CCPs. Additional to the two channels with MOPs, a third channel was measured with GFP-clathrin, whose images were stacked to check for co-localization with interactions that lasted longer than 20 frames. Therefore, the CCPs were localized by fitting a 2-D Gaussian, also giving the estimated width L of the pits. An interaction was defined as 'inside a CCP' when one of the co-localizing particles was localized once during the interaction within L of one CCP. If the co-localizing particles were not within less than L of any CCP, then the co-localization was considered as 'outside CCPs'.

1.5. Non-fluorescent Opioid Ligands selectively targeting Opioid Receptor Heterodimers (unpublished research work)

1.5.1. Aim of the Work

Objective of this work was to synthesize and investigate morphinan-based ligands, which were described to bind selectively on OR heterodimers with high affinity. Thus, these ligands could represent interesting tools to study OR heterodimerization at single-molecule level by an alternative approach. Therefore, co-transfected cells expressing each two OR subtypes of choice could be used. When the receptors are epitope-tagged and labeled with a pair of fluorophores, heterodimerization could be investigated in the presence and absence of the respective, selective ligand (Fig. 19). This approach would allow to determine the influence of the ligand on heterodimerization and enable a statement, to which extent certain heterodimer-binding ligands recruit two receptors to dimerize or bind to pre-formed heterodimers. This experimental design could even represent an interesting supplement for the respective strategy with two homomer subtype-selective, fluorescent ligands and two wild-type receptors, expressed on the surface of co-transfected cells (cf. chapter 1.3.).

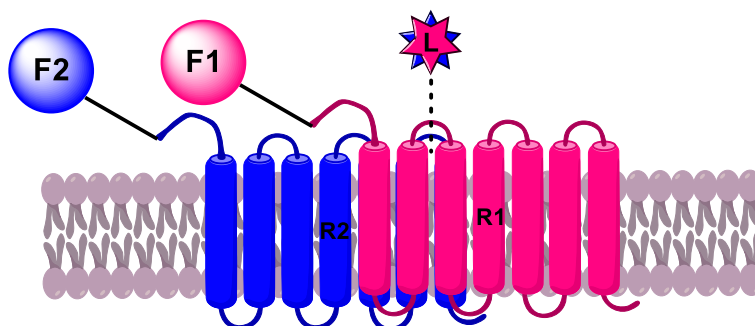


Fig. 19. Heterodimerization of two OR subtypes R1 and R2. The pair of receptors is labeled with the fluorophores F1 and F2 via an epitope-tag, which enables imaging by SMM. The selective ligand L can either recruit the dimer or bind to the pre-formed species.

For this purpose, three literature-known and heterodimer-selective ligands were chosen, that target MOP/KOP and DOP/KOP heteromers with high affinity and selectivity over the respective receptor homomers. Notably, data for monovalent ligands, that selectively target the MOP/DOP heteromer is scarce (cf. chapter 1.2.).^[66, 121-122] Nevertheless, some studies used selective antibodies and bivalent ligands comprising spacer-bridged homomer-selective pharmacologically active parts.^[68-70, 123-124] One study identified the MOP/DOP heterodimer-biased, non-morphinan agonist CYM51010 by high throughput screening of a small compound library.^[67] This

1.5. Non-fluorescent Opioid Ligands selectively targeting Opioid Receptor Heterodimers

commercially available agonist is currently the only literature known monovalent ligand selectively targeting MOP/DOP heterodimers.

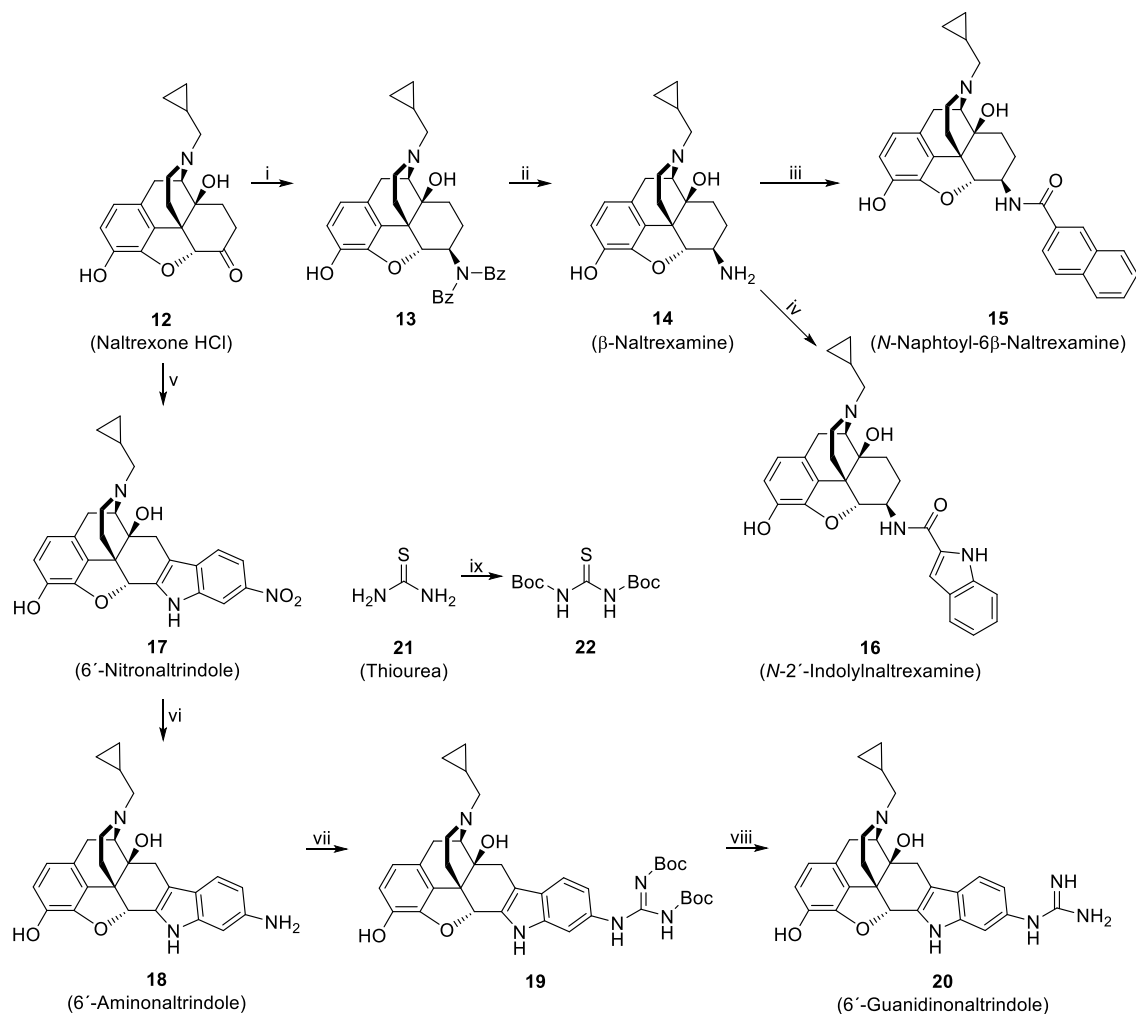
For this work, 6'-GNTI, NNTA and *N*-2'-Indolylnaltrexamine (INTA) were chosen as target compounds due to their promising attributes, which have been partly described before (cf. chapter 1.2.).^[73-74, 77] Notably, INTA is a close derivative of NNTA and selectively activates both KOP heteromers, while NNTA exclusively acts as a potent agonist on MOP/KOP heterodimers.^[125] However, both compounds produced potent antinociception without pronounced side effects like tolerance, dependence and aversive effects, which was attributed to their decreased or missing potential to recruit β -arr to cell membranes co-expressing both of their respective target receptors in the heterodimer.^[125]

Altogether, the unique pharmacological profile of all three compounds bearing a relation to their pronounced affinity for MOP/KOP and DOP/KOP heterodimers and their uncomplicated synthetic access made them interesting ligands to be applied in the experimental design described above.

1.5.2. Synthesis of Unlabeled, Heterodimer-selective Opioid Ligands

Favorably, all three heterodimer-selective opioid ligands could be constructed from naltrexone hydrochloride (**12**), which is not a drug of abuse in contrast to many OR agonists and therefore commercially easier available. At first, a literature-known procedure was used to convert compound **12** stereospecifically into β -naltrexamine (**14**), out of which NNTA **15** and INTA **16** (Scheme 2) could be obtained.^[126] Therefore, compound **12** was turned into its benzoate salt by reaction with silver benzoate under light exclusion. The precipitated silver chloride could easily be removed by filtration.^[126] The benzoate salt of naltrexone, which is more soluble in toluene than the respective hydrochloride, was subsequently condensed with dibenzylamine under azeotropic removal of water and acid catalysis.^[126] Notably, activation of the C6-keto group could also be achieved by Lewis acid catalysis (e.g. with zinc(II)chloride). This procedure yielded the corresponding 6-dibenzyliminium salt, which was directly reduced by sodium cyanoborohydride due to its sensitivity, especially towards water and moisture. Thus, the 6 β -dibenzylamino derivative **13** was generated stereoselectively and subsequently converted to β -naltrexamine (**14**) by catalytic hydrogenation at 1 atm over three days. Complete removal of the *N*-benzyl groups was earliest accomplished after this time.^[126]

1.5. Non-fluorescent Opioid Ligands selectively targeting Opioid Receptor Heterodimers



Scheme 2. Synthesis of OR heterodimer-selective ligands NNTA **15**, INTA **16** and 6'-GNTI **20**. Reagents and conditions: i) 1. Silver benzoate, MeOH : H₂O (9 : 1), 40°C, 90 min; 2. Dibenzylamine, benzoic acid, *p*-TosOH, toluene, 120°C (reflux), 20 h; 3. NaCNBH₃, MeOH (anh.), RT, 8 h, 40% (3 steps). ii) H₂ (1 atm), 10% Pd/C, 1% v/v HCl_{conc}, MeOH, 72 h, 88%. iii) 2-naphtoic acid, HBTU, TEA (anh.), THF (anh.), RT, 18 h, 44%. iv) indole-2-carboxylic acid, HBTU, DIPEA, DMF (anh.), RT, 18 h, 42%. v) 3-nitrophenylhydrazine, MeOH, RT, 24 h → HCl (aqu., conc.), 115°C, 90 min, 96%. vi) H₂, 10% Pd/C, 10% AcOH (aqu.), RT, 24 h, 85%. vii) *N,N*-Di-Boc-thiourea (**22**), HgCl₂, pyridine, DMF, 0°C → RT, 20 h, 59%. viii) F₃C-COOH, CH₂Cl₂, RT, 24 h, 97%. ix) Boc₂O, NaH (60%), THF, 0°C → RT, 3 h, 72%.

Finally, coupling of naphthoyl- and indolyl moieties to the 6 β -amino group of compound **14** was achieved by activating the respective, required acids (2-naphtoic acid for NNTA **15** and indole-2-carboxylic acid for INTA **16**) with HBTU, as described before (cf. chapter 1.4.3.).^[103]

The synthesis of 6'-GNTI was started with the reaction of naltrexone hydrochloride (**12**) and 3-nitrophenylhydrazine hydrochloride under the conditions of Fischer's indole synthesis as described in literature (Scheme 2).^[127] Notably, this procedure led to the formation of 6'-nitronaltrindole (**17**) as main product and the regioisomeric 4'-nitro derivative as side product, which is a consequence of a non-regiospecific [3,3]-sigmatropic rearrangement. Separation of these regioisomers could be achieved by

1.5. Non-fluorescent Opioid Ligands selectively targeting Opioid Receptor Heterodimers

manual column chromatography with 4% triethylamine and mixtures of methanol and dichloromethane according to a method described in literature.^[127] The nitro group was subsequently reduced to the respective primary 6'-amine **18** by catalytic hydrogenation at 1 atm using 10% palladium on activated charcoal as catalyst.^[127] 6'-aminonaltrindole (**18**) was converted to the respective bis-*tert*-butyloxycarbonyl (Boc) protected 6'-guanidino derivative **19** by using *N,N*-bis-Boc-thiourea (**22**) in the presence of mercury(II)chloride and pyridine for guanylation.^[128] Compound **22** was synthesized beforehand by reacting thiourea (**21**) with di-*tert*-butyl dicarbonate (Boc₂O).^[129] Finally, deprotection of both Boc-groups of compound **19** was accomplished by reaction with trifluoroacetic acid in dichloromethane,^[128] yielding 6'-GNTI **20** as twofold trifluoroacetate salt. Final purification of target compound **20** was performed by flash chromatography on a reversed phase column due to the high polarity of the target compound.

1.5.3. Binding Affinity and Intrinsic Activity of Heterodimer-selective Opioid Ligands

All three synthesized ligands were checked for their binding affinity on all *hOR* subtypes via radioligand binding studies using [³H]-diprenorphine as standard ligand. Thus, it was controlled that the ligands exhibit the highest affinities on the respective receptor protomers, that are part of the heterodimer on which they are described to bind to (table 2). As expected, 6'-GNTI had the highest affinities on KOP and DOP,

Table 2. Binding affinities (K_i) of the heterodimer-selective ligands 6'-GNTI **20**, INTA **16** and NNTA **15** on human OR subtypes, determined by radioligand binding with [³H]-diprenorphine. Data is presented as mean \pm Standard Deviation (SD).

Compound	K_i [nM] \pm S.E.M., <i>hMOP</i>	K_i [nM] \pm S.E.M., <i>hKOP</i>	K_i [nM] \pm S.E.M., <i>hDOP</i>
6'-GNTI 20	23 \pm 4.9	0.28 \pm 0.035	2.9 \pm 1.1
INTA 16	0.16 \pm 0.002	0.21 \pm 0.081	1.7 \pm 0.83
NNTA 15	0.14 \pm 0.034	0.17 \pm 0.01	3.3 \pm 0.13

which is consistent with previous results.^[73] However, murine, epitope-tagged versions of the ORs were used in this study,^[73] probably explaining the higher affinity for singly expressed *mDOP* than for *mKOP*, which is contrary to the results presented here (table 2). Notably, in cells co-expressing both *mKOP* and *mDOP* as heterodimers the competition curve for displacement of [³H]-diprenorphine binding was monophasic for 6'-GNTI and biphasic for the selective antagonists nor-binaltorphimine (KOP) and

1.5. Non-fluorescent Opioid Ligands selectively targeting Opioid Receptor Heterodimers

naltrindole (DOP).^[73] Thus, a homogenous population of binding sites for 6'-GNTI was suggested, as it would be expected for a heterodimeric receptor species.

NNTA and its derivative INTA expectedly exhibited highest binding affinities on *hMOP* and *hKOP* with K_i values in the sub-nanomolar range, whereby INTA also had a two-fold increased affinity for DOP, when compared with NNTA.^[77, 125] Since INTA was described to bind additionally to DOP/KOP heterodimers, this result met the expectations as well.^[125]

Since all three ligands were described to act as agonists on their respective addressed OR heterodimers, while their pharmacological profile on the respective protomers was different in parts, the compounds were tested in the assays for G-protein mediated signaling and β -arr recruitment, as described before (cf. chapter 1.4.4. and 1.4.7.). 6'-GNTI acted as agonist on the KOP ($EC_{50} = 1.2$ nM, 93% of max. stimulation of dynorphine A) and exhibited minor KOP mediated β -arr recruitment ($EC_{50} = 9.1$ nM, 26% of max. stimulation), while it was not active on both other receptor subtypes (Fig. 20). These results are consistent with the functional activity of compound **20** measured

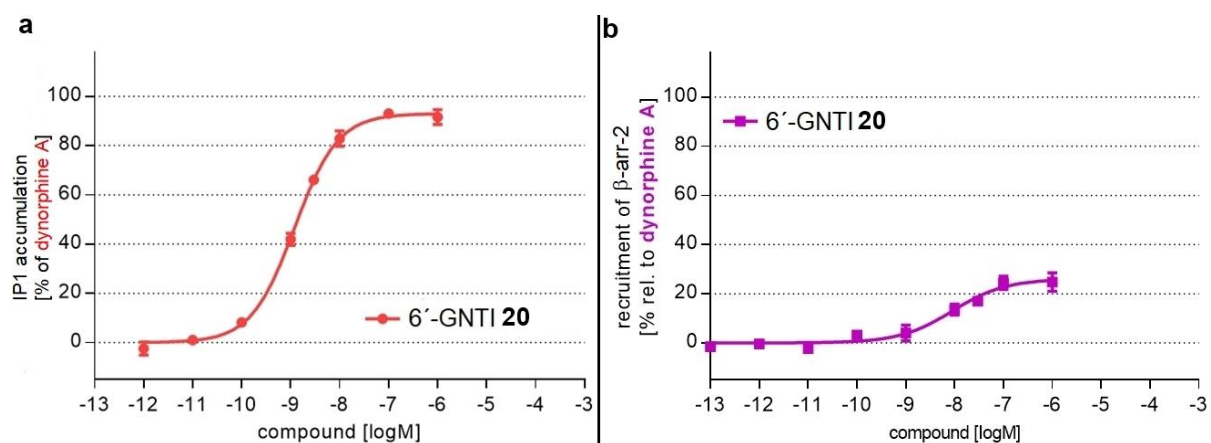


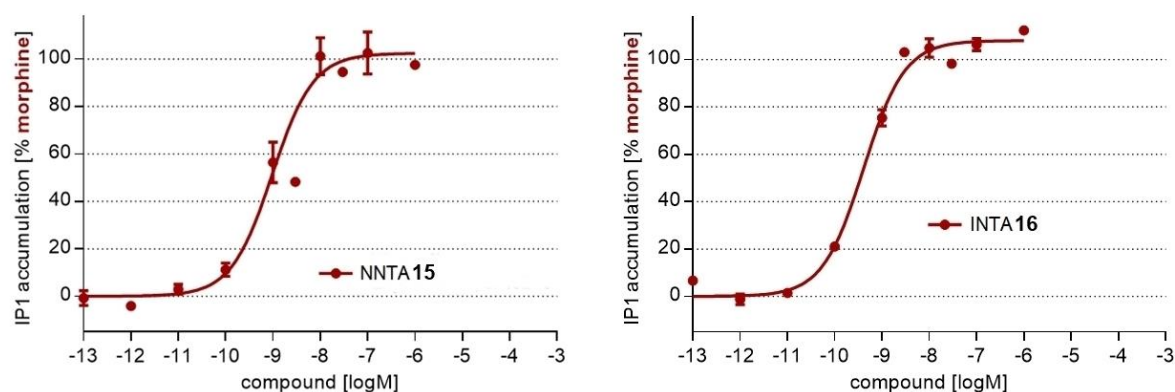
Fig. 20. Intrinsic activity of 6'-GNTI **20** on *hKOP*. **a)** IP₁ accumulation assay for G-protein mediated signaling. IP₁ accumulation in percentage of dynorphine A was plotted against the logarithmic ligand concentration (range from 0.1 pM up to 10 μ M). Data is presented as means \pm S.E.M. for duplicates of the respective experiments. **b)** β -arr-2 recruitment assay with compound **20**. Recruitment of β -arr-2 in percentage relative to dynorphine A was plotted against the logarithmic ligand concentration (range from 1 pM to 10 μ M).

via Ca^{2+} release on HEK-293 cells expressing epitope-tagged *mORs*. However, in this assay 6'-GNTI was most potent in cells co-expressing DOP/KOP and MOP/KOP, while its agonist activity was weaker in cells expressing individual KOPs.^[73] On the other hand, the presented results are also in agreement with a later study, which described 6'-GNTI as extremely G-protein biased KOP agonist, that lacks β -arr recruitment.^[74] The potency determined in a BRET-based assay for G-protein mediated signaling

1.5. Non-fluorescent Opioid Ligands selectively targeting Opioid Receptor Heterodimers

matches the data presented here (Fig. 20, $EC_{50} = 1.2 \text{ nM}$ vs. $1.6 \pm 1.3 \text{ nM}$).^[74] Additionally, a BRET-based assay measuring recruitment of β -arr-2 showed a comparable, minor effect of compound **20**.^[74] Interestingly, NNTA **15** and INTA **16** exhibited a very similar profile of functional activity, what could be expected due to their structural relationship. Importantly, both compounds acted as G-protein biased agonists on *hMOP* (Fig. 21). This result seems contradictory to the characterization of NNTA **15** as antagonist in cells expressing individual MOPs.^[77] However, in this study it was shown in a Ca^{2+} release assay, that compound **15** could antagonize the effect of the standard ligand DAMGO in HEK-293 cells stably expressing individual MOPs.^[77] DAMGO is known to produce robust recruitment of β -arr on *hMOP*, while NNTA did not show any effect in the respective assay (Fig. 21b). Moreover, the same study demonstrated that compound **15** was efficacious in two independent assays (Ca^{2+} release and [^{35}S]GTP γ S) for G-protein mediated signaling on HEK-293 cells and

a



b

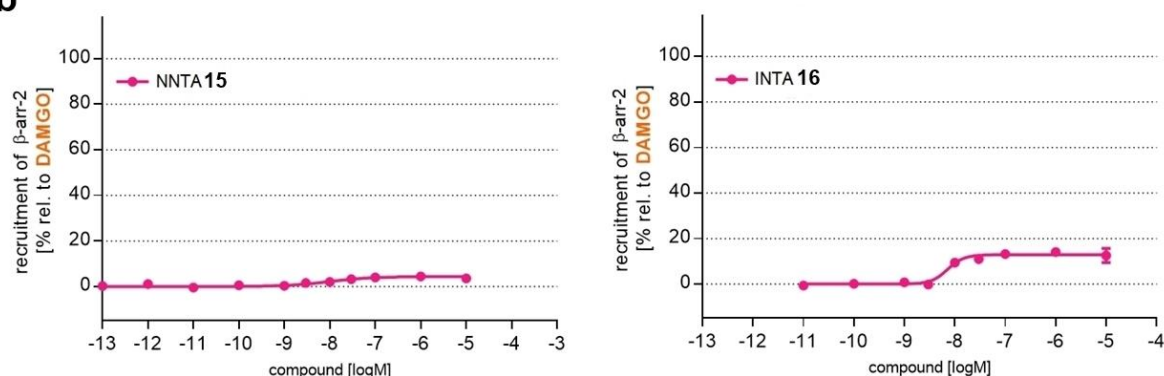


Fig. 21. Functional activity of NNTA **15** and INTA **16** on *hMOP*. **a**) IP₁ accumulation assay for G-protein mediated signaling. IP₁ accumulation in percentage of the maximum effect of morphine was plotted against the logarithmic ligand concentration of NNTA **15** and INTA **16** (range from 0.1 pM up to 10 μ M). Data is presented as means \pm S.E.M. for duplicates of the respective experiments. **b**) β -arr-2 recruitment assay with compound **15** and **16**. Recruitment of β -arr-2 in percentage relative to the maximum effect of DAMGO was plotted against the logarithmic ligand concentration of NNTA **15** and INTA **16** (range from 1 pM to 10 μ M).

1.5. Non-fluorescent Opioid Ligands selectively targeting Opioid Receptor Heterodimers

respective cell membranes stably expressing individual MOPs, even though its efficacy was way more pronounced at the co-transfected cell line expressing both MOPs and KOPs.^[77] INTA **16** exhibited a similar profile as NNTA **15** in the respective Ca²⁺ release assay, apart from its additional increased efficacy in cell lines co-expressing KOPs and DOPs.^[125] Like NNTA **15**, INTA **16** acted as agonist on all *hOR* subtypes (Fig. 21 and table 3) in the IP1 accumulation assay, which is consistent with the results from previous studies.^[77, 125] Considerable recruitment of β -arr-2 was only detectable on KOP and DOP (Fig. 21 and table 3), which seems partly contradictory to the results of a respective assay measuring fluorescence of the cell surface membrane after treatment of the respective cell lines with primary immunofluorescent β -arr-2 antibodies.^[125] All three cell lines expressing the individual OR subtypes were found to recruit β -arr-2 after treatment with compound **16**, even though the criterion “brightness of cell surface membrane” for positive β -arr-2 recruitment seems rather subjective and was not quantified. Nevertheless, the cell lines co-expressing MOP/KOP and especially DOP/KOP showed strongly reduced or abolished recruitment after treatment with INTA.^[125] Interestingly, NNTA **15** was used as control ligand for the MOP/KOP cells and 6'-GNTI **20** for the KOP/DOP pair in this study, leading to some visible recruitment of β -arr-2. Even though this is a rather opposing result to the studies with 6'-GNTI, that described the compound as a strongly G-protein biased KOP agonist devoid of β -arr-signaling,^[74, 130] this is in agreement with the results of the β -arr-2 recruitment assay on *hKOP*, where some minor efficacy was detected for both compounds **15** and **20** (Fig. 20 and table 3).

Table 3. Intrinsic activities of the three OR heterodimer-targeting ligands **15**, **16** and **20**. Shown are EC₅₀ values for IP1 accumulation and recruitment of β -arr-2 and the respective percental maximal effect relative to a standard ligand (MOP: Morphine for IP1, DAMGO for β -arr-2; KOP: Dynorphine A; DOP: Leu-enkephalin).

Compound	EC ₅₀ [nM] / % max. effect relative to morphine (IP1) or DAMGO (β -arr-2) (MOP)	EC ₅₀ [nM] / % max. effect relative to dynorphine A (KOP)	EC ₅₀ [nM] / % max. effect relative to Leu-enkephalin (DOP)
6'-GNTI 20	IP1: - / 20% at 1 μ M	IP1: 1.2 nM / 93%	IP1: 71 nM / 13%
	β -arr: - / <5%	β -arr: 9.1 nM / 26%	β -arr: - / 0%
NNTA 15	IP1: 0.96 nM / 102%	IP1: 0.22 nM / 101%	IP1: 9.5 nM / 98%
	β -arr: - / <5%	β -arr: 2.5 nM / 102%	β -arr: 98 nM / 40%
INTA 16	IP1: 0.41 nM / 108%	IP1: 0.12 nM / 101%	IP1: 2.9 nM / 96%
	β -arr: 7.2 nM / 13%	β -arr: 2.0 nM / 100%	β -arr: 26 nM / 79%

1.5. Non-fluorescent Opioid Ligands selectively targeting Opioid Receptor Heterodimers

Altogether, the three opioid agonists exhibited high binding affinities on *h*ORs, especially on the receptor protomers, which are part of the respective heterodimer on which they are described to bind to (cf. table 2). NNTA **15** and INTA **16** acted as agonists on all subtypes with subnanomolar EC₅₀ values for *h*MOP and *h*KOP and nanomolar affinities for *h*DOP. Consistent with the binding affinity data, the efficacy of **16** on *h*DOP was increased compared to NNTA **15** (cf. tables 2 and 3). Concerning the potential to recruit β -arr-2, 6'-GNTI **20** showed only a marginal effect on KOP, while NNTA **15** and INTA **16** exhibited non or very low β -arr-2 recruitment on MOP and their effects were more pronounced on *h*DOP and especially *h*KOP (cf. table 3). The binding properties and efficacies, in combination with their unique pharmacological profiles represent these ligands as interesting tool compounds to study heterodimerization of ORs via SMM. This approach could potentially enable new insights into the effect of agonists on heterodimerization. Moreover, the kind of controversial debate towards the influence of biased agonism and receptor oligomerization on the pharmacological output of OR agonists could gain new important results. This might be of peculiar interest, since all three ligands were described to produce significantly reduced or no side effects at all, when compared to opioid analgesics in clinical use.^[73-74, 77, 125, 130-131]

1.5.4. Experimental Procedures

Common reagents and methods for chemical synthesis

Common reagents and solvents were obtained from commercial suppliers (Sigma-Aldrich, Steinheim, Germany; Merck, Darmstadt, Germany) and were used without any further purification, unless stated otherwise. The thin layer chromatography (TLC) for controlling reaction progress was performed on precoated plates (Silica Gel 60 F254, Macherey-Nagel GmbH & Co. KG, Düren, Germany). The substances were either visualized by their fluorescence, when irradiated with UV-light (254 nm), by spray-reagents (Dragendorff's reagent, Ehrlich's reagent) or by their discoloration in an iodine chamber. Silica gels with grain sizes of 0.063 - 0.2 mm (Merck, Darmstadt, Germany) were used for manual column chromatography. The columns were packed wet. The composition of the eluents is indicated in percentage by volume.

NMR spectra were recorded at room temperature on a Bruker AV 400 FT-NMR Spectrometer (company Bruker Biospin, Karlsruhe, Germany) (¹H: 400 MHz, ¹³C: 100 MHz). The residual protons and the ¹³C-resonance signals of the deuterated solvents

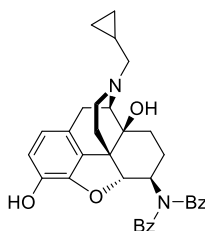
1.5. Non-fluorescent Opioid Ligands selectively targeting Opioid Receptor Heterodimers

were used as internal standards. The chemical shifts δ are indicated in [ppm] and the coupling constants in [Hz]. The signal multiplicities are abbreviated as follows: s = singlet, d = doublet, t = triplet, q = quartet, dd = doublet of doublets, m = multiplet.

Analytical HPLC was performed on a Shimadzu LC20AB system equipped with a DGU-20A3R controller, and a SPD-20A UV/Vis detector. The stationary phase was a Synergi 4u Fusion-RP (150×4.6 mm) column. A MeOH/water gradient + 0.1% formic acid (phase A/ phase B) was used as mobile phase. For analytical HPLC a flow rate of 1 mL/min was used. For semi-preparative HPLC, a Synergi 4u Fusion-RP 80A (250×10.0 mm) column was used as stationary phase and the flow rate was 2.5 mL/min.

ESI-MS spectral data were acquired on a Shimadzu LCMS-2020 single quadrupole LC/MS (Shimadzu Europe, Duisburg, Germany).

Synthesis of *N,N*-dibenzyl-6 β -naltrexamine (**13**)



500 mg (1.323 mmol, 1.00 eq) of Naltrexone hydrochloride (**12**) were dissolved in 20 mL of MeOH : H₂O (9 : 1) at room temperature while stirring and 318.1 mg (1.3892 mmol, 1.05 eq) of silver benzoate were added under light exclusion. This suspension was stirred for 90 min at 40°C, before it was passed through a filter. The filtrate solution was evaporated to dryness. The residue was dissolved in dry toluene and 159.1 μ L (163.2 mg, 0.827 mmol, 1.25 eq) of dibenzylamine, 101 mg (0.827 mmol, 1.25 eq) of benzoic acid and a trace of *p*-toluenesulfonic acid were given to the solution. The yellow suspension was refluxed for 20 h at 120 °C, using a Dean-Stark trap for azeotropic removal of water. After the reaction had completed, MeOH (LC/MS-grade) was given to the solution, until it became clear. Then 52.0 mg (0.827 mmol, 1.25 eq) of sodium cyanoborohydride were added and the suspension was stirred for 24 h at room temperature. After this reaction completed, it was passed through a filter and washed with methanol. The solvent was removed, and the residue was partitioned between chloroform and 3% ammoniac. The organic phase was washed with water and brine, then dried over sodium sulphate. Finally, the crude product was recrystallized from ethanol to yield a white solid.

1.5. Non-fluorescent Opioid Ligands selectively targeting Opioid Receptor Heterodimers

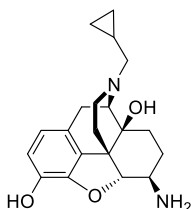
Yield: 278.5 mg, 0.53282 mmol, 40%.

$^1\text{H-NMR}$ (400 MHz, CDCl_3) δ [ppm]: 7.33 (d, $^3J = 7.3$ Hz, 4H, $\text{H}_{\text{ar, Bz}}$), 7.17 (t, $^3J = 7.4$ Hz, 4H, $\text{H}_{\text{ar, Bz}}$), 7.08 (t, $^3J = 7.2$ Hz, 2H, $\text{H}_{\text{ar, Bz}}$), 6.39 (dd, $J = 52.6, 8.1$ Hz, 2H, H_{ar}), 4.60 (d, $^3J = 7.8$ Hz, 1H, H-5), 3.78 (d, $^4J = 14.2$ Hz, 2H, CH_2, Bz), 3.50 (d, $^4J = 14.2$ Hz, 2H, CH_2, Bz), 2.88 (dd, $J = 28.7, 11.9$ Hz, 2H, CH_2), 2.52 - 2.36 (m, 3H, $\text{CH} + \text{CH}_2$), 2.27 - 2.19 (m, 2H, $\text{N-CH}_2, \text{cycloprop}$), 2.11 (td, $J = 12.3, 4.8$ Hz, 1H, CH), 2.01 - 1.86 (m, 2H, CH_2), 1.40 (dd, $J = 65.5, 11.9$ Hz, 2H, CH_2), 1.19 - 1.08 (m, 2H, CH_2), 0.77 - 0.66 (m, 1H, $\text{CH}_{\text{cycloprop}}$), 0.40 (d, $^3J = 7.1$ Hz, 2H, $\text{CH}_2, \text{cycloprop}$), -0.01 (d, $^3J = 4.3$ Hz, 2H, $\text{CH}_2, \text{cycloprop}$).

$^{13}\text{C-NMR}$ (100 MHz, CDCl_3) δ [ppm]: 142.52 (C_q), 140.53 (C_q), 139.42 (C_q), 131.85 (C_q), 128.64 (4x C_t, Bz), 128.19 (4x C_t, Bz), 126.95 (2x C_t, Bz), 124.79 (C_q), 118.55 (C_t, ar), 116.80 (C_t, ar), 92.38 ($\text{C}_t\text{-5}$), 70.54 (C_q), 62.65 (C_t), 59.76 (C_t), 59.34 (C_s), 54.56 (C_s), 47.89 (C_q), 44.13 (C_s), 30.97 (C_s), 30.60 (C_s), 22.79 (C_s), 18.24 (C_s), 9.59 ($\text{C}_t, \text{cycloprop}$), 3.98 (2x $\text{C}_s, \text{cycloprop}$).

ESI-MS: 262.20 m/z [$\text{M}+2\text{H}$] $^{2+}$, 523.15 m/z [$\text{M}+\text{H}$] $^+$, calculated 523.30 m/z (100%).

Synthesis of β -naltrexamine (**14**)



278.5 mg (533 μmol , 1.00 eq) of *N,N*-dibenzyl-6 β -naltrexamine (**13**) were dissolved in 14.2 mL of methanol at room temperature, while stirring. Then 112 μL (~1% v/v) of concentrated, aqueous hydrochloric acid were added, followed by 44.6 mg (16 wt-%) of palladium on activated charcoal (10% Pd), which was added carefully under argon

1.5. Non-fluorescent Opioid Ligands selectively targeting Opioid Receptor Heterodimers

protection. After that, the atmosphere was replaced by hydrogen gas using a balloon and the solution was hydrogenated for three days at 1 atm, until TLC indicated complete removal of both benzyl groups. Subsequently, the catalyst was filtered off with a pad of celite and the solvent was evaporated to yield β -naltrexamine dihydrochloride (**14**) as a white to beige solid, which was used without further purification.

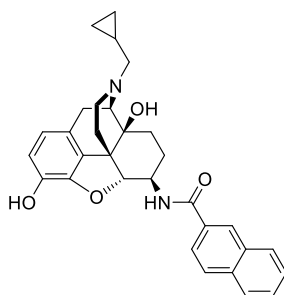
Yield: 193.9 mg, 467 μ mol, 88%.

$^1\text{H-NMR}$ (400 MHz, CDCl_3) δ [ppm]: 6.72 (dd, $J = 8.2, 2.2$ Hz, 2H, H_{ar}), 4.62 (d, $^3J = 7.6$ Hz, 1H, H-5), 3.35 - 3.26 (m, 2H, CH_2), 3.11 - 3.05 (m, 2H, CH_2), 2.97 - 2.84 (m, 2H, CH_2), 2.65 (s, 1H, CH), 2.61 - 2.56 (m, 2H, CH_2), 2.03 (tt, $J = 13.1, 6.7$ Hz, 1H), 1.81 (tt, $J = 9.3, 8.3$ Hz, 2H, CH_2), 1.58 - 1.46 (m, 2H, CH_2), 1.11 - 1.01 (m, 1H, $\text{CH}_{\text{cycloprop}}$), 0.78 - 0.63 (m, 2H, CH_2 , cycloprop), 0.45 (pd, $J = 9.2, 4.9$ Hz, 2H, CH_2 , cycloprop).

$^{13}\text{C-NMR}$ (100 MHz, CDCl_3) δ [ppm]: 143.12 (C_q), 143.04 (C_q), 130.28 (C_q), 122.34 (C_q), 121.71 ($\text{C}_{\text{t, ar}}$), 119.71 ($\text{C}_{\text{t, ar}}$), 90.13 ($\text{C}_{\text{t-5}}$), 71.10 (C_q), 63.85 (C_{t}), 58.90 (C_{s}), 54.40 (C_{t}), 47.94 (C_{s}), 47.70 (C_q), 30.54 (C_{s}), 28.90 (C_{s}), 24.40 (C_{s}), 22.96 (C_{s}), 7.09 ($\text{C}_{\text{t, cycloprop}}$), 6.08 (C_{s} , cycloprop), 3.54 (C_{s} , cycloprop).

ESI-MS: 343.15 m/z [$\text{M}+\text{H}$] $^+$, calculated 343.20 m/z (100%).

Synthesis of *N*-naphthoyl-6 β -naltrexamine (NNTA, **15**)



8.03 mg (46.6 μ mol, 1.05 eq) of 2-naphthoic acid were dissolved in 3 mL of dry THF under an argon atmosphere. Then 9.23 μ L (66.6 μ mol, 1.50 eq) of dry triethylamine

1.5. Non-fluorescent Opioid Ligands selectively targeting Opioid Receptor Heterodimers

were added to the solution, followed by 18.5 mg (48.8 μmol , 1.10 eq) of HBTU. Finally, 15.2 mg (44.4 μmol , 1.00 eq) of β -naltrexamine (**14**) were given to the reaction mixture, after everything had been dissolved and a slight color change indicated complete activation of the acid. After that, the reaction was stirred for 18 h at room temperature. After completion, the solvent was removed under reduced pressure and the crude product was purified by manual column chromatography (normal phase, eluent: CH_2Cl_2 : MeOH = 99 : 1) to yield NNTA **15** as white solid.

Yield: 9.7 mg, 19.5 μmol , 44%.

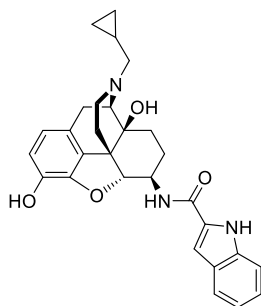
$^1\text{H-NMR}$ (400 MHz, D_3COD) δ [ppm]: 8.47 (s, 1H, CH_{naph}), 7.99 (dt, J = 16.0, 8.4 Hz, 4H, CH_{naph}), 7.66 - 7.60 (m, 2H, CH_{naph}), 6.81 (dd, J = 8.5, 1.4 Hz, 2H, H_{ar}), 4.92 (d, 3J = 7.9 Hz, 1H, H-5), 4.02 - 3.96 (m, 1H, CH-6), 3.28 - 3.25 (m, 1H), 3.22 - 3.15 (m, 2H), 2.96 (dd, J = 13.5, 7.6 Hz, 1H), 2.77 - 2.70 (m, 4H, 2x CH_2), 2.13 (td, J = 11.2, 1.7 Hz, 1H, CH-9), 1.86 - 1.84 (m, 2H, CH_2), 1.69 (t, J = 13.4 Hz, 2H, CH_2), 1.24 - 1.12 (m, 1H, $\text{CH}_{\text{cycloprop}}$), 0.82 - 0.75 (m, 2H, CH_2 , cycloprop), 0.62 - 0.52 (m, 2H, CH_2 , cycloprop).

$^{13}\text{C-NMR}$ (100 MHz, D_3COD) δ [ppm]: 170.10 (C_q), 143.84 (C_q), 143.06 (C_q), 136.33 (C_q), 134.04 (C_q), 132.77 (C_q), 130.82 (C_q), 130.06 ($\text{C}_{\text{t, naph}}$), 129.34 ($\text{C}_{\text{t, naph}}$), 128.93 ($\text{C}_{\text{t, naph}}$), 128.78 ($\text{C}_{\text{t, naph}}$), 127.89 ($\text{C}_{\text{t, naph}}$), 124.91 ($\text{C}_{\text{t, naph}}$), 121.88 (C_q), 120.97 ($\text{C}_{\text{t, ar}}$), 119.74 ($\text{C}_{\text{t, ar}}$), 92.06 ($\text{C}_{\text{t-5}}$), 71.43 (C_q -14), 64.35 ($\text{C}_{\text{t-6}}$), 64.31 (C_s), 58.75 (C_s), 53.29 (C_{t}), 48.34 (C_s), 47.67 (C_q), 35.37 (C_{t}), 31.19 (C_s), 28.95 (C_s), 24.77 (C_s), 24.48 (C_s), 6.87 ($\text{C}_{\text{t, cycloprop}}$), 6.18 (C_s , cycloprop), 3.41 (C_s , cycloprop).

ESI-MS: 497.15 m/z [$\text{M}+\text{H}$] $^+$, calculated 497.24 m/z (100%).

1.5. Non-fluorescent Opioid Ligands selectively targeting Opioid Receptor Heterodimers

Synthesis of N-2'-indolylnaltrexamine (INTA, **16**)



14.7 mg (91.1 μmol , 1.20 eq) of indole-2-carboxylic acid were dissolved in 2 mL of dry DMF at room temperature under an argon atmosphere and 38.7 μL (228 μmol , 3.00 eq) of DIPEA were added. Then 43.2 mg (114 μmol , 1.50 eq) of HBTU were given to the solution and 26 mg (75.9 μmol , 1.00 eq) of β -naltrexamine (**14**) were transferred to the reaction mixture in 1 mL of dry DMF, after everything was dissolved and a slight color change appeared. The reaction was subsequently stirred for 18 h at room temperature. After completion, an excess of ethyl acetate was added and the organic phase was washed with portions of aqueous, saturated sodium hydrogen carbonate solution, water and brine. After drying over sodium sulphate, the solvent was removed under reduced pressure and the crude residue was purified by manual column chromatography (normal phase, eluent: CH_2Cl_2 : MeOH + 0.1% NH_3 = 97 : 3 \rightarrow 96.5 : 3.5) to yield INTA **16** as a white solid.

Yield: 15.45 mg, 31.8 μmol , 42%.

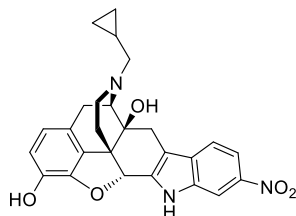
$^1\text{H-NMR}$ (400 MHz, D_3COD) δ [ppm]: 7.67 (d, $^3J = 8.0$ Hz, 1H, $\text{CH}_{\text{indole}}$), 7.50 (d, $^3J = 8.3$ Hz, 1H, $\text{CH}_{\text{indole}}$), 7.28 (t, $^3J = 7.6$ Hz, 1H, $\text{CH}_{\text{indole}}$), 7.20 (s, 1H, $\text{CH}_{\text{indole}}$), 7.13 (t, $^3J = 7.5$ Hz, 1H, $\text{CH}_{\text{indole}}$), 6.84 - 6.79 (m, 2H, CH_{ar}), 4.85 (s, 1H, H-5), 3.98 (d, $J = 5.4$ Hz, 1H, H-6), 3.42 (dd, $J = 13.2, 6.3$ Hz, 2H, CH_2), 3.24 (d, $J = 5.4$ Hz, 1H), 3.17 (dd, $J = 12.2, 8.1$ Hz, 1H), 2.94 (dd, $J = 13.5, 7.6$ Hz, 1H), 2.79 - 2.65 (m, 2H, CH_2), 2.13 (td, $J = 26.4, 12.1$ Hz, 1H), 1.87 - 1.77 (m, 2H, CH_2), 1.67 (t, $J = 12.2$ Hz, 3H, CH_2 + CH), 1.21 - 1.15 (m, 1H, $\text{CH}_{\text{cycloprop}}$), 0.91 - 0.76 (m, 2H, CH_2 , cycloprop), 0.62 - 0.52 (m, 2H, CH_2 , cycloprop).

1.5. Non-fluorescent Opioid Ligands selectively targeting Opioid Receptor Heterodimers

^{13}C -NMR (100 MHz, D_3COD) δ [ppm]: 163.91 (C_q), 143.77 (C_q), 142.95 (C_q), 138.30 (C_q), 132.08 (C_q), 130.76 (C_q), 128.96 (C_q), 125.16 (C_t), 122.81 (C_t), 121.92 (C_q), 121.23 (C_t), 121.00 (C_t), 119.73 (C_t), 113.09 (C_t), 104.50 (C_t), 92.09 (C_t), 71.37 (C_q), 64.35 (C_t), 58.74 (C_s), 52.71 (C_t), 48.26 (C_s), 47.62 (C_q), 31.10 (C_s), 28.94 (C_s), 24.90 (C_s), 24.38 (C_s), 6.82 (C_t , cycloprop), 6.14 (C_s , cycloprop), 3.36 (C_s , cycloprop).

ESI-MS: 486.15 m/z $[\text{M}+\text{H}]^+$, calculated 486.24 m/z (100%).

Synthesis of 6'-nitronaltrindole (**17**)



750 mg (1.99 mmol, 1.00 eq) of naltrexone hydrochloride (**12**) were dissolved in MeOH and 395 mg (2.08 mmol, 1.05 eq) of 3-nitrophenylhydrazine hydrochloride were added. This solution was stirred at room temperature for 24 h before the solvent was evaporated and the mixture was heated up to 115°C in 20 mL of concentrated hydrochloric acid for 90 min. Then the solution was cooled to 0°C and concentrated, aqueous sodium hydroxide was added, until the pH value was basic. The aqueous phase was extracted with five portions of a mixture of 25% EtOH in CH_2Cl_2 and the combined, organic phases were dried over sodium sulphate. After evaporation of the solvent, the crude product was purified by manual column chromatography (normal phase, eluent = CH_2Cl_2 : MeOH = 9.5 : 0.5 \rightarrow 9 : 1) to yield a yellow solid.

Yield: 881 mg, 1.92 mmol, 96%.

^1H -NMR (400 MHz, D_3COD) δ [ppm]: 0.16 - 0.26 (m, 2H, CH_2 , cycloprop), 0.52 - 0.64 (m, 2H, CH_2 , cycloprop), 0.85 - 1.00 (m, 1H, $\text{CH}_{\text{cycloprop}}$), 1.21 - 1.27 (m, 2H, CH_2 -15), 2.01 (s, 1H, $-\text{OH}_{\text{tert}}$), 2.56 (d, $^3J = 15.8$ Hz, 1H, H-8), 3.20 (d, $^3J = 18.8$ Hz, 1H, H-8), 2.31 - 3.09 (m, 6H, N- CH_2 , H-16, H-10), 5.60 (s, 1H, H-5), 6.58

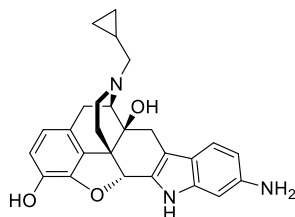
1.5. Non-fluorescent Opioid Ligands selectively targeting Opioid Receptor Heterodimers

- 6.64 (m, 2H, H-1 & H-2), 7.28 (d, $^3J = 8.8$ Hz, 1H, H-4'), 7.72 (dd, $^3J = 8.8$ Hz, $^4J = 2.0$ Hz, 1H, H-5'), 8.03 (d, $^4J = 1.9$ Hz, 1H, H-7').

^{13}C -NMR (100 MHz, D_3COD) δ [ppm]: 4.10 (C_s , cycloprop), 4.70 (C_s , cycloprop), 10.0 (C_t , cycloprop), 24.10 (C_s -10), 29.50 (C_s -8), 32.51 (C_s -15), 44.92 (C_s -16), 49.18 (C_q -13), 60.37 (N- C_s , cycloprop), 63.39 (C_t -9), 74.18 (C_q -14), 85.15 (C_t -5), 108.81 (C_t -7'), 112.23 (C_q -7), 114.90 (C_t -5'), 118.53 (C_t -4'), 119.34 (C_t -2), 120.32 (C_t -1), 126.20 (C_q -11), 131.85 (C_q -12), 132.30 (C_q -3'), 136.69 (C_q -6), 137.43 (C_q -3), 141.08 (C_q -2'), 144.34 (C_q -6'), 144.72 (C_q -4).

ESI-MS: 460.15 m/z [$\text{M}+\text{H}$] $^+$, calculated 460.19 m/z (100%).

Synthesis of 6'-aminonaltrindole (**18**)



138 mg (0.30 mmol, 1.00 eq) of 6'-nitronaltrindole (**17**) were dissolved in 36 mL of 10% aqueous acetic acid and 14.0 mg (~ 10 wt.-%) of palladium on activated charcoal (10% Pd) were added, while stirring under an argon atmosphere. The solution was hydrogenated at room temperature with a balloon for 24 h, then the catalyst was filtered off through a small pad of celite under suction. The filtrate was made alkaline by addition of 0.1 M aqueous sodium hydroxide and the basic phase was extracted with five portions of a mixture of 25% EtOH in CH_2Cl_2 . After drying over sodium sulphate, the solvents were removed under reduced pressure and the crude product was purified by manual column chromatography (normal phase, eluent = CH_2Cl_2 : MeOH = 9.5 : 0.5 + 0.1% NH_3) to yield a brown solid.

Yield: 110 mg, 256 μmol , 85%.

^1H -NMR (400 MHz, DMSO-d_6) δ [ppm]: 0.19 (brs, 2H, CH_2 , cycloprop), 0.48–0.57 (m, 2H, CH_2 , cycloprop), 0.82–0.89 (m, 1H, CH , cycloprop),

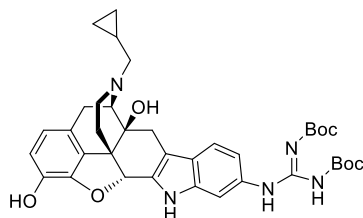
1.5. Non-fluorescent Opioid Ligands selectively targeting Opioid Receptor Heterodimers

5.44 (s, 1H, H-5), 6.32 (dd, $J_1 = 8.4$ Hz, $J_2 = 1.9$ Hz, 1H, H-5'), 6.49 (d, $^4J = 1.7$ Hz, 1H, H-7'), 6.50 (dd, $J_1 = 26.3$ Hz, $J_2 = 8.1$ Hz, 2H, H-1 / H-2), 6.98 (d, $^3J = 8.3$ Hz, 1H, H-4').

^{13}C -NMR (100 MHz, D_3COD) δ [ppm]: 3.88 (C_s , cycloprop), 4.31 (C_s , cycloprop), 9.58 (C_t , cycloprop), 23.45 (C_s -10), 29.11 (C_s -8), 31.75 (C_s -15), 44.14 (C_s -16), 48.13 (C_q -13), 59.74 (N-C_s , cycloprop), 62.62 (C_t -9), 73.42 (C_q -14), 85.61 (C_t -5), 98.03 (C_t -7'), 110.68 (C_t -5'), 110.90 (C_q -7), 117.35 (C_t -2), 118.96 (C_t -4'), 119.60 (C_t -1), 121.19 (C_q -3'), 124.91 (C_q -11), 127.85 (C_q -6), 131.24 (C_q -12), 139.00 (C_q -2'), 139.95 (C_q -3), 142.24 (C_q -4), 143.65 (C_q -6').

ESI-MS: 430.20 m/z [$\text{M}+\text{H}$] $^+$, calculated 430.21 m/z (100%).

Synthesis of *N,N'*-bis-Boc-6'-guanidinonaltrindole (**19**)



30 mg (69.9 μmol , 1.00 eq) of 6'-aminonaltrindole (**18**) were dissolved in 2 mL of DMF at room temperature and 30 mg (109 μmol , 1.55 eq) of *N,N'*-di-Boc-thiourea (**22**) were added to the solution, before it was cooled down to 0°C. Then 18.6 μL (231 μmol , 3.30 eq) of pyridine were added, followed by 21 mg (76.8 μmol , 1.10 eq) of mercury(II)chloride. The reaction mixture was allowed to warm up to room temperature and stirred for 20 h. After completion, an excess of ethyl acetate was added and the solution was filtered. The filtrate solution was washed with water and brine and the organic phase was dried over sodium sulphate. After removal of the solvent under reduced pressure, the crude product was purified by manual column chromatography (normal phase, eluent = CH_2Cl_2 : MeOH = 9.5 : 0.5 \rightarrow 9 : 1) to yield the product as beige solid.

Yield: 27.7 mg, 41.2 μmol , 59%.

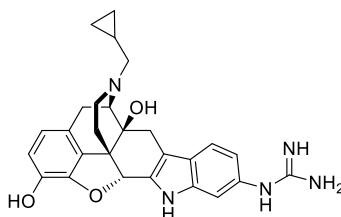
1.5. Non-fluorescent Opioid Ligands selectively targeting Opioid Receptor Heterodimers

$^1\text{H-NMR}$ (400 MHz, D_3COD) δ [ppm]: 7.77 (s, 1H, $\text{CH}_{\text{indole}}$), 7.34 (d, $^3J = 8.4$ Hz, 1H, $\text{CH}_{\text{indole}}$), 6.95 (dd, $^3J_1 = 8.4$, $^4J_2 = 1.6$ Hz, 1H, $\text{CH}_{\text{indole}}$), 6.63 - 6.58 (m, 2H, CH_{ar}), 5.62 (s, 1H, H-5), 3.67 - 3.54 (m, 2H, CH_2) 3.38 (s, 15H, CH_3, Boc), 3.24 (d, $J = 18.8$ Hz, 1H), 2.96 (dd, $J = 18.8$, 6.2 Hz, 1H), 2.87 (d, $J = 4.8$ Hz, 1H), 2.82 (s, 2H, CH_2), 2.63 (d, $J = 15.9$ Hz, 3H), 2.43 (d, $J = 7.4$ Hz, 2H), 1.76 (d, $J = 9.6$ Hz, 2H, CH_2), 1.05 - 0.95 (m, 1H, $\text{CH}_{\text{cycloprop}}$), 0.71 - 0.58 (m, 2H, $\text{CH}_2, \text{cycloprop}$), 0.29 (d, $J = 4.1$ Hz, 2H, $\text{CH}_2, \text{cycloprop}$).

$^{13}\text{C-NMR}$ (100 MHz, D_3COD) δ [ppm]: 217.52 (C_q), 180.18 (C_q), 144.73 (C_q), 138.66 (C_q), 131.58 (C_q), 125.86 (C_q), 119.95 (C_t, ar), 119.68 (C_t, ar), 118.53 (C_t, ar), 115.98 (C_t, ar), 107.36 (C_t, ar), 85.80 ($\text{C}_t\text{-5}$), 74.21 (C_q), 72.60 (C_q), 63.57 ($\text{C}_t\text{-9}$), 60.89 (C_q), 60.08 ($\text{N-C}_s, \text{cycloprop}$), 49.85 (C_p, Boc), 45.50 (C_s), 31.95 (C_s), 30.73 (C_s), 29.87 (C_s), 28.38 (C_p, Boc), 24.27 (C_s), 9.44 ($\text{C}_t, \text{cycloprop}$), 4.99 ($\text{C}_s, \text{cycloprop}$), 3.93 ($\text{C}_s, \text{cycloprop}$).

ESI-MS: 672.25 m/z $[\text{M}+\text{H}]^+$, 336.75 $[\text{M}+2\text{H}]^{2+}$, calculated 672.34 m/z (100%).

Synthesis of 6'-guanidinonaltrindole (6'-GNTI, **20**)



20.3 mg (30.2 μmol , 1.00 eq) of *N,N'*-bis-Boc-6'-guanidinonaltrindole (**19**) were dissolved in 3 mL of dichloromethane at room temperature, while stirring. Then 0.5 mL of trifluoroacetic acid were added carefully and an immediate color change from orange to brown appeared. The solution was stirred for 18 h at room temperature. After completion, the solvent was evaporated under reduced pressure. The crude residue was directly purified by flash chromatography on a reversed phase column (eluent:

1.5. Non-fluorescent Opioid Ligands selectively targeting Opioid Receptor Heterodimers

MeOH : H₂O + 0.1% formic acid) to obtain the pure product as its twofold trifluoroacetate salt.

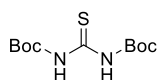
Yield: 20.59 mg, 43.7 μmol, 97%.

¹H-NMR (400 MHz, D₃COD) δ [ppm]: 7.57 (d, ³J = 8.3 Hz, 1H, H_{ar, indole}), 7.38 (s, 1H, H-7'), 6.97 (d, ³J = 8.0 Hz, 1H, H_{ar, indole}), 6.74 (q, ³J = 8.2 Hz, 2H, H-1, H-2), 5.81 (s, 1H, H-5), 3.54 - 3.40 (m, 4H, 2x CH₂), 3.29 (dd, J = 12.8, 3.1 Hz, 1H), 3.09 (d, J = 16.1 Hz, 2H, CH₂), 3.04 - 2.97 (m, 1H), 2.84 (dd, J = 13.5, 4.5 Hz, 1H), 2.77 (d, J = 16.3 Hz, 1H), 2.02 (d, J = 12.6 Hz, 1H), 1.27 - 1.18 (m, 1H, CH_{cycloprop}), 0.89 (ddd, J = 17.3, 12.6, 8.3 Hz, 2H, CH_{2, cycloprop}), 0.61 (d, J = 4.3 Hz, 2H, CH_{2, cycloprop}).

¹³C-NMR (100 MHz, DMSO-d₆) δ [ppm]: 156.80 (C_q), 143.04 (C_q), 139.94 (C_q), 136.88 (C_q), 130.91 (C_q), 130.80 (C_q), 129.54 (C_q), 125.05 (C_q), 119.31 (C_t), 118.42 (C_t), 116.94 (C_t), 116.66 (C_t), 109.99 (C_q), 108.65 (C_t), 83.68 (C_{t-5}), 72.11 (C_{q-14}), 61.57 (C_{t-9}), 58.44 (N-C_{s, cycloprop}), 47.13 (C_{q-13}), 45.39 (C_s), 43.58 (C_s), 28.72 (C_s), 22.78 (C_s), 9.03 (C_{t, cycloprop}), 4.00 (C_{s, cycloprop}), 3.38 (C_{s, cycloprop}).

ESI-MS: 472.30 m/z [M+H]⁺, 236.60 [M+2H]²⁺, calculated 472.23 m/z (100%).

Synthesis of N,N'-Di-Boc-thiourea (**22**)



50.0 mg (657 μmol, 1.00 eq) of thiourea (**21**) were dissolved in dry THF at room temperature. This solution was cooled to 0°C, before 71.0 mg (2.96 mmol, 4.50 eq) of sodium hydride were added. The solution was allowed to warm up to room temperature and stirred for 10 min. After that, it was cooled to 0°C again and 315.4 mg (1.45 mmol, 2.20 eq) of di-*tert*-butyl dicarbonate (Boc₂O) were given to the solution. Then the reaction mixture was stirred for 2 h at room temperature, before aqueous, saturated

1.5. Non-fluorescent Opioid Ligands selectively targeting Opioid Receptor Heterodimers

sodium hydrogen carbonate was added. The solution was poured into water, before it was extracted with three portions of ethyl acetate. The combined organic layers were dried over magnesium sulphate. Finally, the solvent was evaporated to yield a white solid, which was pure enough to be used without further purification.

Yield: 131.4 mg, 475 μ mol, 72%.

$^1\text{H-NMR}$ (400 MHz, acetone- d_6) δ [ppm]: 1.51 (s, 18H, CH_3 , Boc),
10.80 (brs, 1H, -NH-).

$^{13}\text{C-NMR}$ (100 MHz, acetone- d_6) δ [ppm]: 28.09 (C_p , Boc), 83.67 (C_q , Boc), 151.58 (C=O),
179.01 (C=S).

Binding affinity (radioligand binding studies)

Binding affinities towards *hDOP*, *hKOP* and *hMOP* were determined as follows: Membranes were prepared from HEK293T cells each transiently transfected with the cDNAs for DOP, KOP (both cDNAs obtained from the cDNA resource center, www.cdna.org) and MOP, respectively (generous gift from the Ernest Gallo Clinic and Research Center, UCSF, CA). Receptor densities (B_{max} value) and specific binding affinities (K_D value) for the radioligand [^3H]diprenorphine (specific activity 31 Ci/mmol, PerkinElmer, Rodgau, Germany) were determined to be 1,700 fmol/mg protein, 0.25 nM for DOP, 6,500 fmol/mg protein, 0.13 nM for KOP, and 1,400 \pm 780 fmol/mg protein, 0.078 \pm 0.002 nM for MOP, respectively. Competition binding experiments were performed by incubating membranes in binding buffer (50 mM Tris, 5 mM MgCl_2 , 0.1 mM EDTA, 5 $\mu\text{g/mL}$ bacitracin and 5 $\mu\text{g/mL}$ soybean trypsin inhibitor at pH 7.4) at a final protein concentration of 2-14 $\mu\text{g/well}$, together with the radioligand (final concentration 0.3 nM for DOP, KOP, 0.2-0.3 nM for MOP) and varying concentrations of the competing ligands for 60 minutes at 37°C. Non-specific binding was determined in the presence of naloxone at a final concentration of 10 μM . The protein concentration was established using the method of Lowry.^[132] The resulting competition curves were analyzed by nonlinear regression using the algorithms implemented in PRISM 6.0 (GraphPad Software, San Diego, CA) to provide an IC_{50} value, which was subsequently transformed into the K_i value employing the equation of Cheng and Prusoff.^[133]

1.5. Non-fluorescent Opioid Ligands selectively targeting Opioid Receptor Heterodimers

Intrinsic activity

Accumulation of inositol monophosphate (IP1): Determination of the activation of MOP, KOP and DOP was measured applying the IP-One HTRF® assay (Cisbio, Codolet, France) according to the manufacturer's protocol. HEK-293T cells were grown to a confluence of approx. 70% and transiently co-transfected with the cDNA of the human DOP, KOP (both from the cDNA Resource Center, Bloomsberg, PA) or MOP (gift from Ernest Gallo Clinic and Research Center, UCSF, CA) and of the hybrid G-protein $G_{\alpha_{qi}}$ (G_{α_q} protein with the last five amino acids at the C-terminus replaced by the corresponding sequence of G_{α_i} ; gift from The J. David Gladstone Institutes, San Francisco, CA) applying the Mirus TransIT-293 transfection reagent (PepLab, Erlangen, Germany). After one day cells were detached from the culture dish with Versene (Life Technologies, Darmstadt, Germany), seeded into black 384-well plates (10000 cells/well) (Greiner Bio-One, Frickenhausen, Germany) and maintained for 24 h at 37°C. Agonist properties were determined by incubating the test compounds (final range of concentration from 0.1 pM up to 10 µM) in duplicates for 180 min at 37°C. Incubation was stopped by addition of the detection reagents (IP1-d2 conjugate and Anti-IP1 cryptate TB conjugate each dissolved in lysis buffer) for further 60 min at room temperature. Homogenous time resolved fluorescence resonance energy transfer (HTRF) was measured using the Clariostar plate reader (BMG, Ortenberg, Germany). Data analysis was performed by nonlinear regression using the algorithms for log(agonist) vs. response of PRISM 6.0 (GraphPad, San Diego, CA) and normalization of the raw data to basal (0%) and the maximum effect of morphine (MOP), Leu-enkephalin (DOP), or dynorphin A (KOP) (100%).

Recruitment of β -arr-2: Measurement of β -arr-2 recruitment was done applying the PathHunter® assay (DiscoverX, Birmingham, U.K.) according to the manufacturer's protocol. HEK-293 cells stably expressing the enzyme acceptor (EA) tagged β -arr-2 fusion protein were transiently transfected with the ProLink tagged MOP-PK1, DOP-PK2, or KOP-PK2 construct, respectively, employing the Mirus TransIT-293 transfection reagent. After 24 h cells were transferred into white clear bottom 384-well plates (5000 cells/well) (Greiner Bio-One) and maintained for further 24 h at 37°C, 5% CO₂. To start receptor stimulated β -arr-2 recruitment, the test compounds were added to the cells to get a final concentration in a range of 1 pM to 10 µM. Incubation was continued for 90 min (MOP-PK1, DOP-PK2) or 300 min (KOP-PK2) at 37°C.

1.5. Non-fluorescent Opioid Ligands selectively targeting Opioid Receptor Heterodimers

Stimulation was stopped by addition of the detection mix and further incubation for 60 min at room temperature. Chemiluminescence was determined using a Clariostar plate reader. Data analysis was done by nonlinear regression using the algorithms for log(agonist) vs. response of PRISM 6.0 (GraphPad, San Diego, CA) and normalization of the raw data to basal (0%) and the maximum effect of DAMGO (MOP-PK1), Leu-enkephalin (DOP-PK2), or dynorphin A (KOP-PK2) (100%).

2. Imaging of Butyrylcholinesterase Activity by Positron Emission Tomography with ^{18}F -Radiotracers

The enzyme butyrylcholinesterase (BChE) is a serine hydrolase and an isoenzyme of acetylcholinesterase (AChE). While AChE specifically catalyzes the hydrolysis of acetylcholine, BChE exhibits a broader acceptance of substrates and hydrolyzes also non-choline esters, e.g. cocaine, heroin or acetylsalicylic acid.^[134-137] After its discovery in 1932, BChE gained interest in the field of anesthesia, since it essentially regulates the degradation of the muscle relaxants succinylcholine and mivacurium. Consequently, patients with BChE variants of reduced or missing catalytic activity got into critical apnea after administration.^[138] Moreover, BChE contributes to the scavenging of toxic parasymphomimetics such as organophosphates or naturally occurring alkaloids like physostigmine.^[134]

The catalytic activity of *h*BChE basically results from three amino acids, called the catalytic triad, which are serine 226, glutamic acid 353 and histidine 466.^[139] This sequence is positioned in an active site-gorge, which additionally contains an anionic site composed of tryptophan 82, that interacts with the positively charged, quaternary nitrogen of choline.^[140] Moreover, the active site is equipped with an acyl binding pocket composed of lysine 286 and valine 288, which directs the acyl group of choline esters in the right position for efficient catalysis.^[140] Interestingly, the side chains of these amino acids are sterically less demanding than the respective phenylalanine-comprised acyl binding pocket of AChE. Thus, the decreased substrate specificity of BChE can be explained.^[134]

The distribution of BChE in various human tissues is significantly different to AChE, which can be found predominantly in the nervous system and in muscles, obviously due to its main task of regulating cholinergic neurotransmission. While BChE is present there in minor levels, too, it also occurs in the liver, from where it is secreted into blood plasma.^[141] Additionally, high levels of BChE can be found in heart and lung, which was revealed by Northern blot analysis of *h*BChE mRNA in different tissues. This distribution of BChE in combination with its ability to hydrolyze and deactivate a broad variety of ester or carbamate based substrates led to the suggestion, that the enzyme serves as a first wall of defense against potentially harmful xenobiotics.^[142] Notably,

2. Imaging of Butyrylcholinesterase Activity by Positron Emission Tomography with ¹⁸F-Radiotracers

there are healthy humans exhibiting catalytically inactive (“silent”) forms of BChE. This has raised a debate about the physiological role and importance of the enzyme.^[134, 143] Under certain conditions BChE can serve as surrogate of AChE in the central nervous system (CNS) and at neuromuscular junctions, which was demonstrated by studies with AChE knock-out mice.^[144-146] Additionally, there is growing evidence that BChE might contribute in some areas of the development of the nervous system.^[147-149] This finding is further supported by structural accordances of the ChEs with cell adhesion molecules, suggesting a potential non-catalytic function.^[150]

Importantly, expression levels and activity of BChE were found to be altered in the process of several pathologies of neurodegenerative, oncologic, cardiovascular and other diseases.^[151] In Alzheimer’s disease (AD), BChE expression is elevated along with amyloid- β (A β) plaques in the cerebral cortex.^[152-153] These A β plaques can impair neurovascular homeostasis by causing endothelial dysfunction,^[154] however, on the other hand A β deposits are also found in up to 30% of aged adults with no symptoms of dementia.^[155] Additionally, investigations of a BChE knock-out mouse model of AD revealed considerably fewer fibrillar A β plaques.^[152, 156] Consequently, these results raised interest in the applicability of BChE activity as diagnostic biomarker for AD. Moreover, both ChEs contribute to cellular proliferation and differentiation, which suggests a potential influence on tumorigenesis.^[148, 157-158] Indeed, certain variants of cancer exhibit a down- and/or upregulation of BChE activity and expression levels.^[151] Notably, a distinctive decrease of BChE expression was observed in large-cell- and squamous-cell lung carcinoma.^[159] Moreover, advanced cancer patients have decreased plasma BChE levels, which seems to be independent of hepatic involvement. Interestingly, most strongly decreased BChE activities were found in patients with liver metastases, despite otherwise unremarkable liver function tests.^[151, 160-161] Thus, it seems promising to employ BChE activity values and levels in prognosis, diagnosis and disease monitoring of the mentioned cancer types. Concerning cardiovascular pathologies, low BChE activities were evaluated for their prognostic value of mortality in acute myocardial infarction and interestingly, the predictive value seemed to be associated to the relationship of low enzyme activity with poor cardiac function.^[162]

Due to this variety of BChE involvements in different pathologic conditions and diseases, tracers for positron emission tomography were developed, however, most of them with the aim to target the enzyme in the CNS and thus, to enable diagnosis or

2. Imaging of Butyrylcholinesterase Activity by Positron Emission Tomography with ^{18}F -Radiotracers

disease monitoring of neurodegenerative diseases like AD. PET is an imaging technique enabling to determine the spatial and temporal distribution of an injected, radiolabeled compound with high sensitivity.^[163] Therefore, the compound requires a positron-emitting radionuclide, since PET detects high energy photons emitted into opposite directions upon positron annihilation, therefore enabling the localization of the event by coincident detection.^[163] A PET tracer targeting BChE can be designed as substrate or inhibitor of the enzyme, while the latter can be further categorized into reversibly or irreversibly acting compounds. Notably, substrates usually have high rates of hydrolysis, which can be disadvantageous due to poor delivery into the desired tissue.^[164] Consequently, the PET results rather represent the plasma delivery rate of the tracer than the tissue enzyme distribution in this case.^[165] On the other hand, substrate-based PET tracers are usually blood-brain barrier (BBB) permeable, which is essential for a BChE PET tracer in CNS imaging. Concerning inhibitor based BChE PET tracers, a common problem is a complex mechanism of enzyme inactivation, which hampers the precise determination of *in vivo* kinetics and biodistribution.^[164, 166] Examples of literature-known substrate-type BChE PET tracers include 1- ^{11}C -Methyl-4-piperidiny *n*-butyrate (^{11}C -MP4B), *N*- ^{18}F fluoroethylpiperidin-4-ylmethyl butyrate and *N*-methylpiperidin-4-yl 4- ^{123}I iodobenzoate (^{123}I MP4Bz) (Fig. 22).^[167-169]

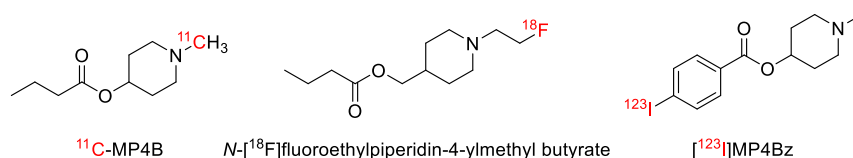


Fig. 22. Substrate-based, specific radiotracers for *h*BChE, labeled with different radionuclides for PET (in red).

Expectedly, ^{11}C -MP4B exhibited quick hydrolysis rates, followed by fast excretion through the renal system, but the tracer was able to enter the brain. However, brain uptake was highest in regions beyond cortical areas, where BChE associated $\text{A}\beta$ plaques develop during AD.^[168] *N*- ^{18}F fluoroethylpiperidin-4-ylmethyl butyrate represents an optimized derivative of ^{11}C -MP4B concerning hydrolysis rates, specificity for BChE and the chosen radionuclide. However, the *in vivo* characterization in this study was preliminary and the hydrolysis rates were still elevated.^[169] Thus, further studies would be required to evaluate the tracer as diagnostic tool in neurodegenerative diseases. Notably, the substrate-based tracer ^{123}I MP4Bz demonstrated slow and specific hydrolysis by BChE and could enter the brain, which indicated good BBB permeability. Interestingly, brain retention was significantly more

2. Imaging of Butyrylcholinesterase Activity by Positron Emission Tomography with ^{18}F -Radiotracers

pronounced in an AD mouse model (5XFAD) than in its wild-type counterpart, especially in the cerebral cortex, as indicated by single photon emission computed tomography (SPECT) studies.^[167] Thus, evidence for the potential diagnostic value of BChE in AD was provided.

Concerning inhibitor-based radiotracers for labeling of ChEs, it must be mentioned beforehand, that real irreversible inhibition of ChEs is often accompanied by high toxicity. Prominent examples are organophosphates and some of them were even developed as nerve agents for war purposes (e.g. “G-series” of nerve agents: Tabun, soman, sarin, GV, cyclosarin). Nevertheless, an organophosphate-based ^{18}F -labeled PET tracer was investigated to gain deeper insights into temporal *in vivo* mechanisms of actions of this class of compounds.^[170] Better candidates for clinically applicable PET tracers are carbamate-based ChE inhibitors, particularly because of their “pseudo-irreversible” binding mode. This means the enzyme is only inhibited transiently by covalent bond formation with the catalytically active serine 226.^[171] The resulting functional group after reaction with this serine is a new enzyme-bound carbamate, which is hydrolyzing over time and enzyme activity is subsequently regenerated. An example of such a tracer is phenyl 4- ^{123}I -iodophenylcarbamate (^{123}I -PIP, Fig. 23), which was used in autoradiographic studies on human brain tissue.^[172] Indeed, accumulation of radioactivity occurred in AD brain tissue, where $\text{A}\beta$ plaques had ChE activity.^[172] On the other hand, this tracer is not selective for BChE and was not investigated *in vivo*. An example of a selective and highly affine pseudo-irreversible BChE inhibitor as PET tracer was based on a tetracyclic carbamate (Fig. 23).^[164] This compound was labeled at the carbamate site either with ^{11}C or ^{18}F to achieve transient covalent labeling of the enzyme, when the radioactive moiety is transferred by reaction with serine 226.^[173-174]

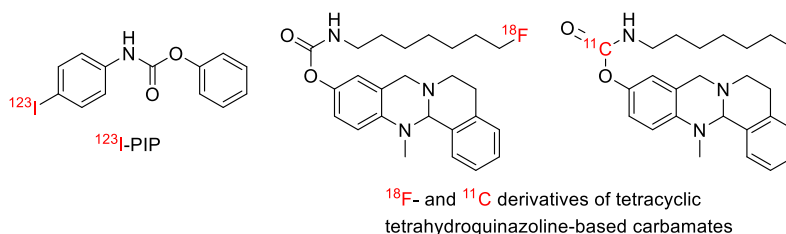


Fig. 23. Carbamate-based PET tracers for ChE imaging: Non-selective inhibitor ^{123}I -PIP (left)^[172] and selective BChE inhibitors based on tetrahydroquinazoline (middle, right).^[164]

Concerning reversible BChE inhibitors as PET tracers, it must be noted that the few literature described compounds published at that date were not selective for BChE and

designed as AChE PET tracers, respectively (e.g. [^{11}C]galantamine, [^{11}C]donepezil, [^{11}C]tacrine).^[175-177] However, a recent study used an ^{11}C -labeled radiotracer based on a potent and selective sulfonamide-type BChE inhibitor with reversible binding mode.^[178] This inhibitor also represented the scaffold of an ^{18}F -labeled derivative in a previous study, which is part of this thesis (cf. chapter 2.1.).^[179] The respective ^{11}C -labeled tracer was assessed as early *in vivo* biomarker in a mouse model of AD. BBB permeability was confirmed by dynamic whole-body PET imaging studies. Biodistribution data revealed fast clearance of radioactivity from the blood and accumulation of radioactivity in liver and kidneys, followed by an increase in the bladder. Importantly, significantly higher initial brain uptake of the tracer was observed in the AD mouse model as compared to the wild-type counterpart. Moreover, longitudinal, dynamic PET imaging studies demonstrated an increased uptake of the tracer in AD mice, when compared to wild-type counterparts, but only after late time points (6-8 months). No differences were detected at the age of 4 months and interestingly, differences disappeared again after 10 and 12 months, which was however partly contradictory to *ex vivo* staining results. Despite some drawbacks, like the quick appearance of some metabolites and a rapid wash-out from the brain, the results with this tracer mostly confirmed BChE as a promising biomarker in AD.^[178]

2.1. Synthesis and Initial Characterization of a Reversible, Selective ^{18}F -Labeled Radiotracer for Human Butyrylcholinesterase (published research work)^[179]

The content of this chapter has been published^[179] (Gentzsch, C.; Chen, X.; Spatz, P.; Kořak, U.; Knez, D.; Nose, N.; Gobec, S.; Higuchi, T.; Decker, M. Synthesis and Initial Characterization of a Reversible, Selective ^{18}F -Labeled Radiotracer for Human Butyrylcholinesterase. *Mol. Imaging Biol.* **2021**, <https://doi.org/10.1007/s11307-021-01584-2>.) and is adapted with permission from the respective authors.

Author contributions:

- C. Gentzsch performed synthesis and analytical characterization of the precursor for ^{18}F -labeling and the respective non-radioactive BChE inhibitor under the supervision of M. Decker
- U. Kořak and D. Knez (working group of S. Gobec) provided a synthetic building block, contributed with ideas regarding the tracer design and performed assays to

2.1. Synthesis and Initial Characterization of a Reversible, Selective ^{18}F -Labeled Radiotracer for Human Butyrylcholinesterase

characterize binding kinetics and inhibitory potency. P. Spatz performed additional assays to characterize inhibitory potency (Ellman's assay) under the supervision of M. Decker

- X. Chen (working group of T. Higuchi) performed radiolabeling and *ex vivo* / *in vivo* studies with the help of N. Nose

2.1.1. Aim of the Study

The objective of the presented work was to design and synthesize a reversible inhibitor of *h*BChE for evaluation as PET tracer after ^{18}F -labeling. The compound should have high inhibitory potency as well as pronounced selectivity over *h*AChE to enable a preferable precise *in vivo* mapping of the target enzyme. Further requirements on the compound were a lipophilic character and low molecular weight (<500 g/mol) to potentially enable PET imaging of BChE in the human brain, if the compound exhibited BBB permeability. Quick and uncomplicated radiolabeling in preferably few steps should be enabled by a suitable tosylate precursor for labeling with ^{18}F , which is a common radionuclide for PET studies due to advantageous properties (e.g. long half-life, high positron yields, low positron energies). Finally, the radiotracer should be investigated in *ex vivo* autoradiography and *in vivo* microPET studies to initially evaluate its properties as PET tracer and its suitability to monitor BChE activity.

2.1.2. Design and Synthesis

The design of the radiotracer was based on a novel, reversible sulfonamide-type BChE inhibitor, which exhibited promising characteristics for PET tracer development in previous studies (Fig. 24).^[180] These include high inhibitory potency ($\text{IC}_{50} = 4.9 \pm 0.3$ nM) in combination with excellent selectivity over *h*AChE (percental residual activity at $10 \mu\text{M} = 97\% \pm 2\%$).^[180] Moreover, pharmacokinetics of the relatively small and lipophilic compound had been investigated. Interestingly, an *in vitro* assay on Caco-2 cells expressing membrane transport proteins like P-glycoprotein or breast cancer

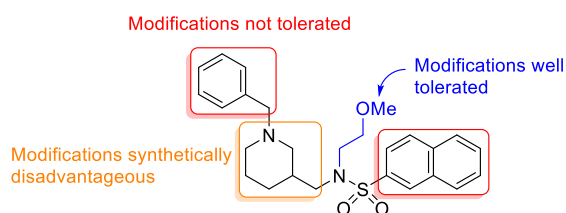


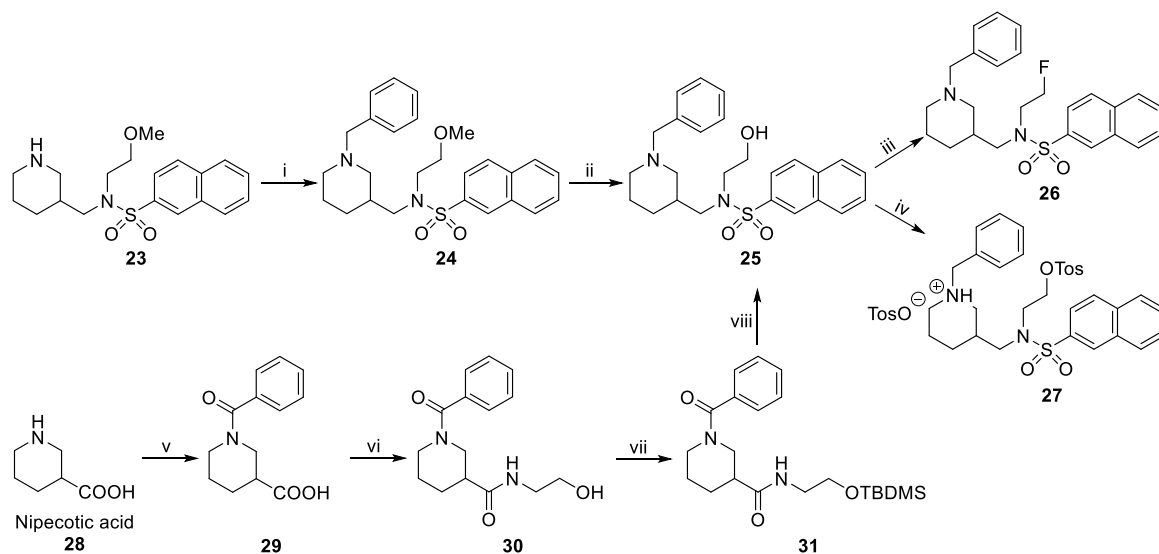
Fig. 24. Structure and SARs of the potent, selective sulfonamide-based *h*BChE inhibitor, which served as template for PET tracer design.

2.1. Synthesis and Initial Characterization of a Reversible, Selective ¹⁸F-Labeled Radiotracer for Human Butyrylcholinesterase

resistance protein demonstrated that the compound is not a substrate of active efflux mechanisms.^[180] However, incubation of human blood plasma with the inhibitor and subsequent equilibrium dialysis showed high plasma protein binding (96%).^[180] The compound was degraded in plasma with a half-life $t_{1/2} > 120$ min, while hepatic clearance happened faster ($t_{1/2} = 54$ min).^[180] Importantly, *in vivo* measurements of the compound's distribution between blood plasma and brain indicated a modest, but existing BBB permeability.^[180] Favorably, the described structure-activity relationships (SARs) facilitated the important decision, where fluorine should be introduced in the molecule (Fig. 24).^[180] Consequently, the methoxy-group at the end of the ethylene-chain on the sulfonamidic nitrogen was replaced with fluorine to obtain the non-radioactive, "cold" inhibitor, which served as reference compound during radiolabeling and for *in vitro* assays. This position was chosen, because the methoxyethylene moiety had been described to point out of the binding pocket, as indicated by the *h*BChE crystal structure in complex with the inhibitor. Consequently, modifications had the slightest impact on inhibitory potencies, which was verified by measuring inhibitory potencies of several derivatives.^[180]

The synthesis of both precursor **27** and cold, fluorinated inhibitor **26** is presented in scheme 3 and was performed by Christian Gentsch under the supervision of Prof. Dr. Michael Decker (Julius-Maximilian-University of Würzburg, Institute of Pharmacy and Food Chemistry). Starting point was the building block **23**, which is not commercially available and was provided as precursor from the laboratory of Prof. Dr. Stanislav Gobec (Chair of Pharmaceutical Chemistry, Faculty of Pharmacy, University of Ljubljana). It enabled the facile synthesis of the parent compound **24** as intermediate, which was favorable for comparison purposes with fluorinated derivative **26**. Synthesis of compound **24** was carried out by reductive amination of benzaldehyde under Leuckart-Wallach conditions in formic acid, leading to benzylation of the secondary piperidine nitrogen in low yields.^[181] The use of freshly distilled benzaldehyde is advantageous due to its slow autoxidation.^[182] Demethylation of the methoxy group was achieved with boron trifluoride etherate in propane-1-thiol in satisfying yields.^[183] This reaction progressed very slowly, however, slightly elevated temperatures accelerated the conversion to a more reasonable time of 60 h. Advantageously, the resulting alcohol **25** could be subsequently used to generate both precursor **27** and cold inhibitor **26**. Fluorination of **25** was achieved with diethylaminosulfur trifluoride (DAST) in low yields,^[184] which is likely due to the described, slow decomposition of

2.1. Synthesis and Initial Characterization of a Reversible, Selective ^{18}F -Labeled Radiotracer for Human Butyrylcholinesterase



Scheme 3. Synthesis of non-radioactive, fluorinated hBChE inhibitor **26** and a respective precursor **27** for ^{18}F -radiolabeling. Reagents and conditions: i) benzaldehyde, formic acid, 6 h, 180°C , 44%; ii) $\text{BF}_3 \cdot \text{Et}_2\text{O}$, propane-1-thiol, 50°C , 60 h, 60%; iii) DAST, CH_2Cl_2 , $-10^\circ\text{C} \rightarrow \text{RT}$, 24%; iv) 1. TosCl, NEt_3 , CH_2Cl_2 , RT, 18 h, 98%, 2. *p*-TosOH, MeOH; (v) benzoyl chloride, K_2CO_3 , THF/ H_2O , $0^\circ\text{C} \rightarrow \text{RT}$, 20 h, 88 %; (vi) ethanolamine, HBTU, NEt_3 , DMF, RT, 18 h, 88%; (vii) TBDMS-Cl, imidazole, DMF, RT, 24 h, 69%; (viii) 1. LiAlH_4 , THF, reflux, 1 h; 2. naphthalene-2-sulfonyl chloride, DIPEA, CH_2Cl_2 , $0^\circ\text{C} \rightarrow \text{RT}$, 54% (two steps).

the DAST reagent, especially in the presence of moisture. Moreover, DAST is known to cause side reactions possibly decreasing yields (e.g. eliminations, carbonium-ion type rearrangements).^[184] In contrast, tosylation of the alcohol under standard conditions using tosyl chloride (TosCl) proceeded almost quantitatively,^[185] however, the tosylated precursor was slowly decomposing due to intramolecular cyclization by nucleophilic attack of the tertiary piperidine nitrogen, as indicated by LC/MS analysis. Consequently, the precursor was stabilized by salt formation with toluenesulfonic acid. Since building block **23** is not commercially available, an alternative synthesis of alcohol **25** was established, which started from nipicotic acid **28** (scheme 3).^[186] At first, the piperidine nitrogen was benzoylated applying Schotten-Baumann conditions, which gave *N*-benzoylnipicotic acid **29** in excellent yields.^[186] Next, the carboxylic acid was activated and coupled to 2-aminoethanol using the HBTU method, as described before (cf. chapters 1.4.3. and 1.5.2.).^[103] The resulting *N*-benzoylnipicotic ethanolamide **30** was subsequently protected with the *tert* butyldimethylsilyl (TBDMS) group at the primary hydroxy group, which gave the respective silyl ether **31** in good yields.^[187] Interestingly, the subsequent reduction of both amide carbonyl groups with lithium aluminum hydride could be combined with the coupling to naphthalene-2-sulfonyl chloride in a one-pot manner, which additionally included TBDMS deprotection, likely due to the harsh basic conditions during the reduction step.^[180, 186]

2.1. Synthesis and Initial Characterization of a Reversible, Selective ^{18}F -Labeled Radiotracer for Human Butyrylcholinesterase

Subsequently, this procedure directly gave alcohol **25** in satisfying yields over two steps.

2.1.3. Inhibitory Potency and Binding Kinetics

To control for retained, high inhibitory potency of the synthesized, cold fluorinated inhibitor **26** (scheme 3), a colorimetric assay was performed by Dr. Urban Košak and Assist. Prof. Dr. Damijan Knez (University of Ljubljana, Faculty of Pharmacy, Chair of Pharmaceutical Chemistry, Head: Prof. Dr. Stanislav Gobec) according to the method of Ellman.^[188] Therefore, *h*BChE in phosphate buffer was incubated with the stock solution of inhibitor **26** and Ellman's reagent (5,5'-dithiobis-(2-nitrobenzoic acid) = DTNB). Then the synthetic substrate butyrylthiocholine iodide (BTCl) was added to start hydrolysis reactions. Thereby DTNB reacts with the hydrolyzed thiols and allows their photochemical quantification. Finally, after plotting residual enzyme activities against seven different concentrations of inhibitor **26**, the IC_{50} value was calculated. Compared to the parent compound, methoxy-derivative **24**, the inhibitory potency dropped significantly, resulting in a low, submicromolar IC_{50} value of 118.3 ± 19.6 nM (cf. IC_{50} (**24**) = 4.9 ± 0.3 nM^[180]). Based on the crystal structure of *h*BChE in complex with the parent inhibitor **24** (scheme 3), it was shown that the methoxy-oxygen can act as H-bond acceptor with a structural water and Asn68.^[180] Since the methoxy group was replaced with fluorine to obtain the cold inhibitor **26**, the potency drop could be explained and still represented a good compromise, because substitutions on other positions caused a way more pronounced decrease of potency. This had been demonstrated based on several derivatives with substituted benzyl- or naphthyl-moieties.^[180] Moreover, a derivative with 4-fluoromethyl-substitution on the benzyl group was synthesized (Fig. 25) and exhibited no relevant inhibitory effect on *h*BChE.

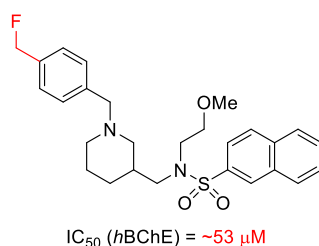
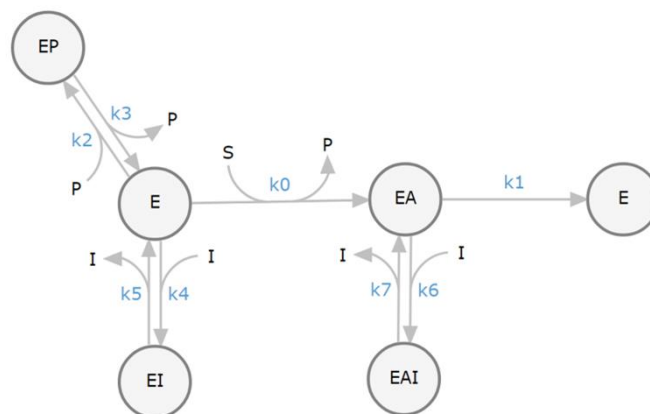


Fig. 25. Derivative of parent *h*BChE inhibitor **24** (scheme 3) with 4-fluoromethyl-substitution on the benzyl group (red), which caused almost complete loss of inhibitory potency.

Consequently, the work was continued with compound **26** and its binding kinetics were investigated by Assist. Prof. Dr. Damijan Knez with the help of Dr. Jure Stojan

2.1. Synthesis and Initial Characterization of a Reversible, Selective ^{18}F -Labeled Radiotracer for Human Butyrylcholinesterase

(University of Ljubljana, Medical Faculty). Therefore, the dissociation constants K_1 (binding to the free enzyme) and K_2 (binding to the acylated enzyme) were measured based on time-dependent progress curves of product formation with BTCl as substrate according to Ellman's method.^[188] DTNB served again as detecting reagent for the hydrolyzed thiols. The underlying mechanism of reversible BChE inhibition is presented in scheme 4.



Scheme 4. Reversible inhibition of BChE-catalyzed BTCl hydrolysis by inhibitor **26**. Abbreviations: E = free enzyme, EA = intermediately acylated enzyme, S = substrate BTCl, P = stoichiometrically released products (thiocholine-TNB, TNB⁻), I = inhibitor **26** (scheme 3). Constants: k_1 = catalytic constant for BTCl turnover (k_{cat}), k_0 = Michaelis constant (K_m), $k_3/k_2 = K_p$ = inhibition constant for binding of the product thiocholine-TNB, $k_5/k_4 = K_1$ = dissociation constant for inhibitor binding to the free enzyme, $k_7/k_6 = K_2$ = dissociation constant for inhibitor binding to the acylated enzyme.

Hydrolysis of BTCl was measured until completion in the absence and presence of three different concentrations of inhibitor **26** (Fig. 26). Additionally, experimental

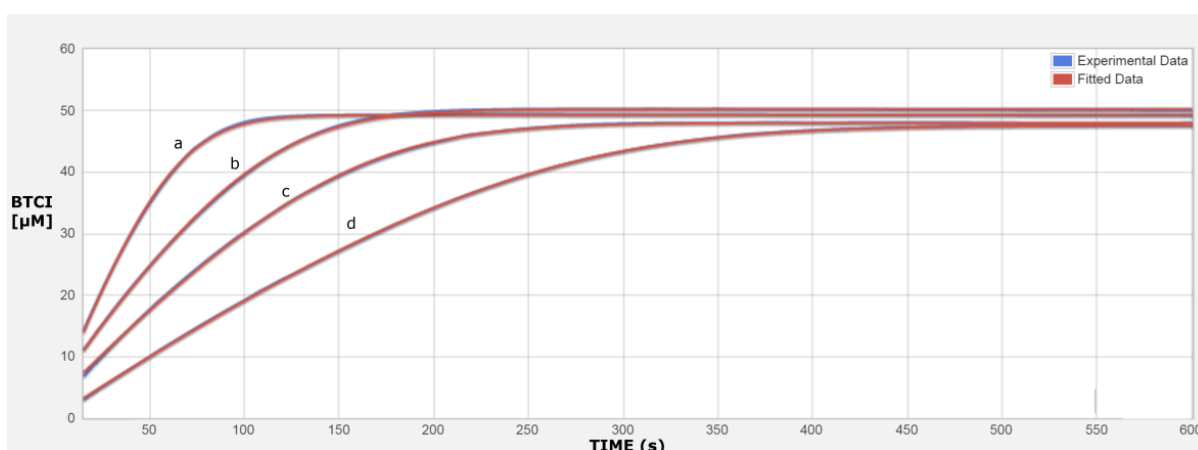


Fig. 26. Time-dependent product formation for the hydrolysis of $\sim 46 \mu\text{M}$ BTCl by *h*BChE (1 nM) in the absence (a) and presence of inhibitor **26** (b: 40 nM, c: 80 nM, d: 160 nM). Experimental data (blue) was fitted to a theoretical model (red) for a mixed, reversible inhibition mechanism of the free and acylated enzyme.

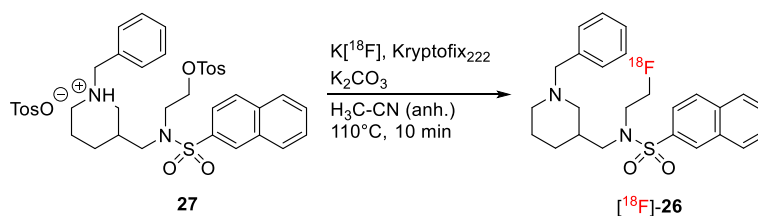
progress curves were compared with a theoretical model, that describes a mixed reaction mechanism for binding of the inhibitor **26** to both the free and acylated BChE

2.1. Synthesis and Initial Characterization of a Reversible, Selective ^{18}F -Labeled Radiotracer for Human Butyrylcholinesterase

(Fig. 26). Consequently, both dissociation constants could be determined and showed high, nanomolar binding potential of the inhibitor **26** to hBChE ($K_1 = 32.9$ nM, $K_2 = 68.0$ nM) with an approximately two-fold higher constant for binding to the acylated enzyme.

2.1.4. ^{18}F -Radiolabeling and preliminary *ex vivo* and *in vivo* Characterization

Due to the promising characteristics of the cold, fluorinated inhibitor **26** (scheme 3), the respective tosylate precursor **27** was subjected to ^{18}F -radiolabeling in an established procedure based on nucleophilic substitution of the tosylate leaving group with $[\text{}^{18}\text{F}]\text{F}^-$ (scheme 5). Labeling was performed by Dr. Xinyu Chen (University Hospital of Würzburg, Department of Nuclear Medicine, Prof. Dr. Takahiro Higuchi).



Scheme 5. Procedure for the radiolabeling of tosylate precursor **27** with $[\text{}^{18}\text{F}]\text{F}^-$ to generate the respective radiotracer $[\text{}^{18}\text{F}]\text{-26}$.

Labeling was carried out in dry acetonitrile at elevated temperatures for 10 min in the presence of a cryptand to generate nucleophilic fluoride ions. Purification of the crude product was achieved by semi-preparative HPLC on a reversed phase column, yielding the sufficiently pure radiotracer $[\text{}^{18}\text{F}]\text{-26}$ in an average radiochemical yield of $20 \pm 3\%$ ($n = 2$, corrected for decay). The identity and radiochemical purity were controlled by TLC autoradiography (purity $\geq 95.3\%$). The whole labeling process including identification and purification was completed manually in approximately 120 min. Notably, a fluorination progress of more than 33% was measured in a previous radiolabeling attempt by TLC autoradiography. Moreover, the retention time of the cold compound **26** on analytical HPLC with UV detection corresponded to that of the radiotracer $[\text{}^{18}\text{F}]\text{-26}$ using γ detection.

After the successful and quick radiolabeling with good yields and sufficient purities, the tracer was subsequently investigated *ex vivo* for its binding to mice brain tissue using freshly prepared horizontal slices (performed by Dr. Xinyu Chen with the help of Naoko Nose, Okayama University, Graduate School of Medicine, Dentistry and Pharmaceutical Sciences). The frozen slices of mice brain were incubated with tracer

2.1. Synthesis and Initial Characterization of a Reversible, Selective ^{18}F -Labeled Radiotracer for Human Butyrylcholinesterase

$[^{18}\text{F}]$ -26 in a phosphate buffer (pH = 8.0) in the presence and absence of ethopropazine hydrochloride as BChE-selective blocking agent to prove the specificity of binding. Finally, the brain slices were imaged using an autoradiographic system (Fig. 27).

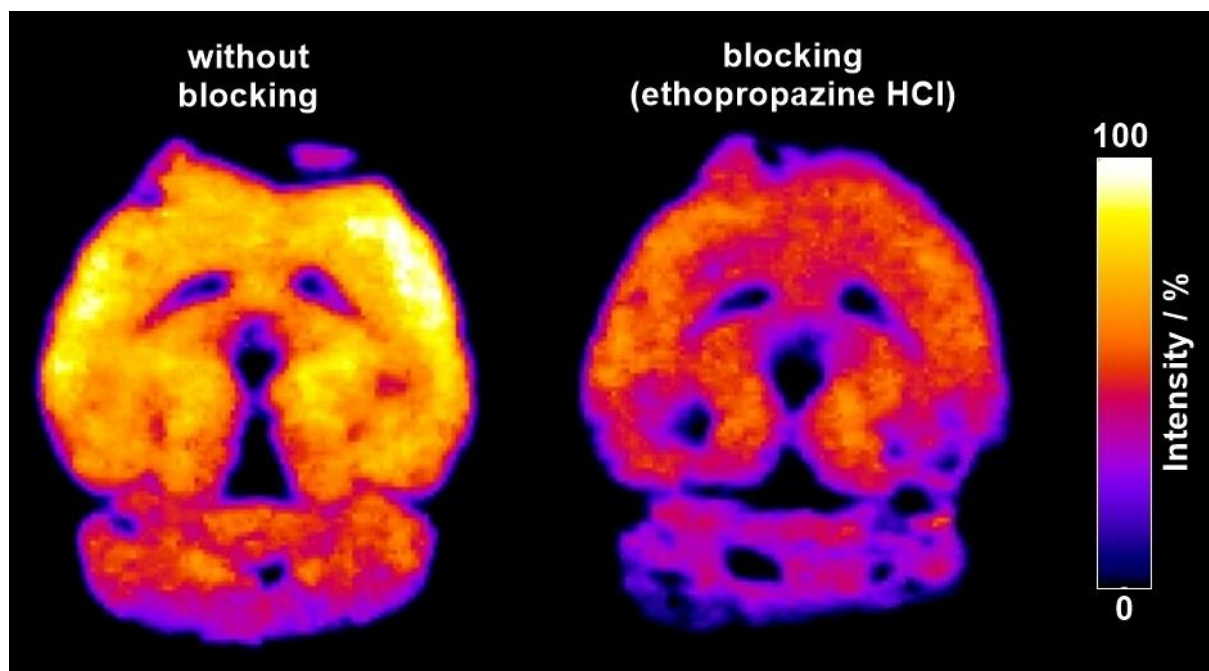


Fig. 27. Images of brain slices of a healthy mouse after incubation with BChE selective radiotracer $[^{18}\text{F}]$ -26 and subsequent autoradiography. Left: Image recorded without preincubation with the selective BChE inhibitor ethopropazine hydrochloride, right: Image recorded after previous preincubation with ethopropazine hydrochloride as blocking agent.

Interestingly, the tracer demonstrated good binding to brain tissue, which was indicated by high intensities in most of the brain area, especially at the cerebral cortex.

Considering the known BChE distribution in mice brain, this result was in good agreement.^[146, 189-190] Expectedly, binding of the tracer to ethopropazine-preincubated mice brain tissue was significantly decreased, which suggests the specific binding to BChE. However, some significant intensity was still observed despite preincubation with ethopropazine hydrochloride. This could indicate possible non-specific binding promoted by the high lipophilicity of the tracer and/or potential off-target effects.

Finally, an initial micro-PET study was performed by Dr. Xinyu Chen with the help of Naoko Nose to investigate the distribution of radiotracer $[^{18}\text{F}]$ -26 *in vivo*. Therefore, a solution of the tracer in saline was prepared and injected via tail vein to a male Wistar rat, which was anesthetized and maintained beforehand. Immediately after that, the rat was scanned in a micro-PET system using a dynamic imaging protocol of 60 min. The resulting PET images were analyzed with a software for medical imaging data

2.1. Synthesis and Initial Characterization of a Reversible, Selective ^{18}F -Labeled Radiotracer for Human Butyrylcholinesterase

examination (cf. chapter 2.1.5. for details) and time-activity curves of respective regions of interest were obtained (Fig. 28).

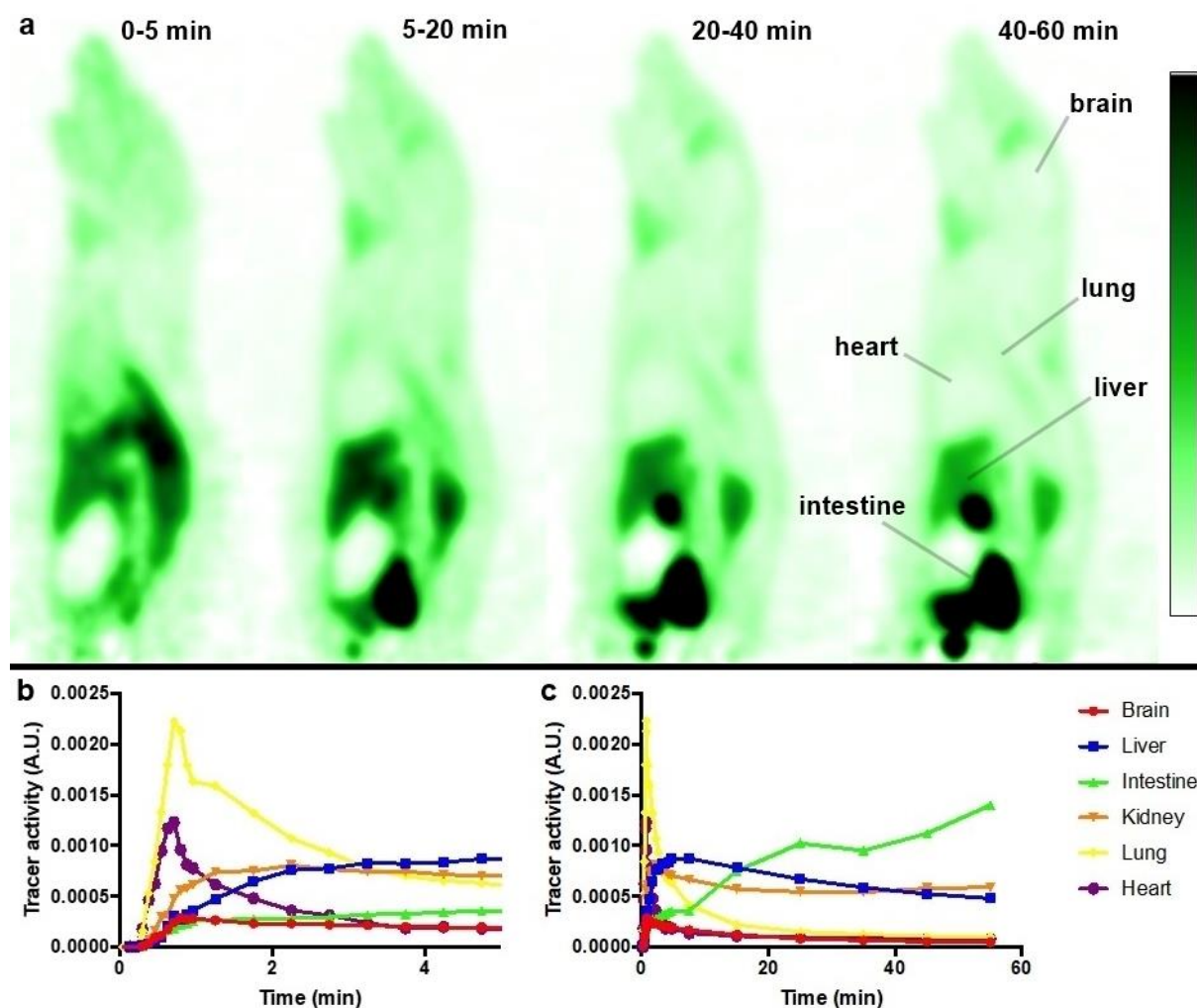


Fig. 28. a) Dynamic, sagittal PET images of a healthy, male Wistar rat after tail vein injection of tracer $[^{18}\text{F}]\text{-26}$ and subsequent imaging over 60 min in a micro-PET system. Dark-green areas correspond to a high tracer uptake, light-green areas represent low tracer uptake. b) Time-activity curves resulting from the respective PET images above (initial 5 min). c) Time-activity curves over the whole 60 min.

The PET images revealed a quick uptake in heart and lung during the first two minutes. Expectedly, these organs should be reached first after intravenous injection, but they also express BChE in an elevated manner (cf. chapter 2).^[142] After this initial blood pool circulation, high activity was found in liver and kidneys and finally, the tracer (or its metabolites) were secreted into intestine and urine. Importantly, uptake in the brain was - unexpectedly - very low, which precludes an application as CNS PET tracer, especially since there are selective substrate-type tracers, that had been shown to enter the brain (cf. chapter 2).^[167-169] Nevertheless, possible reasons for the limited brain uptake should be investigated, since the parent compound **24** is not a substrate

2.1. Synthesis and Initial Characterization of a Reversible, Selective ^{18}F -Labeled Radiotracer for Human Butyrylcholinesterase

of efflux pumps and could passively permeate the BBB with moderate efficiency.^[180] The lipophilicity of compound **24** is pronounced, while the molar mass is rather small (< 500 g/mol). On the other hand, the parent compound **24** demonstrated high plasma protein binding.^[180] Notably, a close derivative of the alcohol **25** (scheme 3), which carries a propylene chain in contrast to the ethylene chain on the sulfonamidic nitrogen of compound **24**, was used as precursor for ^{11}C -labeling with $[^{11}\text{C}]\text{H}_3\text{Cl}$ (cf. chapter 2).^[178] Even though ^{11}C has a much shorter half-life than ^{18}F , which complicates radiolabeling procedures and subsequent investigations, this approach enabled studies with a structurally more similar radiotracer compared to parent compound **24**. In contrast, this tracer exhibited better BBB permeability, but was rapidly washed out from the brain. The specificity of binding, as assessed in blocking studies with ethopropazine hydrochloride, was comparable to $[^{18}\text{F}]\text{-26}$. Moreover, a comparison of tracer accumulation in AD- and wild type mice in longitudinal PET studies revealed increased activities in AD affected brain areas during the early disease stage. The biodistribution profile was almost identical to $[^{18}\text{F}]\text{-26}$ apart from the brain uptake (e.g. high activities in liver and kidneys).^[178] Thus, an application of the tracer $[^{18}\text{F}]\text{-26}$ could be conceivable in diagnosis, prognosis or monitoring of diseases without involvement of CNS BChE (cf. chapter 2). However, future studies should also focus on investigating the reasons for the different brain uptake of $[^{18}\text{F}]\text{-26}$ and the ^{11}C -labeled close derivative.

2.1.5. Experimental Procedures

The following section describes detailed procedures for all performed experiments in the published research work of chapter 2.1.^[179] These experimental details were published separately as electronic supplementary material.

Common reagents and methods for chemical synthesis

TLC for reaction control was performed on precoated sheets (ALUGRAM[®] Xtra SIL G/UV₂₅₄, Layer: 0.20 mm silica gel 60 with fluorescent indicator UV₂₅₄) of the company Macherey-Nagel GmbH & Co. KG, 52355 Düren, Germany. The substances were visualized by their fluorescence, when irradiated with UV light (254 nm).

Silica gel with a grain size of 0.04 - 0.063 mm (company Macherey-Nagel GmbH & Co. KG, 52355 Düren, Germany) was used for manual column chromatography. The

2.1. Synthesis and Initial Characterization of a Reversible, Selective ¹⁸F-Labeled Radiotracer for Human Butyrylcholinesterase

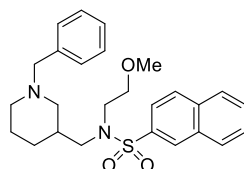
columns were packed wet. The composition of the eluents is indicated in percentage by volume.

NMR spectra were recorded at room temperature on a Bruker AV 400 FT-NMR-Spectrometer (company Bruker Biospin, Karlsruhe, Germany) (¹H: 400 MHz, ¹³C: 100 MHz). The residual protons and the ¹³C resonance signals of the deuterated solvents were used as internal standard. The chemical shifts δ were indicated in [ppm] and the coupling constants in [Hz]. The signal multiplicities were abbreviated as follows: s = singlet, brs = broad singlet, d = doublet, t = triplet, q = quartet, dd = doublet of doublets, m = multiplet.

Analytical HPLC was performed on a Shimadzu LC20AB system equipped with a DGU-20A3R controller, and a SPD-20A UV/Vis detector. Stationary phase was a Synergi 4u Fusion-RP (150×4.6 mm) column. A gradient of MeOH/water + 0.1% formic acid (phase A/ phase B) was used as mobile phase. For analytical HPLC a flow rate of 1 mL/min was used.

ESI-MS spectral data were acquired on a Shimadzu LCMS-2020 single quadrupole LC/MS (Shimadzu Europe, Duisburg, Germany).

Synthesis of *N*-((1-benzylpiperidin-3-yl)methyl)-*N*-(2-methoxyethyl)naphthalene-2-sulfonamide (**24**)



250 mg (0.69 mmol, 1.00 eq) of *N*-(2-methoxyethyl)-*N*-(piperidin-3-ylmethyl)naphthalene-2-sulfonamide (**23**) were dissolved in 1.00 mL (26.5 mmol, 38.4 eq) of formic acid at room temperature, while vigorous stirring. Then 348.6 mL (3.45 mmol, 5.00 eq) of freshly distilled benzaldehyde were added to the solution, before the mixture was heated up to 180°C for 6 h. After cooling down to room temperature, distilled water was added and the pH value was adjusted below 3 by addition of aqueous hydrochloric acid (2 M). After that, the aqueous phase was washed with diethylether to remove unpolar byproducts. Then the aqueous phase was adjusted to a pH value above 10 by addition of sodium hydroxide, before it was extracted with each two portions of diethylether and chloroform. The combined organic phases were dried over sodium sulphate, concentrated in vacuo and the crude product was purified by column chromatography (eluent = CH₂Cl₂ : MeOH : NH₃ = 98.5 : 1.4 : 0.1 → 98 : 1.9 :

2.1. Synthesis and Initial Characterization of a Reversible, Selective ¹⁸F-Labeled Radiotracer for Human Butyrylcholinesterase

0.1) to yield *N*-((1-benzylpiperidin-3-yl)methyl)-*N*-(2-methoxyethyl)naphthalene-2-sulfonamide (**24**) as a transparent, viscid gel.

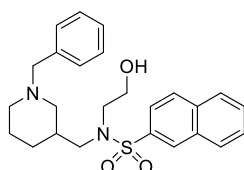
Yield: 138 mg, 305 μmol, 44%.

¹H-NMR (400 MHz, CDCl₃) δ [ppm]: 8.39 (s, 1H, H_{naph}), 7.94 (td, *J* = 11.7, 7.6 Hz, 3H, H_{naph}), 7.78 (dd, *J* = 8.6, 1.7 Hz, 1H, H_{naph}), 7.66-7.60 (m, 2H, H_{naph}), 7.33-7.22 (m, 5H, H_{benz}), 3.51-3.43 (m, 4H), 3.32 (t, *J* = 6.2 Hz, 2H, CH₂-OMe), 3.23 (s, 3H, -OCH₃), 3.13 (qd, 2H, *J* = 13.7, 7.5 Hz), 2.77 (dd, *J* = 35.3, 10.6 Hz, 2H), 2.00 (t, *J* = 9.6 Hz, 2H), 1.80-1.66 (m, 3H), 1.59-1.49 (m, 1H), 1.28 (s, 1H).

¹³C-NMR (100 MHz, CDCl₃) δ [ppm]: 138.49 (C_q), 136.68 (C_q), 134.80 (C_q), 132.29 (C_q), 129.31 (C_t), 129.30 (C_t), 129.24 (C_t), 128.73 (C_t), 128.55 (C_t), 128.24 (C_t), 127.97 (C_t), 127.57 (C_t), 127.02 (C_t), 122.74 (C_t), 71.31 (C_s), 63.52 (C_s), 58.83 (C_p), 57.81 (C_s), 54.09 (C_s), 53.38 (C_s), 48.24 (C_s), 35.03 (C_t), 28.41 (C_s), 24.72 (C_s).

ESI-MS: 453.20 [M+H]⁺, calculated: 453.22 (100%).

Synthesis of N-((1-benzylpiperidin-3-yl)methyl)-*N*-(2-hydroxyethyl)naphthalene-2-sulfonamide (**25**)



138 mg (0.305 mmol, 1.00 eq) of *N*-((1-benzylpiperidin-3-yl)methyl)-*N*-(2-methoxyethyl)naphthalene-2-sulfonamide (**24**) were dissolved in 1.5 mL of propane-1-thiol at room temperature, while vigorous stirring. Then 1.5 mL of borontrifluoride etherate were added dropwise to the solution. After foaming had stopped, the clear solution was heated up to 50°C for 60 h. Then saturated, aqueous sodium hydrogencarbonate solution was added to the reaction mixture and the aqueous phase was extracted with three portions of dichloromethane. After that, the organic phase

2.1. Synthesis and Initial Characterization of a Reversible, Selective ¹⁸F-Labeled Radiotracer for Human Butyrylcholinesterase

was washed with water and brine, then dried over sodium sulphate. After removal of the solvent under reduced pressure, the crude product was purified by column chromatography (eluent = CH₂Cl₂ : MeOH : NH₃ = 96.5 : 3.4 : 0.1) to obtain *N*-((1-benzylpiperidin-3-yl)methyl)-*N*-(2-hydroxyethyl)naphthalene-2-sulfonamide (**25**) as a transparent, viscid gel.

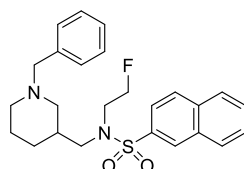
Yield: 80 mg, 182 μmol, 60%.

¹H-NMR (400 MHz, CDCl₃) δ [ppm]: 8.32 (s, 1H, H_{naph}), 7.94 – 7.86 (m, 3H, H_{naph}), 7.71 (dd, *J* = 8.6, 1.4 Hz, 1H, H_{naph}), 7.63 – 7.56 (m, 2H, H_{naph}), 7.28 – 7.20 (m, 5H, H_{benz}), 3.69 (t, *J* = 5.2 Hz, 2H, -H₂C-OH), 3.47 (dd, *J* = 13, 5.5 Hz, 2H, CH₂), 3.28 (dt, *J* = 12, 4.8 Hz, 1H, CH₂), 3.19 – 3.04 (m, 4H, 2xCH₂), 2.66 (d, *J* = 9.1 Hz, 1H), 2.48 (brs, 1H), 2.16 (d, *J* = 27.6 Hz, 3H), 1.64 – 1.44 (m, 4H).

¹³C-NMR (100 MHz, CDCl₃) δ [ppm]: 137.00 (C_q), 135.42 (C_q), 134.95 (C_q), 132.32 (C_q), 129.81 (C_t), 129.56 (C_t), 129.38 (C_t), 128.95 (C_t), 128.90 (C_t), 128.37 (C_t), 128.04 (C_t), 127.74 (C_t), 127.47 (C_t), 122.70 (C_t), 63.61 (C_s), 62.06 (C_s), 56.78 (C_s), 53.85 (C_s), 53.57 (C_s), 52.49 (C_s), 34.76 (C_t), 27.70 (C_s), 23.58 (C_s).

ESI-MS: 439.20 [M+H]⁺, calculated 439.20 (100%).

Synthesis of *N*-((1-benzylpiperidin-3-yl)methyl)-*N*-(2-fluoroethyl)naphthalene-2-sulfonamide (**26**)



50 mg (0.114 mmol, 1.00 eq) of *N*-((1-benzylpiperidin-3-yl)methyl)-*N*-(2-hydroxyethyl)naphthalene-2-sulfonamide (**25**) in 1 mL of dry dichloromethane were given to a solution of 18.1 μL (0.137 mmol, 1.20 eq) diethylaminosulfur trifluoride (DAST) in 1 mL of dry dichloromethane, while stirring at -10°C. The reaction was allowed to warm up to room temperature and stirred for 24 h. Then the organic phase

2.1. Synthesis and Initial Characterization of a Reversible, Selective ^{18}F -Labeled Radiotracer for Human Butyrylcholinesterase

was washed with aqueous, saturated sodium hydrogencarbonate solution, water and brine and dried over sodium sulphate. The crude product was purified by manual column chromatography (eluent = CH_2Cl_2 : MeOH : NH_3 = 98.5 : 1.4 : 0.1 \rightarrow 98 : 1.9 : 0.1). The product was obtained as slight yellow, transparent viscid gel.

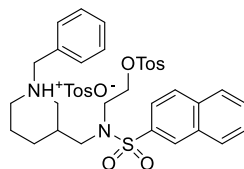
Yield: 12 mg, 27.2 μmol , 24%.

$^1\text{H-NMR}$ (400 MHz, CDCl_3) δ [ppm]: 8.38 (s, 1H, H_{naph}), 7.98 – 7.90 (m, 3H, H_{naph}), 7.75 (dd, 1H, $J = 8.6, 1.8$ Hz, H_{naph}), 7.64 (pd, 2H, $J = 6.9, 1.5$ Hz, H_{naph}), 7.31 – 7.23 (m, 5H, H_{benz}), 4.57 (t, 1H, $J = 5.4$ Hz, $-\text{CH}_2\text{F}$), 4.45 (t, 1H, $J = 5.4$ Hz, $-\text{CH}_2\text{F}$), 3.54 – 3.37 (m, 4H), 3.14 (ddd, 2H, $J = 34.8, 13.8, 7.5$ Hz), 2.72 (dd, 2H, $J = 27.9, 10.4$ Hz), 2.10 – 1.89 (m, 2H), 1.81 – 1.64 (m, 5H).

$^{13}\text{C-NMR}$ (100 MHz, CDCl_3) δ [ppm]: 24.56 (C_s), 29.84 (C_s), 34.79 (C_t), 48.58 (C_s), 48.81 (C_s), 53.31 (C_s), 53.56 (C_s), 63.50 (C_s), 82.54 (C_s), 122.60 (C_t), 127.10 (C_t), 127.75 (C_t), 128.05 (C_t), 128.29 (C_t), 128.75 (C_t), 128.95 (C_t), 129.31 (C_t), 129.38 (C_t), 129.59 (C_t), 132.32 (C_q), 134.94 (C_q), 136.29 (C_q).

ESI-MS: 441.20 $[\text{M}+\text{H}]^+$, calculated 441.20 (100%).

Synthesis of 1-benzyl-3-((N-(2-(tosyloxy)ethyl)naphthalene-2-sulfonamido)methyl)-piperidin-1-ium-4-methylbenzenesulfonate (27)



53 mg (0.121 mmol, 1.00 eq) of *N*-((1-benzylpiperidin-3-yl)methyl)-*N*-(2-hydroxyethyl)naphthalene-2-sulfonamide (**25**) were dissolved in 5 mL of dry dichloromethane at room temperature, while stirring and 33.5 μL (0.2426 mmol, 2.00 eq) of dry triethylamine were added, followed by 34.5 mg (0.181 mmol, 1.50 eq) of *p*-toluenesulfonyl chloride. The reaction was stirred for 18 h at room temperature. After that, the organic phase was washed with aqueous, saturated sodium hydrogen

2.1. Synthesis and Initial Characterization of a Reversible, Selective ¹⁸F-Labeled Radiotracer for Human Butyrylcholinesterase

carbonate solution, water and brine and dried over sodium sulphate. After removal of the solvent under reduced pressure, the crude product was purified by manual column chromatography (eluent = CH₂Cl₂ : MeOH : NH₃ = 97.75 : 2.15 : 0.1 → 97.5 : 2.4 : 0.1) to obtain 2-(*N*-((1-benzylpiperidin-3-yl)methyl)naphthalene-2-sulfonamido)ethyl 4-methylbenzenesulfonate as a transparent, viscid gel. Yield and analytical data were determined for the free base (M = 592.77 g/mol), afterwards the compound was dissolved in purified methanol and an equimolar amount of *p*-toluenesulfonic acid was added to stabilize the precursor as tosylate salt. Finally, the solvent was removed under reduced pressure and the compound was stored in the desiccator.

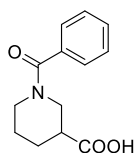
Yield: 70 mg, 118 μmol, 98%.

¹H-NMR (400 MHz, CDCl₃) δ [ppm]: 8.30 (s, 1H, H_{naph}), 7.86 – 7.94 (m, 3H, H_{naph}), 7.57 – 7.69 (m, 5H, H_{naph}/H_{tos}), 7.18 – 7.26 (m, 7H, H_{benz}/H_{tos}), 4.09 (t, 2H, J = 6.3 Hz, -CH₂OTs), 3.31 – 3.43 (m, 4H), 2.91 – 3.09 (m, 2H), 2.62 (d, 2H, ³J = 8.3 Hz), 2.39 (s, 3H, -CH_{3, tos}), 1.94 – 1.99 (m, 1H), 1.85 (s, 1H), 1.69 -1.74 (m, 1H), 1.60 (d, 3H, ³J = 10 Hz).

¹³C-NMR (100 MHz, CDCl₃) δ [ppm]: 21.79 (C_p), 24.39 (C_s), 29.83 (C_s), 34.76 (C_t), 47.45 (C_s), 53.36 (C_s), 53.99 (C_s), 57.52 (C_s), 63.42 (C_s), 68.18 (C_s), 122.56 (C_t), 127.09 (C_t), 127.77 (C_t), 128.04 (C_t), 128.08 (C_t), 128.29 (C_t), 128.82 (C_t), 129.02 (C_t), 129.21 (C_t), 129.41 (C_t), 129.65 (C_t), 130.06 (C_t), 132.29 (C_q), 132.72 (C_q), 134.97 (C_q), 135.76 (C_q), 145.18 (C_q).

ESI-MS: 593.15 [M+H]⁺, calculated 593.21 (100%).

Synthesis of 1-benzoylpiperidine-3-carboxylic acid (**29**)



500 mg (3.87 mmol, 1.00 eq) of nipecotic acid (**28**) were dissolved in a mixture of tetrahydrofuran and water (10 mL of each) and the solution was cooled down to 0°C. Then 2.86 g (19.36 mmol, 5.00 eq) of potassium carbonate were added, followed by

2.1. Synthesis and Initial Characterization of a Reversible, Selective ¹⁸F-Labeled Radiotracer for Human Butyrylcholinesterase

535.2 μ L (4.65 mmol, 1.20 eq) of benzoyl chloride, which was added dropwise while vigorous stirring. The reaction mixture was allowed to warm up to room temperature and stirred for 20 h. Then the aqueous phase was washed with three portions of ethyl acetate, before it was acidified to pH = 1-2 by addition of 2 M hydrochloric acid, while cooling with ice. A solid precipitated slowly and the aqueous phase was kept at 3°C over night, after which time more crystalline solid appeared. The product was collected by suction filtration and dried in the desiccator.

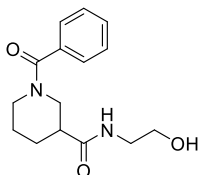
Yield: 793.2 mg, 3.4 mmol, 88%.

¹H-NMR (400 MHz, DMSO-d₆) δ [ppm]: 12.49 (brs, 1H, COOH), 7.37-7.96 (m, 5H, H_{ar}), 4.14-4.42 (m, 1H), 3.17-3.64 (m, 2H), 3.01 (t, J=11.2 Hz, 1H), 2.43-2.46 (m, 1H), 2.01-1.97 (m, 1H), 1.66-1.45 (m, 3H).

¹³C-NMR (100 MHz, DMSO-d₆) δ [ppm]: 8.91 (C_t), 26.97 (C_s), 45.14 (C_s), 126.66 (C_t), 128.36 (C_t), 128.56 (C_t), 129.22 (C_t), 129.33 (C_t), 136.34 (C_q), 169.17 (C_q), 174.39 (C_q).

ESI-MS: 234.05 [M+H]⁺, calculated 234.11 (100%).

Synthesis of 1-benzoyl-N-(2-hydroxyethyl)piperidine-3-carboxamide (**30**)



788.3 mg (3.38 mmol, 1.00 eq) of 1-benzoylpiperidine-3-carboxylic acid (**29**) were dissolved in dry DMF at room temperature, while stirring. 1.72 mL (10.14 mmol, 3.00 eq) of DIPEA and 1.92 g (5.07 mmol, 1.50 eq) of HBTU were added to the solution, before 354 μ L (5.91 mmol, 1.75 eq) of 2-aminoethanol were added dropwise. The reaction mixture was stirred for 18 h at room temperature. After that, the solvent was removed under reduced pressure by a high-vacuum pump and the residue was taken up in dichloromethane. The organic phase was washed with aqueous, saturated sodium hydrogencarbonate solution, water and brine, then dried over sodium sulphate. Finally, the crude product was purified by manual column chromatography (normal phase, eluent = CH₂Cl₂ : MeOH : NH₃ = 9.65 : 0.34 : 0.01 \rightarrow 9.60 : 0.39 : 0.01 \rightarrow 9.50

2.1. Synthesis and Initial Characterization of a Reversible, Selective ¹⁸F-Labeled Radiotracer for Human Butyrylcholinesterase

: 0.49 : 0.01) to yield 1-benzoyl-*N*-(2-hydroxyethyl)piperidine-3-carboxamide (**30**) as transparent, viscid gel.

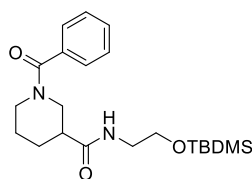
Yield: 818.7 mg, 2.96 mmol, 88%.

¹H-NMR (400 MHz, CDCl₃) δ [ppm]: 7.36-7.42 (m, 5H, H_{ar}), 4.10 (d, J=10.7 Hz, 1H), 3.42-3.75 (m, 6H), 3.30 (dd, 2H, J₁=13.7, J₂=4.9 Hz), 2.52 (brs, 1H), 2.06-2.16 (m, 1H), 1.88 (brs, 1H), 1.63 (brs, 1H), 1.32-1.36 (m, 2H).

¹³C-NMR (100 MHz, CDCl₃) δ [ppm]: 24.76 (C_s), 27.24 (C_s), 42.40 (C_t), 42.62 (C_s), 44.96 (C_s), 48.77 (C_s), 62.18 (C_s), 126.92 (C_t), 128.76 (C_t), 130.13 (C_t), 135.47 (C_q), 171.21 (C_q), 173.58 (C_q).

ESI-MS: 277.15 [M+H]⁺, calculated 277.15 (100%).

Synthesis of 1-benzoyl-*N*-(2-((*tert*-butyldimethylsilyl)oxy)ethyl)piperidine-3-carboxamide (**31**)



513 mg (1.86 mmol, 1.00 eq) of 1-benzoyl-*N*-(2-hydroxyethyl)piperidine-3-carboxamide (**30**) were dissolved in 2.5 mL of dry DMF at room temperature, while vigorous stirring. Then 759.8 mg (11.16 mmol, 6.00 eq) of imidazole were added to the solution, followed by 841 mg (5.58 mmol, 3.00 eq) of *tert*-butyldimethylsilyl chloride. After that, the reaction mixture was stirred at room temperature for 24 h. Ethylacetate was added to the solution and the organic phase was washed with aqueous, saturated sodium bicarbonate solution, water and brine. Finally, the organic phase was dried over sodium sulfate. The crude product was purified by manual column chromatography (normal phase, eluent = CH₂Cl₂ : MeOH : NEt₃ = 99 : 0.8 : 0.2).

Yield: 503 mg, 1.29 mmol, 69%.

¹H-NMR (400 MHz, CDCl₃) δ [ppm]: 7.38 (s, 5H, H_{ar}), 6.32-5.82 (m, 1H), 4.56 (d, J = 77.0 Hz, 1H), 3.66 (brs, 3H), 3.36-3.23 (m, 3H), 2.94 (s, 2H), 2.87 (s, 2H), 2.31 (d, J = 74.9 Hz,

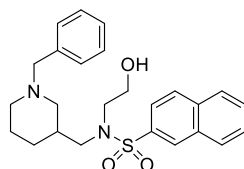
2.1. Synthesis and Initial Characterization of a Reversible, Selective ¹⁸F-Labeled Radiotracer for Human Butyrylcholinesterase

1H), 1.95 (s, 3H), 1.54 (d, *J* = 72.4 Hz, 2H),
0.88 (s, 9H, H_{tBu}), 0.05 (s, 6H, H_{SiMe}).

¹³C-NMR (100 MHz, CDCl₃) δ [ppm]: 172.63 (C_q), 170.73 (C_q), 135.97 (C_q), 129.84 (C_t), 128.62 (C_t), 127.02 (C_t), 61.89 (C_s), 41.82 (C_s), 36.57 (C_t), 31.53 (C_p), 26.03 (C_p), 18.41 (C_q), -5.22 (C_p).

ESI-MS: 391.70 [M+H]⁺, calculated 391.24 (100%).

Alternative synthesis of N-((1-benzylpiperidin-3-yl)methyl)-N-(2-hydroxyethyl)-naphthalene-2-sulfonamide (25)



53.13 mg (1.40 mmol, 5.00 eq) of lithium aluminum hydride were suspended in 4 mL of dry tetrahydrofuran at room temperature, while vigorous stirring. After that, 100 mg (0.28 mmol, 1.00 eq) 1-benzoyl-*N*-(2-((*tert*-butyldimethylsilyl)oxy)ethyl)piperidine-3-carboxamide **31** were dissolved in 1 mL of dry tetrahydrofuran and added dropwise to the reaction mixture. The solution was heated up to reflux (70°C) for 1 h. Then, the reaction mixture was cooled down to 0°C and water was added dropwise to quench excessive lithium aluminum hydride. Finally, the suspension was filtered and the residue was carefully washed with each five portions of tetrahydrofuran and dichloromethane. After removal of the solvents, the crude product was dissolved in 5 mL of dry dichloromethane and the solution was cooled down to 0°C. Then 47.6 mL (0.28 mmol, 1.00 eq) of diisopropylethylamine were added, followed by 63.5 mg (0.28 mmol, 1.00 eq) of naphthalene-2-sulfonylchloride. The solution was allowed to warm up to room temperature and stirred for 20 h. Then the organic phase was washed with aqueous, saturated sodium hydrogen carbonate, water and brine and dried over sodium sulfate. The crude product was purified by manual column chromatography (normal phase, eluent = CH₂Cl₂ : MeOH : NH₃ = 9.65 : 0.34 : 0.01) to obtain *N*-((1-benzylpiperidin-3-yl)methyl)-*N*-(2-hydroxyethyl)naphthalene-2-sulfonamide (**25**) as a transparent, viscid gel.

Yield: 64 mg, 146 μmol, 54% (two steps).

2.1. Synthesis and Initial Characterization of a Reversible, Selective ¹⁸F-Labeled Radiotracer for Human Butyrylcholinesterase

Analytical data (¹H-, ¹³C-NMR, ESI-MS) for compound **25** was presented after the first synthetic procedure (p. 79).

Colorimetric Ellman's assay

The inhibitory potency of compound **26** against *h*BChE was determined using the method of Ellman.^[188] The compound stock solution (100% in DMSO) was incubated with Ellman's reagent (DTNB) and the *h*BChE (final concentrations: 370 μM Ellman's reagent, ~1 nM *h*BChE, in 0.1 M phosphate buffer, pH 8.0) for 5 min at room temperature. The reactions were started by addition of the synthetic substrate (final concentration: 500 μM butyrylthiocholine iodide). The final content of DMSO was always 1%. The increase in absorbance at 412 nm was monitored for 1 min using a 96-well microplate reader (Synergy H4 and Synergy HT; BioTek Instruments, Inc., USA). The initial velocities in the presence (v_i) and absence (v_o) of the test compound were calculated. The inhibitory potency was expressed as the residual activity, according to the following equation:

$$RA = (v_i - b) / (v_o - b),$$

where b is the blank value using phosphate buffer instead of *h*BChE. For IC₅₀ determinations, seven different concentrations of each compound were used. The IC₅₀ values were obtained by plotting the residual *h*BChE activities against the applied inhibitor concentrations, with the experimental data fitted to a four-parameter logistic function. For the fitting procedure, GraphPad Prism 8.4.3 was used. Tacrine served as the positive control.

Kinetic studies

Compound **26** was tested by measuring the progress curves for BTCl hydrolysis by *h*BChE in the absence and presence of the compound at three concentrations (i.e. 40 nM, 80 nM, 160 nM). Assays were carried out over 10 min, in a 0.6 mL cuvette, using the method of Ellman.^[188] The experiments were carried out at 25°C in 25 mM phosphate buffer, pH = 7.0. The concentration of purified *h*BChE, which was always the final addition to these assays, was approximately 1 nM. The hydrolysis of 46 μM BTCl was followed until completion, in the presence of 1 mM DTNB. Reaching the plateau was important to get a precise estimate of the actual added BTCl concentration. For the calculation, the molar absorption coefficient of $13800 \frac{1}{\text{mol}\cdot\text{cm}}$ was used. All the measurements were performed using a conventional UV/Vis

2.1. Synthesis and Initial Characterization of a Reversible, Selective ^{18}F -Labeled Radiotracer for Human Butyrylcholinesterase

spectrophotometer (Cary 3500 UV-Vis spectrophotometer; Agilent). Due to the experimental manipulation, a dead time of 15 s was added to each measurement, and all progress curves were extrapolated accordingly prior to the analysis.

The progress-curve analysis was performed using the ENZO web application, implemented at www.enzo.cmm.ki.si.^[191] This program is designed to generate differential equations from drawn reaction schemes and subsequently to fit the coefficients of these equations according to least squares methodology to reproduce the experimental data using a numerical integration algorithm. For determination of the kinetics mechanisms and parameters, the van Slyke-Cullen single intermediate reaction scheme^[192] for substrate hydrolysis by hBChE was combined with a reversible mixed inhibition mechanism (scheme 4). In all of the evaluations, the k_1 of 814 s^{-1} , the substrate specificity constant k_1/K_m of $1 \cdot 10^8\text{ M}^{-1}\text{ s}^{-1}$, and the inhibition constant of $38.3\text{ }\mu\text{M}$ for the binding of thiocholine-TNB (k_3/k_2) in the hydrolysis of BTCI by purified hBChE were constrained, as these values had been determined previously.^[193]

Radiochemistry

^{18}F]HF in ^{18}O]H₂O was trapped on a QMA cartridge. The cartridge was eluted with 66 mM K₂CO₃ aq. (300 μL) into a v-vial containing a solution of Kryptofix₂₂₂ (15 mg) in acetonitrile (500 μL), which was then dried azeotropically at 120°C. The drying was repeated twice with anhydrous acetonitrile (2 \times 500 μL). After the drying procedure, a solution of the precursor **27** (1 mg) in anhydrous acetonitrile (400 μL) was added to the v-vial and reacted at 110°C for 10 min. After cooling the reaction mixture with a nitrogen flow, 5% acetic acid (300 μL) was added to neutralize the base. It was diluted with water (10 mL) and slowly applied to a Sep-Pak light C18 cartridge to remove the free fluorine-18. The trapped compound was eluted with ethanol (0.5 mL) and was purified via preparative HPLC. The collected fraction ($R_t = 8.7\text{-}9.7\text{ min}$) was diluted with water (10 mL) and slowly applied to a Sep-Pak light C18 cartridge. The cartridge was washed with water (5 mL), then eluted with ethanol (0.5 mL). The ^{18}F -labeled tracer [^{18}F]-**26** was diluted with saline for further *ex vivo* and *in vivo* applications.

Prep. HPLC: Shimadzu HPLC with COSMOSIL C18 ARII 6.0 \times 150 mm column, eluent: Phase A H₂O (with 0.1% TFA), Phase B MeCN (with 0.1% TFA). Method: B conc. 0-2 min: 40%, 2-15 min: 40-65%, 15-17 min: 65-96%, 17-20 min: 95%, 20-22 min: 95-40%, 22-30 min: 40%, flow rate = 1.7 mL/min. The radiolabeling was finished manually within approximately 120 min. The average radiochemical yield was $20 \pm 3\%$ (decay-

2.1. Synthesis and Initial Characterization of a Reversible, Selective ¹⁸F-Labeled Radiotracer for Human Butyrylcholinesterase

corrected, n = 2) without reaction condition optimization. Both the tracer identity and the radiochemical purity ($\geq 95\%$) were confirmed by TLC autoradiography.

Ex vivo autoradiography on mice brain slices

In the *ex vivo* autoradiography study, frozen mice brain slices were incubated in a buffer at pH = 8.0 (150 mM NaCl, 5 mM EDTA, 50 mM Na₂HPO₄) containing the tracer [¹⁸F]-26 (1.44 MBq each) with or without ethopropazine (60 μ M) for 30 min at 25°C. The slices were rinsed subsequently in PBS five times, 1 min each time. The slices were dried at room temperature with a hairdryer and then exposed to a phosphor imaging plate (Fuji SR-type image plate, Fujifilm Corporation, Tokyo, Japan) for 30 min. The film was scanned in a GE Amersham Typhoon biomolecular imager (Typhoon FLA 7000). The obtained images were processed using AMIDE medical imaging software (version 1.01 for Mac).

In vivo PET imaging

A male Wistar rat (weight 195 g) was anaesthetized using 2% isoflurane. Immediately after the injection of a solution of radiotracer [¹⁸F]-26 in 5% ethanol in saline (6.3 MBq) via tail vein, a 60 min dynamic imaging protocol was started using a dedicated small-animal PET system (microPET FOCUS 120, SIEMENS, Munich, Germany). The data was sorted into 3-dimensional sinograms, which were then reconstructed with a Fourier transform to produce dynamic images using a 2-dimensional ordered-subset expectation maximization (OSEM) algorithm. The obtained PET images were analyzed with the public domain tool AMIDE. Time-activity curves of regions of interest derived from the dynamic images were generated. All applicable international, national, and/or institutional guidelines for the care and use of animals were followed. Animal protocols were approved by the local Animal Care and Use Committee and conducted according to the Guide for the Care and Use of Laboratory Animals.

2.2. Synthesis and Initial Characterization of a Pseudo-irreversible, Selective Inhibitor of Human Butyrylcholinesterase as PET Tracer (published research work)^[194]

The content of this chapter has been published^[194] (Gentzsch, C.; Hoffmann, M.; Ohshima, Y.; Nose, N.; Chen, X.; Higuchi, T.; Decker, M. Synthesis and Initial Characterization of a Selective, Pseudo-irreversible Inhibitor of Human Butyrylcholinesterase as PET Tracer, *ChemMedChem* **2021**, *16*, 1427–1437, <https://doi.org/10.1002/cmdc.202000942>) and is adapted with permission from the respective authors.

Author contributions:

- C. Gentzsch and M. Hoffmann performed synthesis and analytical characterization of the precursor for ¹⁸F-radiolabeling and the non-radioactive reference compound under the supervision of M. Decker
- Y. Ohshima performed *in vitro* protein binding studies with the radiotracer under the supervision of T. Higuchi
- M. Hoffmann performed assays to characterize inhibitory potency and binding kinetics under the supervision of M. Decker
- X. Chen performed radiolabeling and *ex vivo* / *in vivo* studies with the help of N. Nose under the supervision of T. Higuchi

2.2.1. Aim of the Study

This work focused on the design and synthesis of a carbamate-based, ¹⁸F-labeled PET tracer inhibiting *h*BChE in a pseudo-irreversible manner and especially with long residence time on the enzyme. The characterization of the compound's inhibitory potency and binding kinetics with a subsequent comparison of those attributes with the non-fluorinated parent compound should enable a first estimation of the compound's suitability as radiotracer for *h*BChE. Importantly, the respective precursor for ¹⁸F-radiolabeling should be designed in a way, that enables the radiolabeling process, since carbamates can easily decompose under the harsh radiolabeling conditions.^[164] If a successful radiolabeling can be performed in reasonable time and without excessive efforts for isolation and purification, the respective radiotracer should be investigated in preliminary *ex vivo* autoradiography and *in vivo* PET studies, as

2.2. Synthesis and Initial Characterization of a Pseudo-irreversible, Selective Inhibitor of Human Butyrylcholinesterase as PET Tracer

described before (cf. chapter 2.1.4.). Consequently, the tracer could be evaluated for a potential application in BChE-involved diseases as diagnostic or prognostic tool and/or for disease monitoring (cf. chapter 2). Additionally, a comparison of selective BChE inhibitors as PET tracers with different binding modes could be made by comparison to the results of the previous study with a reversible BChE PET tracer (cf. chapter 2.1.).

2.2.2. Design and Synthesis

For the design of a pseudo-irreversible BChE PET tracer with preferably long duration of action, a carbamate with a tetracyclic tetrahydroquinazoline-based “carrier” scaffold and an alkylene linker with a morpholine moiety at its end was chosen as template (Figure 29).

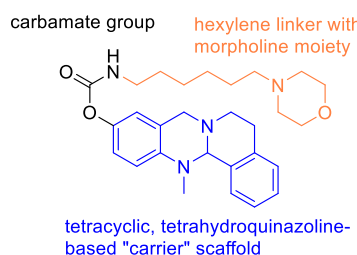
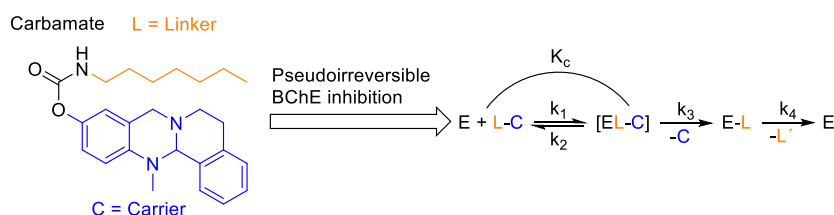


Fig. 29. Parent BChE inhibitor, that served as design schedule for a PET tracer with pseudo-irreversible binding mode and long duration of action.

Even though this compound exhibited slightly decreased inhibitory potency ($IC_{50} = 49.3$ nM^[195]) on *h*BChE compared to a respective derivative with an unsubstituted heptyl chain on the carbamate nitrogen (scheme 6, $IC_{50} = 6.4$ nM^[164]), extraordinary selectivity over *h*AChE was retained (selectivity index >1000^[195]) and even more importantly, the duration of enzyme inhibition was strongly increased, since the morpholino-hexylene moiety is transferred on the enzyme by reaction with the catalytically active serine 226,^[195] as described before (cf. chapter 2). The mechanism of pseudo-irreversible *h*BChE inhibition is presented in scheme 6. At first, the formation of a reversible



Scheme 6. Potent, selective *h*BChE inhibitor with unsubstituted heptyl chain on the carbamate nitrogen (left) and pseudo-irreversible mechanism of BChE inhibition (right); E = enzyme (BChE).

2.2. Synthesis and Initial Characterization of a Pseudo-irreversible, Selective Inhibitor of Human Butyrylcholinesterase as PET Tracer

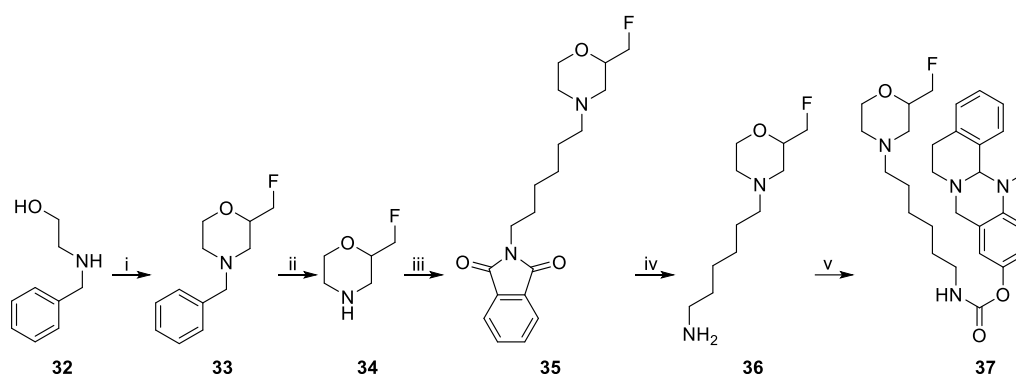
complex [EL-C] of the respective carbamate-based inhibitor L-C with the enzyme E occurs, which is described by the equilibrium constant K_c . Importantly, the affinity of such an inhibitor can only be described by K_c , if the complex formation (described by rate constant k_1) is distinctly faster than the subsequent transfer of the carbamate-linker group L to the enzyme. This step leads to the covalently inhibited enzyme E-L and is kinetically described by rate constant k_3 . Consequently, the carrier scaffold C is released as free phenol. However, since the covalent inhibition happens due to a nucleophilic substitution reaction of the serine 226 hydroxy group with the carbamate functionality, a new carbamate is formed on the enzyme. Because of the sensitivity of carbamates against hydrolysis, the covalent inhibition is only transient and enzyme activity is regenerated again, while the linker is released as L' (likely a carbamic acid decomposing to the respective primary amine). This step is kinetically characterized by rate constant k_4 and reproduces the catalytically active enzyme E.^[173-174, 195-196] Consequently, there are two additional important criteria for the design of a pseudo-irreversible BChE PET tracer: 1) An appropriate carbamoylation rate k_3 . Excessive rates can lead to a premature labeling of BChE in the bloodstream, thus causing an imaging of vascularized areas ("perfusion scan"). However, true BChE tissue distribution would not be reflected this way. On the other hand, low k_3 rates can lead to a metabolization of the tracer before it actually binds to the target enzyme in the tissue. Hence, a suitable k_3 rate should be a compromise to obtain a "molecular scan" as PET result. 2) A preferably low decarbamoylation rate k_4 and thus, a long half-life $t_{1/2}$ of enzyme reactivation. After labeling, the enzyme should remain in the carbamoylated state for a preferably long time to enable increased times of PET observation in the interesting areas and thus, a flexible study design with precise mapping of BChE's tissue distribution. As mentioned above, the morpholino-substituted derivative exhibited way better kinetic characteristics for a suitable PET tracer than the unsubstituted *n*-heptyl compound, concerning its k_3 , k_4 and $t_{1/2}$ values (table 4).^[164, 195]

Table 4. Kinetic rate constants for carbamoylation k_3 and decarbamoylation k_4 and respective half-life $t_{1/2}$ of enzyme reactivation of hBChE of two tetracyclic carbamates with *n*-heptyl- (scheme 6) and morpholino-hexylene (Fig. 29) substitution on the carbamate nitrogen. Data is presented with SEM (standard error of the mean) for three independent experiments.

Linker moiety L	$k_3 \pm \text{SEM}$ [min ⁻¹]	$k_4 \pm \text{SEM}$ [h ⁻¹]	$t_{1/2}$ [h]
Morpholino-hexylene	0.16 ± 0.02	0.042 ± 0.004	16.50
<i>n</i> -heptyl	0.66 ± 0.32	0.62 ± 0.04	1.12

2.2. Synthesis and Initial Characterization of a Pseudo-irreversible, Selective Inhibitor of Human Butyrylcholinesterase as PET Tracer

Moreover, an ^{18}F - and ^{11}C -PET tracer derived from the *n*-heptyl carbamate (Fig. 23 and scheme 6) required quite complicated, harsh and time consuming radiolabeling procedures, while the ^{18}F -derivative retained the characteristics of its parent compound, concerning kinetics and inhibitory potency.^[164] Notably, a decreased rate of carbamoylation k_3 , which avoids a perfusion PET scan, and a strongly decreased decarbamoylation rate k_4 , allowing for prolonged observation times with a long half-life of enzyme reactivation, represented the motivation to design a respective PET tracer. Consequently, syntheses for a respective fluorinated, cold compound and a tosylate precursor were developed (scheme 7 and 8) and performed by Christian Gentsch and Dr. Matthias Hoffmann under the supervision of Prof. Dr. Michael Decker (Julius-Maximilian-University of Würzburg, Institute of Pharmacy and Food Chemistry). A fluoromethyl group was introduced on the morpholine ring, since this moiety is transferred to the enzyme (cf. scheme 6) and the respective compound was synthetically most easily accessible.



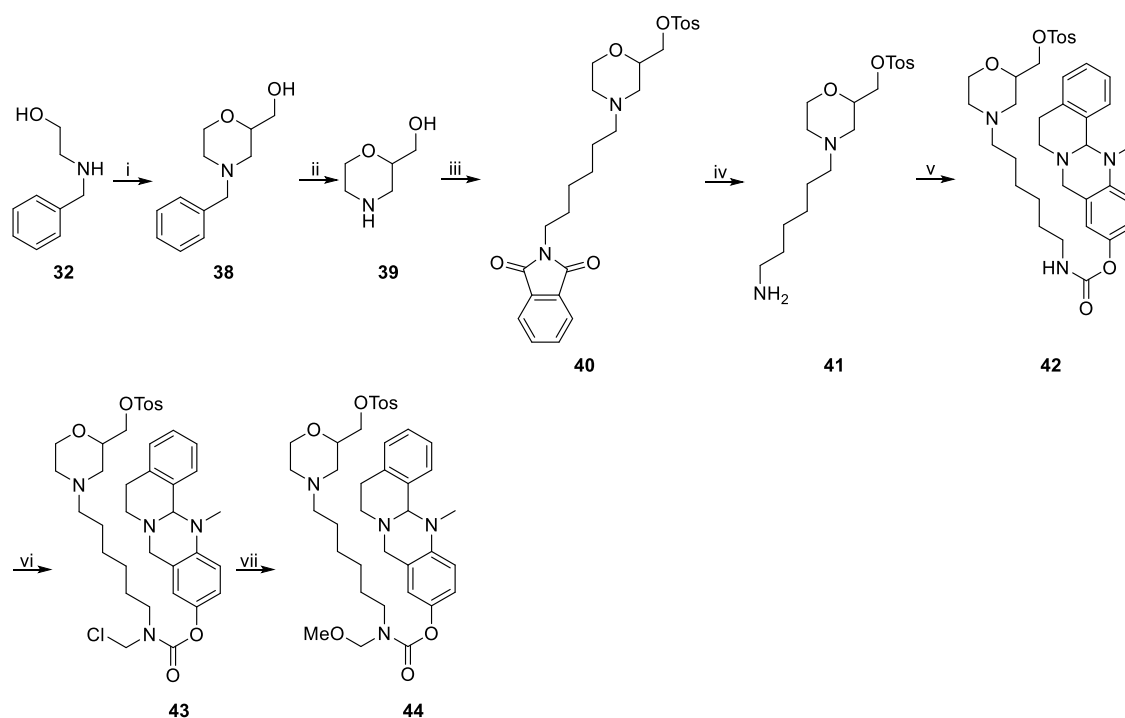
Scheme 7. Synthesis of the cold, fluorinated pseudo-irreversible *h*BChE inhibitor **37**. Reagents and conditions: i) 1. epifluorohydrin, RT, 3 h; 2. H_2SO_4 , 140°C , 1 h, 67%; ii) H_2 (1 atm), Pd/C, MeOH, RT, 1 h, quant.; iii) 2-(6-bromohexyl)isoindoline-1,3-dione, NEt_3 , DMF, 105°C , 4 h, 63%; iv) $\text{H}_4\text{N}_2 \cdot \text{H}_2\text{O}$, EtOH, 85°C , 4 h, 77 %; v) 1. *p*-nitrophenyl chloroformate, NEt_3 , CH_2Cl_2 , 2 h, RT, 67 %; 2. 13-methyl-5,8,13,13a-tetrahydro-6*H*-isoquinolino[1,2-*b*]quinazolin-10-ol, NaH, CH_2Cl_2 , 1 h, RT, 75%.

At first, 4-benzyl-2-(fluoromethyl)morpholine (**33**) was synthesized using *N*-benzyl-2-aminoethanol (**32**), which was reacted with epifluorohydrin at room temperature and directly cyclized intramolecularly using sulfuric acid at elevated temperatures to generate the morpholine heterocycle in satisfying yields.^[197-198] The benzyl group was removed quantitatively by catalytic hydrogenation (1 atm) to yield 2-(fluoromethyl)morpholine (**34**).^[199] This building block was reacted with 2-(6-bromohexyl)isoindoline-1,3-dione in a nucleophilic substitution reaction to obtain the respective alkylated phthalimide **35** in satisfying yields. Hydrazinolysis of compound **35**

2.2. Synthesis and Initial Characterization of a Pseudo-irreversible, Selective Inhibitor of Human Butyrylcholinesterase as PET Tracer

according to the conditions of Gabriel synthesis gave the respective primary amine **36** in good yields. Activation of compound **36** as reactive carbamate was achieved with *p*-nitrophenyl chloroformate in satisfying yields and the activated compound was directly reacted with the carrier scaffold 13-methyl-5,8,13,13a-tetrahydro-6*H*-isoquinolino[1,2-*b*]quinazolin-10-ol, to obtain the desired target compound, 13-methyl-5,8,13,13a-tetrahydro-6*H*-isoquinolino[1,2-*b*]quinazolin-10-yl(6-(2-(fluoromethyl)morpholino)-hexyl)carbamate (**37**) in good yields. The detailed synthesis of 13-methyl-5,8,13,13a-tetrahydro-6*H*-isoquinolino[1,2-*b*]quinazolin-10-ol itself was previously described in literature (Sawatzky et al., **2014**).^[200] As described before (chapter 2.1.2.), the cold compound **37** was essential to investigate its inhibitory potency and binding kinetics for comparison with the non-fluorinated derivative (Fig. 29) and it served as reference during radiolabeling.

Synthesis of a respective tosylate precursor for ¹⁸F-radiolabeling was achieved in a similar way including methoxymethyl (MOM) protection of the carbamate nitrogen (scheme 8), because direct radiolabeling of the unprotected carbamate precursor can't be accomplished due to decomposition (cf. chapter 2.2.1.).^[164]



Scheme 8. Synthesis of tosylated, MOM-protected precursor **44** for ¹⁸F-radiolabeling. Reagents and conditions: i) 1. epichlorohydrine, RT, 3 h; 2. H₂SO₄, 140°C, 1 h, 67% over two steps; 3. H₂O, CHONH₂, 145°C, 20 h, 93%; ii) H₂ (1 atm), Pd/C, MeOH, RT, 1 h, quant.; iii) 1. 2-(6-bromohexyl)isoindolin-1,3-dione, *N,N*-diisopropylethylamine (DIPEA), DMF, 100°C, 20 h, 66%; 2. TosCl, NEt₃, CH₂Cl₂, RT, 20 h, 71%; iv) H₄N₂ · H₂O, EtOH, 80°C, 1.5 h, 88%; v) 1. *p*-nitrophenyl chloroformate, NEt₃, CH₂Cl₂, 3 h, RT, 55%; 2. 13-methyl-5,8,13,13a-tetrahydro-6*H*-isoquinolino[1,2-*b*]quinazolin-10-ol, NaH, CH₂Cl₂, 2 h, RT, 94%; vi) TMS-Cl, paraformaldehyde, CH₂Cl₂, RT, 18 h; vii) MeOH, RT, 1 h, 85% (two steps).

2.2. Synthesis and Initial Characterization of a Pseudo-irreversible, Selective Inhibitor of Human Butyrylcholinesterase as PET Tracer

N-Benzyl-2-aminoethanol (**32**) was reacted with epichlorohydrin, followed by intramolecular, acid-mediated cyclization as described above with epifluorohydrin.^[197-198] This procedure yielded 4-benzyl-2-(chloromethyl)morpholine in satisfying yields. Chlorine was subsequently replaced by a hydroxy group in a nucleophilic substitution reaction with water at high temperatures, which gave (4-benzylmorpholin-2-yl)methanol (**38**) in excellent yields.^[199] Catalytic hydrogenation of compound **38** at 1 atm with 10% palladium on activated charcoal as catalyst proceeded quantitatively to yield morpholin-2-ylmethanol (**39**). This building block was reacted with 2-(6-bromohexyl)isoindoline-1,3-dione as described above, yielding the respective *N*-alkylated phthalimide for an upcoming Gabriel synthesis. However, first the hydroxy group was tosylated to avoid reaction of the primary amine after hydrazinolysis with the applied tosyl chloride.^[185] This gave the respective, tosylated phthalimide **40** in good yields, which was then subjected to a hydrazinolysis to obtain the respective primary amine **41** in very good yields. Activation of amine **41** with *p*-nitrophenyl chloroformate and subsequent transfer on the phenolic, tetracyclic carrier scaffold was conducted as described above and gave the unprotected tosylate precursor **42** in excellent yields. For MOM protection of the carbamate nitrogen, a method was chosen, that avoids the use of methoxymethyl chloride, which is highly cancerogenic.^[201] The procedure included the *in situ* attachment of a chloromethyl group to the carbamate nitrogen with trimethylsilyl chloride (TMS-Cl) and paraformaldehyde to produce the reactive intermediate **43**, which was directly quenched in solution with methanol to give the desired, MOM-protected precursor **44** in very good yields.

2.2.3. Inhibitory Potency and Binding Kinetics

The fluoromethylated, non-radioactive compound **37** was investigated for its inhibitory potency on *h*BChE and *h*AChE by Dr. Matthias Hoffmann under the supervision of Prof. Dr. Michael Decker (Julius-Maximilian-University of Würzburg) using Ellman's colorimetric assay, as described previously (cf. chapter 2.1.3 and 2.1.5.).^[188] A solution of DTNB and the respective *h*ChE was incubated with solutions of inhibitor **37** in different concentrations. Hydrolysis reactions were started by adding the respective synthetic substrate for each ChE (BTCI for *h*BChE and acetylthiocholine iodide ATCI for *h*AChE). Subsequently, the hydrolyzed thiols were quantified photometrically and enzyme activity was calculated. IC₅₀ values were determined after plotting percental enzyme activities against the logarithmic concentrations of compound **37**. The IC₅₀

2.2. Synthesis and Initial Characterization of a Pseudo-irreversible, Selective Inhibitor of Human Butyrylcholinesterase as PET Tracer

value of inhibitor **37** on *hBChE* was determined as 66.6 nM, while no activity on *hAChE* was observed ($IC_{50} > 100 \mu M$). As expected, these values were in good accordance with the parent, non-fluorinated compound (Fig. 29, $IC_{50} = 49.3$ nM on *hBChE*, $IC_{50} > 100 \mu M$ on *hAChE*^[195]), since the introduction of the fluoromethyl group was just a minor alteration of the molecular structure.

Consequently, kinetic studies with inhibitor **37** were performed by Dr. Matthias Hoffmann to determine K_c , k_3 , k_4 and $t_{1/2}$ (scheme 6). The equilibrium constant K_c and the rate constant of carbamoylation k_3 were measured with the same general setup as for IC_{50} determination, but the enzyme was pre-incubated for certain times during 40 min with different inhibitor concentrations, before the synthetic substrate BTCl was added. The resulting, time-dependent plots of enzyme activities allowed for determination of the first-order rate constant k_{obs} according to the following equation:

$$A = A_0 \cdot e^{-k_{obs} \cdot t} + A_{\infty}$$

In that respect, A is the enzyme activity at the time “ t ” (A_0 at the beginning $t = 0$ and A_{∞} at infinite time). Consequently, rate constants k_{obs} were obtained for the different concentrations of inhibitor **37**, whose reciprocals were plotted against the inverse concentration according to the next equation:

$$\frac{1}{k_{obs}} = \frac{K_c}{k_3} \cdot \frac{1}{[37]} + \frac{1}{k_3}$$

The linear equation allowed determining k_3 from the y-intercept and K_c from the slope. The equilibrium constant was measured as $K_c = 199.9 \pm 160.4$ nM and the rate constant of carbamoylation $k_3 = 0.42 \pm 0.25 \text{ min}^{-1}$. The k_3 value was a bit higher than that of the parent compound (Fig. 29, $k_3 = 0.16 \pm 0.02 \text{ min}^{-1}$)^[195], but lower than that of the *n*-heptyl derivative (scheme 6, $k_3 = 0.66 \pm 0.32 \text{ min}^{-1}$)^[164, 195]. The K_c value was in good accordance with the parent compound ($K_c = 202 \pm 55$ nM).^[195] Generally, these values were in a promising range to potentially achieve a molecular PET scan with the respective radiolabeled tracer. The decarbamoylation rate constant k_4 and the respective half-life of enzyme reactivation were measured in dilution experiments after incubation of the enzyme solution with a saturating concentration of **37** to inhibit > 85% of *hBChE* by carbamoylation. Subsequent dilution of 1 : 1000 should prevent further enzyme inhibition and lead to a regeneration of enzyme activity by time-dependent decarbamoylation (cf. scheme 6). Thus, enzyme activity was measured at several time points after dilution. The plot was fitted to a first-order exponential curve allowing to calculate k_4 from the following equation:

2.2. Synthesis and Initial Characterization of a Pseudo-irreversible, Selective Inhibitor of Human Butyrylcholinesterase as PET Tracer

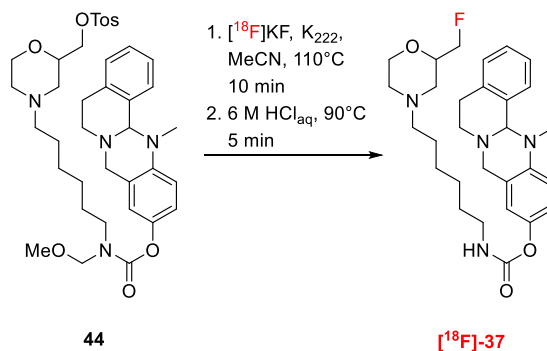
$$A = (1 - e^{-k_4 t}) \cdot (1 - A_0) + A_0$$

In this way, the decarbamylation rate constant was determined as $k_4 = 0.043 \pm 0.003 \text{ h}^{-1}$ and the corresponding half-life of enzyme regeneration was $t_{1/2} = 16.13 \text{ h}$. These values were in excellent agreement with those of the parent compound ($k_4 = 0.042 \pm 0.004 \text{ h}^{-1}$, $t_{1/2} = 16.50 \text{ h}$, cf. table 4).^[195] Importantly, a comparison with the respective values of the *n*-heptyl derivative (scheme 6) revealed, that the enzyme is carbamoylated significantly longer ($k_4 = 0.62 \pm 0.04 \text{ h}^{-1}$, $t_{1/2} = 1.12 \text{ h}$, cf. table 4).^[164, 195]

2.2.4. ¹⁸F-Radiolabeling and preliminary *ex vivo* and *in vivo*

Characterization

Due to the promising binding kinetics and inhibitory potency of the cold, fluorinated *h*BChE inhibitor **37**, radiolabeling of the respective MOM protected tosylate precursor **44** (scheme 8) was attempted in a two-step procedure by Dr. Xinyu Chen under the supervision of Prof. Dr. Takahiro Higuchi (University Hospital of Würzburg, Department of Nuclear Medicine), including nucleophilic substitution with [¹⁸F]F⁻, as described before (chapter 2.1.4. and 2.1.5.) and subsequent MOM deprotection with hydrochloric acid (scheme 9).



Scheme 9. ¹⁸F-radiolabeling of MOM protected tosylate precursor **44** and subsequent deprotection yielding the respective radiotracer [¹⁸F]-**37**.

Precursor **44** was reacted for 10 min with [¹⁸F]KF at elevated temperatures and in the presence of a [2.2.2.]cryptand (Kryptofix₂₂₂ = K₂₂₂). Next, removal of the MOM protecting group was accomplished by adding 6 M aqueous hydrochloric acid and heating for further 5 min. Purification after radiolabeling was conducted with semi-preparative HPLC. In this way, radiotracer [¹⁸F]-**37** was obtained in a radiochemical yield of 13% after decay correction and a radiochemical purity of 95.3%, as indicated by TLC autoradiography. The whole radiolabeling process was feasible in a time frame of 180 min. This process was an obvious improvement compared to the complicated

2.2. Synthesis and Initial Characterization of a Pseudo-irreversible, Selective Inhibitor of Human Butyrylcholinesterase as PET Tracer

and time-consuming 4-step radiolabeling of the “first generation” carbamate PET tracers, that had been developed based on the *n*-heptyl derivative (scheme 6, Fig. 23).^[164] Thus, this procedure represents an advantageous, novel strategy for ¹⁸F-radiolabeling of carbamates in general.

Consequently, the radiotracers binding to mice brain tissue was investigated by Dr. Xinyu Chen with the help of Naoko Nose (Okayama University, Graduate School of Medicine, Dentistry and Pharmaceutical Sciences) in *ex vivo* autoradiography experiments in an identical way as described before (chapter 2.1.4. and 2.1.5.). Freshly prepared horizontal slices of mice brain were prepared and incubated with a solution of [¹⁸F]-37 in a phosphate buffer at pH = 8. Ethopropazine hydrochloride served again as blocking agent to prove the specificity of binding (Fig. 30).

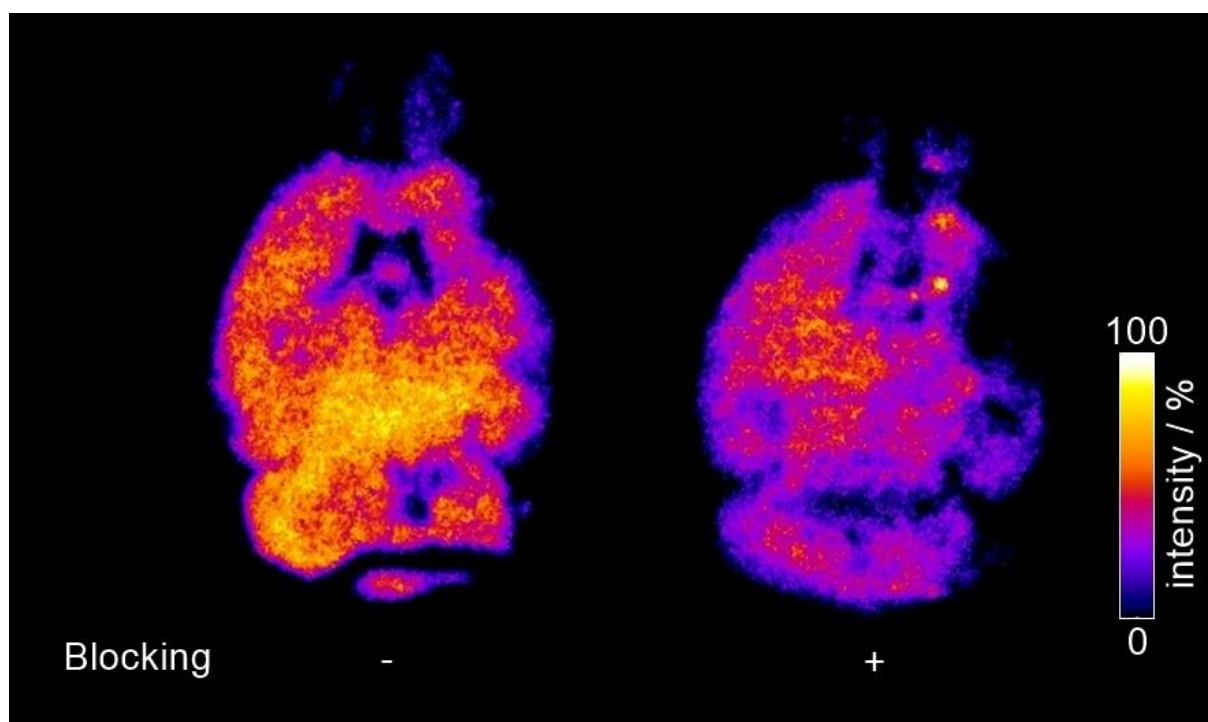


Fig. 30. Images after *ex vivo* autoradiography on horizontal slices of mice brain tissue incubated with radiotracer [¹⁸F]-37. Right: Pre-incubation with ethopropazine hydrochloride as BChE-specific blocking agent, left: Without blocking agent.

The tracer exhibited good binding to the tissue, as indicated by high levels of radioactivity in relevant brain areas like white matter bundles, thalamus, upper brainstem and cerebral cortex. Pre-incubation with ethopropazine hydrochloride led to a strongly decreased binding, however, as some intensity was still detectable, the tracer could have off-target effects or at least exhibit non-specific binding due to its pronounced lipophilicity. Notably, these results are similar to the analogous experiment with the reversible ¹⁸F-labeled radiotracer [¹⁸F]-26 (chapter 2.1.4.).

2.2. Synthesis and Initial Characterization of a Pseudo-irreversible, Selective Inhibitor of Human Butyrylcholinesterase as PET Tracer

Finally, the radiotracer's *in vivo* distribution was initially investigated in micro-PET studies by Dr. Xinyu Chen with the help of Naoko Nose, as described before (chapter 2.1.4. and 2.1.5.). After injection of a solution of the tracer in saline to a healthy, male Wistar rat via tail vein, the anesthetized rat was scanned in a small-animal PET system to obtain dynamic PET images, which were subsequently analyzed to generate time-activity curves of regions of interest (Fig. 31).

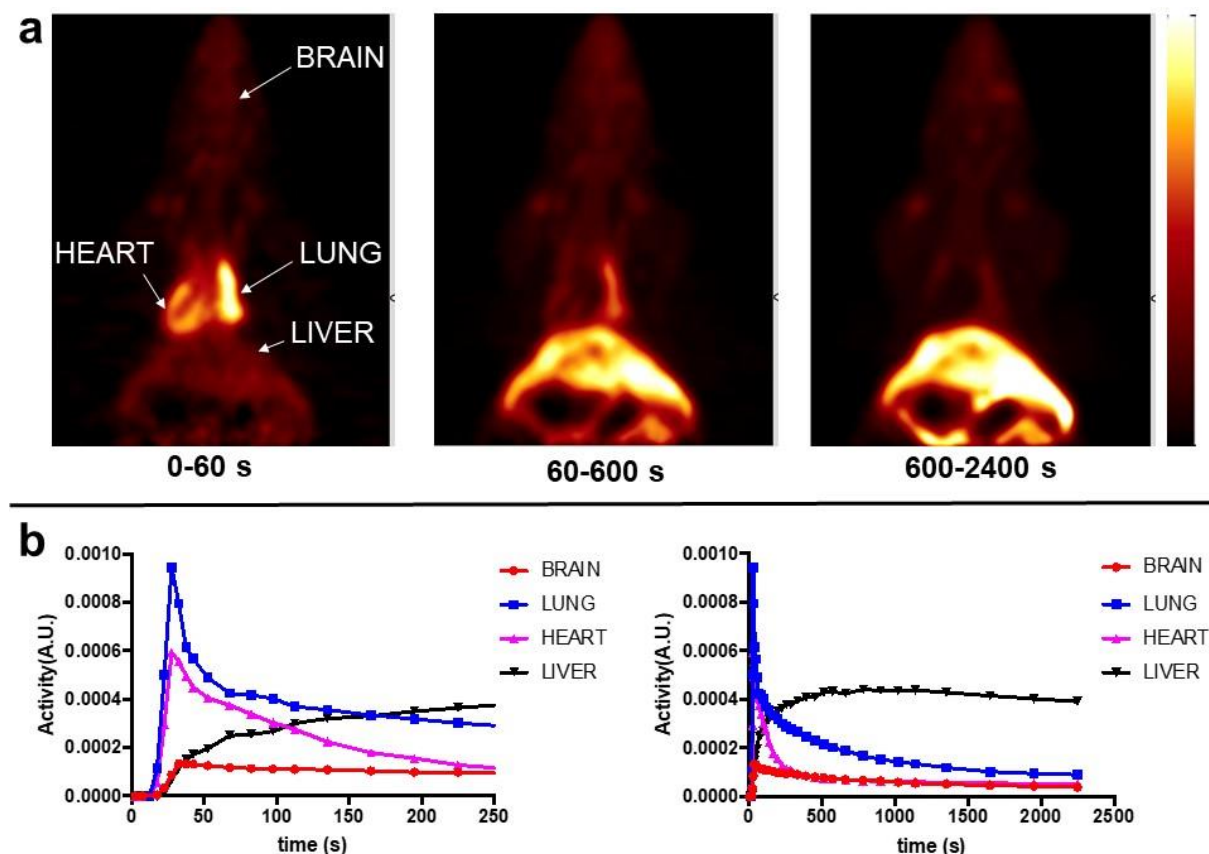


Fig 31. Preliminary characterization of *in vivo* distribution of radiotracer [^{18}F]-37 via micro-PET with a healthy, male Wistar rat. **a)** Dynamic PET images after scanning for 40 min directly after tail vein injection. **b)** Time-activity curves of regions of interest generated from the images above, left: Initial 250 s, right: Complete 40 min.

Interestingly, the images and corresponding curves revealed a similar distribution profile as for the analogous experiment with the reversible radiotracer [^{18}F]-26. A rapid enrichment in heart and lung occurred after initial blood pool circulation during the first minute. Then an accumulation of activity was mainly observed in the liver, while brain uptake was comparably very low. It is noteworthy, that the parent compound (Fig. 29) exhibited pro-cognitive and neuroprotective effects in a mouse model of AD with i.c.v. injected $\text{A}\beta_{25-35}$.^[195] However, the respective behavioral assays were carried out after seven days of daily i.p. injections of the compound, consequently a minor brain uptake

2.2. Synthesis and Initial Characterization of a Pseudo-irreversible, Selective Inhibitor of Human Butyrylcholinesterase as PET Tracer

represents no comparable limitation of use as for a PET tracer to target BChE in the CNS for diagnostic purposes. Thus, both *in vivo* distribution results with the reversible tracer [¹⁸F]-26 (chapter 2.1.4.) and the pseudo-irreversible tracer [¹⁸F]-37 might be indicative of a limited use of inhibitor-type PET tracers targeting CNS BChE. Substrate-type tracers should likely be more appropriate in this context, even though they must be designed properly, too, considering their partly quick hydrolysis (cf. chapter 2). Nevertheless, an application of both tracers in diagnosis, prognosis or disease monitoring of pathologies with altered BChE activities outside the CNS (e.g. certain lung cancer types or cardiovascular diseases, cf. chapter 2) is conceivable, especially since both tracers quickly reach heart and lung. Additionally, reasons for the limited brain uptake of both tracers should be ascertained (e.g. limited BBB penetration due to low passive diffusion or extrusion by efflux pumps) to enable the design of more convenient CNS PET tracers for BChE.

2.2.5. Experimental Procedures

The following section describes detailed procedures for all performed experiments in the published research work of chapter 2.2.^[194] Some of the experimental details were published separately as [Supporting Information](#).

Common reagents and methods for chemical synthesis

Reagents and solvents were obtained from commercial suppliers in reagent grade and were used without further purification unless stated otherwise. Dichloromethane as solvent was distilled from CaH₂ under argon.

The reaction progress was controlled with analytical thin-layer chromatography (TLC) on precoated silica gel GF₂₅₄ plates (Macherey Nagel, Düren, Germany). Compounds were detected under UV light (254 and 366 nm) or through staining with iodine, KMnO₄, or Ehrlich's reagent.

Crude products were purified after work-up by manual flash column chromatography. Silica gel (particle size of 40-63 μm; VWR chemicals, Leuven, Belgium) was used as the stationary phase and mixtures from petroleum ether/ethyl acetate or dichloromethane/methanol as eluent systems.

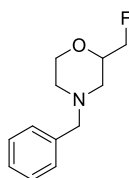
The pure compounds were submitted for nuclear magnetic resonance spectra on an AV-400 NMR instrument (Bruker) in deuterated solvents (DMSO-d₆, CDCl₃, CD₂Cl₂,

2.2. Synthesis and Initial Characterization of a Pseudo-irreversible, Selective Inhibitor of Human Butyrylcholinesterase as PET Tracer

CD₃OD). Chemical shifts are expressed in ppm relative to DMSO-d₆, CDCl₃, CD₂Cl₂, or CD₃OD (2.50/7.26/5.32/3.31 for ¹H; 39.5/77.2/53.5/49.0 for ¹³C).

Purity of the compounds was controlled with analytical HPLC on a Shimadzu system equipped with a DGU-20A3R controller, LC20AB liquid chromatograph, and SPD-20 A UV/Vis detector (Shimadzu): Stationary phase: Synergi 4 U fusion RP (Synergi, Aschaffenburg, Germany) column; mobile phase: water + 0.1% formic acid (phase A) and methanol + 0.1% formic acid (phase B) with a flow of 1.0 mL/min. Method: conc. B, gradient 5 → 90% from 0 to 8 min, 90% isocratic from 8 to 13 min, gradient 90 → 5% from 13 to 15 min, 5% isocratic from 15 to 18 min. Compounds were detected at λ = 254 nm, and target compounds were ≥ 95% pure.

Synthesis of 4-benzyl-2-(fluoromethyl)morpholine (**33**)



In a flask, 2-(benzylamino)ethan-1-ol (**32**; 1.866 mL, 1.988 g, 13.15 mmol, 1 eq) and epifluorohydrin (1 g, 13.15 mmol, 1 eq) were mixed and stirred for 3 h at room temperature. Then concentrated sulfuric acid (5 mL) was added carefully and the mixture was heated up to 140°C for 1 h. Afterwards, the reaction mixture was allowed to cool down to room temperature and was poured onto ice. The aqueous layer was basified with aqueous sodium hydroxide (10 M) and extracted with three portions of ethyl acetate. The combined organic layers were washed with water and brine, dried over sodium sulphate, filtered, and evaporated to dryness under reduced pressure. The residue was purified by manual flash column chromatography (petroleum ether/ethyl acetate = 3:1, *R_f* = 0.35) to yield 4-benzyl-2-(fluoromethyl)morpholine (**33**; 1.31 g, 6.26 mmol, 48%) as colorless oil.

¹H-NMR (400 MHz, CDCl₃): δ [ppm] = 7.29-7.14 (m, 5H), 4.41-4.31 (m, 1H), 4.29-4.21 (m, 1H), 3.89-3.58 (m, 3H), 3.53-3.35 (m, 2H), 2.74-2.55 (m, 2H), 2.14 (td, *J* = 11.4, 3.3 Hz, 1H), 2.04-1.86 (m, 1H).

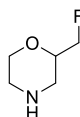
¹³C NMR (101 MHz, CDCl₃): δ [ppm] = 137.7 (1 C), 129.3 (2 C), 128.5 (2 C), 127.4 (1 C), 85.0 (1 C), 83.3 (1 C), 74.5 (0.5 C), 74.3

2.2. Synthesis and Initial Characterization of a Pseudo-irreversible, Selective Inhibitor of Human Butyrylcholinesterase as PET Tracer

(0.5 C), 66.9 (1 C), 63.5 (1 C), 53.9 (1 C), 53.8 (1 C), 53.0 (1 C).

MS (ESI): $[M+H]^+$ calculated for $C_{12}H_{16}NOF$ = 210.13, found 210.10.

Synthesis of 2-(fluoromethyl)morpholine (**34**)



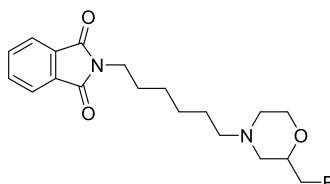
A solution of 4-benzyl-2-(fluoromethyl)morpholine (**33**; 1.3 g, 6.21 mmol, 1 eq) in MeOH (30 mL) was prepared and formic acid (0.5 mL) was added. No precipitation was observed. Then palladium on activated charcoal (10 wt-%, 130 mg) was added and the atmosphere was replaced with hydrogen. The mixture was stirred for 1 h at room temperature. After that, the catalyst was filtered off by a pad of celite, which was washed with methanol. The filtrate was evaporated to dryness in vacuo to yield 2-(fluoromethyl)morpholine as its formiate salt (**34**; 1.025 g, 6.21 mmol, quant.) as colorless oil.

1H -NMR (400 MHz, CD_3OD): δ [ppm] = 8.37 (s, 1H), 4.57-4.49 (m, 1H), 4.44-4.37 (m, 1H), 4.15-4.06 (m, 1H), 4.04-3.90 (m, 1H), 3.90-3.80 (m, 1H), 3.39-3.32 (m, 1H), 3.29-3.26 (m, 1H), 3.25 (dt, J = 2.5, 1.3 Hz, 1H), 3.18-3.12 (m, 1H), 3.10-2.99 (m, 1H).

^{13}C -NMR (101 MHz, CD_3OD): δ [ppm] = 168.2 (1 C), 84.8 (1 C), 83.1 (1 C), 73.6 (0.5 C), 73.4 (0.5 C), 64.9 (1 C), 43.8 (1 C).

MS (ESI): $[M+H]^+$ calculated for $C_5H_{10}FNO$ = 120.08; found 120.15.

Synthesis of 2-(6-(2-(fluoromethyl)morpholino)hexyl)isoindoline-1,3-dione (**35**)



2-(Fluoromethyl)morpholine hydroformiate (**34**; 1001 mg, 6.06 mmol, 1 eq) was dissolved in dry dimethylformamide (10 mL) and triethylamine (3 mL) was added. Then 2-(6-bromohexyl)isoindoline-1,3-dione (2 g, 6.45 mmol, 1.06 eq) was added and the

2.2. Synthesis and Initial Characterization of a Pseudo-irreversible, Selective Inhibitor of Human Butyrylcholinesterase as PET Tracer

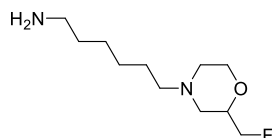
resulting solution was heated to 105°C for 4 h. The mixture was allowed to cool down to room temperature and water was added. The aqueous layer was extracted with three portions of ethyl acetate. Then the combined organic layers were washed with water and brine, dried over sodium sulphate, filtered, and the solvent was evaporated under reduced pressure. The residue was purified by manual column chromatography (CH₂Cl₂/MeOH = 98:2, *R_f* = 0.33) to yield 2-(6-[2-(fluoromethyl)morpholino]hexyl)isoindoline-1,3-dione (**35**; 1.334 g, 3.83 mmol, 63%) as colorless oil.

¹H-NMR (400 MHz, CDCl₃): δ [ppm] = 7.80-7.74 (m, 2H), 7.66-7.61 (m, 2H), 4.41-4.36 (m, 1H), 4.29-4.24 (m, 1H), 3.83 (ddd, *J* = 11.3, 3.3, 1.7 Hz, 1H), 3.66-3.50 (m, 4H), 2.74-2.67 (m, 1H), 2.61 (dd, *J* = 11.5, 1.9 Hz, 1H), 2.34-2.22 (m, 2H), 2.05 (td, *J* = 11.4, 3.3 Hz, 1H), 1.94-1.82 (m, 1H), 1.69-1.56 (m, 3H), 1.50-1.36 (m, 3H), 1.37-1.24 (m, 4H).

¹³C-NMR (101 MHz, CDCl₃): δ [ppm] = 168.4 (1 C), 133.9 (2 C), 132.2 (1 C), 123.3 (2 C), 84.9 (1 C), 83.1 (1 C), 74.3 (0.5 C), 74.1 (0.5 C), 66.8 (1 C), 58.8 (1 C), 54.0 (1 C), 52.9 (1 C), 37.9 (1 C), 28.5 (1 C), 27.0 (1 C), 26.7 (1 C), 26.4 (1 C).

MS (ESI): [M+H]⁺ calculated for C₁₉H₂₆N₂O₄ = 349.19, found 349.15.

Synthesis of 6-(2-(fluoromethyl)morpholino)hexan-1-amine (**36**)



To a solution of 2-{6-[2-(fluoromethyl)morpholino]hexyl}isoindoline-1,3-dione (**35**; 1.2 g, 3.44 mmol, 1 eq) in ethanol (50 mL), hydrazine hydrate (1 mL, > 5 eq) was added. The solution was heated to 85°C for 4 h. Then the mixture was allowed to cool down to room temperature and the precipitate was filtered off. The filtrate was evaporated to dryness under reduced pressure. The residue was triturated with dichloromethane, filtered, and the filtrate was evaporated under reduced pressure to yield 6-[2-

2.2. Synthesis and Initial Characterization of a Pseudo-irreversible, Selective Inhibitor of Human Butyrylcholinesterase as PET Tracer

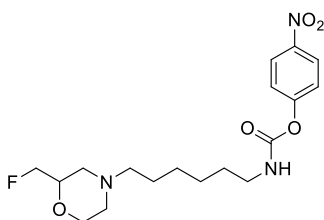
(fluoromethyl)morpholino]hexan-1-amine (**36**; 577 mg, 2.64 mmol, 77%) as colorless oil without further purification.

$^1\text{H-NMR}$ (400 MHz, CDCl_3): δ [ppm] = 4.48-4.42 (m, 1H), 3.95-3.86 (m, 1H), 3.72-3.64 (m, 1H), 3.64-3.58 (m, 1H), 2.80-2.74 (m, 1H), 2.71-2.63 (m, 3H), 2.37-2.29 (m, 2H), 2.12 (td, $J=11.5, 3.4$ Hz, 1H), 2.01-1.89 (m, 1H), 1.55-1.41 (m, 4H), 1.39-1.27 (m, 4H).

$^{13}\text{C-NMR}$ (101 MHz, CDCl_3): δ [ppm] = 85.0 (1 C), 83.3 (1 C), 74.4 (0.5 C), 74.2 (0.5 C), 67.0 (1 C), 59.1 (1 C), 54.2 (1 C), 54.1 (1 C), 53.1 (1 C), 42.2 (1 C), 33.7 (1 C), 27.4 (1 C), 26.9 (1 C), 26.6 (1 C).

MS (ESI): $[\text{M}+\text{H}]^+$ calculated for $\text{C}_{11}\text{H}_{23}\text{FN}_2\text{OH}$ = 219.19; found 219.20.

Synthesis of 4-Nitrophenyl-{6-[2-(fluoromethyl)morpholino]hexyl}carbamate



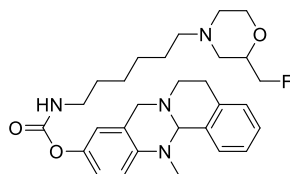
To a solution of 6-[2-(fluoromethyl)morpholino]hexan-1-amine (**36**; 500 mg, 2.29 mmol) in dry dichloromethane (10 mL), triethylamine (0.5 mL) and 4-nitrophenylchloroformate (508 mg, 2.52 mmol) were added. The resulting solution was stirred for 2 h at room temperature. Then the solvent was evaporated under reduced pressure and the residue was purified by manual flash column chromatography (eluent = $\text{CH}_2\text{Cl}_2/\text{MeOH}$ 99:1, R_f = 0.11) to yield 4-nitrophenyl {6-[2-(fluoromethyl)morpholino]hexyl}carbamate (588 mg, 1.53 mmol, 67%) as yellow oil.

MS (ESI): $[\text{M}+\text{H}]^+$ calculated for $\text{C}_{18}\text{H}_{26}\text{FN}_3\text{O}_5$ = 384.20, found 384.05.

Due to high instability of the title compound only LC/MS data was measured, before directly reacting it in the next step.

2.2. Synthesis and Initial Characterization of a Pseudo-irreversible, Selective Inhibitor of Human Butyrylcholinesterase as PET Tracer

Synthesis of 13-methyl-5,8,13,13a-tetrahydro-6H-isoquinolino[1,2-b]quinazolin-10-yl (6-(2-(fluoromethyl)morpholino)hexyl)carbamate (**37**)



To a solution of 4-nitrophenyl [6-(2-(fluoromethyl)morpholino)hexyl]carbamate (86 mg, 0.23 mmol, 1.2 eq) and 13-methyl-5,8,13,13a-tetrahydro-6H-isoquinolino[1,2-b]quinazolin-10-ol (50 mg, 0.19 mmol, 1 eq), sodium hydride (60% suspension in paraffin oil, 9 mg, 0.23 mmol, 1 eq) was added. The resulting mixture was stirred for 1 h at room temperature. Then water was added and the aqueous layer was extracted with three portions of dichloromethane. The combined organic layers were washed with water, saturated aqueous sodium hydrogen carbonate solution and brine, dried over sodium sulphate, filtered, and evaporated to dryness under reduced pressure. The residue was purified by manual flash column chromatography ($\text{CH}_2\text{Cl}_2/\text{MeOH} = 98:2$, $R_f = 0.14$) to yield 13-methyl-5,8,13,13a-tetrahydro-6H-isoquinolino[1,2-b]quinazolin-10-yl{6-[2-(fluoromethyl)morpholino]hexyl}carbamate (**37**; 72 mg, 0.14 μmol , 75%) as colorless oil.

$^1\text{H-NMR}$ (400 MHz, CD_2Cl_2): δ [ppm] = 7.38-7.32 (m, 1H), 7.22-7.15 (m, 2H), 7.14-7.09 (m, 1H), 6.89-6.81 (m, 2H), 6.74-6.68 (m, 1H), 4.77 (s, 1H), 4.42-4.35 (m, 1H), 4.30-4.22 (m, 1H), 3.94 (d, $J = 15.6$ Hz, 1H), 3.89-3.79 (m, 2H), 3.78-3.58 (m, 2H), 3.24-3.11 (m, 3H), 3.10-2.98 (m, 1H), 2.83-2.60 (m, 4H), 2.51 (s, 3H), 2.34-2.26 (m, 2H), 2.06 (td, $J = 11.4, 3.3$ Hz, 1H), 1.94-1.82 (m, 1H), 1.55-1.39 (m, 4H), 1.37-1.26 (m, 4H).

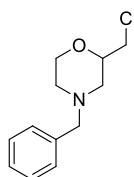
$^{13}\text{C-NMR}$ (101 MHz, CD_2Cl_2): δ [ppm] = 155.5 (1 C), 146.3 (1 C), 144.9 (1 C), 136.7 (1 C), 134.5 (1 C), 129.1 (1 C), 128.9 (1 C), 127.7 (1 C), 126.1 (1 C), 120.7 (1 C), 120.5 (1 C), 120.0 (1 C), 85.5 (1 C), 83.8 (1 C), 76.8 (1 C), 74.8 (0.5 C), 74.6 (0.5 C), 67.0 (1 C), 56.5

2.2. Synthesis and Initial Characterization of a Pseudo-irreversible, Selective Inhibitor of Human Butyrylcholinesterase as PET Tracer

(1 C), 54.38 (1 C), 54.33 (1 C), 54.26 (1 C),
53.8 (1 C), 53.4 (1 C), 48.3 (1 C), 41.5 (1 C),
38.2 (1 C), 30.2 (1 C), 29.0 (1 C), 27.4 (1 C),
27.0 (1 C), 26.8 (1 C).

MS (ESI): $[M+H]^+$ calculated for $C_{29}H_{39}FN_4O_3 = 511.31$, found 511.15; HPLC: $t_R = 6.74$ min, 97.5% purity.

Synthesis of 4-Benzyl-2-(chloromethyl)morpholine



2-(benzylamino)ethan-1-ol (**32**) (4.72 mL, 5 g, 33.7 mmol, 1 eq) and epichlorohydrin (2.59 mL, 3.06 g, 33.7 mmol, 1 eq) were mixed and stirred together for 3 h at room temperature until TLC ($CH_2Cl_2/MeOH = 95/5$; $R_f(\text{intermediate}) = 0.42$) indicated complete conversion. Then concentrated sulfuric acid ($V = 6.5$ mL) was added dropwise and the resulting mixture was heated up to $140^\circ C$ for 1 h. The mixture was allowed to cool down to room temperature and poured onto ice. The pH value was adjusted to $pH = 9$ with aqueous sodium hydroxide solution (5 M). The separated oil was extracted with three portions of toluene. The combined organic layers were washed with water and brine, dried over sodium sulphate, filtered, and evaporated to dryness in vacuo. NMR data indicated sufficient purity. 4-Benzyl-2-(chloromethyl)morpholine (5.11 g, 22.6 mmol, 67%) was obtained as pale yellow oil.

1H -NMR (400 MHz, $CDCl_3$): δ [ppm] = 7.30-7.15 (m, 5H), 3.88-3.79 (m, 1H), 3.74-3.58 (m, 2H), 3.48-3.36 (m, 4H), 2.82-2.72 (m, 1H), 2.62-2.52 (m, 1H), 2.14 (td, $J = 11.3, 3.3$ Hz, 1H), 1.94 (dd, $J = 11.1, 9.8$ Hz, 1H).

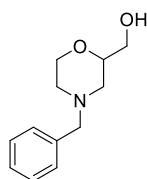
^{13}C -NMR (101 MHz, $CDCl_3$): δ [ppm] = 137.6 (1C), 129.2 (2C), 128.4 (2C), 127.4 (1C), 75.2 (1C), 66.9 (1C), 63.3 (1C), 56.0 (1C), 52.82 (1C), 45.0 (1C).

MS (ESI): $[M+H]^+$ calculated for $C_{12}H_{16}ClNOH = 227.10$; found 227.15;

TLC: petroleum ether/ethyl acetate = 1/1, $R_f = 0.6$.

2.2. Synthesis and Initial Characterization of a Pseudo-irreversible, Selective Inhibitor of Human Butyrylcholinesterase as PET Tracer

Synthesis of (4-benzylmorpholin-2-yl)methanol (**38**)



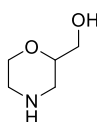
A solution of 4-benzyl-2-(chloromethyl)morpholine (2 g, 8.86 mmol, 1 eq) in formamide ($V = 20$ mL) was prepared and water ($V = 5$ mL) was added. The resulting mixture was heated up to 145°C for 20 h. Then the reaction was stopped and the reaction mixture was cooled down to room temperature. Water was added and the aqueous layer was extracted with three portions of ethyl acetate. The combined organic layers were washed with water and brine, dried over sodium sulphate, filtered, and evaporated to dryness in vacuo. The oily residue was purified by manual flash column chromatography ($\text{CH}_2\text{Cl}_2/\text{MeOH} = 95/5$, $R_f = 0.32$) to yield 4-(benzylmorpholine-2-yl)methanol (**38**) (1.71 g, 8.25 mmol, 93%) as colorless oil.

$^1\text{H-NMR}$ (400 MHz, CDCl_3): δ [ppm] = 7.26-7.14 (m, 5H), 3.86-3.78 (m, 1H), 3.68-3.37 (m, 6H), 2.64-2.56 (m, 2H), 2.12 (td, $J = 11.4, 3.3$ Hz, 1H), 1.93 (dd, $J = 11.4, 10.0$ Hz, 1H).

$^{13}\text{C-NMR}$ (101 MHz, CDCl_3): δ [ppm] = 137.7 (1C), 129.3 (2C), 128.4 (2C), 127.4 (1C), 76.1 (1C), 66.8 (1C), 64.4 (1C), 63.5 (1C), 54.7 (1C), 53.2 (1C).

MS (ESI): $[\text{M}+\text{H}]^+$ calculated for $\text{C}_{12}\text{H}_{17}\text{NO}_2\text{H} = 208.14$; found 208.05.

Synthesis of morpholin-2-ylmethanol (**39**)



To a solution of 4-(benzylmorpholine-2-yl)methanol (**38**) (700 mg, 3.38 mmol, 1 eq) in methanol ($V = 20$ mL), palladium on activated charcoal (10% Pd) (100 mg, 14 wt.-%) and formic acid ($V = 0.2$ mL) were added. The atmosphere was replaced with hydrogen using a balloon (1 atm) and the resulting mixture was stirred for 1 h at room temperature until TLC indicated the full conversion of the starting material. Then the catalyst was filtered off over a pad of celite. The celite was washed with methanol and

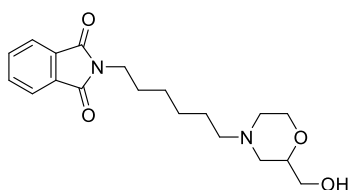
2.2. Synthesis and Initial Characterization of a Pseudo-irreversible, Selective Inhibitor of Human Butyrylcholinesterase as PET Tracer

the filtrate was evaporated to dryness in vacuo. Morpholin-2-ylmethanol (**39**) (550 mg, 3.37 mmol, quant.) was obtained as its formiate salt (colorless oil) and was used without further purification.

TLC: CH₂Cl₂/MeOH = 95/5; R_f = 0.05.

MS (ESI): [M+H]⁺ calculated for C₅H₁₁NO₂H = 118.09; found 118.15.

Synthesis of 2-(6-(2-(hydroxymethyl)morpholino)hexyl)isoindoline-1,3-dione



Morpholine-2-ylmethanol formiate (**39**) (500 mg, 3.06 mmol, 1 eq) was dissolved in dimethylformamide and diisopropylethylamine (V = 1.56 ml, 1.19 g, 9.18 mmol, 3 eq) and 2-(6-bromohexyl)isoindoline-1,3-dione (1044 mg, 3.37 mmol, 1.1 eq) were added. The solution was heated up to 100°C for 20 h. After that, the reaction mixture was cooled down to room temperature and water was added. The aqueous layer was extracted with three portions of ethyl acetate. The combined organic layers were washed with water and brine, dried over sodium sulphate, filtered, and evaporated to dryness under reduced pressure. The residue was purified by flash column chromatography (Ø = 3 cm, h = 15 cm, V = 20 mL, CH₂Cl₂/MeOH = 95/5, R_f = 0.22) to yield 2-{6-[2-(hydroxymethyl)morpholino]hexyl}isoindoline-1,3-dione (700 mg, 2.02 mmol, 66%) as colorless oil.

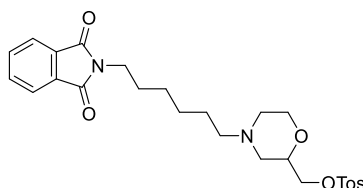
¹H-NMR (400 MHz, CDCl₃): δ [ppm] = 7.86-7.79 (m, 2H), 7.73-7.64 (m, 2H), 3.98-3.83 (m, 1H), 3.80-3.49 (m, 4H), 2.78-2.61 (m, 2H), 2.39-2.25 (m, 2H), 2.17-2.02 (m, 2H), 2.02-1.83 (m, 2H), 1.7-1.59 (m, 2H), 1.57-1.41 (m, 2H), 1.42-1.30 (m, 4H).

¹³C-NMR (101 MHz, CDCl₃): δ [ppm] = 168.6 (2C), 134.0 (2C), 132.3 (2C), 123.3 (2C), 76.0 (1C), 66.7 (1C), 64.5 (1C), 59.0 (1C), 54.9 (1C), 53.3 (1C), 38.1 (1C), 28.6 (1C), 27.1 (1C), 26.9 (1C), 26.5 (1C).

MS (ESI): [M+H]⁺ calculated for C₁₉H₂₆N₂O₄ = 347.20, found 347.05.

2.2. Synthesis and Initial Characterization of a Pseudo-irreversible, Selective Inhibitor of Human Butyrylcholinesterase as PET Tracer

Synthesis of (4-(6-(1,3-dioxoisindolin-2-yl)hexyl)morpholin-2-yl)methyl 4-methylbenzenesulfonate (**40**)



Triethylamine ($V = 197 \mu\text{L}$, 144 mg, 1.42 mmol, 1.2 eq) was added to a solution of 2-{6-[2-(hydroxymethyl)morpholino]hexyl}isoindoline-1,3-dione (410 mg, 1.18 mmol, 1 eq) in dry dichloromethane ($V = 10 \text{ mL}$). After addition of *p*-toluenesulfonyl chloride (271 mg, 1.42 mmol, 1.2 eq) the solution was stirred for 20 h at room temperature. The reaction was stopped by addition of water and the layers were separated. The aqueous phase was extracted with two portions of dichloromethane. The combined organic layers were washed with water, saturated sodium hydrogen carbonate solution and brine, then dried over sodium sulphate, filtered and evaporated to dryness in vacuo. The residue was purified by manual flash column chromatography ($\text{CH}_2\text{Cl}_2/\text{MeOH} = 98/2$, $R_f = 0.31$) to yield 4-{6-[1,3-dioxoisindolin-2-yl]hexyl}morpholin-2-yl}methyl 4-methylbenzenesulfonate (**40**) (417 mg, 0.83 mmol, 71%) as colorless oil.

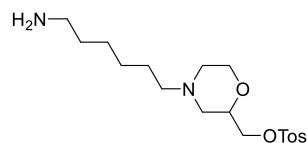
$^1\text{H-NMR}$ (400 MHz, CDCl_3): δ [ppm] = 7.86-7.81 (m, 2H), 7.81-7.76 (m, 2H), 7.74-7.68 (m, 2H), 7.36-7.31 (m, 2H), 4.06-3.93 (m, 2H), 3.83-3.63 (m, 4H), 3.64-3.52 (m, 1H), 2.70 (d, $J = 11.1 \text{ Hz}$, 1H), 2.62 (d, $J = 11.4 \text{ Hz}$, 1H), 2.32-2.22 (m, 2H), 2.10-2.00 (m, 1H), 1.84 (t, $J = 10.6 \text{ Hz}$, 1H), 1.73-1.61 (m, 3H), 1.48-1.39 (m, 2H), 1.39-1.29 (m, 6H).

$^{13}\text{C-NMR}$ (101 MHz, CDCl_3): δ [ppm] = 168.6 (2C), 145.0 (1C), 134.0 (2C), 133.0 (1C), 132.3 (2C), 130.0 (2C), 128.2 (2C), 123.3 (2C), 73.0 (1C), 70.5 (1C), 66.8 (1C), 58.8 (1C), 54.8 (1C), 53.6 (1C), 52.9 (1C), 38.0 (1C), 28.6 (1C), 27.0 (1C), 26.8 (1C), 26.4 (1C), 21.8 (1C).

MS (ESI): $[\text{M}+\text{H}]^+$ calculated for $\text{C}_{26}\text{H}_{32}\text{N}_2\text{O}_6\text{SH} = 501.21$; found 501.15.

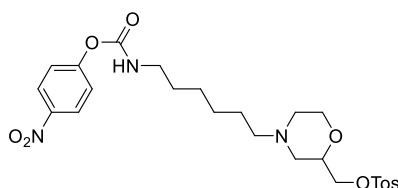
2.2. Synthesis and Initial Characterization of a Pseudo-irreversible, Selective Inhibitor of Human Butyrylcholinesterase as PET Tracer

Synthesis of (4-(6-aminohexyl)morpholin-2-yl)methyl-4-methylbenzenesulfonate (**41**)



Hydrazine hydrate ($V = 0.2$ mL) was added to a solution of 4-{6-[1,3-dioxisoindolin-2-yl]hexyl}morpholin-2-yl}methyl 4-methylbenzenesulfonate (**40**) (193 mg, 0.39 mmol) in ethanol ($V = 20$ mL). The resulting mixture was heated up to 80°C and stirred for 1.5 h. After that, the solution was cooled down to room temperature and the precipitated solid was filtered off. The filtrate was evaporated to dryness under reduced pressure and the residue was triturated with dichloromethane, filtered and evaporated to dryness under reduced pressure to yield [4-(6-aminohexyl)morpholin-2-yl]methyl 4-methylbenzenesulfonate (**41**) (126 mg, 0.34 mmol, 88%) as colorless oil which was used without further purification.

Synthesis of (4-(6-(((4-nitrophenoxy)carbonyl)amino)hexyl)morpholin-2-yl)methyl-4-methylbenzenesulfonate

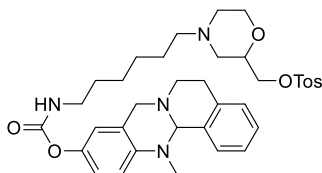


A solution of [4-(6-aminohexyl)morpholin-2-yl]methyl-4-methylbenzenesulfonate (**41**) (377 mg, 1.02 mmol, 1 eq) in dry dichloromethane ($V = 10$ mL) was prepared and triethylamine ($V = 162$ μL , 123 mg, 1.22 mmol, 1.2 eq) was added. Finally 4-nitrophenylchloroformate was added and the resulting solution was stirred for 3 h at room temperature. After TLC indicated the completion of reaction, the solvent was evaporated under reduced pressure and the residue was purified by flash column chromatography ($\text{CH}_2\text{Cl}_2/\text{MeOH} = 98/2$, $R_f = 0.15$) to yield [4-(6-(((4-nitrophenoxy)carbonyl)amino)hexyl)morpholin-2-yl]methyl 4-methylbenzenesulfonate (302 mg, 0.56 mmol, 55%) as yellow oil.

Due to the high instability of the title compound, the compound was used directly in the next step.

2.2. Synthesis and Initial Characterization of a Pseudo-irreversible, Selective Inhibitor of Human Butyrylcholinesterase as PET Tracer

Synthesis of (4-(6-(((13-methyl-5,8,13,13a-tetrahydro-6H-isoquinolino[1,2-b]-quinazolin-10-yl)oxy)carbonyl)amino)hexyl)morpholin-2-yl)methyl 4-methylbenzenesulfonate (**42**)



To a solution of [4-(6-(((4-nitrophenoxy)carbonyl)amino)hexyl)morpholin-2-yl)methyl 4-methylbenzenesulfonate (117 mg, 0.22 mmol, 1.2 eq) in dry dichloromethane ($V = 10$ mL), 13-methyl-5,8,13,13a-tetrahydro-6H-isoquinolino[1,2-b]quinazolin-10-ol (52 mg, 0.20 mmol, 1 eq) and sodium hydride (60% in paraffin oil, 13 mg, 0.33 mmol, 1.65 eq) were added. The resulting mixture was stirred for 2 h at room temperature. After that, water was added and the aqueous layer was extracted with three portions of dichloromethane. The combined organic layers were washed with water, two portions of saturated, aqueous sodium hydrogen carbonate solution, and brine, then dried over sodium sulphate. The solvent was evaporated to dryness under reduced pressure. The residue was purified by flash column chromatography (petroleum ether/ethyl acetate = 1/1, $R_f = 0$ to remove unreacted 13-methyl-5,8,13,13a-tetrahydro-6H-isoquinolino[1,2-b]quinazolin-10-ol ($R_f = 0.5$), then $\text{CH}_2\text{Cl}_2/\text{MeOH} = 98/2$, $R_f = 0.12$) to yield {4-[6-(((13-methyl-5,8,13,13a-tetrahydro-6H-isoquinolino[1,2-b]quinazolin-10-yl)oxy)carbonyl)-amino)hexyl)morpholin-2-yl)methyl 4-methylbenzenesulfonate (**42**) (122 mg, 0.18 mmol, 94%) as colorless oil.

$^1\text{H-NMR}$ (400 MHz, CDCl_3): δ [ppm] = 7.81-7.76 (m, 2H), 7.40-7.36 (m, 1H), 7.35-7.31 (m, 2H), 7.24-7.19 (m, 2H), 7.17-7.13 (m, 1H), 6.91-6.87 (m, 2H), 6.78-6.75 (m, 1H), 4.84 (s, 1H), 4.00 (qd, $J = 10.4, 5.1$ Hz, 3H), 3.90-3.75 (m, 3H), 3.71-3.58 (m, 2H), 3.33-3.18 (m, 3H), 3.18-3.02 (m, 1H), 2.91-2.64 (m, 2H), 2.58 (s, 3H), 2.42 (s, 3H), 2.33 (dd, $J = 7.5, 5.2$ Hz, 2H), 2.17-2.06 (m, 1H), 1.99-1.87 (m, 1H), 1.61-1.43 (m, 4H), 1.42-1.28 (m, 6H).

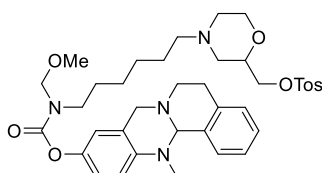
$^{13}\text{C-NMR}$ (101 MHz, CDCl_3): δ [ppm] = 155.3 (1C), 145.9 (1C), 145.0 (1C), 144.4 (1C), 136.1 (1C), 134.0 (1C), 133.0 (1C),

2.2. Synthesis and Initial Characterization of a Pseudo-irreversible, Selective Inhibitor of Human Butyrylcholinesterase as PET Tracer

130.0 (2C), 128.92 (1C), 128.86 (1C), 128.1 (2C), 127.6 (1C), 125.9 (1C), 125.3 (1C), 120.4 (1C), 120.1 (1C), 119.7 (1C), 77.4 (1C), 72.9 (1C), 70.4 (1C), 66.6 (1C), 58.8 (1C), 56.3 (1C), 54.7 (1C), 52.9 (1C), 47.9 (1C), 41.2 (1C), 38.0 (1C), 29.9 (1C), 28.7 (1C), 27.1 (1C), 26.7 (1C), 26.3 (1C), 21.8 (1C).

MS (ESI): $[M+H]^+$ calculated for $C_{36}H_{46}N_4O_6SH$ = 663.32; found 663.20; HPLC: R_t = 6.74 min, purity = 97.5%.

Synthesis of (4-(6-((methoxymethyl)((13-methyl-5,8,13,13a-tetrahydro-6H-isoquinolino[1,2-b]quinazolin-10-yl)oxy)carbonyl)amino)hexyl)morpholin-2-yl)methyl 4-methylbenzenesulfonate (**44**)



To a solution of {4-[6-({[(13-methyl-5,8,13,13a-tetrahydro-6H-isoquinolino[1,2-b]quinazolin-10-yl)oxy]carbonyl)amino]hexyl]morpholin-2-yl}methyl-4-methylbenzenesulfonate (**12**) (51 mg, 77 μ mol, 1 eq) in dry dichloromethane (V = 5 mL), paraformaldehyde (3.5 mg, 115 μ mol, 1.5 eq) and fresh trimethylsilyl chloride (V = 29.3 μ L, 25.1 mg, 231 μ mol, 3 eq) were added. The resulting mixture was stirred for 18 h at room temperature. After that, methanol (V = 2 mL) was added and the mixture was stirred at room temperature for 1 h. Saturated sodium hydrogen carbonate solution was added afterwards and the aqueous layer was extracted with three portions of dichloromethane. The combined organic layers were washed with water and brine, dried over sodium sulphate and filtered. The solvent was removed under reduced pressure. The residue was purified by flash column chromatography (CH_2Cl_2 /methanol = 98/2, R_f = 0.15) to yield (4-{6-[(methoxymethyl){[(13-methyl-5,8,13,13a-tetrahydro-6H-isoquinolino[1,2-b]quinazolin-10-yl)oxy]carbonyl)amino]hexyl}morpholin-2-yl)methyl 4-methylbenzenesulfonate (**44**) (46 mg, 65 μ mol, 84%) as colorless oil.

1H -NMR (400 MHz, CD_2Cl_2): δ [ppm] = 7.80-7.75 (m, 2H), 7.42-7.35 (m, 3H), 7.27-7.20 (m, 2H), 7.19-7.14 (m, 1H), 6.95-6.85 (m, 2H), 6.79-6.74 (m, 1H), 4.88-4.73 (m, 3H),

2.2. Synthesis and Initial Characterization of a Pseudo-irreversible, Selective Inhibitor of Human Butyrylcholinesterase as PET Tracer

4.04-3.93 (m, 3H), 3.89 (d, $J = 15.7$ Hz, 1H), 3.78 (d, $J = 11.3$ Hz, 1H), 3.73-3.66 (m, 1H), 3.56 (t, $J = 10.8$ Hz, 1H), 3.47-3.31 (m, 5H), 3.29-3.20 (m, 1H), 3.13-3.02 (m, 1H), 2.82 (dt, $J = 9.6, 4.6$ Hz, 1H), 2.76-2.59 (m, 3H), 2.56 (s, 3H), 2.45 (s, 3H), 2.33-2.24 (m, 2H), 2.05 (t, $J = 10.7$ Hz, 1H), 1.82 (t, $J = 10.6$ Hz, 1H), 1.76-1.58 (m, 2H), 1.52-1.26 (m, 6H).

^{13}C -NMR (101 MHz, CD_2Cl_2): δ [ppm] = 155.7 (1C), 146.1 (1C), 145.2 (1C), 144.6 (1C), 136.4 (1C), 134.2 (1C), 132.9 (1C), 129.9 (2C), 128.8 (1C), 128.6 (1C), 128.0 (2C), 127.4 (1C), 125.8 (2C), 120.3 (1C), 120.0 (1C), 119.6 (1C), 79.3 (0.5C), 79.1 (0.5C), 76.5 (1C), 73.0 (1C), 70.7 (1C), 66.6 (1C), 58.7 (1C), 56.1 (1C), 55.6 (0.5C), 55.4 (0.5C), 54.6 (1C), 52.9 (1C), 47.9 (1C), 37.8 (1C), 28.6 (1C), 27.1 (1C), 26.8 (1C), 26.5 (1C), 21.4 (1C).

MS (ESI): $[\text{M}+\text{H}]^+$ calculated for $\text{C}_{38}\text{H}_{50}\text{N}_4\text{O}_7\text{SH} = 707.35$; found 707.20; HPLC: $R_t = 8.66$ min, purity 95.5%.

Colorimetric Ellman's assay

hAChE (EC 3.1.1.7, from human erythrocytes), DTNB (Ellman's reagent), ATCI and BTCl were purchased from Sigma-Aldrich. *hBChE* (E.C. 3.1.1.8) was kindly donated by Dr. Oksana Lockridge, Nebraska Medical Centre. For the assays, the inhibitors were dissolved in ethanol (absolute, reagent grade, Ph. Eur.) to give a concentration of 3.33 mM (100 μM in the assay) and stepwise diluted to 3.33 nM (0.1 nM in the assay). The buffer was prepared from 3.12 g of potassium dihydrogen phosphate in 500 mL of doubly distilled water. After the potassium dihydrogen phosphate was dissolved, the pH value was adjusted 8.0 with 0.1 M sodium hydroxide solution. Both enzymes were dissolved in assay buffer and diluted to 2.5 units/mL. The solutions were stabilized with 1 mg/mL of bovine serum albumin (Sigma-Aldrich) and were stored at 7°C until usage. DTNB was dissolved in buffer at 10 mM (0.3 mM in the assay). The substrates ATCI and BTCl

2.2. Synthesis and Initial Characterization of a Pseudo-irreversible, Selective Inhibitor of Human Butyrylcholinesterase as PET Tracer

were prepared with a concentration of 75 mM (452 μ M in the assay) in assay buffer and kept frozen until usage. The absorbance of probes was measured with a Shimadzu UVmini-1240 spectrometer at 412 nm.

IC₅₀ determination: The assay was carried out at room temperature (25 °C). Thereby, 900 μ L of the buffer, 30 μ L of DTNB solution (10 mM, 0.3 mM in the assay) and 30 μ L of enzyme solution (*hAChE* or *hBChE*, 2.5 units/mL) were mixed in a cuvette. The incubation was started directly after the addition of 30 μ L of solutions of inhibitor **37** (scheme 7) in different concentrations. The solutions were mixed well by manual stirring. After 20 min incubation, 6 μ L of substrate solution (ATCI or BTCl; 75 mM, 452 μ M in the assay) were added. The mixture was left for 2.5 min to allow substrate hydrolysis, and the absorbance was measured at $\lambda = 412$ nm, whereas enzyme activity was determined three times for every concentration with at least seven different concentrations. A blank value was determined by replacing the enzyme solution with buffer, the compound solution was replaced with ethanol. The maximum enzyme activity was determined with 30 μ L of ethanol instead of the compound solution. 10% of ethanol did not reduce enzyme activity. The enzyme activity in percent of maximum activity was plotted against the logarithmic inhibitor concentration, from which IC₅₀ values were calculated with the software GraphPad Prism 5.

Kinetic studies

For determination of K_c and k_3 values, the same general setup was used (900 μ L of the assay buffer, 30 μ L of DTNB solution (10 mM, 0.3 mM in the assay), and 30 μ L of *hBChE* solution (2.5 units/mL) were mixed at room temperature). Then, 30 μ L of solutions of inhibitor **37** (scheme 7) in different concentrations were added, but enzyme activity was determined after 1, 2, 4, 6, 10, 15, 20, 30, and 40 min of incubation by addition of 6 μ L of BTCl solution (75 mM, 452 μ M in the assay). The absorbance at $\lambda = 412$ nm was measured after 2.5 min. All concentrations were measured three times, at least five different concentrations were measured for at least seven time points. The obtained enzyme activities in percent of maximum enzyme activity were plotted in a time-dependent manner and fitted to the following equation (cf. chapter 2.2.3.) to determine the rate constant k_{obs} using the software GraphPad Prism 5.

$$A = A_0 \cdot e^{-k_{obs} \cdot t} + A_\infty$$

The obtained inverse rate constants k_{obs} were plotted against the reciprocal concentration $[I]^{-1}$, and k_3 was calculated from the y-intercept of the resulting curve,

2.2. Synthesis and Initial Characterization of a Pseudo-irreversible, Selective Inhibitor of Human Butyrylcholinesterase as PET Tracer

and K_c from the slope of the resulting linearization according to the following equation (cf. chapter 2.2.3.) using the software GraphPad Prism 5.

$$\frac{1}{k_{obs}} = \frac{K_c}{k_3} \cdot \frac{1}{[I]} + \frac{1}{k_3}$$

For the measurement of decarbamylation kinetics, the enzyme was incubated with inhibitor **37** (scheme 7) to carbamoylate > 85% of the enzyme. After 1 h, the solution was diluted 1000-fold to stop any further carbamoylation. The enzyme activity was measured at several (at least 8) time points. For the determination of full enzyme activity, a batch of the enzyme was treated with ethanol instead of inhibitor solution and diluted 1000-fold in the same manner. The enzyme activity in percent was plotted against time after dilution to give the first-order rate constant k_4 according to the following equation (cf. chapter 2.2.3.) using the software GraphPad Prism 5.

$$A = (1 - e^{-k_4 \cdot t}) \cdot (1 - A_0) + A_0$$

All experiments were carried out in triplicates.

Radiochemistry

Solvents and chemicals were purchased from Sigma-Aldrich and directly used without further purification. $[^{18}\text{F}]\text{F}^-$ was produced by a cyclotron (GE Medical Systems, Uppsala) at the Department of Nuclear Medicine of the University Hospital of Würzburg. Enriched $[^{18}\text{O}]\text{H}_2\text{O}$ was irradiated with protons to produce $[^{18}\text{F}]\text{F}^-$ and radiofluorination was carried out manually. HPLC was used for purification and analyses of radioactive products (Shimadzu system equipped with UV detector, $\lambda=220$ and 254 nm, and γ -detector). The purified radiotracer $[^{18}\text{F}]\text{-37}$ (scheme 9) was diluted with either PBS or saline to the corresponding concentration for further evaluation.

13-Methyl-5,8,13,13a-tetrahydro-6*H*-isoquinolino[1,2-*b*] quinazolin-10-yl-{6-[2-([^{18}F]-fluoromethyl)morpholino]-hexyl}carbamate ($[^{18}\text{F}]\text{-37}$): $[^{18}\text{F}]\text{F}^-$ was separated from $[^{18}\text{O}]\text{H}_2\text{O}$ by an anion exchange cartridge (Sep-Pak QMA Cartridge) and eluted with 0.5 mL of 25 mM potassium carbonate and 50 mM Kryptofix₂₂₂ solution in MeCN/H₂O (6 : 2) into a V-vial. The solution was dried at 120°C under a nitrogen flow, which was repeated twice with 500 μL of anhydrous acetonitrile. Labeling was carried out using 1.3 mg of precursor **44** (scheme 8) dissolved in 0.4 mL of anhydrous MeCN at 110°C for 20 min, followed by addition of 100 μL of hydrochloric acid (6 M) with further 5 min heating at 90°C. After addition of 500 μL of 1 M aqueous sodium hydrogen carbonate

2.2. Synthesis and Initial Characterization of a Pseudo-irreversible, Selective Inhibitor of Human Butyrylcholinesterase as PET Tracer

solution and 10 mL of water to quench the reaction, the crude product was trapped on a Sep-Pak light C18, which was washed with 5 mL of water and eluted with 0.5 mL of ethanol. The crude radiotracer was purified via semi-preparative HPLC. Column: 10x100 mm C18 Phenomenex Onyx Monolithic, Mobile phase: Phase A: H₂O, Phase B: MeCN, 0-20 min, 20% → 80% B, 20-26 min, 95% B, 28-30 min 20% B, Flow rate: 1.5 ml/min. The collected fraction was diluted with 10 mL of water and trapped on a Sep-Pak light C18, which was dried with 5 mL of air and eluted with 0.3 mL ethanol. The total radiolabeling procedure was feasible in 180 min in a radiochemical yield of 13% (corrected for decay). Sufficient radiochemical purity was determined by TLC autoradiography (95.3 %).

Ex vivo autoradiography on mice brain slices

Ex vivo tissue binding studies were carried out with one C57BL/6 N mouse from Charles River. Two series of horizontal brain slices with 20 µm thickness were prepared for either control or blocking group. A buffer (150 mM NaCl, 5 mM EDTA, 50 mM Na₂HPO₄, pH 8.0) containing [¹⁸F]-**37** (A=1.44 MBq) with or without ethopropazine hydrochloride (60 µM) as blocking agent was prepared for incubation with the mice brain slices. Slices were incubated for 30 min at 25°C and then rinsed five times in PBS buffer (1 min each time). The slices were dried at room temperature and exposed to a phosphor imaging plate (GE healthcare, BAS IP MS 2025 E, Munich, Germany). Images were produced with a digital autoradiographic system (Typhoon FLA 7000).

In vivo PET imaging

A healthy, male Wistar rat was anesthetized and maintained with isoflurane for *in vivo* PET imaging using a micro PET system (FOCUS, Siemens, Erlangen, Germany). A 60-min dynamic imaging protocol was started directly after the injection of a solution of [¹⁸F]-**37** (5% ethanol in saline, 6.3 MBq). Analysis of the obtained PET images was performed with the public domain tool AMIDE imaging software (A Medical Imaging Data Examiner, version 1.01) and time-activity curves of regions of interest were generated.

All applicable international, national, and/or institutional guidelines for the care and use of animals were followed. Animal protocols were approved by the local Animal Care and Use Committee (approval no. 15063) and conducted according to the Guide for the Care and Use of Laboratory Animals.

3. Summary

The present thesis concerns the molecular imaging of ORs and *h*BChE with the aid of tailored probes, which are suitable for the respective applied imaging techniques. The first part focusses on imaging of ORs with selective probes using TIRF- and SM microscopy. Initially, a pair of fluorescent probes for the MOP was designed based on the potent and selective, irreversible ligand CACO.^[92] A tetraglycine linker was attached at the C6 position of the CACO scaffold and the sulfo-cyanine dyes Cy3 and Cy5 were coupled at the end of the linker in a synthesis of seven steps, starting from thebaine. The dyes were chosen due to their relatively small size, high photostability, quantum yields and absorption coefficients, and minor potential to induce non-specific binding.^[94] The respective fluorescent probes exhibited retained selectivity over the other OR subtypes, as measured in a HTRF assay for the Cy5 derivative. Binding affinity was expectedly decreased due to the synthetic modifications on the pharmacologically active part, but still in the nanomolar range. The Cy3 derivative of CACO acted as partial agonist in an IP1 accumulation assay and was inactive in a β -arr-2 recruitment assay. Both fluorescent ligands exhibited wash resistance in a wash-out assay, likely due to a *p*-nitrocinnamoylamino side chain forming a covalent bond on the receptor.^[92] The Cy3 derivative of CACO was used in SMM experiments to investigate the diffusion behavior of wild-type MOP on the surface of CHO cells. Receptor movement was heterogenous and classified into four categories (immobile, normal-, sub-, and super-diffusion). The percentages of receptors in each category were in good agreement with the diffusion profile of other GPCRs.^[106] Finally, the pair of fluorescent ligands was used in two-color SMM experiments to investigate the homodimerization of wild-type MOP. The results revealed a small, consistent fraction of homodimers (4-5%) with a lifetime of 1-2 s, that stopped diffusing during their interaction. Importantly, the dimerization was not forced due to recruitment of two individual receptors to CCPs, which was proved with a SMM experiment using co-transfected CHO cells, that express wild-type MOP and GFP tagged clathrin. An estimation of the mono- and dimeric MOP fraction in relation to the receptor density on the plasma membrane revealed, that a density of approximately 27 receptor particles per μm^2 would produce a dimer-fraction of ~50%. The density of MOP expressed by the transfected CHO cells was only 1.7 particles / μm^2 . The required receptor densities

3. Summary

for ~50% MOP dimers can be achieved at synapses,^[111-113] meaning a pronounced fraction of dimers could exist *in vivo*.^[114]

Next, three ligands were synthesized, that had been described to selectively target OR heterodimers. These ligands should serve as tools to investigate the extent of heterodimerization between the three different OR subtypes. 6'-GNTI was described to bind to the DOP/KOP heterodimer and exhibited the highest binding affinities on the respective homomers in radioligand binding studies.^[73] The ligand acted as agonist on the KOP in the IP1 accumulation assay and exhibited minor potential to recruit β -arr-2. NNTA was described as potent agonist on MOP/KOP heterodimers.^[77] Its binding affinity was highest on the respective OR protomers. Interestingly, it acted as full agonist on all three OR subtypes in the IP1 accumulation assay. The potential to recruit β -arr-2 was highest on the KOP and minor on the DOP, while β -arr-2 recruitment could not be determined on the MOP. INTA was described to target both possible KOP heterodimers and is a close derivative of NNTA.^[125] Indeed, its profile of binding affinity was similar, however, with a two-fold increased K_i value on the DOP. INTA also acted as agonist on all three OR subtypes in the IP1 accumulation assay and β -arr-2 recruitment appeared mainly on the KOP but was also increased on the DOP compared to NNTA. Altogether, these ligands could represent interesting tools for SMM to investigate the role of agonists on heterodimerization and clarify the influence of biased agonism and heterodimerization on the interesting pharmacological profile of the three ligands, since all three compounds were described to lack certain typical side effects of opioids.^[73, 77, 125]

The second part of this thesis focused on the development of ^{18}F -labeled, selective radiotracers for PET imaging of BChE. The first tracer was developed based on a reversible BChE inhibitor with excellent selectivity over AChE and high, nanomolar inhibitory potency.^[180] The replacement of a methoxy group with fluorine in the molecular structure of the sulfonamide-based inhibitor led to a significant decrease of potency, however, the value was still in the three-digit nanomolar range. The kinetics of the reversible binding mode were investigated and the dissociation constants for binding to the free- and acylated enzyme were measured. Binding potential was higher on the free enzyme and two-fold lower on the acylated enzyme with two-digit nanomolar values. Radiolabeling of a stabilized tosylate precursor in an established procedure based on nucleophilic substitution of the tosylate group with $^{18}\text{F}^-$ gave the respective radiotracer in a good radiochemical yield and purity in a reasonable time

3. Summary

frame. Subsequently, the tracer was investigated *ex vivo* for its binding to mice brain tissue using autoradiography, where it showed high, specific binding, even though off-target effects and/or non-specific binding could not be ruled out completely. Preliminary *in vivo* imaging of the tracer via micro-PET revealed low brain uptake, rapid enrichment in heart and lung and accumulation in liver tissue before excretion via intestine and urine.

Additionally, a carbamate-based pseudo-irreversible ^{18}F -PET tracer was developed based on a potent and selective *h*BChE inhibitor with long duration of action on the enzyme.^[195] The parent carbamate consisted of a tetracyclic, tetrahydroquinazoline based carrier scaffold and a morpholine moiety at the end of a hexylene linker, which is attached to the carbamate nitrogen and transferred onto the enzyme.^[195] A fluoromethyl-group was introduced on the morpholine moiety in a synthetic procedure of five steps, starting from epifluorohydrin and *N*-benzylaminoethanol. A respective MOM-protected tosylate precursor was developed and synthesized using a similar approach starting from epichlorohydrin and *N*-benzylaminoethanol. The cold, non-radioactive compound exhibited retained high inhibitory potency on *h*BChE in the two-digit nanomolar range and the kinetic values of the carbamoylation- and decarbamoylation step were not significantly altered as well. Radiolabeling was achieved by nucleophilic substitution of the tosylate group with $[^{18}\text{F}]\text{F}^-$ and subsequent MOM deprotection, which represented a novel, facile approach for the radiolabeling of sensitive carbamates. The tracer showed high and specific binding to mice brain tissue in *ex vivo* autoradiography experiments. However, some remaining activity despite blocking with the selective BChE inhibitor ethopropazine hydrochloride indicated potential off-target effects or non-specific binding due to the lipophilicity of the tracer. This result was similar as for the reversible ^{18}F -PET tracer. Moreover, analogous *in vivo* micro-PET experiments with the pseudo-irreversible tracer revealed a similar distribution profile as for the reversible tracer with little brain uptake and rapid enrichment in heart and lung, followed by accumulation in the liver, before excretion. Consequently, these results suggest that the design of substrate-type tracers for PET imaging of CNS BChE could be more straightforward since they usually can pass the BBB. The inhibitor-type tracers might be suitable for determining altered BChE activities in the organs with high tracer accumulation (e.g. heart and lung). Nevertheless, investigating the reasons for the limited brain uptake of both tracers should be the subject of future studies.

4. Zusammenfassung

Die vorliegende Arbeit beschäftigt sich mit der molekularen Bildgebung von Opioidrezeptoren und der humanen Butyrylcholinesterase mithilfe von maßgeschneiderten Verbindungen, die jeweils optimal geeignet für die angewendeten Bildgebungstechniken sind. Der erste Teil behandelt die Bildgebung von Opioidrezeptoren durch selektive Liganden mittels TIRF- und SM Mikroskopie. Zunächst wurden zwei Fluoreszenzliganden für den MOP designt, als Grundlage diente hierbei der potente und selektive, irreversible Ligand CACO.^[92] Ein Tetraglycin Linker wurde an die C6 Position der CACO Struktur angehängt und die Sulfo-cyanin Farbstoffe Cy3 und Cy5 wurden in einer siebenstufigen Synthese ausgehend von Thebain an das Ende des Linkers gekuppelt. Die Fluorophore wurden wegen ihrer relativ geringen Größe, ausgeprägter Photostabilität, hohen Quantenausbeuten und Absorptionskoeffizienten, und ihrem geringen Potenzial unspezifisch zu Binden ausgewählt.^[94] Die entsprechenden Fluoreszenzliganden behielten ihre Selektivität gegenüber den beiden anderen Opioidrezeptor-Subtypen bei, was mittels eines HTRF Assays mit dem Cy5-Derivat ermittelt wurde. Die Bindungsaffinität wurde erwartungsgemäß durch die synthetischen Modifikationen am pharmakologisch wirksamen Teil erniedrigt, lag aber dennoch im nanomolaren Bereich. Das Cy3 Derivat von CACO wirkte als Partialagonist in einem IP1-Anreicherungsassay und war inaktiv in einem β -arr-2-Rekrutierungsassay. Beide Fluoreszenzliganden wiesen Auswasch-Stabilität in einem entsprechenden Assay auf, was wahrscheinlich an der *p*-Nitrocinnamoylamino-Seitenkette liegt, die eine kovalente Bindung am Rezeptor ausbilden kann.^[92] Das Cy3-Derivat von CACO wurde in SMM Experimenten eingesetzt, um das Diffusionsverhalten des Wildtyp-MOP auf der Oberfläche von CHO Zellen zu untersuchen. Die Rezeptorbewegung war heterogen und wurde in vier Kategorien unterteilt (unbeweglich, normal-, sub-, und super-diffusiv). Der prozentuale Anteil der Rezeptoren in jeder Kategorie stimmte gut mit dem Diffusionsprofil anderer GPCRs überein.^[106] Schließlich wurde das Paar der Fluoreszenzliganden in Zwei-Farben-SMM-Experimenten eingesetzt, um die Homodimerisierung des Wildtyp MOP zu untersuchen. Die Ergebnisse offenbarten einen kleinen, beständigen Anteil von Homodimeren (4-5%) mit einer Lebenszeit von 1-2 s, die ihre Diffusion während der Interaktion unterbrachen. Die Dimerisierung war nicht durch die Rekrutierung von zwei Rezeptoren zur selben CCP forciert. Dies wurde in einem SMM Experiment mit co-

4. Zusammenfassung

transfizierten CHO Zellen, die den Wildtyp-MOP und GFP markiertes Clathrin exprimieren, überprüft. Eine Einschätzung des monomeren und dimeren MOP Anteils bezogen auf die Rezeptordichte in der Plasmamembran zeigte, dass eine Dichte von etwa 27 Rezeptoren pro μm^2 einen Dimer-Anteil von etwa 50% erzeugen würde. Die Dichte von MOPs, die von den transfizierten CHO Zellen exprimiert wurden, war lediglich 1.7 Rezeptoren / μm^2 . Die erforderliche Rezeptordichte für ~50% MOP Dimere kann an Synapsen erreicht werden,^[111-113] weshalb ein ausgeprägter Anteil von Dimeren *in vivo* existieren könnte.^[114]

Nachfolgend wurden drei Liganden synthetisiert, die selektiv an Opioidrezeptor-Heterodimeren binden. Diese Liganden sollten als Werkzeuge dienen, um das Ausmaß der Heterodimerisierung zwischen den drei verschiedenen Opioidrezeptor-Subtypen zu untersuchen. 6'-GNTI wurde als selektiver DOP/KOP Heterodimer-Ligand beschrieben und wies in Radioligand-Bindungsstudien die höchsten Affinitäten an den entsprechenden Rezeptor-Homomeren auf.^[73] Der Ligand stellte sich als KOP-Agonist im IP1-Anreicherungsassay heraus und wies ein sehr geringes Potenzial auf, β -arr-2 zu rekrutieren. NNTA wurde als potenter Agonist an MOP/KOP-Heterodimeren beschrieben.^[77] Die Bindungsaffinität war an den entsprechenden Protomeren am größten. Die Verbindung verhielt sich im IP1-Assay als Vollagonist an allen Opioidrezeptor-Subtypen. Das Potenzial, β -arr-2 zu rekrutieren, war am KOP am höchsten und geringfügig auch am DOP vorhanden, während β -arr-2 Rekrutierung am MOP nicht festgestellt werden konnte. INTA wurde als Ligand an beiden KOP-Heterodimeren beschrieben und ist ein strukturell nahes Derivat von NNTA.^[125] In der Tat waren die Bindungsaffinitäten ähnlich, allerdings mit einem zweifach höheren K_i am DOP. INTA war im IP1-Assay auch ein Agonist an allen Opioidrezeptor-Subtypen und β -arr-2 Rekrutierung wurde vor allem am KOP festgestellt, war aber im Vergleich zu NNTA auch am DOP erhöht. Insgesamt könnten diese Liganden interessante Werkzeuge für die SMM darstellen, um die Rolle von Agonisten bei der Opioidrezeptor-Heterodimerisierung zu untersuchen und den Einfluss von funktioneller Selektivität und Heterodimerisierung auf das interessante pharmakologische Profil dieser drei Liganden zu klären, da alle drei Verbindungen *in vivo* weniger typische Opioid-Nebenwirkungen aufwiesen.^[73, 77, 125]

Der zweite Teil der Arbeit beschäftigt sich mit der Entwicklung von ^{18}F -markierten, selektiven Radiotracern für die Bildgebung der BChE mittel PET. Der erste Tracer wurde auf Grundlage eines reversiblen BChE Inhibitors mit exzellenter Selektivität

4. Zusammenfassung

über die AChE und hoher, nanomolarer inhibitorischer Wirksamkeit entwickelt.^[180] Der Austausch einer Methoxy-Gruppe durch Fluor in der molekularen Struktur des sulfonamid-basierten Inhibitors führte zu einer signifikanten Abnahme der Wirksamkeit, aber der IC₅₀-Wert lag noch im dreistellig-nanomolaren Bereich. Die Kinetik des reversiblen Bindungsmechanismus wurde untersucht und Dissoziationskonstanten für das Binden an das freie und acylierte Enzym wurden gemessen. Das Bindungspotenzial war höher am freien Enzym und zweifach niedriger am acylierten Enzym mit jeweils zweistellig nanomolaren Werten. Die Radiomarkierung einer stabilisierten Vorstufe wurde in einem etablierten Verfahren auf Grundlage von nukleophiler Substitution der Tosylat-Gruppe mit [¹⁸F]F⁻ durchgeführt und ergab den entsprechenden Radiotracer in guter radiochemischer Ausbeute und Reinheit bei geringem Zeitaufwand. Anschließend wurde der Tracer *ex vivo* auf seine Bindung zu Mäusehirn-Gewebeschnitten mittels Autoradiographie untersucht, und zeigte ein hohes, spezifisches Binden, auch wenn off-target Effekte und/oder unspezifisches Binden nicht ganz ausgeschlossen werden konnten. Die vorläufige *in vivo* Bildgebung der Verteilung des Tracers mittels micro-PET offenbarte eine geringe Hirnaufnahme, eine schnelle Anreicherung in Herz und Lunge und Akkumulierung in der Leber vor der Ausscheidung über Darm und Urin.

Zusätzlich wurde ein carbamat-basierter, pseudo-irreversibler ¹⁸F-PET-Tracer entwickelt, der auf einem wirksamen, selektiven Inhibitor der hBChE mit langer Wirkdauer am Enzym basiert.^[195] Das Vorläufer-Carbamat bestand aus einem tetrazyklischen, Tetrahydrochinazolin-basierten "Träger"-Grundgerüst und einem Morpholin-Teil am Ende eines Hexyl-Linkers, der am Carbamat-Stickstoff angebracht ist und auf das Enzym übertragen wird.^[195] Eine Fluoromethyl-gruppe wurde in einer fünfstufigen Synthese ausgehend von Epifluorhydrin und *N*-Benzylaminoethanol an den Morpholin-Teil angefügt. Eine entsprechende MOM-geschützte Tosylat-Vorstufe wurde entwickelt und in einer ähnlichen Herangehensweise ausgehend von Epichlorhydrin und *N*-Benzylaminoethanol synthetisiert. Die kalte, nicht-radioaktive Verbindung behielt hohe inhibitorische Wirksamkeit an der hBChE im zweistellig-nanomolaren Bereich und die kinetischen Werte für den Carbamoylierungs- und Decarbamoylierungsschritt wurden auch nicht signifikant verändert. Die Radiomarkierung wurde durch nucleophile Substitution der Tosylat-Gruppe durch [¹⁸F]F⁻ und nachfolgender MOM-Entschützung erreicht, was eine neuartige, schnelle und einfache Herangehensweise für die Radiomarkierung von sensiblen Carbamaten

4. Zusammenfassung

darstellt. Der Tracer zeigte starkes, spezifisches Binden an Mäusehirn-Gewebeschnitten in *ex vivo* Autoradiografie-Experimenten, aber einige verbleibende Aktivität trotz Blockierung des Enzyms mit dem selektiven BChE Inhibitor Ethopropazin hydrochlorid deutete auf mögliche off-target Effekte und/oder unspezifisches Binden wegen der hohen Lipophilie des Tracers hin. Dieses Ergebnis war vergleichbar mit dem entsprechenden Experiment des reversiblen ^{18}F -PET Tracers. Darüber hinaus zeigte ein analoges *in vivo* micro-PET Experiment mit dem pseudo-irreversiblen Tracer ein ähnliches Verteilungsprofil mit geringer Hirnaufnahme und schneller Anreicherung in Herz und Lunge, gefolgt von Akkumulation in der Leber vor der Ausscheidung. Folglich deuten diese Ergebnisse an, dass das Design von substrat-basierten Tracern zur Bildgebung der BChE im zentralen Nervensystem unkomplizierter sein dürfte, da sie für gewöhnlich die Blut-Hirn Schranke passieren können. Die inhibitor-basierten Tracer könnten für die Bestimmung veränderter BChE Aktivitäten in den Organen mit hoher Anreicherung von Radioaktivität geeignet sein (z.B. Herz und Lunge). Trotzdem sollte die Untersuchung der Gründe für die geringe Hirnaufnahme beider inhibitor-basierten Radiotracer Gegenstand zukünftiger Studien sein.

References

1. Walwyn, W. M.; Miotto, K. A.; Evans, C. J. Opioid pharmaceuticals and addiction: The issues, and research directions seeking solutions. *Drug Alcohol Depend.* **2010**, *108* (3), 156–165.
2. Feng, Y.; He, X.; Yang, Y.; Chao, D.; Lazarus, L. H.; Xia, Y. Current research on opioid receptor function. *Curr. Drug Targets* **2012**, *13* (2), 230–246.
3. Filizola, M.; Devi, L. A. Grand opening of structure-guided design for novel opioids. *Trends Pharmacol. Sci.* **2013**, *34* (1), 6–12.
4. Cox, B. M.; Christie, M. J.; Devi, L.; Toll, L.; Traynor, J. R. Challenges for opioid receptor nomenclature: IUPHAR Review 9. *Br. J. Pharmacol.* **2015**, *172* (2), 317–323.
5. M. Waldhoer, S. E. Bartlett; Whistler, J. L. Opioid Receptors. *Annu. Rev. Biochem.* **2004**, *73* (1), 953–990.
6. Meunier, J.-C.; Mollereau, C.; Toll, L.; Suaudeau, C.; Moisand, C.; Alvinerie, P.; Butour, J.-L.; Guillemot, J.-C.; Ferrara, P.; Monsarrat, B.; Mazarguil, H.; Vassart, G.; Parmentier, M.; Costentin, J. Isolation and structure of the endogenous agonist of opioid receptor-like ORL1 receptor. *Nature* **1995**, *377* (6549), 532–535.
7. Reinscheid, R. K.; Nothacker, H.-P.; Bourson, A.; Ardati, A.; Henningsen, R. A.; Bunzow, J. R.; Grandy, D. K.; Langen, H.; Monsma, F. J.; Civelli, O. Orphanin FQ: A Neuropeptide That Activates an Opioidlike G Protein-Coupled Receptor. *Science* **1995**, *270* (5237), 792–794.
8. Mollereau, C.; Parmentier, M.; Mailleux, P.; Butour, J.-L.; Moisand, C.; Chalon, P.; Caput, D.; Vassart, G.; Meunier, J.-C. ORL1, a novel member of the opioid receptor family: Cloning, functional expression and localization. *FEBS Lett.* **1994**, *341* (1), 33–38.
9. Günther, T.; Dasgupta, P.; Mann, A.; Miess, E.; Klieber, A.; Fritzwanker, S.; Steinborn, R.; Schulz, S. Targeting multiple opioid receptors – improved analgesics with reduced side effects? *Br. J. Pharmacol.* **2018**, *175* (14), 2857–2868.
10. Bruchas, M. R.; Chavkin, C. Kinase cascades and ligand-directed signaling at the kappa opioid receptor. *Psychopharmacology* **2010**, *210* (2), 137–147.
11. Ahlbeck, K. Opioids: a two-faced Janus. *Curr. Med. Res. Opin.* **2011**, *27* (2), 439–448.
12. McNicol, E.; Horowicz-Mehler, N.; Fisk, R. A.; Bennett, K.; Gialetti-Goudas, M.; Chew, P. W.; Lau, J.; Carr, D. Management of opioid side effects in cancer-related and chronic noncancer pain: a systematic review. *J. Pain* **2003**, *4* (5), 231–256.
13. Al-Hasani, R.; Bruchas, M. R. Molecular Mechanisms of Opioid Receptor-dependent Signaling and Behavior. *Anesthesiology* **2011**, *115* (6), 1363–1381.
14. Childers, S. R.; Snyder, S. H. Guanine nucleotides differentiate agonist and antagonist interactions with opiate receptors. *Life Sci.* **1978**, *23* (7), 759–761.
15. Childers, S. R.; Creese, I.; Snowman, A. M.; Snyder, S. H. Opiate receptor binding affected differentially by opiates and opioid peptides. *Eur. J. Pharmacol.* **1979**, *55* (1), 11–18.
16. Barchfeld, C. C.; Medzihradsky, F. Receptor-mediated stimulation of brain GTPase by opiates in normal and dependent rats. *Biochem. Biophys. Res. Commun.* **1984**, *121* (2), 641–648.
17. Minneman, K. P.; Iversen, L. L. Enkephalin and opiate narcotics increase cyclic GMP accumulation in slices of rat neostriatum. *Nature* **1976**, *262* (5566), 313–314.
18. Wickman, K.; Clapham, D. E. Ion channel regulation by G proteins. *Physiol. Rev.* **1995**, *75* (4), 865–885.
19. Sadjia, R.; Alagem, N.; Reuveny, E. Gating of GIRK Channels: Details of an Intricate, Membrane-Delimited Signaling Complex. *Neuron* **2003**, *39* (1), 9–12.
20. Ippolito, D. L.; Temkin, P. A.; Rogalski, S. L.; Chavkin, C. N-terminal Tyrosine Residues within the Potassium Channel Kir3 Modulate GTPase activity of Gai*. *J. Biol. Chem.* **2002**, *277* (36), 32692–32696.
21. Torrecilla, M.; Quillinan, N.; Williams, J. T.; Wickman, K. Pre- and postsynaptic regulation of locus coeruleus neurons after chronic morphine treatment: a study of GIRK-knockout mice. *Eur. J. Neurosci.* **2008**, *28* (3), 618–624.
22. Torrecilla, M.; Marker, C. L.; Cintora, S. C.; Stoffel, M.; Williams, J. T.; Wickman, K. G-Protein-Gated Potassium Channels Containing Kir3.2 and Kir3.3 Subunits Mediate the Acute Inhibitory Effects of Opioids on Locus Coeruleus Neurons. *J. Neurosci.* **2002**, *22* (11), 4328–4334.
23. Rusin, K. I.; Giovannucci, D. R.; Stuenkel, E. L.; Moises, H. C. κ -Opioid Receptor Activation Modulates Ca^{2+} Currents and Secretion in Isolated Neuroendocrine Nerve Terminals. *J. Neurosci.* **1997**, *17* (17), 6565–6574.

References

24. Zamponi, G. W.; Snutch, T. P. Modulating modulation: crosstalk between regulatory pathways of presynaptic calcium channels. *Mol. Interv.* **2002**, *2* (8), 476–478.
25. Zamponi, G. W.; Snutch, T. P. Modulation of voltage-dependent calcium channels by G proteins. *Curr. Opin. Neurobiol.* **1998**, *8* (3), 351–356.
26. Tan, L.; Yan, W.; McCorvy, J. D.; Cheng, J. Biased Ligands of G Protein-Coupled Receptors (GPCRs): Structure–Functional Selectivity Relationships (SFSRs) and Therapeutic Potential. *J. Med. Chem.* **2018**, *61* (22), 9841–9878.
27. Singla, N.; Minkowitz, H. S.; Soergel, D. G.; Burt, D. A.; Subach, R. A.; Salamea, M. Y.; Fossler, M. J.; Skobieranda, F. A randomized, Phase IIb study investigating oliceridine (TRV130), a novel μ -receptor G-protein pathway selective (μ -GPS) modulator, for the management of moderate to severe acute pain following abdominoplasty. *J. Pain Res.* **2017**, *10*, 2413–2424.
28. Manglik, A.; Lin, H.; Aryal, D. K.; McCorvy, J. D.; Dengler, D.; Corder, G.; Levit, A.; Kling, R. C.; Bernat, V.; Hübner, H.; Huang, X.-P.; Sassano, M. F.; Giguère, P. M.; Löber, S.; Da, D.; Scherrer, G.; Kobilka, B. K.; Gmeiner, P.; Roth, B. L.; Shoichet, B. K. Structure-based discovery of opioid analgesics with reduced side effects. *Nature* **2016**, *537* (7619), 185–190.
29. Pitcher, J. A.; Freedman, N. J.; Lefkowitz, R. J. G Protein–Coupled Receptor Kinases. *Annu. Rev. Biochem.* **1998**, *67* (1), 653–692.
30. Kahsai, A. W.; Pani, B.; Lefkowitz, R. J. GPCR signaling: conformational activation of arrestins. *Cell Res.* **2018**, *28* (8), 783–784.
31. Mafi, A.; Kim, S.-K.; Goddard, W. A. Mechanism of β -arrestin recruitment by the μ -opioid G protein-coupled receptor. *Proc. Natl. Acad. Sci. U.S.A.* **2020**, *117* (28), 16346–16355.
32. Pitcher, J.; Inglese, J.; Higgins, J.; Arriza, J.; Casey, P.; Kim, C.; Benovic, J.; Kwatra, M.; Caron, M.; Lefkowitz, R. Role of $\beta\gamma$ Subunits of G proteins in Targeting the β -Adrenergic Receptor Kinase to Membrane-Bound Receptors. *Science* **1992**, *257* (5074), 1264–1267.
33. Pitcher, J. A.; Touhara, K.; Payne, E. S.; Lefkowitz, R. J. Pleckstrin Homology Domain-mediated Membrane Association and Activation of the β -Adrenergic Receptor Kinase Requires Coordinate Interaction with $G_{\beta\gamma}$ Subunits and Lipid*. *J. Biol. Chem.* **1995**, *270* (20), 11707–11710.
34. Li, J.; Xiang, B.; Su, W.; Zhang, X.; Huang, Y.; Ma, L. Agonist-induced Formation of Opioid Receptor-G Protein-coupled Receptor Kinase (GRK)- $G_{\beta\gamma}$ Complex on Membrane Is Required for GRK2 Function *in Vivo**. *J. Biol. Chem.* **2003**, *278* (32), 30219–30226.
35. Hilger, D.; Masureel, M.; Kobilka, B. K. Structure and dynamics of GPCR signaling complexes. *Nat. Struct. Mol. Biol.* **2018**, *25* (1), 4–12.
36. Williams, J. T.; Ingram, S. L.; Henderson, G.; Chavkin, C.; von Zastrow, M.; Schulz, S.; Koch, T.; Evans, C. J.; Christie, M. J. Regulation of μ -opioid receptors: desensitization, phosphorylation, internalization, and tolerance. *Pharmacol. Rev.* **2013**, *65* (1), 223–254.
37. Kliewer, A.; Schmiedel, F.; Sianati, S.; Bailey, A.; Bateman, J. T.; Levitt, E. S.; Williams, J. T.; Christie, M. J.; Schulz, S. Phosphorylation-deficient G-protein-biased μ -opioid receptors improve analgesia and diminish tolerance but worsen opioid side effects. *Nat. Commun.* **2019**, *10* (1), 367.
38. Arttamangkul, S.; Heinz, D. A.; Bunzow, J. R.; Song, X.; Williams, J. T. Cellular tolerance at the μ -opioid receptor is phosphorylation dependent. *eLife* **2018**, *7*, e34989.
39. Bouvier, M. Oligomerization of G-protein-coupled transmitter receptors. *Nat. Rev. Neurosci.* **2001**, *2* (4), 274–286.
40. Milligan, G.; Bouvier, M. Methods to monitor the quaternary structure of G protein-coupled receptors. *FEBS J.* **2005**, *272* (12), 2914–2925.
41. Pin, J.-P.; Neubig, R.; Bouvier, M.; Devi, L.; Filizola, M.; Javitch, J. A.; Lohse, M. J.; Milligan, G.; Palczewski, K.; Parmentier, M.; Spedding, M. International Union of Basic and Clinical Pharmacology. LXVII. Recommendations for the Recognition and Nomenclature of G Protein-Coupled Receptor Heteromultimers. *Pharmacol. Rev.* **2007**, *59* (1), 5–13.
42. Ferré, S.; Baler, R.; Bouvier, M.; Caron, M. G.; Devi, L. A.; Durroux, T.; Fuxe, K.; George, S. R.; Javitch, J. A.; Lohse, M. J.; Mackie, K.; Milligan, G.; Pflieger, K. D. G.; Pin, J.-P.; Volkow, N. D.; Waldhoer, M.; Woods, A. S.; Franco, R. Building a new conceptual framework for receptor heteromers. *Nat. Chem. Biol.* **2009**, *5* (3), 131–134.
43. Chun, L.; Zhang, W.-H.; Liu, J.-F. Structure and ligand recognition of class C GPCRs. *Acta Pharmacol. Sin.* **2012**, *33* (3), 312–323.
44. Rondard, P.; Goudet, C.; Kniazeff, J.; Pin, J.-P.; Prézeau, L. The complexity of their activation mechanism opens new possibilities for the modulation of mGlu and GABAB class C G protein-coupled receptors. *Neuropharmacology* **2011**, *60* (1), 82–92.
45. Kniazeff, J.; Prézeau, L.; Rondard, P.; Pin, J.-P.; Goudet, C. Dimers and beyond: The functional puzzles of class C GPCRs. *Pharmacol. Ther.* **2011**, *130* (1), 9–25.
46. Kuszak, A. J.; Pitchiaya, S.; Anand, J. P.; Mosberg, H. I.; Walter, N. G.; Sunahara, R. K. Purification and Functional Reconstitution of

References

- Monomeric μ -Opioid Receptors: Allosteric Modulation of Agonist Binding by G_{i2} . *J. Biol. Chem.* **2009**, *284* (39), 26732–26741.
47. Bayburt, T. H.; Leitz, A. J.; Xie, G.; Oprian, D. D.; Sligar, S. G. Transducin Activation by Nanoscale Lipid Bilayers Containing One and Two Rhodopsins*. *J. Biol. Chem.* **2007**, *282* (20), 14875–14881.
48. Whorton, M. R.; Bokoch, M. P.; Rasmussen, S. G. F.; Huang, B.; Zare, R. N.; Kobilka, B.; Sunahara, R. K. A monomeric G protein-coupled receptor isolated in a high-density lipoprotein particle efficiently activates its G protein. *Proc. Natl. Acad. Sci. U.S.A.* **2007**, *104* (18), 7682–7687.
49. Whorton, M. R.; Jastrzebska, B.; Park, P. S. H.; Fotiadis, D.; Engel, A.; Palczewski, K.; Sunahara, R. K. Efficient coupling of transducin to monomeric rhodopsin in a phospholipid bilayer. *J. Biol. Chem.* **2008**, *283* (7), 4387–4394.
50. Ferré, S.; Casadó, V.; Devi, L. A.; Filizola, M.; Jockers, R.; Lohse, M. J.; Milligan, G.; Pin, J.-P.; Guitart, X. G protein-coupled receptor oligomerization revisited: functional and pharmacological perspectives. *Pharmacol. Rev.* **2014**, *66* (2), 413–434.
51. Cvejic, S.; Devi, L. A. Dimerization of the δ Opioid Receptor: Implication for a Role in Receptor Internalization*. *J. Biol. Chem.* **1997**, *272* (43), 26959–26964.
52. Jordan, B. A.; Devi, L. A. G-protein-coupled receptor heterodimerization modulates receptor function. *Nature* **1999**, *399* (6737), 697–700.
53. He, L.; Fong, J.; von Zastrow, M.; Whistler, J. L. Regulation of Opioid Receptor Trafficking and Morphine Tolerance by Receptor Oligomerization. *Cell* **2002**, *108* (2), 271–282.
54. Manglik, A.; Kruse, A. C.; Kobilka, T. S.; Thian, F. S.; Mathiesen, J. M.; Sunahara, R. K.; Pardo, L.; Weis, W. I.; Kobilka, B. K.; Granier, S. Crystal structure of the μ -opioid receptor bound to a morphinan antagonist. *Nature* **2012**, *485* (7398), 321–326.
55. Möller, J.; Isbilir, A.; Sungkaworn, T.; Osberg, B.; Karathanasis, C.; Sunkara, V.; Grushevskiy, E. O.; Bock, A.; Annibale, P.; Heilemann, M.; Schütte, C.; Lohse, M. J. Single-molecule analysis reveals agonist-specific dimer formation of μ -opioid receptors. *Nat. Chem. Biol.* **2020**, *16* (9), 946–954.
56. Gentzsch, C.; Seier, K.; Drakopoulos, A.; Jobin, M.-L.; Lanoiselée, Y.; Koszegi, Z.; Maurel, D.; Sounier, R.; Hübner, H.; Gmeiner, P.; Granier, S.; Calebiro, D.; Decker, M. Selective and Wash-Resistant Fluorescent Dihydrocodeinone Derivatives Allow Single-Molecule Imaging of μ -Opioid Receptor Dimerization. *Angewandte Chemie International Edition* **2020**, *59* (15), 5958–5964.
57. Gomes, I.; Jordan, B. A.; Gupta, A.; Trapaidze, N.; Nagy, V.; Devi, L. A. Heterodimerization of μ and δ Opioid Receptors: A Role in Opiate Synergy. *J. Neurosci.* **2000**, *20* (22), RC110.
58. Gomes, I.; Gupta, A.; Filipovska, J.; Szeto, H. H.; Pintar, J. E.; Devi, L. A. A role for heterodimerization of μ and δ opiate receptors in enhancing morphine analgesia. *Proc. Natl. Acad. Sci. U.S.A.* **2004**, *101* (14), 5135–5139.
59. George, S. R.; Fan, T.; Xie, Z.; Tse, R.; Tam, V.; Varghese, G.; O'Dowd, B. F. Oligomerization of μ - and δ -Opioid Receptors: Generation of Novel Functional Properties*. *J. Biol. Chem.* **2000**, *275* (34), 26128–26135.
60. Gomes, I.; IJzerman, A. P.; Ye, K.; Maillet, E. L.; Devi, L. A. G Protein-Coupled Receptor Heteromerization: A Role in Allosteric Modulation of Ligand Binding. *Mol. Pharmacol.* **2011**, *79* (6), 1044–1052.
61. Hasbi, A.; Nguyen, T.; Fan, T.; Cheng, R.; Rashid, A.; Alijaniam, M.; Rasenick, M. M.; O'Dowd, B. F.; George, S. R. Trafficking of Preassembled Opioid μ - δ Heterooligomer-G α Signaling Complexes to the Plasma Membrane: Coregulation by Agonists. *Biochemistry* **2007**, *46* (45), 12997–13009.
62. Fan, T.; Varghese, G.; Nguyen, T.; Tse, R.; O'Dowd, B. F.; George, S. R. A Role for the Distal Carboxyl Tails in Generating the Novel Pharmacology and G Protein Activation Profile of μ and δ Opioid Receptor Hetero-oligomers*. *J. Biol. Chem.* **2005**, *280* (46), 38478–38488.
63. Law, P.-Y.; Erickson-Herbrandson, L. J.; Zha, Q. Q.; Solberg, J.; Chu, J.; Sarre, A.; Loh, H. H. Heterodimerization of μ - and δ -Opioid Receptors Occurs at the Cell Surface Only and Requires Receptor-G Protein Interactions*. *J. Biol. Chem.* **2005**, *280* (12), 11152–11164.
64. Milan-Lobo, L.; Whistler, J. L. Heteromerization of the μ - and δ -opioid receptors produces ligand-biased antagonism and alters μ -receptor trafficking. *J. Pharmacol. Exp. Ther.* **2011**, *337* (3), 868–875.
65. Décaillot, F. M.; Rozenfeld, R.; Gupta, A.; Devi, L. A. Cell surface targeting of μ - δ opioid receptor heterodimers by RTP4. *Proc. Natl. Acad. Sci. U.S.A.* **2008**, *105* (41), 16045–16050.
66. Fujita, W.; Gomes, I.; Devi, L. A. Revolution in GPCR signalling: opioid receptor heteromers as novel therapeutic targets: IUPHAR Review 10. *Br. J. Pharmacol.* **2014**, *171* (18), 4155–4176.
67. Gomes, I.; Fujita, W.; Gupta, A.; Saldanha, S. A.; Negri, A.; Pinello, C. E.; Eberhart, C.; Roberts, E.; Filizola, M.; Hodder, P.; Devi, L. A. Identification of a μ - δ opioid receptor heteromer-biased agonist with antinociceptive activity. *Proc. Natl. Acad. Sci. U.S.A.* **2013**, *110* (29), 12072–12077.

References

68. Daniels, D. J.; Lenard, N. R.; Etienne, C. L.; Law, P.-Y.; Roerig, S. C.; Portoghese, P. S. Opioid-induced tolerance and dependence in mice is modulated by the distance between pharmacophores in a bivalent ligand series. *Proc. Natl. Acad. Sci. U.S.A.* **2005**, *102* (52), 19208–19213.
69. Lenard, N. R.; Daniels, D. J.; Portoghese, P. S.; Roerig, S. C. Absence of conditioned place preference or reinstatement with bivalent ligands containing mu-opioid receptor agonist and delta-opioid receptor antagonist pharmacophores. *Eur. J. Pharmacol.* **2007**, *566* (1), 75–82.
70. Harvey, J. H.; Long, D. H.; England, P. M.; Whistler, J. L. Tuned-Affinity Bivalent Ligands for the Characterization of Opioid Receptor Heteromers. *ACS Med. Chem. Lett.* **2012**, *3* (8), 640–644.
71. Ramsay, D.; Kellett, E.; McVey, M.; Rees, S.; Milligan, G. Homo- and hetero-oligomeric interactions between G-protein-coupled receptors in living cells monitored by two variants of bioluminescence resonance energy transfer (BRET): hetero-oligomers between receptor subtypes form more efficiently than between less closely related sequences. *Biochem. J.* **2002**, *365* (2), 429–440.
72. Berg, K. A.; Rowan, M. P.; Gupta, A.; Sanchez, T. A.; Silva, M.; Gomes, I.; McGuire, B. A.; Portoghese, P. S.; Hargreaves, K. M.; Devi, L. A.; Clarke, W. P. Allosteric Interactions between δ and κ Opioid Receptors in Peripheral Sensory Neurons. *Mol. Pharmacol.* **2012**, *81* (2), 264–272.
73. Waldhoer, M.; Fong, J.; Jones, R. M.; Lunzer, M. M.; Sharma, S. K.; Kostenis, E.; Portoghese, P. S.; Whistler, J. L. A heterodimer-selective agonist shows *in vivo* relevance of G protein-coupled receptor dimers. *Proc. Natl. Acad. Sci. U.S.A.* **2005**, *102* (25), 9050–9055.
74. Rives, M.-L.; Rossillo, M.; Liu-Chen, L.-Y.; Javitch, J. A. 6'-Guanidinonaltrindole (6'-GNTI) Is a G Protein-biased κ -Opioid Receptor Agonist That Inhibits Arrestin Recruitment *. *J. Biol. Chem.* **2012**, *287* (32), 27050–27054.
75. Chakrabarti, S.; Liu, N.-J.; Gintzler, A. R. Formation of μ - κ -opioid receptor heterodimer is sex-dependent and mediates female-specific opioid analgesia. *Proc. Natl. Acad. Sci. U.S.A.* **2010**, *107* (46), 20115–20119.
76. Wang, D.; Sun, X.; Bohn, L. M.; Sadée, W. Opioid Receptor Homo- and Heterodimerization in Living Cells by Quantitative Bioluminescence Resonance Energy Transfer. *Mol. Pharmacol.* **2005**, *67* (6), 2173–2184.
77. Yekkirala, A. S.; Lunzer, M. M.; McCurdy, C. R.; Powers, M. D.; Kalyuzhny, A. E.; Roerig, S. C.; Portoghese, P. S. *N*-naphthoyl- β -naltrexamine (NNTA), a highly selective and potent activator of μ / κ -opioid heteromers. *Proc. Natl. Acad. Sci. U.S.A.* **2011**, *108* (12), 5098–5103.
78. Ciruela, F.; Jacobson, K. A.; Fernández-Dueñas, V. Portraying G Protein-Coupled Receptors with Fluorescent Ligands. *ACS Chem. Biol.* **2014**, *9* (9), 1918–1928.
79. Cardullo, R. A., Theoretical Principles and Practical Considerations for Fluorescence Resonance Energy Transfer Microscopy. In *Methods in Cell Biology*, Academic Press: 2007; Vol. 81, pp 479–494.
80. Förster, T. Zwischenmolekulare Energiewanderung und Fluoreszenz. *Ann. Phys.* **1948**, *437* (1-2), 55–75.
81. Stryer, L.; Haugland, R. P. Energy transfer: a spectroscopic ruler. *Proc. Natl. Acad. Sci. U.S.A.* **1967**, *58* (2), 719–726.
82. Piston, D. W.; Kremers, G.-J. Fluorescent protein FRET: the good, the bad and the ugly. *Trends Biochem. Sci.* **2007**, *32* (9), 407–414.
83. Lavis, L. D.; Raines, R. T. Bright Building Blocks for Chemical Biology. *ACS Chem. Biol.* **2014**, *9* (4), 855–866.
84. Böhme, I.; Beck-Sickinger, A. G. Illuminating the life of GPCRs. *Cell Commun. Signal.* **2009**, *7* (1), 16.
85. Rao, J.; Dragulescu-Andrasi, A.; Yao, H. Fluorescence imaging *in vivo*: recent advances. *Curr. Opin. Biotechnol.* **2007**, *18* (1), 17–25.
86. Drakopoulos, A.; Decker, M. Development and Biological Applications of Fluorescent Opioid Ligands. *ChemPlusChem* **2020**, *85* (6), 1354–1364.
87. Zwier, J. M.; Roux, T.; Cottet, M.; Durroux, T.; Douzon, S.; Bdioui, S.; Gregor, N.; Bourrier, E.; Oueslati, N.; Nicolas, L.; Tinel, N.; Boisseau, C.; Yverneau, P.; Charrier-Savournin, F.; Fink, M.; Trinquet, E. A Fluorescent Ligand-Binding Alternative Using Tag-lite® Technology. *J. Biomol. Screen.* **2010**, *15* (10), 1248–1259.
88. Lam, R.; Gondin, A. B.; Canals, M.; Kellam, B.; Bridson, S. J.; Graham, B.; Scammells, P. J. Fluorescently Labeled Morphine Derivatives for Bioimaging Studies. *J. Med. Chem.* **2018**, *61* (3), 1316–1329.
89. Cunningham, C. W.; Mercer, S. L.; Hassan, H. E.; Traynor, J. R.; Eddington, N. D.; Coop, A. Opioids and Efflux Transporters. Part 2: P-Glycoprotein Substrate Activity of 3- and 6-Substituted Morphine Analogs. *J. Med. Chem.* **2008**, *51* (7), 2316–2320.
90. Schembri, L. S.; Stoddart, L. A.; Bridson, S. J.; Kellam, B.; Canals, M.; Graham, B.; Scammells, P. J. Synthesis, Biological Evaluation, and Utility of

References

- Fluorescent Ligands Targeting the μ -Opioid Receptor. *J. Med. Chem.* **2015**, *58* (24), 9754–9767.
91. Pergolizzi, J.; Aloisi, A. M.; Dahan, A.; Filitz, J.; Langford, R.; Likar, R.; Mercadante, S.; Morlion, B.; Raffa, R. B.; Sabatowski, R.; Sacerdote, P.; Torres, L. M.; Weinbroum, A. A. Current Knowledge of Buprenorphine and Its Unique Pharmacological Profile. *Pain Pract.* **2010**, *10* (5), 428–450.
92. McLaughlin, J. P.; Hill, K. P.; Jiang, Q.; Sebastian, A.; Archer, S.; Bidlack, J. M. Nitrocinnamoyl and Chlorocinnamoyl Derivatives of Dihydrocodeinone: In Vivo and In Vitro Characterization of μ -Selective Agonist and Antagonist Activity. *J. Pharmacol. Exp. Ther.* **1999**, *289* (1), 304–311.
93. Emmerson, P. J.; Archer, S.; El-Hamouly, W.; Mansour, A.; Akil, H.; Medzihradsky, F. Synthesis and Characterization of 4,4-Difluoro-4-bora-3a,4a-Diaza-s-Indacene (BODIPY)-Labeled Fluorescent Ligands for the Mu Opioid Receptor. *Biochem. Pharmacol.* **1997**, *54* (12), 1315–1322.
94. Southwick, P. L.; Ernst, L. A.; Tauriello, E. W.; Parker, S. R.; Mujumdar, R. B.; Mujumdar, S. R.; Clever, H. A.; Waggoner, A. S. Cyanine dye labeling reagents—carboxymethylindocyanine succinimidyl esters. *Cytometry* **1990**, *11* (3), 418–430.
95. Gentsch, C. Synthesis of a μ -opioid receptor-selective, fluorescent probe Julius-Maximilian-University of Würzburg, unpublished, 2016.
96. Stoddart, L. A.; Vernall, A. J.; Briddon, S. J.; Kellam, B.; Hill, S. J. Direct visualisation of internalization of the adenosine A₃ receptor and localization with arrestin3 using a fluorescent agonist. *Neuropharmacology* **2015**, *98*, 68–77.
97. Chang, A.-C.; Chao, C. C.; Takemori, A. E.; Gekker, G.; Hu, S.; Peterson, P. K.; Portoghese, P. S. Arylacetamide-Derived Fluorescent Probes: Synthesis, Biological Evaluation, and Direct Fluorescent Labeling of κ Opioid Receptors in Mouse Microglial Cells. *J. Med. Chem.* **1996**, *39* (8), 1729–1735.
98. Kshirsagar, T.; Nakano, A. H.; Law, P.-Y.; Elde, R.; Portoghese, P. S. NT14F: a non-peptide fluorescent probe selective for functional delta opioid receptors. *Neurosci. Lett.* **1998**, *249* (2), 83–86.
99. Berényi, S.; Csutoras, C.; Sipos, A. Recent Developments in the Chemistry of Thebaine and its Transformation Products as Pharmacological Targets. *Curr. Med. Chem.* **2009**, *16*, 3215–3242.
100. Kirby, G. W.; McGuigan, H.; Mackinnon, J. W. M.; McLean, D.; Sharma, R. P. Formation and reactions of C-nitrosoformate esters, a new class of transient dienophiles. *J. Chem. Soc., Perkin Trans. 1* **1985**, (0), 1437–1442.
101. Sebastian, A.; Bidlack, J. M.; Jiang, Q.; Deecher, D.; Teitler, M.; Glick, S. D.; Archer, S. 14 β -[(*p*-Nitrocinnamoyl)amino]morphinones, 14 β -[(*p*-Nitrocinnamoyl)amino]-7,8-dihydromorphinones, and Their Codeinone Analogs: Synthesis and Receptor Activity. *J. Med. Chem.* **1993**, *36* (21), 3154–3160.
102. Kirby, G. W.; McLean, D. An Efficient Synthesis of 14 β -Aminocodeinone from Thebaine. *J. Chem. Soc., Perkin Trans. 1* **1985**, (0), 1443–1445.
103. Burke, M. J.; Trantow, B. M. An efficient route to 3-aminoindazoles and 3-amino-7-azaindazoles. *Tetrahedron Lett.* **2008**, *49* (31), 4579–4581.
104. Dar, M.; Giesler, T.; Richardson, R.; Cai, C.; Cooper, M.; Lavasani, S.; Kille, P.; Voet, T.; Vermeesch, J. Development of a novel ozone- and photo-stable HyPer5 red fluorescent dye for array CGH and microarray gene expression analysis with consistent performance irrespective of environmental conditions. *BMC Biotechnol.* **2008**, *8* (1), 86.
105. Calebiro, D.; Rieken, F.; Wagner, J.; Sungkaworn, T.; Zabel, U.; Borzi, A.; Cocucci, E.; Zürn, A.; Lohse, M. J. Single-molecule analysis of fluorescently labeled G-protein-coupled receptors reveals complexes with distinct dynamics and organization. *Proc. Natl. Acad. Sci. U.S.A.* **2013**, *110* (2), 743–748.
106. Sungkaworn, T.; Jobin, M.-L.; Burnecki, K.; Weron, A.; Lohse, M. J.; Calebiro, D. Single-molecule imaging reveals receptor–G protein interactions at cell surface hot spots. *Nature* **2017**, *550* (7677), 543–547.
107. Jaqaman, K.; Danuser, G. Computational image analysis of cellular dynamics: a case study based on particle tracking. *Cold Spring Harb. Protoc.* **2009**, *4*, doi:10.1101/pdb.top65 (12).
108. Murase, K.; Fujiwara, T.; Umemura, Y.; Suzuki, K.; Iino, R.; Yamashita, H.; Saito, M.; Murakoshi, H.; Ritchie, K.; Kusumi, A. Ultrafine Membrane Compartments for Molecular Diffusion as Revealed by Single Molecule Techniques. *Biophys. J.* **2004**, *86* (6), 4075–4093.
109. Hern, J. A.; Baig, A. H.; Mashanov, G. I.; Birdsall, B.; Corrie, J. E. T.; Lazareno, S.; Molloy, J. E.; Birdsall, N. J. M. Formation and dissociation of M₁ muscarinic receptor dimers seen by total internal reflection fluorescence imaging of single molecules. *Proc. Natl. Acad. Sci. U.S.A.* **2010**, *107*, 2693–2698.
110. Tabor, A.; Weisenburger, S.; Banerjee, A.; Purkayastha, N.; Kaindl, J. M.; Hübner, H.; Wei, L.; Grömer, T. W.; Kornhuber, J.; Tschammer, N.; Birdsall, N. J. M.; Mashanov, G. I.; Sandoghdar, V.; Gmeiner, P. Visualization and ligand-induced modulation of dopamine receptor dimerization at the single molecule level. *Sci. Rep.* **2016**, *6*, 1–16.

References

111. Tobin, S. J.; Wakefield, D. L.; Terenius, L.; Vukojević, V.; Jovanović-Talisman, T. Ethanol and Naltrexone Have Distinct Effects on the Lateral Nano-organization of Mu and Kappa Opioid Receptors in the Plasma Membrane. *ACS Chem. Neurosci.* **2019**, *10*, 667–676.
112. Van Bockstaele, E. J.; Colago, E. E. O.; Moriwaki, A.; Uhl, G. R. Mu-opioid receptor is located on the plasma membrane of dendrites that receive asymmetric synapses from axon terminals containing leucine-enkephalin in the rat nucleus locus coeruleus. *J. Comp. Neurol.* **1996**, *376*, 65–74.
113. Milner, T. A.; Drake, C. T. Ultrastructural evidence for presynaptic μ opioid receptor modulation of synaptic plasticity in NMDA-receptor-containing dendrites in the dentate gyrus. *Brain Res. Bull.* **2001**, *54*, 131–140.
114. Le Merrer, J.; Becker, J. A. J.; Befort, K.; Kieffer, B. L. Reward Processing by the Opioid System in the Brain. *Physiol. Rev.* **2009**, *89* (4), 1379–1412.
115. Drakopoulos, A.; Koszegi, Z.; Lanoiselée, Y.; Hübner, H.; Gmeiner, P.; Calebiro, D.; Decker, M. Investigation of Inactive-State κ Opioid Receptor Homodimerization via Single-Molecule Microscopy Using New Antagonistic Fluorescent Probes. *J. Med. Chem.* **2020**, *63* (7), 3596–3609.
116. Jaqaman, K.; Loerke, D.; Mettlen, M.; Kuwata, H.; Grinstein, S.; Schmid, S. L.; Danuser, G. Robust single-particle tracking in live-cell time-lapse sequences. *Nat. Methods* **2008**, *5*, 695–702.
117. Metzler, R.; Jeon, J.-H.; Cherstvy, A. G.; Barkai, E. Anomalous diffusion models and their properties: non-stationarity, non-ergodicity, and ageing at the centenary of single particle tracking. *Phys. Chem. Chem. Phys.* **2014**, *16* (44), 24128–24164.
118. Andrianov, A.; Grebenkov, D. S. Time-averaged MSD of Brownian motion. *J. Stat. Mech. Theory Exp.* **2012**, *2012* (07), P07001.
119. Lanoiselée, Y.; Sikora, G.; Grzesiek, A.; Grebenkov, D. S.; Wyłomańska, A. Optimal parameters for anomalous-diffusion-exponent estimation from noisy data. *Phys. Rev. E* **2018**, *98* (6), 062139.
120. Lucy, L. B. An iterative technique for the rectification of observed distributions. *Astron. J.* **1974**, *79*, 745–754.
121. Milan-Lobo, L.; Enquist, J.; van Rijn, R. M.; Whistler, J. L. Anti-Analgesic Effect of the Mu/Delta Opioid Receptor Heteromer Revealed by Ligand-Biased Antagonism. *PLOS ONE* **2013**, *8* (3), e58362.
122. Fujita, W.; Gomes, I.; Devi, L. A. Heteromers of μ - δ opioid receptors: new pharmacology and novel therapeutic possibilities. *Br. J. Pharmacol.* **2015**, *172* (2), 375–387.
123. Yekkirala, A. S.; Kalyuzhny, A. E.; Portoghese, P. S. An Immunocytochemical-Correlate for Evaluating the Bridging of Heteromeric Mu-Delta Opioid Protomers by Bivalent Ligands. *ACS Chem. Biol.* **2013**, *8* (7), 1412–1416.
124. Gupta, A.; Mulder, J.; Gomes, I.; Rozenfeld, R.; Bushlin, I.; Ong, E.; Lim, M.; Maillet, E.; Junek, M.; Cahill, C. M.; Harkany, T.; Devi, L. A. Increased Abundance of Opioid Receptor Heteromers After Chronic Morphine Administration. *Sci. Signal.* **2010**, *3* (131), ra54.
125. Le Naour, M.; Lunzer, M. M.; Powers, M. D.; Kalyuzhny, A. E.; Benneyworth, M. A.; Thomas, M. J.; Portoghese, P. S. Putative Kappa Opioid Heteromers As Targets for Developing Analgesics Free of Adverse Effects. *J. Med. Chem.* **2014**, *57* (15), 6383–6392.
126. Sayre, L. M.; Portoghese, P. S. Stereospecific Synthesis of the 6α - and 6β -Amino Derivatives of Naltrexone and Oxymorphone. *J. Org. Chem.* **1980**, *45* (16), 3366–3368.
127. Portoghese, P. S.; Sultana, M.; Nelson, W. L.; Klein, P.; Takemori, A. E. δ Opioid Antagonist Activity and Binding Studies of Regioisomeric Isothiocyanate Derivatives of Naltrindole: Evidence for δ Receptor Subtypes. *J. Med. Chem.* **1992**, *35* (22), 4086–4091.
128. Kim, K. S.; Qian, L. Improved method for the preparation of guanidines. *Tetrahedron Lett.* **1993**, *34* (48), 7677–7680.
129. Iwanowicz, E. J.; Poss, M. A.; Lin, J. Preparation of *N,N'*-bis-*tert*-Butoxycarbonylthiourea. *Synth. Commun.* **1993**, *23* (10), 1443–1445.
130. Schmid, C. L.; Streicher, J. M.; Groer, C. E.; Munro, T. A.; Zhou, L.; Bohn, L. M. Functional Selectivity of 6'-Guanidinonaltrindole (6'-GNTI) at κ -Opioid Receptors in Striatal Neurons*. *J. Biol. Chem.* **2013**, *288* (31), 22387–22398.
131. Le Naour, M.; Lunzer, M. M.; Powers, M. D.; Portoghese, P. S. Opioid Activity of Spinally Selective Analogues of *N*-Naphthoyl- β -naltrexamine in HEK-293 Cells and Mice. *J. Med. Chem.* **2012**, *55* (2), 670–677.
132. Lowry, O. H.; Rosebrough, N. J.; Farr, A. L.; Randall, R. J. Protein measurement with the Folin phenol reagent. *J. Biol. Chem.* **1951**, *193* (1), 265–275.
133. Yung-Chi, C.; Prusoff, W. H. Relationship between the inhibition constant (K_i) and the concentration of inhibitor which causes 50 per cent inhibition (I_{50}) of an enzymatic reaction. *Biochem. Pharmacol.* **1973**, *22* (23), 3099–3108.

References

134. Darvesh, S.; Hopkins, D. A.; Geula, C. Neurobiology of butyrylcholinesterase. *Nat. Rev. Neurosci.* **2003**, *4* (2), 131–138.
135. Masson, P.; Froment, M.-T.; Fortier, P.-L.; Visicchio, J.-E.; Bartels, C. F.; Lockridge, O. Butyrylcholinesterase-catalysed hydrolysis of aspirin, a negatively charged ester, and aspirin-related neutral esters. *Biochim. Biophys. Acta, Protein Struct. Mol. Enzymol.* **1998**, *1387* (1), 41–52.
136. Gately, S. J. Activities of the enantiomers of cocaine and some related compounds as substrates and inhibitors of plasma butyrylcholinesterase. *Biochem. Pharmacol.* **1991**, *41* (8), 1249–1254.
137. Lockridge, O.; Mottershaw-Jackson, N.; Eckerson, H. W.; La Du, B. N. Hydrolysis of diacetylmorphine (heroin) by human serum cholinesterase. *J. Pharmacol. Exp. Ther.* **1980**, *215* (1), 1–8.
138. Evans, F. T.; Gray, P. W. S.; Lehmann, H.; Silk, E. Sensitivity to Succinylcholine in Relation to Serum-Cholinesterase. *Lancet* **1952**, *259* (6721), 1229–1230.
139. Lockridge, O.; Bartels, C. F.; Vaughan, T. A.; Wong, C. K.; Norton, S. E.; Johnson, L. L. Complete amino acid sequence of human serum cholinesterase. *J. Biol. Chem.* **1987**, *262* (2), 549–557.
140. Vellom, D. C.; Radic, Z.; Li, Y.; Pickering, N. A.; Camp, S.; Taylor, P. Amino acid residues controlling acetylcholinesterase and butyrylcholinesterase specificity. *Biochemistry* **1993**, *32* (1), 12–17.
141. Massoulié, J.; Pezzementi, L.; Bon, S.; Krejci, E.; Vallette, F.-M. Molecular and cellular biology of cholinesterases. *Prog. Neurobiol.* **1993**, *41* (1), 31–91.
142. Jbilo, O.; Bartels, C. F.; Chatonnet, A.; Toutant, J. P.; Lockridge, O. Tissue distribution of human acetylcholinesterase and butyrylcholinesterase messenger RNA. *Toxicol.* **1994**, *32* (11), 1445–1457.
143. Lockridge, O.; Duysen, E.; Masson, P., Butyrylcholinesterase: Overview, Structure, and Function. In *Anticholinesterase Pesticides*, Satoh, T.; Gupta, R. C., Eds. Wiley-VCH: 2011; pp 25–41.
144. Girard, E.; Bernard, V.; Minic, J.; Chatonnet, A.; Krejci, E.; Molgó, J. Butyrylcholinesterase and the control of synaptic responses in acetylcholinesterase knockout mice. *Life Sci.* **2007**, *80* (24), 2380–2385.
145. Hartmann, J.; Kiewert, C.; Duysen, E. G.; Lockridge, O.; Greig, N. H.; Klein, J. Excessive hippocampal acetylcholine levels in acetylcholinesterase-deficient mice are moderated by butyrylcholinesterase activity. *J. Neurochem.* **2007**, *100* (5), 1421–1429.
146. Mesulam, M. M.; Guillozet, A.; Shaw, P.; Levey, A.; Duysen, E. G.; Lockridge, O. Acetylcholinesterase knockouts establish central cholinergic pathways and can use butyrylcholinesterase to hydrolyze acetylcholine. *Neuroscience* **2002**, *110* (4), 627–639.
147. Robertson, R. T.; Mostamand, F. Development of 'non-specific' cholinesterase-containing neurons in the dorsal thalamus of the rat. *Brain Res. Dev. Brain Res.* **1988**, *41* (1), 43–60.
148. Layer, P. G. Cholinesterases during development of the avian nervous system. *Cell. Mol. Neurobiol.* **1991**, *11* (1), 7–33.
149. Dubovy, P.; Haninec, P. Non-specific cholinesterase activity of the developing peripheral nerves and its possible function in cells in intimate contact with growing axons of chick embryo. *Int. J. Dev. Neurosci.* **1990**, *8* (5), 589–597.
150. Tsigelny, I.; Taylor, P.; Bourne, P. E.; Shindyalov, I. N.; Südhof, T. C. Common EF-hand motifs in cholinesterases and neurolygins suggest a role for Ca²⁺ binding in cell surface associations. *Protein Sci.* **2000**, *9* (1), 180–185.
151. Santarpia, L.; Grandone, I.; Contaldo, F.; Pasanisi, F. Butyrylcholinesterase as a prognostic marker: a review of the literature. *J. Cachexia Sarcopenia Muscle* **2013**, *4* (1), 31–39.
152. Reid, G. A.; Darvesh, S. Butyrylcholinesterase-knockout reduces brain deposition of fibrillar β -amyloid in an Alzheimer mouse model. *Neuroscience* **2015**, *298*, 424–435.
153. Macdonald, I. R.; Maxwell, S. P.; Reid, G. A.; Cash, M. K.; DeBay, D. R.; Darvesh, S. Quantification of Butyrylcholinesterase Activity as a Sensitive and Specific Biomarker of Alzheimer's Disease. *J. Alzheimer's Dis.* **2017**, *58*, 491–505.
154. Koizumi, K.; Wang, G.; Park, L. Endothelial Dysfunction and Amyloid- β -Induced Neurovascular Alterations. *Cell. Mol. Neurobiol.* **2016**, *36* (2), 155–165.
155. Katzman, R.; Terry, R.; DeTeresa, R.; Brown, T.; Davies, P.; Fuld, P.; Renbing, X.; Peck, A. Clinical, pathological, and neurochemical changes in dementia: A subgroup with preserved mental status and numerous neocortical plaques. *Ann. Neurol.* **1988**, *23* (2), 138–144.
156. Darvesh, S. Butyrylcholinesterase as a Diagnostic and Therapeutic Target for Alzheimer's Disease. *Curr. Alzheimer Res.* **2016**, *13*, 1–5.
157. Aziz-Aloya, R. B.; Sternfeld, M.; Soreq, H., Chapter 16: Promoter elements and alternative splicing in the human AChE gene. In *Progress in Brain Research*, Cuello, A. C., Ed. Elsevier: 1993; Vol. 98, pp 147–153.

References

158. Layer, P. G.; Willbold, E. Novel Functions of Cholinesterases in Development, Physiology and Disease. *Prog. Histochem. Cytochem.* **1994**, *29* (3), III–92.
159. Martínez-Moreno, P.; Nieto-Cerón, S.; Torres-Lanzas, J.; Ruiz-Espejo, F.; Tovar-Zapata, I.; Martínez-Hernández, P.; Rodríguez-López, J. N.; Vidal, C. J.; Cabezas-Herrera, J. Cholinesterase activity of human lung tumours varies according to their histological classification. *Carcinogenesis* **2005**, *27* (3), 429–436.
160. Ogunkeye, O. O.; Roluga, A. I. Serum cholinesterase activity helps to distinguish between liver disease and non-liver disease aberration in liver function tests. *Pathophysiology* **2006**, *13* (2), 91–93.
161. Gu, S.-Z. Alterations of serum cholinesterase in patients with gastric cancer. *World J. Gastroenterol.* **2005**, *11*, 4604–4606.
162. Sun, L.; Qi, X.; Tan, Q.; Yang, H.; Qi, X. Low Serum-Butyrylcholinesterase Activity as a Prognostic Marker of Mortality Associates with Poor Cardiac Function in Acute Myocardial Infarction. *Clin. Lab.* **2016**, *62* (6), 1093–1099.
163. Vaquero, J. J.; Kinahan, P. Positron Emission Tomography: Current Challenges and Opportunities for Technological Advances in Clinical and Preclinical Imaging Systems. *Annu. Rev. Biomed.* **2015**, *17*, 385–414.
164. Sawatzky, E.; Al-Momani, E.; Kobayashi, R.; Higuchi, T.; Samnick, S.; Decker, M. A Novel Way To Radiolabel Human Butyrylcholinesterase for Positron Emission Tomography through Irreversible Transfer of the Radiolabeled Moiety. *ChemMedChem* **2016**, *11* (14), 1540–1550.
165. Logan, J.; Fowler, J. S.; Ding, Y.-S.; Franceschi, D.; Wang, G.-J.; Volkow, N. D.; Felder, C.; Alexoff, D. Strategy for the Formation of Parametric Images under Conditions of Low Injected Radioactivity Applied to PET Studies with the Irreversible Monoamine Oxidase a Tracers [¹¹C]Clorgyline and Deuterium-Substituted [¹¹C]Clorgyline. *J. Cereb. Blood Flow Metab.* **2002**, *22* (11), 1367–1376.
166. Fowler, J. S.; Logan, J.; Volkow, N. D.; Wang, G.-J.; MacGregor, R. R.; Ding, Y.-S. Monoamine oxidase: radiotracer development and human studies. *Methods* **2002**, *27* (3), 263–277.
167. DeBay, D. R.; Reid, G. A.; Pottie, I. R.; Martin, E.; Bowen, C. V.; Darvesh, S. Targeting butyrylcholinesterase for preclinical single photon emission computed tomography (SPECT) imaging of Alzheimer's disease. *Alzheimers Dement. (N Y)* **2017**, *3* (2), 166–176.
168. Roivainen, A.; Rinne, J.; Virta, J.; Järvenpää, T.; Salomäki, S.; Yu, M.; Nägren, K. Biodistribution and blood metabolism of 1-¹¹C-methyl-4-piperidinyl n-butyrate in humans: an imaging agent for in vivo assessment of butyrylcholinesterase activity with PET. *J. Nucl. Med.* **2004**, *45* (12), 2032–2039.
169. Kikuchi, T.; Zhang, M.-R.; Ikota, N.; Fukushi, K.; Okamura, T.; Suzuki, K.; Arano, Y.; Irie, T. N-[¹⁸F]fluoroethylpiperidin-4-ylmethyl butyrate: a novel radiotracer for quantifying brain butyrylcholinesterase activity by positron emission tomography. *Bioorg. Med. Chem. Lett.* **2004**, *14* (8), 1927–1930.
170. James, S. L.; Ahmed, S. K.; Murphy, S.; Braden, M. R.; Belabassi, Y.; VanBrocklin, H. F.; Thompson, C. M.; Gerdes, J. M. A Novel Fluorine-18 β-Fluoroethoxy Organophosphate Positron Emission Tomography Imaging Tracer Targeted to Central Nervous System Acetylcholinesterase. *ACS Chem. Neurosci.* **2014**, *5* (7), 519–524.
171. Darvesh, S.; Darvesh, K. V.; McDonald, R. S.; Mataija, D.; Walsh, R.; Mothana, S.; Lockridge, O.; Martin, E. Carbamates with Differential Mechanism of Inhibition Toward Acetylcholinesterase and Butyrylcholinesterase. *J. Med. Chem.* **2008**, *51* (14), 4200–4212.
172. Macdonald, I. R.; Reid, G. A.; Pottie, I. R.; Martin, E.; Darvesh, S. Synthesis and Preliminary Evaluation of Phenyl 4-¹²³I-Iodophenylcarbamate for Visualization of Cholinesterases Associated with Alzheimer Disease Pathology. *J. Nucl. Med.* **2016**, *57* (2), 297–302.
173. Huang, G.; Kling, B.; Darras, F. H.; Heilmann, J.; Decker, M. Identification of a neuroprotective and selective butyrylcholinesterase inhibitor derived from the natural alkaloid evodiamine. *Eur. J. Med. Chem.* **2014**, *81*, 15–21.
174. Darras, F. H.; Kling, B.; Heilmann, J.; Decker, M. Neuroprotective Tri- and Tetracyclic BChE Inhibitors Releasing Reversible Inhibitors upon Carbamate Transfer. *ACS Med. Chem. Lett.* **2012**, *3* (11), 914–919.
175. De Vos, F.; Santens, P.; Vermeirsch, H.; Dewolf, I.; Dumont, F.; Slegers, G.; Dierckx, R. A.; De Reuck, J. Pharmacological Evaluation of [¹¹C]Donepezil as Tracer for Visualization of Acetylcholinesterase by PET. *Nucl. Med. Biol.* **2000**, *27* (8), 745–747.
176. Kimura, H.; Kawai, T.; Hamashima, Y.; Kawashima, H.; Miura, K.; Nakaya, Y.; Hirasawa, M.; Arimitsu, K.; Kajimoto, T.; Ohmomo, Y.; Ono, M.; Node, M.; Saji, H. Synthesis and evaluation of (–)- and (+)-[¹¹C]galanthamine as PET tracers for cerebral acetylcholinesterase imaging. *Bioorganic & Medicinal Chemistry* **2014**, *22* (1), 285–291.
177. Tavitian, B.; Pappata, S.; Bonnot-Lours, S.; Prenant, C.; Jobert, A.; Cruzel, C.; Di Giambardino, L. Positron emission tomography study of [¹¹C]methyl-tetrahydroaminoacridine (methyl-tacrine) in baboon brain. *Eur. J. Pharmacol.* **1993**, *236* (2), 229–238.

References

178. Rejc, L.; Gómez-Vallejo, V.; Joya, A.; Moreno, O.; Egimendia, A.; Castellnou, P.; Ríos-Anglada, X.; Cossío, U.; Baz, Z.; Passannante, R.; Tobalina-Larrea, I.; Ramos-Cabrer, P.; Giralt, A.; Sastre, M.; Capetillo-Zarate, E.; Košak, U.; Knez, D.; Gobec, S.; Marder, M.; Martin, A.; Llop, J. Longitudinal evaluation of a novel BChE PET tracer as an early *in vivo* biomarker in the brain of a mouse model for Alzheimer disease. *Theranostics* **2021**, *11* (13), 6542–6559.
179. Gentzsch, C.; Chen, X.; Spatz, P.; Košak, U.; Knez, D.; Nose, N.; Gobec, S.; Higuchi, T.; Decker, M. Synthesis and Initial Characterization of a Reversible, Selective ¹⁸F-Labeled Radiotracer for Human Butyrylcholinesterase. *Mol. Imaging Biol.* **2021**, doi: 10.1007/s11307-021-01584-2.
180. Košak, U.; Brus, B.; Knez, D.; Šink, R.; Žakelj, S.; Trontelj, J.; Pišlar, A.; Šlenc, J.; Gobec, M.; Živin, M.; Tratnjek, L.; Perše, M.; Sačat, K.; Podkowa, A.; Filipek, B.; Nachon, F.; Brazzolotto, X.; Więckowska, A.; Malawska, B.; Stojan, J.; Raščan, I. M.; Kos, J.; Coquelle, N.; Colletier, J.-P.; Gobec, S. Development of an *in-vivo* active reversible butyrylcholinesterase inhibitor. *Sci. Rep.* **2016**, *6* (1), 39495.
181. Ignatovich, Z. V.; Gusak, K. N.; Chernikhova, T. V.; Kozlov, N. G.; Koroleva, E. V. Interaction of secondary amines with aromatic aldehydes-efficient method for synthesis of the functionalized heterocyclic amines. *Chem. Heterocycl. Compd.* **2007**, *43* (12), 1540–1543.
182. Jorissen, W. P.; van der Beek, P. A. A. The oxidation of benzaldehyde. *Recl. Trav. Chim. Pays-Bas* **1930**, *49* (2), 138–141.
183. Node, M.; Hori, H.; Fujita, E. Demethylation of aliphatic methyl ethers with a thiol and boron trifluoride. *J. Chem. Soc. Perkin Trans. I* **1976**, (20), 2237–2240.
184. Middleton, W. J. New fluorinating reagents. Dialkylaminosulfur fluorides. *J. Org. Chem.* **1975**, *40* (5), 574–578.
185. Kabalka, G. W.; Varma, M.; Varma, R. S.; Srivastava, P. C.; Knapp, F. F. Tosylation of Alcohols. *J. Org. Chem.* **1986**, *51* (12), 2386–2388.
186. Košak, U.; Brus, B.; Gobec, S. Straightforward synthesis of orthogonally protected piperidin-3-ylmethanamine and piperidin-4-ylmethanamine derivatives. *Tetrahedron Lett.* **2014**, *55* (12), 2037–2039.
187. Porto, R. S.; Vasconcellos, M. L. A. A.; Ventura, E.; Coelho, F. Diastereoselective Epoxidation of Allylic Diols Derived from Baylis-Hillman Adducts. *Synthesis* **2005**, *2005* (14), 2297–2306.
188. Ellman, G. L.; Courtney, K. D.; Andres, V.; Featherstone, R. M. A new and rapid colorimetric determination of acetylcholinesterase activity. *Biochem. Pharmacol.* **1961**, *7* (2), 88–95.
189. Reid, G. A.; Chilukuri, N.; Darvesh, S. Butyrylcholinesterase and the cholinergic system. *Neuroscience* **2013**, *234*, 53–68.
190. Geula, C.; Nagykerly, N. Butyrylcholinesterase activity in the rat forebrain and upper brainstem: Postnatal development and adult distribution. *Exp. Neurol.* **2007**, *204* (2), 640–657.
191. Bevc, S.; Konc, J.; Stojan, J.; Hodošek, M.; Penca, M.; Praprotnik, M.; Janežič, D. ENZO: A Web Tool for Derivation and Evaluation of Kinetic Models of Enzyme Catalyzed Reactions. *PLOS ONE* **2011**, *6* (7), e22265.
192. Kuzmič, P. Application of the Van Slyke–Cullen irreversible mechanism in the analysis of enzymatic progress curves. *Anal. Biochem.* **2009**, *394* (2), 287–289.
193. Stojan, J. The mechanism and benefit of human butyrylcholinesterase activation by what would otherwise be inhibitors. *Chem.-Biol. Interact.* **2019**, *308*, 350–356.
194. Gentzsch, C.; Hoffmann, M.; Ohshima, Y.; Nose, N.; Chen, X.; Higuchi, T.; Decker, M. Synthesis and Initial Characterization of a Selective, Pseudo-irreversible Inhibitor of Human Butyrylcholinesterase as PET Tracer. *ChemMedChem* **2021**, *16*, 1427–1437.
195. Hoffmann, M.; Stiller, C.; Endres, E.; Scheiner, M.; Gunesch, S.; Sotriffer, C.; Maurice, T.; Decker, M. Highly Selective Butyrylcholinesterase Inhibitors with Tunable Duration of Action by Chemical Modification of Transferable Carbamate Units Exhibit Pronounced Neuroprotective Effect in an Alzheimer's Disease Mouse Model. *J. Med. Chem.* **2019**, *62* (20), 9116–9140.
196. Sawatzky, E.; Wehle, S.; Kling, B.; Wendrich, J.; Bringmann, G.; Sotriffer, C. A.; Heilmann, J.; Decker, M. Discovery of Highly Selective and Nanomolar Carbamate-Based Butyrylcholinesterase Inhibitors by Rational Investigation into Their Inhibition Mode. *J. Med. Chem.* **2016**, *59* (5), 2067–2082.
197. Fehler, S. K.; Maschauer, S.; Höfling, S. B.; Bartuschat, A. L.; Tschammer, N.; Hübner, H.; Gmeiner, P.; Prante, O.; Heinrich, M. R. Fast and Efficient ¹⁸F-Labeling by [¹⁸F]Fluorophenylazocarboxylic Esters. *Chem. Eur. J.* **2014**, *20* (2), 370–375.
198. Kato, S.; Morie, T.; Hino, K.; Kon, T.; Naruto, S.; Yoshida, N.; Karasawa, T.; Matsumoto, J. Novel Benzamides as Selective and Potent Gastric Prokinetic Agents. 1. Synthesis and Structure-Activity Relationships of *N*-[(2-Morpholinyl)alkyl]benzamides. *J. Med. Chem.* **1990**, *33* (5), 1406–1413.

References

199. Lainton, J. A. H.; Allen, M. C.; Burton, M.; Cameron, S.; Edwards, T. R. G.; Harden, G.; Hogg, R.; Leung, W.; Miller, S.; Morrish, J. J.; Rooke, S. M.; Wendt, B. Design and Synthesis of A Diverse Morpholine Template Library. *J. Comb. Chem.* **2003**, *5* (4), 400–407.
200. Sawatzky, E.; Bukowczan, J.; Decker, M. Investigation into selective debenzoylation and ring cleavage of quinazoline based heterocycles. *Tetrahedron Lett.* **2014**, *55* (18), 2973–2976.
201. Barnes, D. M.; Barkalow, J.; Plata, D. J. A Facile Method for the Preparation of MOM-Protected Carbamates. *Org. Lett.* **2009**, *11* (2), 273–275.

Single-Molecule Microscopy

International Edition: DOI: 10.1002/anie.201912683

German Edition: DOI: 10.1002/ange.201912683



Selective and Wash-Resistant Fluorescent Dihydrocodeinone Derivatives Allow Single-Molecule Imaging of μ -Opioid Receptor Dimerization

Christian Gentsch⁺, Kerstin Seier⁺, Antonios Drakopoulos, Marie-Lise Jobin, Yann Lanoiselée, Zsombor Koszegi, Damien Maurel, Rémy Sounier, Harald Hübner, Peter Gmeiner, Sébastien Granier, Davide Calebiro,* and Michael Decker*

Abstract: μ -Opioid receptors (μ -ORs) play a critical role in the modulation of pain and mediate the effects of the most powerful analgesic drugs. Despite extensive efforts, it remains insufficiently understood how μ -ORs produce specific effects in living cells. We developed new fluorescent ligands based on the μ -OR antagonist *E-p-nitrocinnamoylamino-dihydrocodeinone* (CACO), that display high affinity, long residence time and pronounced selectivity. Using these ligands, we achieved single-molecule imaging of μ -ORs on the surface of living cells at physiological expression levels. Our results reveal a high heterogeneity in the diffusion of μ -ORs, with a relevant immobile fraction. Using a pair of fluorescent ligands of different color, we provide evidence that μ -ORs interact with each other to form short-lived homodimers on the plasma membrane. This approach provides a new strategy to investigate μ -OR pharmacology at single-molecule level.

Introduction

Opioid receptors (ORs) belong to the family A of rhodopsin-like G protein-coupled receptors and occur in three major subtypes, μ , δ and κ .^[1] They are predominantly found in the central and peripheral nervous system, where they modulate transmission and perception of pain. Importantly, μ -ORs mediate most therapeutic effects of opioids, which are the most powerful, but also most addictive

analgesics known to date.^[2] In contrast, κ - and δ -OR activation causes weaker analgesia, but has been associated with less side effects.^[3] The effects of opioids on neurons are mainly mediated by activation of heterotrimeric G_i proteins, which inhibit cAMP production, while opening G protein-coupled inward rectifying potassium channels (GIRK) and closing voltage-dependent N-type Ca²⁺ channels via G _{$\beta\gamma$} subunits.^[2,3]

Because of their importance as drug targets, μ -ORs have been intensively investigated both, in vitro and in vivo.^[1–4] A major breakthrough in the field has been the determination of high-resolution three-dimensional structures of the μ -OR in complex with an antagonist and, later on, with an agonist and G protein mimetic nanobodies, as well as most recently by cryo-electron microscopy.^[5] These studies have provided important insights into the mechanisms of ligand binding and receptor activation, which might pave the way to the rational design of new analgesics with improved efficacy and less side effects, such as addiction. Interestingly, in the above studies μ -ORs were found to crystallize as dimers.^[5a,b] Largely based on previous experiments applying resonance energy transfer methods, these findings support the hypothesis that μ -ORs might form homodimers.^[1,4b,6] However, the nanoscale organization and dynamics of μ -ORs on the surface of living cells remain largely unknown, mostly due to technical limitations of conventional methods. These typically include

[*] C. Gentsch,^[†] A. Drakopoulos, Prof. Dr. M. Decker
 Pharmaceutical and Medicinal Chemistry, Institute of Pharmacy and Food Chemistry, Julius Maximilian University of Würzburg
 Am Hubland, 97074 Würzburg (Germany)
 E-mail: michael.decker@uni-wuerzburg.de

K. Seier,^[†] Dr. M. L. Jobin, Prof. Dr. D. Calebiro
 Institute of Pharmacology and Toxicology,
 Julius Maximilian University of Würzburg
 Versbacher Strasse 9, 97078 Würzburg (Germany)


Dr. Y. Lanoiselée, Dr. Z. Koszegi, Prof. Dr. D. Calebiro
 Institute of Metabolism and Systems Research & Centre of Membrane Proteins and Receptors, University of Birmingham
 IBR Tower, Level 2, Edgbaston, Birmingham, B152TT (UK)
 E-mail: d.calebiro@bham.ac.uk


Dr. D. Maurel
 ARPEGE (Pharmacology Screening Interactome) platform facility,
 Institut de Génétique Fonctionnelle, Université de Montpellier,
 CNRS, INSERM 141, rue de la Cardonille, 34094 Montpellier Cedex 05 (France)

Dr. R. Sounier, Dr. S. Granier
 Institut de Génétique Fonctionnelle, Université de Montpellier,
 CNRS, INSERM
 141, rue de la Cardonille, 34094 Montpellier Cedex 05 (France)

Dr. H. Hübner, Prof. Dr. P. Gmeiner
 Medicinal Chemistry, Department of Chemistry and Pharmacy,
 Friedrich-Alexander University of Erlangen-Nuremberg
 91058 Erlangen (Germany)

[†] These authors contributed equally to this work.

 Supporting information and the ORCID identification number(s) for the author(s) of this article can be found under:
<https://doi.org/10.1002/anie.201912683>.

 © 2019 The Authors. Published by Wiley-VCH Verlag GmbH & Co. KGaA. This is an open access article under the terms of the Creative Commons Attribution License, which permits use, distribution and reproduction in any medium, provided the original work is properly cited.

the requirement of cell disruption, insufficient spatiotemporal resolution and/or averaging over thousands or even millions of receptors.^[7]

In an attempt to overcome such limitations, we and others have developed innovative methods based on single-molecule microscopy, which allow imaging of individual receptors and other molecules on the surface of living cells with a temporal resolution of approximately 28.4 ms and a spatial resolution of approximately 20 nm, which is at least 10 times below the best theoretical resolution of conventional fluorescence microscopy.^[8] This approach can provide a highly quantitative characterization of dynamic events, such as protein-protein interactions among membrane receptors,^[9] even when involving only a small fraction of the investigated molecules.^[9a,c,10]

Here, we present the synthesis and single-molecule microscopy application of new fluorescent, selective μ -OR ligands to study unmodified receptors in living cells at physiological expression levels.

Results and Discussion

The structure of the ligands consists of a pharmacologically active compound, a fluorophore, and a linker (Figure 1).

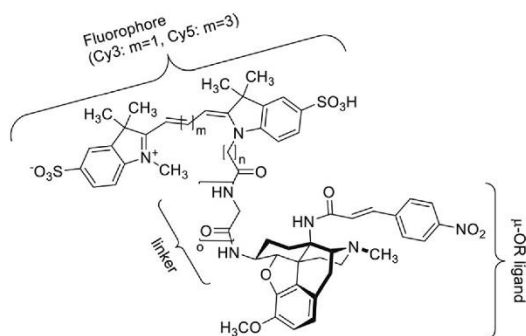


Figure 1. Structure of the fluorescent, selective μ -opioid receptor ligands ($n=5$, $o=4$).

All three units have been chosen with regard to their individual and specific characteristics to achieve high affinity and selectivity as well as optimal optical properties for single-molecule fluorescence microscopy, for example, high signal-to-noise ratios and low blinking and bleaching rates.

The pharmacologically active moiety (parent ligand) is based upon *E-p*-nitrocinnamoylamino-dihydrocodeinone (CACO), which had been described to be a potent and selective μ -OR ligand, and to retain such properties upon conjugation with the small organic fluorophore BODIPY ($EC_{50}=24.4$ nM, $\delta/\kappa > 1000$ nM) through a small alkylene linker.^[11] The unlabeled ligand has been described to act as short-term agonist and long-term antagonist with an IC_{50} value of 0.46 ± 0.003 nM for μ -OR ($\delta = 4.2 \pm 1.3$ nM, $\kappa = 19 \pm 2.8$ nM). A K_d of 0.52 ± 0.14 nM was measured by means of saturation binding experiments with [³H]DAMGO.^[12] The nitrocinnamoyl part of the active compound contains a Mi-

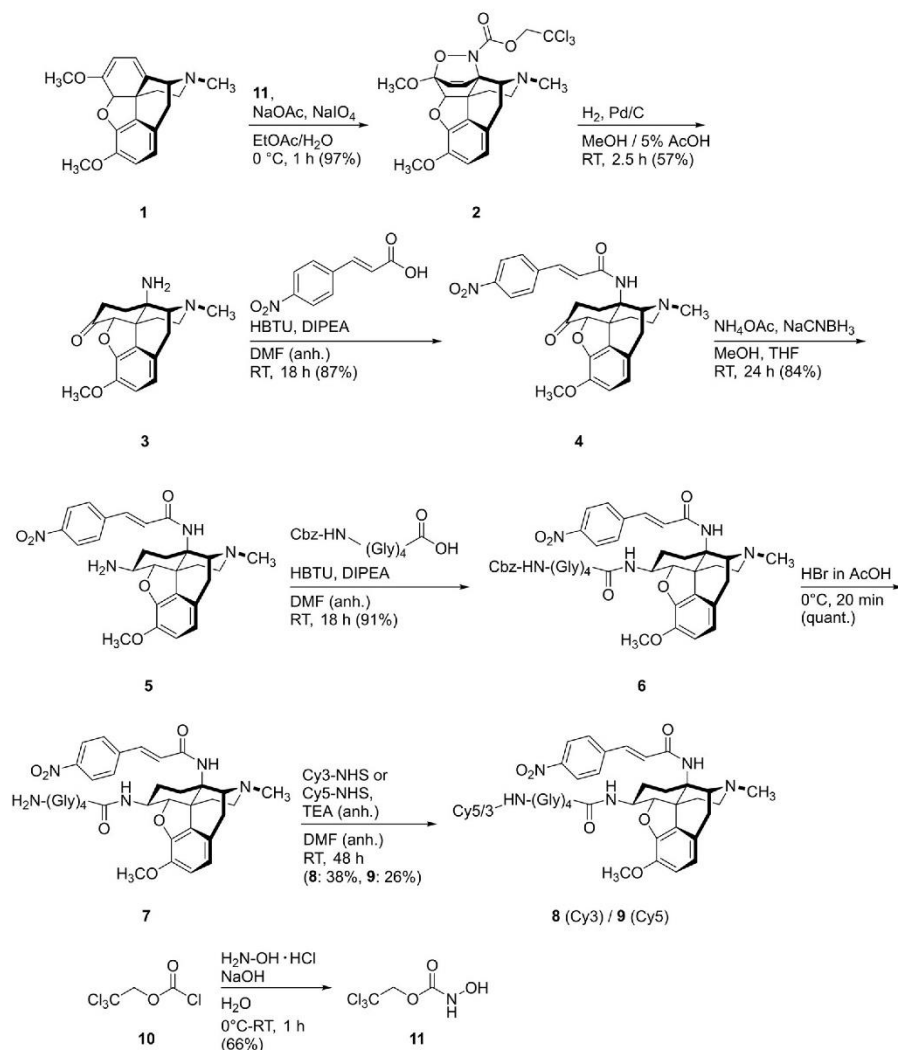
chael acceptor, which potentially forms covalent bonds with nucleophilic side-chains of amino acids in the μ -OR binding pocket. This has been shown in the μ -OR crystal structure for β -funaltrexamine.^[5a]

The pentylene linker connects the pharmacologically active moiety and the fluorophore. In our probe design, we incorporated a tetraglycine into the linker, inspired by previous studies based on GPCR-imaging with fluorescent ligands, which yielded improved results.^[13] Cyanine 3 and 5 (Cy3/5) were chosen as fluorophores because of their advantageous optical properties which make them particularly suited for single-molecule microscopy, including emission in the red and near infrared regions of the spectrum, respectively, as well as high absorption coefficients and quantum yields.^[14]

The synthesis shown in Scheme 1 started with a hetero-Diels–Alder reaction of thebaine **1** and the intermediately oxidized *N*-hydroxycarbamate **11**, prepared from the respective chloroformate **10**.^[15] The resulting cycloadduct **2** was hydrogenated to give dihydrocodeinone **3**.^[16] A nitrocinnamoyl moiety was introduced by coupling the C14-amino group of **3** with the respective activated acid, yielding compound **4**.^[17] Subsequent reductive amination of the C-6-keto group led to compound **5**.^[11] In a preliminary approach, we directly used the NHS-activated dyes to couple them to the newly introduced amino-group. However, these probes had shown high background and a poor signal-to-noise ratio in single-molecule microscopy experiments (see Supporting Information). While an alkylene chain might be sufficient to bridge pharmacophore and fluorophore and define the distance between the bulky residues, the tetraglycine moiety additionally increases the polarity of the compound and prevents sticking to the plasma membrane (Figure 1). This led to a major increase in selectivity and reduction of background. The newly introduced amino group of **5** was coupled to *N*-Cbz-protected tetraglycine, yielding compound **6**.^[17] After deprotection of Cbz with hydrobromic acid, the free amine **7** was coupled to the NHS-activated dyes Cy3 and Cy5 to give the desired fluorescent ligands **8** and **9** (Scheme 1).

Saturation binding curves obtained for compound **9** showed its selectivity for μ -OR (Figure 2A) in a homogenous time-resolved FRET (HTRF) assay with HEK293 cells, which gave optimal results. No significant binding was observed to the other OR-subtypes (Figure 2A). These findings are in good agreement with previous binding studies on the parent compound CACO.^[12]

We then tested compounds **8** (Cy3 conjugate) and **9** (Cy5 conjugate) against wild-type μ -OR expressed in CHO cells, which adhere very well to glass-coverslips, resulting in a particularly flat plasma membrane. Compounds **8** and **9** bound to cell-surface receptors were selectively imaged by total internal reflection fluorescence microscopy (TIRF), which illuminates only approximately 200 nm at the interface between the coverslip and the cells (Figure 2B). CHO cells devoid of μ -OR expression were used as control for unspecific binding. The results confirmed a highly specific binding of the compounds to μ -ORs, with negligible unspecific binding to the cells or the coverslip (Figure 2B). This approach also allowed us to obtain concentration-binding relationships for



Scheme 1. Synthesis of the fluorescent, μ -OR selective ligands **8** and **9**.

both compounds. In these experiments, we incubated CHO cells with increasing concentrations of either compound **8** or **9** for 20 min and imaged them by TIRF microscopy. The mean intensities of at least 40 cells per condition were averaged for each concentration of ligand, which allowed us to estimate their affinities (K_D) (Figure 2C). A K_D value of 87 ± 49 nM for compound **8** was reached, whereas compound **9** showed a three-fold lower affinity for μ -ORs with an estimated K_D value of 295 ± 141 nM. The initial affinity of CACO for the μ -OR was reported to be 0.52 ± 0.14 nM.^[12] Intrinsic activity of compound **8** was determined in an inositol mono phosphate-accumulation assay for G-protein mediated signaling. In this assay, the compound acted as a partial agonist ($EC_{50} = 190$ nM, $E_{max} = 57\%$ of maximal response to morphine), while it was inactive in the β -arrestin-2 recruitment assay (cf. Supporting Information). Although chemical modifications often lead to changes in the pharmacological profiles of small molecules, both compounds retain high affinity towards μ -

OR. A 50% wash resistance of CACO has been reported in competition binding experiments with DAMGO, probably due to the capability of the 14β -p-nitrocinnamoylamino-side chain of CACO to bind covalently to the μ -OR.^[12] Fluorescent probes for single-molecule microscopy not only need to possess high labeling efficiency, but ideally, also long residence time on the receptor. Thus, intrigued by the possibility that CACO may bind covalently to μ -OR, we investigated if compounds **8** and **9** also retained a high wash resistance. For this purpose, we performed washing experiments in CHO cells transiently treated with either compound **8** or **9** for 20 min and imaged by TIRF microscopy (Figure 3). During washing, we observed a slow decrease of fluorescence intensity, until it reached a plateau at approximately 33% and 53% of the initial values for compound **8** and **9**, respectively. Importantly, these results indicate that both fluorescent ligands exhibit a long residence time on μ -OR, with a fraction of virtually non-dissociating receptors.

Next, we tested the applicability of the new fluorescent ligands for single-molecule fluorescence microscopy. Both compounds showed excellent photophysical properties, giving rise to easily detectable fluorescent spots in TIRF microscopy. Compound **8** showed slower photobleaching in comparison to compound **9**, consistent with the known photophysical properties of Cy5 and Cy3, respectively.^[18] Therefore, the Cy3 ligand was used for subsequent single-color experiments. CHO cells transiently transfected to express wild-type μ -OR at low physiological densities (approximately 0.8 receptors per μm^2) were incubated with a saturating concentration of compound **8** ($1 \mu\text{M}$) and imaged by fast TIRF microscopy. The transfected cells were easily distinguishable from the background, confirming a highly specific binding (Figure 4A). Individual μ -ORs carrying a fluorescent ligand were detected and tracked using an automated algorithm.^[9a,c,19] A time-averaged mean square displacement (TAMSD) analysis was performed, which allowed investigating the diffusion of the

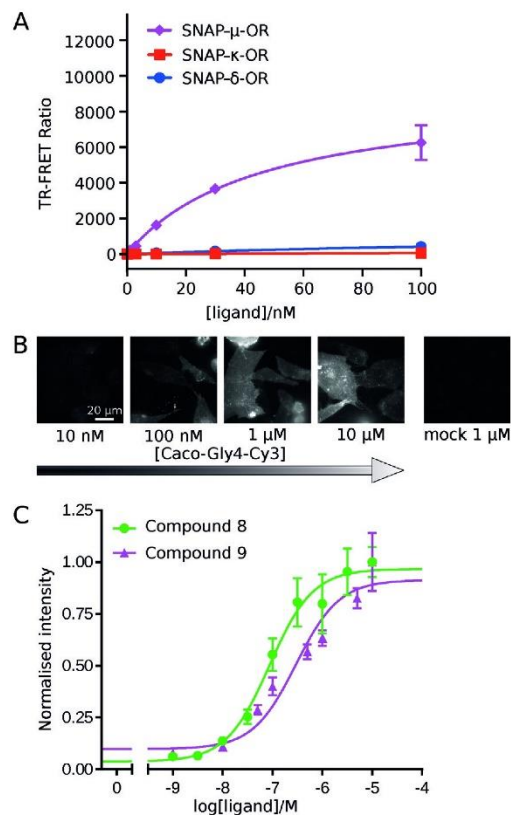


Figure 2. Characterization of compounds **8** and **9**. A) Selectivity of compound **9** for μ -OR versus κ -OR and δ -OR. HEK293 cells were transfected with either OR subtype carrying a SNAP-tag at its N-terminus and labeled with SNAP-Lumi4-Tb. Binding of the fluorescent ligand was detected via HTRF. The mean \pm S.E.M. of three independent experiments is shown. B) Representative TIRF images of CHO cells either transfected with wild-type μ -OR or mock transfected and treated with increasing concentrations of compound **8**. C. Concentration-binding relationships for compounds **8** and **9** obtained from images as in B. The mean \pm S.E.M. of three independent experiments is shown (32 to 86 cells per data point).

receptors within the plasma membrane (cf. Supporting Information). This analysis revealed a high heterogeneity in the mobility of μ -ORs on the plasma membrane. Individual μ -OR particles were classified into four categories based on the type and speed of their motion.^[9c] A percentage of $22 \pm 2\%$ of the receptors were virtually immobile, likely due to trapping in small nanodomains or binding to immobile membrane structures. Sub-diffusive motion was observed for $34 \pm 1\%$, meaning their motion was hindered by either crowding or interactions with their environment. This phenomenon has been previously described for other membrane receptors and can arise from different factors, such as transient trapping in nanodomains.^[9c,20]

Another $34 \pm 1\%$ of the receptors showed normal diffusion, that is, Brownian motion. Super-diffusion, that is, directional motion, was observed for the remaining $10 \pm 1\%$ of particles.

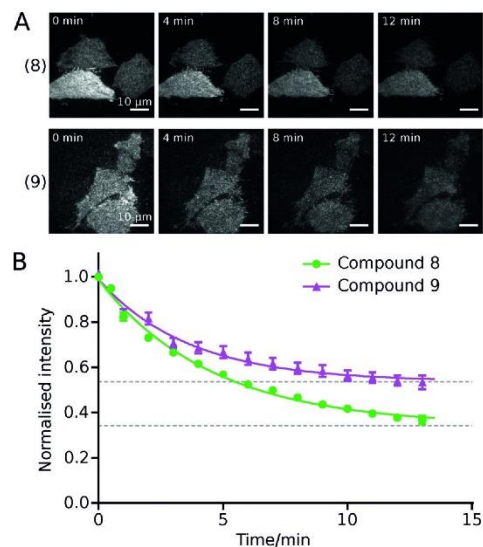


Figure 3. Wash resistance of compounds **8** and **9**. A) Representative TIRF images of CHO cells transiently transfected with wild-type μ -OR and treated with $1 \mu\text{M}$ of compound **8** (top) or **9** (bottom) for 20 min followed by washing. The same cells were imaged every minute during the wash. B) Plots of compound **8/9** dissociation over time obtained from image sequences as in (A). Photobleaching of compounds **8** during this time was negligible; the intensity values of compound **9** were corrected for photobleaching. The mean \pm S.E.M. of four independent experiments is shown (13 and 15 cells per data point, respectively). Data were fitted with a one phase exponential decay plus a constant.

These results are in agreement with previous findings for other prototypical GPCRs like the β_2 - or the α_{2A} -adrenergic receptor.^[9c]

We then explored the applicability of compounds **8** and **9** in single-molecule microscopy experiments to investigate the dimerization of μ -OR at low/physiological expression levels in living cells. For this purpose, CHO cells were transiently transfected with wild-type μ -OR, yielding a total receptor density of around 1.7 particles per μm^2 . The cells were then simultaneously labeled with a mixture of compounds **8** and **9** ($1 \mu\text{M}$ and $0.5 \mu\text{M}$, respectively) to label as many receptors as possible (approximately 80%) with either compound, while keeping unspecific binding to the glass-coverslip low. Then, imaging by fast two-color TIRF microscopy was carried out. The co-localization between receptors labeled with compound **8** and **9** was analyzed by automated computer algorithms as previously described.^[9c] In order to correct for the presence of random co-localizations and to estimate the duration of μ -OR interactions, we applied a previously developed method based on deconvolution of the co-localization times.^[9c] For this purpose, we additionally performed the same experiment using μ -ORs labeled with compound **8** and CD86, a monomeric control protein not interacting with μ -OR, labeled with Alexa Fluor 647 via a SNAP-tag fused at its N-terminus (Figure S2 in the Supporting Information).^[9a] This served as control for the co-localizations expected in the absence of interactions. The deconvolution analysis revealed

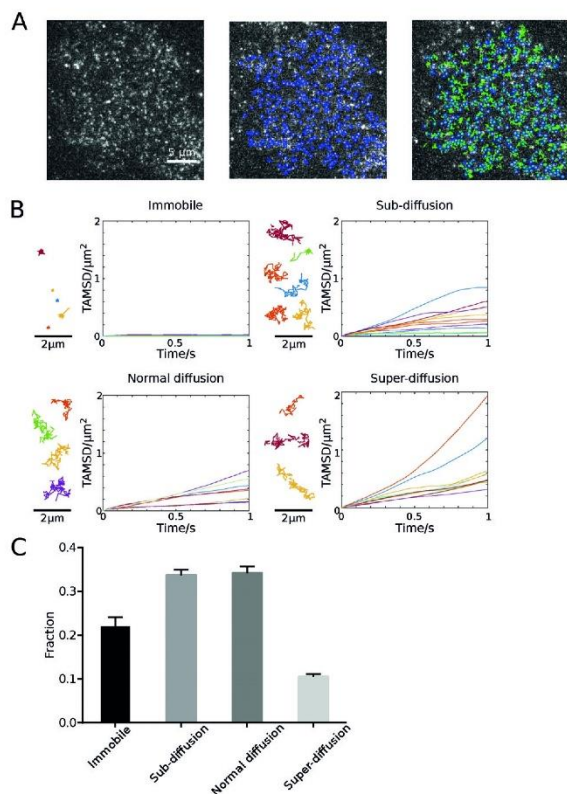


Figure 4. Single-molecule imaging of μ -ORs on the surface of living cells using compound **8**. A) Representative results. A frame of a representative TIRF image sequence (left) and the results of the automated single-particle detection (middle) and tracking algorithm used to follow individual μ -ORs (right) is shown. The current position of individual receptors (blue circles) and their trajectories (green splines) are shown. B) Time-averaged mean square displacement (TAMSD) analysis on the obtained μ -OR trajectories. Based on the results, the trajectories were classified into four categories: virtually immobile, sub-diffusive, normal diffusive and super-diffusive. Shown are examples of trajectories belonging to the four categories and their corresponding TAMSD curves. C) Distribution of μ -ORs trajectories in the four categories identified by the TAMSD analysis. Data are mean \pm S.E.M of 29 individual cells (2,225 trajectories).

that more than 95 % of μ -ORs were diffusing on the plasma membrane as monomers. However, it also revealed a small but consistent fraction of receptors that apparently underwent transient interactions lasting approximately 1–2 seconds. At the low receptor densities analyzed, this fraction of μ -ORs that were interacting at any given time was approximately 4–5 %. Although this represents only a fraction of the receptors, this value is remarkably similar to the one observed between active receptors and G proteins,^[9c] a fundamental interaction in GPCR signaling, suggesting that although involving only a small fraction of receptors it might nevertheless be biologically relevant. Even though the presence of an even smaller fraction of higher order oligomers cannot be completely ruled out, the intensities of the majority of receptor particles and their bleaching behavior (i.e., number of observed photobleaching steps) were consistent with them

being monomers or at most dimers. By deconvolving the distribution of the co-localization times observed between μ -ORs labeled with compounds **8** and **9**, and those obtained between μ -OR and CD86, we were able to estimate the frequency and duration of the interactions between μ -ORs. The resulting relaxation plot of μ -OR interactions (Figure 5B) indicated that μ -ORs were dissociating following an

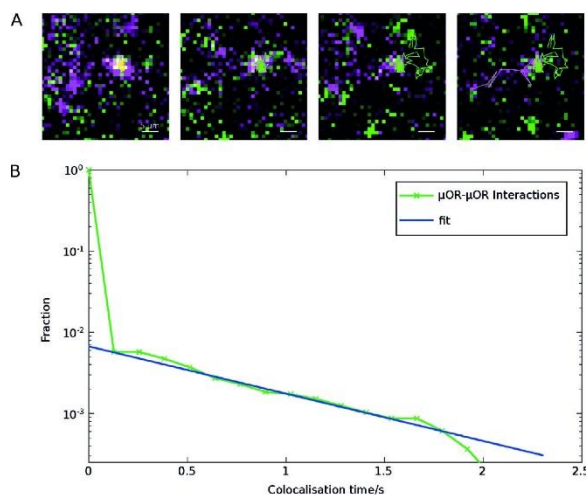


Figure 5. Single-molecule imaging of transient μ -OR interactions. A) Example of a transient co-localization (yellow) observed between two μ -ORs, one labeled with compound **8** (green) and the other with compound **9** (magenta). Both receptors interrupted their motion during the co-localization event. B) Estimation of the frequency and duration of interactions between μ -ORs based on deconvolution of their co-localization times with those obtained between μ -ORs and CD86, where no interactions are expected. Data are from 51832 co-localizations obtained from 25 individual cells for μ -OR- μ -OR and 61259 co-localizations for CD86- μ -OR.

exponential decay, with an estimated time constant (τ) of 1.797 ± 0.487 s (corresponding to a dissociation rate constant, k_{off} of 0.557 ± 0.207 s⁻¹). This value is in good agreement with previous results obtained with prototypical family A GPCRs.^[9a-c,21] This approach also allowed us to calculate the two-dimensional association rate (k_{on}) for interactions between μ -ORs, that is, the formation of dimers, which we estimated to be 0.020 ± 0.004 μm^2 molecule⁻¹ s⁻¹. The estimated k_{on} and k_{off} values give a dissociation equilibrium constant (K_{d}) of 27.43 ± 11.75 molecules per μm^2 , allowing to predict the fraction of μ -ORs in monomeric or dimeric state depending on their density on the plasma membrane. Based on the obtained K_{d} value, we estimate that a μ -OR density of approximately 27 molecules per μm^2 would be required for 50 % of them to be in dimeric state (approximately 7 dimers and 14 monomers per μm^2). Since such densities might occur at synapses,^[22] it is possible that a relevant fraction of μ -ORs might form transient dimers in vivo.^[23]

Interestingly, the majority of receptors seemed to transiently stop diffusing while interacting (Figure 5A). A possible explanation for this is that the observed interactions might represent receptors being simultaneously recruited to

the same clathrin-coated pit (CCP) before internalization. To investigate this possibility, we repeated the same experiment in the presence of co-transfected GFP-tagged clathrin (Figure 6). Computational analyses showed that $77 \pm 9\%$ of all observed μ -OR interactions happen outside of CCPs, with only $23 \pm 9\%$ occurring within or near CCPs. These results suggest that other mechanisms are involved in the observed transient trapping of μ -ORs during their interactions.

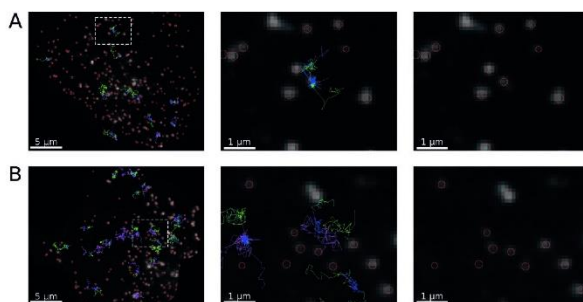


Figure 6. Single-molecule imaging of transient μ -OR interactions in relationship to the location of clathrin coated pits (CCPs). CHO cells were transiently transfected with wild-type μ -OR and GFP-clathrin. The cells were treated with compound **8** ($1 \mu\text{M}$) and compound **9** ($0.5 \mu\text{M}$) for 20 min. After one rapid wash, the cells were imaged by fast two-color TIRF microscopy to track the receptors, followed by acquisition of a CCP image. Shown are images of a representative cell (left) with the obtained trajectories of receptors (green and magenta, respectively) undergoing interactions (blue) overlaid on the CCP image (grey). Red circles correspond to individual CCPs. Middle, enlarged views of the regions delimited by the dashed boxes. Right, same regions without trajectories. A) interactions occurring within or near CCPs. B) interactions occurring outside CCPs.

Conclusion

Whereas GPCRs have long been believed to be solely monomeric receptors, a growing body of evidence obtained mainly using fluorescence and bioluminescence resonance energy transfer (FRET and BRET) suggests that they might form dimers or even higher order oligomers.^[7,10b,24] However, the occurrence of GPCR dimerization at physiological expression levels and their stability remain—with few notable exceptions such as family C GPCRs—controversial. These debates also extend to μ -OR, for which contrasting results have been obtained using methods relying on different expression levels, ranging from physiological levels to over-expression and even purification. Whereas several of the published studies provide evidence in favor of dimerization,^[1,4b,5a,25] others indicate that μ -ORs can function as monomers or the fraction of dimers is negligible.^[26] Our data, obtained on wild-type receptors expressed at levels in living cells contribute to resolve this controversy by showing that whereas most μ -ORs are monomeric, a small, though potentially biologically relevant, fraction of receptors undergo transient dimerization. As the receptors appear to be in equilibrium between monomers and dimers, higher level of dimerization might be achieved at sites of particular high receptor density such as synapses.

In summary, we developed two novel, fluorescent, subtype-selective ligands for the μ -OR with binding affinities in the nanomolar range and the advantageous property of wash resistance. Importantly, we show that the favorable properties of these ligands make them ideal for single-molecule microscopy. We used this set of ligands to investigate the diffusion behavior of μ -ORs as well as their interactions at physiological expression levels. Our results reveal the occurrence of transient receptor interactions, consistent with a dynamic equilibrium between monomers and dimers. As only a small fraction of receptors was found to be interacting with each other in our study, which is too small to be detected in ensemble measurements, our results may help to reconcile some of the apparent discrepancies between previous studies. Importantly, our results reveal dynamic interactions among μ -ORs that occur outside CCPs that would have likely been missed using ensemble methods. This new approach opens up new venues to investigate μ -OR biology and pharmacology in living cells with unprecedented spatiotemporal resolution.

Experimental Section

Comprehensive details of the experimental design can be found in the Supporting Information.

Acknowledgements

This study was supported by the Deutsche Forschungsgemeinschaft (TRR166 ReceptorLight, project C1 to D.C.), a Wellcome Trust Senior Research Fellowship (212313/Z/18/Z to D.C.) and by the National Institutes of Health Grant (NIDA-DA036246 to S.G.). K.S. and A.D. were supported by the Elite Network of Bavaria International Doctoral Program “Receptor Dynamics”.

Conflict of interest

The authors declare no conflict of interest.

Keywords: fluorescent probes · G-protein coupled receptor · homodimerization · opioid ligands · single-molecule microscopy

How to cite: *Angew. Chem. Int. Ed.* **2020**, *59*, 5958–5964
Angew. Chem. **2020**, *132*, 6014–6020

- [1] D. Massotte, *Br. J. Pharmacol.* **2015**, *172*, 420–434.
- [2] M. Waldhoer, S. E. Bartlett, J. L. Whistler, *Annu. Rev. Biochem.* **2004**, *73*, 953–990.
- [3] R. Al-Hasani, M. R. Bruchas, *Anesthesiology* **2011**, *115*, 1363–1381.
- [4] a) B. M. Cox, *Mol. Pharmacol.* **2013**, *83*, 723–728; b) W. Fujita, I. Gomes, A. Devi Lakshmi, *Br. J. Pharmacol.* **2014**, *171*, 4155–4176.
- [5] a) A. Manglik, A. C. Kruse, T. S. Kobilka, F. S. Thian, J. M. Mathiesen, R. K. Sunahara, L. Pardo, W. I. Weis, B. K. Kobilka,

- S. Granier, *Nature* **2012**, *485*, 321–326; b) W. Huang, A. Manglik, A. J. Venkatakrishnan, T. Laemans, E. N. Feinberg, A. L. Sanborn, H. E. Kato, K. E. Livingston, T. S. Thorsen, R. C. Kling, S. Granier, P. Gmeiner, S. M. Husbands, J. R. Traynor, W. I. Weis, J. Steyaert, R. O. Dror, B. K. Kobilka, *Nature* **2015**, *524*, 315–321; c) A. Koehl, H. Hu, S. Maeda, Y. Zhang, Q. Qu, J. M. Paggi, N. R. Latorraca, D. Hilger, R. Dawson, H. Matile, G. F. X. Schertler, S. Granier, W. I. Weis, R. O. Dror, A. Manglik, G. Skiniotis, B. K. Kobilka, *Nature* **2018**, *558*, 547–552.
- [6] F. Ciruela, K. A. Jacobson, V. Fernández-Dueñas, *ACS Chem. Biol.* **2014**, *9*, 1918–1928.
- [7] D. Calebiro, M.-L. Jobin, *Curr. Opin. Cell Biol.* **2019**, *57*, 57–63.
- [8] D. Calebiro, T. Sungkaworn, *Trends Pharmacol. Sci.* **2018**, *39*, 109–122.
- [9] a) D. Calebiro, F. Rieken, J. Wagner, T. Sungkaworn, U. Zabel, A. Borzi, E. Cocucci, A. Zürn, M. J. Lohse, *Proc. Natl. Acad. Sci. USA* **2013**, *110*, 743–748; b) J. A. Hern, A. H. Baig, G. I. Mashanov, B. Birdsall, J. E. T. Corrie, S. Lazareno, J. E. Molloy, N. J. M. Birdsall, *Proc. Natl. Acad. Sci. USA* **2010**, *107*, 2693–2698; c) T. Sungkaworn, M.-L. Jobin, K. Burnecki, A. Weron, M. J. Lohse, D. Calebiro, *Nature* **2017**, *550*, 543–547; d) R. S. Kasai, K. G. N. Suzuki, E. R. Prossnitz, I. Koyama-Honda, C. Nakada, T. K. Fujiwara, A. Kusumi, *J. Cell Biol.* **2011**, *192*, 463–480.
- [10] a) T. Sungkaworn, F. Rieken, M. J. Lohse, D. Calebiro, *J. Vis. Exp.* **2014**, *89*, e51784; b) L. Persani, D. Calebiro, M. Biondi, *Nat. Clin. Pract. Endocrinol. Metab.* **2007**, *3*, 180–190; c) W. Tian, Y. Cao, A. Ismael, D. Stone, J. Liang, in *2014 36th Annual International Conference of the IEEE Engineering in Medicine and Biology Society*, **2014**, pp. 1166–1169.
- [11] P. J. Emmerson, S. Archer, W. El-Hamouly, A. Mansour, H. Akil, F. Medzihradsky, *Biochem. Pharmacol.* **1997**, *54*, 1315–1322.
- [12] J. P. McLaughlin, K. P. Hill, Q. Jiang, A. Sebastian, S. Archer, J. M. Bidlack, *J. Pharmacol. Exp. Ther.* **1999**, *289*, 304–311.
- [13] a) L. A. Stoddart, A. J. Vernall, S. J. Briddon, B. Kellam, S. J. Hill, *Neuropharmacology* **2015**, *98*, 68–77; b) A.-C. Chang, C. C. Chao, A. E. Takemori, G. Gekker, S. Hu, P. K. Peterson, P. S. Portoghese, *J. Med. Chem.* **1996**, *39*, 1729–1735; c) T. Kshirsagar, A. H. Nakano, P.-Y. Law, R. Elde, P. S. Portoghese, *Neurosci. Lett.* **1998**, *249*, 83–86.
- [14] P. L. Southwick, L. A. Ernst, E. W. Tauriello, S. R. Parker, R. B. Mujumdar, S. R. Mujumdar, H. A. Clever, A. S. Waggoner, *Cytometry* **1990**, *11*, 418–430.
- [15] G. W. Kirby, H. McGuigan, J. W. M. Mackinnon, D. McLean, R. P. Sharma, *J. Chem. Soc. Perkin Trans. 1* **1985**, 1437–1442.
- [16] A. Sebastian, J. M. Bidlack, Q. Jiang, D. Deecher, M. Teitler, S. D. Glick, S. Archer, *J. Med. Chem.* **1993**, *36*, 3154–3160.
- [17] M. J. Burke, B. M. Trantow, *Tetrahedron Lett.* **2008**, *49*, 4579–4581.
- [18] M. Dar, T. Giesler, R. Richardson, C. Cai, M. Cooper, S. Lavasani, P. Kille, T. Voet, J. Vermecsch, *BMC Biotechnol.* **2008**, *8*, 86.
- [19] K. Jaqaman, G. Danuser, *Cold Spring Harbor Protoc.* **2009**, *4*, 1–10.
- [20] K. Murase, T. Fujiwara, Y. Umemura, K. Suzuki, R. Ino, H. Yamashita, M. Saito, H. Murakoshi, K. Ritchie, A. Kusumi, *Biophys. J.* **2004**, *86*, 4075–4093.
- [21] A. Tabor, S. Weisenburger, A. Banerjee, N. Purkayastha, J. M. Kaindl, H. Hübner, L. Wei, T. W. Grömer, J. Kornhuber, N. Tschammer, N. J. M. Birdsall, G. I. Mashanov, V. Sandoghdar, P. Gmeiner, *Sci. Rep.* **2016**, *6*, 1–16.
- [22] a) S. J. Tobin, D. L. Wakefield, L. Terenius, V. Vukojević, T. Jovanović-Talisan, *ACS Chem. Neurosci.* **2019**, *10*, 667–676; b) E. J. Van Bockstaele, E. E. O. Colago, A. Moriwaki, G. R. Uhl, *J. Comp. Neurol.* **1996**, *376*, 65–74; c) T. A. Milner, C. T. Drake, *Brain Res. Bull.* **2001**, *54*, 131–140.
- [23] J. Le Merrer, J. A. J. Becker, K. Befort, B. L. Kieffer, *Physiol. Rev.* **2009**, *89*, 1379–1412.
- [24] a) G. Milligan, D. Ramsay, G. Pascal, J. J. Carrillo, *Life Sci.* **2003**, *74*, 181–188; b) M. Bouvier, T. E. Hébert, *J. Physiol.* **2014**, *592*, 2439–2441; c) G. Milligan, R. J. Ward, S. Marsango, *Curr. Opin. Cell Biol.* **2019**, *57*, 40–47; d) G. Milligan, M. Bouvier, *FEBS J.* **2005**, *272*, 2914–2925.
- [25] a) L.-W. Chen, C. Gao, D.-H. Zhou, Q. Wei, X.-J. Xu, J. Chen, Z.-Q. Chi, *Protein Pept. Lett.* **2002**, *9*, 145–152; b) B. A. Jordan, L. A. Devi, *Nature* **1999**, *399*, 697–700; c) I. Gomes, A. Gupta, J. Filipovska, H. H. Szeto, J. E. Pintar, L. A. Devi, *Proc. Natl. Acad. Sci. USA* **2004**, *101*, 5135–5139; d) I. Gomes, B. A. Jordan, A. Gupta, N. Trapaidze, V. Nagy, L. A. Devi, *J. Neurosci.* **2000**, *20*, RC110; e) F. M. Decallot, R. Rozenfeld, A. Gupta, L. A. Devi, *Proc. Natl. Acad. Sci. USA* **2008**, *105*, 16045–16050; f) I. Gomes, J. Filipovska, B. A. Jordan, L. A. Devi, *Methods* **2002**, *27*, 358–365; g) D. Wang, X. Sun, L. Bohn, W. Sadee, *Mol. Pharmacol.* **2005**, *67*, 2173–2184; h) L. He, J. Fong, M. Von Zastrow, J. L. Whistler, *Cell* **2002**, *108*, 271–282; i) D. Provasi, M. B. Boz, J. M. Johnston, M. Filizola, *PLOS Comput. Biol.* **2015**, *11*, e1004148; j) X. Zhang, Y. Yuan, L. Wang, Y. Guo, M. Li, C. Li, X. Pu, *Phys. Chem. Chem. Phys.* **2018**, *20*, 13485–13496.
- [26] a) A. J. Kuszak, S. Pitchaiya, J. P. Anand, H. I. Mosberg, N. G. Walter, R. K. Sunahara, *J. Biol. Chem.* **2009**, *284*, 26732–26741; b) D. Meral, D. Provasi, D. Prada-Gracia, J. Möller, K. Marino, M. J. Lohse, M. Filizola, *Sci. Rep.* **2018**, *8*, 1–13.

Manuscript received: October 9, 2019
Accepted manuscript online: December 6, 2019
Version of record online: January 7, 2020

Appendix II



Mol Imaging Biol (2021)
DOI: 10.1007/s11307-021-01584-2
© The Author(s), 2021. This article is an open access publication



RESEARCH ARTICLE

Synthesis and Initial Characterization of a Reversible, Selective ^{18}F -Labeled Radiotracer for Human Butyrylcholinesterase

Christian Gentsch,¹ Xinyu Chen,^{2,3,4} Philipp Spatz,^{1,3} Urban Košak,⁵ Damijan Knez,⁵ Naoko Nose,⁶ Stanislav Gobec,⁵ Takahiro Higuchi,^{3,4,6} Michael Decker¹

¹Pharmaceutical and Medicinal Chemistry, Institute of Pharmacy and Food Chemistry, Julius-Maximilians-University of Würzburg, Am Hubland, 97074, Würzburg, Germany

²Department of Nuclear Medicine, University Hospital of Augsburg, Stenglinstraße 2, 86156, Augsburg, Germany

³Department of Nuclear Medicine, University Hospital of Würzburg, Oberdürrbacher Straße 6, 97080, Würzburg, Germany

⁴Comprehensive Heart Failure Center, University Hospital of Würzburg, Am Schwarzenberg 15, 97078, Würzburg, Germany

⁵Chair of Pharmaceutical Chemistry, Faculty of Pharmacy, University of Ljubljana, Aškerčeva cesta 7, SI-1000, Ljubljana, Slovenia

⁶Graduate School of Medicine, Dentistry and Pharmaceutical Sciences, Okayama University, 2-5-1 Shikata-cho, Kita-ku, Okayama, Japan

Abstract

Purpose: A neuropathological hallmark of Alzheimer's disease (AD) is the presence of amyloid- β ($\text{A}\beta$) plaques in the brain, which are observed in a significant number of cognitively normal, older adults as well. In AD, butyrylcholinesterase (BChE) becomes associated with $\text{A}\beta$ aggregates, making it a promising target for imaging probes to support diagnosis of AD. In this study, we present the synthesis, radiochemistry, *in vitro* and preliminary *ex* and *in vivo* investigations of a selective, reversible BChE inhibitor as PET-tracer for evaluation as an AD diagnostic.

Procedures: Radiolabeling of the inhibitor was achieved by fluorination of a respective tosylated precursor using $\text{K}[^{18}\text{F}]$. IC_{50} values of the fluorinated compound were obtained in a colorimetric assay using recombinant, human (*h*) BChE. Dissociation constants were determined by measuring *h*BChE activity in the presence of different concentrations of inhibitor.

Results: Radiofluorination of the tosylate precursor gave the desired radiotracer in an average radiochemical yield of 20 ± 3 %. Identity and >95.5 % radiochemical purity were confirmed by HPLC and TLC autoradiography. The inhibitory potency determined in Ellman's assay gave an IC_{50} value of 118.3 ± 19.6 nM. Dissociation constants measured in kinetic experiments revealed lower affinity of the inhibitor for binding to the acylated enzyme ($K_2 = 68.0$ nM) in comparison to the free enzyme ($K_1 = 32.9$ nM).

Conclusions: The reversibly acting, selective radiotracer is synthetically easily accessible and retains promising activity and binding potential on *h*BChE. Radiosynthesis with ^{18}F labeling of tosylates was feasible in a reasonable time frame and good radiochemical yield.

Key words: Alzheimer's disease, Enzyme inhibitor, Positron emission tomography, Biodistribution, Quaternization

Correspondence to: Takahiro Higuchi; e-mail: higuchi_t@ukw.de, Michael Decker; e-mail: michael.decker@uni-wuerzburg.de

Introduction

Alzheimer's disease (AD) is an incurable, progressive neurodegenerative disorder and the most frequent cause of dementia with high prevalence and a long asymptomatic phase [1, 2]. The number of dementia-diseased individuals is expected to further increase, due to a growing average age and demographic change, which is hard to overcome for health care systems and society as a whole [3]. The definitive diagnosis of AD should no longer be solely based on typical, clinical symptoms, since they are not conclusive enough and begin many years after initial neuropathological alterations [4–6]. At this point, a successful disease-modifying or even preventive therapy is already impossible. Due to this fact, there is an urgent need for biological targets and biomarkers of an early disease state to help not only for an early, conclusive diagnosis with respective imaging probes but also to shed new light in the sequences and significances of the various neuropathological processes involved [7]. Three of the four FDA-approved anti-AD medications temporarily ameliorate AD symptoms by inhibiting cholinesterases (ChEs), whereby donepezil and galantamine are selective acetylcholinesterase (AChE) inhibitors and rivastigmine additionally binds to the isoenzyme butyrylcholinesterase (BChE). AChE inhibition prevents degradation of the neurotransmitter acetylcholine, levels of which are decreasing through cell death of cholinergic neurons [8–10]. However, advanced progression of AD involves a rapid decrease of AChE levels in the brain of ~90 %, which is accompanied in later-stage AD by elevated BChE expression. AChE and BChE exhibit very different localisations, biochemical features, and physiological functions [11]; however, BChE can take over the hydrolytic function of AChE [12–16]. These findings make BChE an attractive target for the development of more potent drugs for combatting AD [8–10]. Established pathological AD hallmarks are the abnormal metabolism of amyloid- β (A β), accompanied by hyperphosphorylated tau (τ) proteins, oxidative stress, and alterations concerning microglia cells in nervous tissue [17]. A β peptide can impair neurovascular homeostasis by its cerebrovascular effects, causing endothelial dysfunction [18]. Interestingly, A β deposits develop in nearly 30 % of aged adults, who do not show pathologically deteriorated cognition or memory deficits [19]. However, in AD patients, there is an increased expression of BChE along with A β plaques, especially in the cerebral cortex [20, 21]. In this outer layer of cerebrum, there is usually no considerable amount of BChE in healthy people, suggesting that the enzyme plays a potential key role in generating the detrimental attributes of A β . This finding has been supported in a BChE knockout mouse model, where distinctly fewer fibrillar A β plaques have been detected [15]. In this context, it is highly promising to apply suitable radiotracers in positron emission tomography (PET) studies, since this imaging technique exhibits excellent sensitivity and can provide an accurate estimation of the radiotracers' *in vivo*

concentration and biodistribution [22]. ChE PET tracers have been developed, with the majority of them targeting peripheral or brain AChE [23]. These compounds can be classified in two main categories, substrate-based and ligand-based tracers. The latter can be reversible or irreversible inhibitors. Substrate-based tracers, which usually have a high blood-brain barrier (BBB) permeability, can have intrinsic drawbacks due to quick hydrolysis and delivery limitations into the tissue [24]. In consequence, they may not reflect the regional enzyme distribution, but rather plasma delivery rate of the tracer [25]. Irreversible inhibitor-derived tracers can have a complex mechanism of enzyme inactivation and it is often complicated to accurately determine *in vivo* kinetics and distribution [24, 26]. Examples of substrate-type tracers specific for BChE include *N*-methylpiperidin-4-yl 4- ^{123}I iodobenzoate (^{123}I MP4Bz), *N*- ^{18}F fluoroethylpiperidin-4-ylmethyl butyrate, and 1- ^{11}C -methyl-4-piperidinyl *n*-butyrate (^{11}C MP4B) [16, 27, 28]. ^{11}C MP4B enters the brain, but no enhanced activity can be seen in regions where BChE-associated plaques typically show up in AD, which is likely the same for *N*- ^{18}F fluoroethylpiperidin-4-ylmethyl butyrate. In preliminary *in vivo* studies, the tracer showed high initial uptake in rat cerebral cortex after intravenous injection, but the hydrolysis rate of these ester is presumably still too high [28]. ^{123}I MP4Bz was applied in single-photon emission computed tomography (SPECT) studies, in which it was possible to distinguish cerebral cortical BChE activity in wild-type mice from an AD model [16]. This represents an important proof of concept, which demonstrates that BChE can indeed serve as a promising biomarker in AD diagnostics [15, 21]. This could also be shown for the pseudoirreversible BChE inhibitor phenyl 4- ^{123}I -iodophenylcarbamate (^{123}I -PIP), which accumulated specifically in A β plaques with ChE activity in human AD brain tissue [29]. Additionally, this tracer has been investigated very recently as a potential diagnostic and treatment monitoring tool for BChE activity changes in multiple sclerosis showing promising preliminary results [30]. Regarding irreversible and highly selective inhibitors of BChE as radiotracers, carbamate-based inhibitors were investigated that transfer the radiolabeled moiety onto the enzyme, where it is covalently bound. *Ex vivo* autoradiography on mice brain tissue and kinetic investigations proved such covalent transfer [24]. Furthermore, investigations into the influence of the carbamate structure that is transferred to BChE were made by altering spacer lengths and attached heterocyclic moieties. This resulted in sets of inhibitors with short, medium and long duration of action and pronounced neuroprotectivity in an AD mouse model, showing also the therapeutic potential of such inhibitors [31]. Altogether, these results support BChE not only as a promising biomarker for an early diagnosis of AD but also as an attractive target to be addressed by imaging probes in order to shed the light on the complex neuropathology of AD. Herein, we report on the synthesis, *in vitro* evaluation, radiolabeling, *ex vivo* autoradiography, and

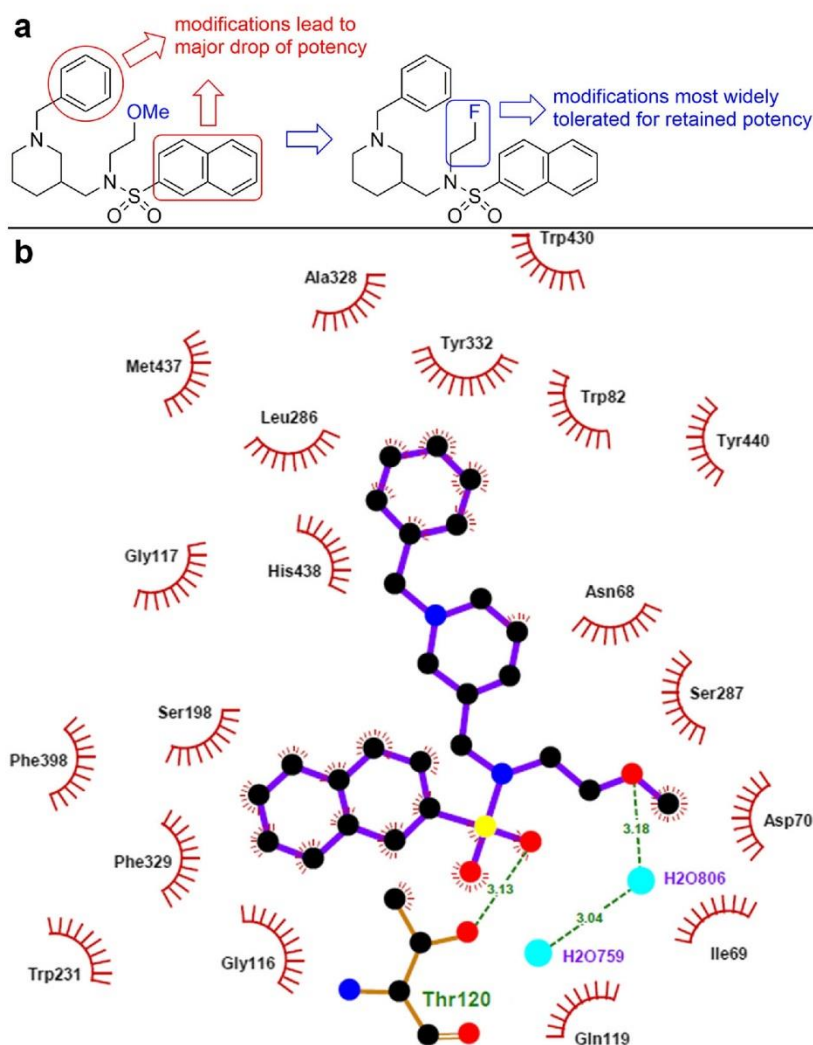


Fig. 1. **a** Design of the radiotracer. A potent, selective, and reversibly acting BChE inhibitor served as parent compound [32]. **b** Parent ligand in the BChE binding pocket [32].

preliminary *in vivo* PET studies of an ^{18}F -labeled BChE selective tracer, based on the structure of a potent, selective BChE inhibitor with reversible binding mode (Fig. 1a, b) [32]. Our intention was to utilize the promising properties of the parent compound for a suitable radiotracer, and these properties include the high affinity and selectivity towards the target enzyme, accompanied by pronounced lipophilicity and a relatively low molecular weight, which is favorable for blood-brain barrier (BBB) penetration [33]. Additionally, we chose a reversible inhibitor to overcome the intrinsic problems of substrate-type and irreversible radiotracers mentioned before, possibly enabling a more precise mapping of BChE distribution. We decided to replace the methoxy group on the ethylene-side chain with fluorine, because this moiety points out of the binding pocket as observed in the resolved crystal structure of the enzyme in complex with the parent inhibitor [32]. We assumed that this modification

would retain most of inhibitory potency. We chose to incorporate ^{18}F as radioisotope to take advantage of a long half-life and high positron yields in combination with a good spatial resolution due to relatively low positron energies in comparison to other radioisotopes commonly used for PET studies (e.g., ^{18}F : 0.65 MeV, ^{68}Ga : 1.90 MeV) [34, 35].

Materials and Methods

Chemistry

The non-radioactive “cold” inhibitor **4** and precursor **5** for radiolabeling were synthesized as shown in Fig. 2. Briefly, the piperidine ring of building block **1** was benzylated under Leuckart-Wallach conditions [36]. Subsequent demethylation of the methoxy group in compound **2** applying $\text{BF}_3 \cdot \text{Et}_2\text{O}$ in propane-1-thiol [37] gave the central building block,

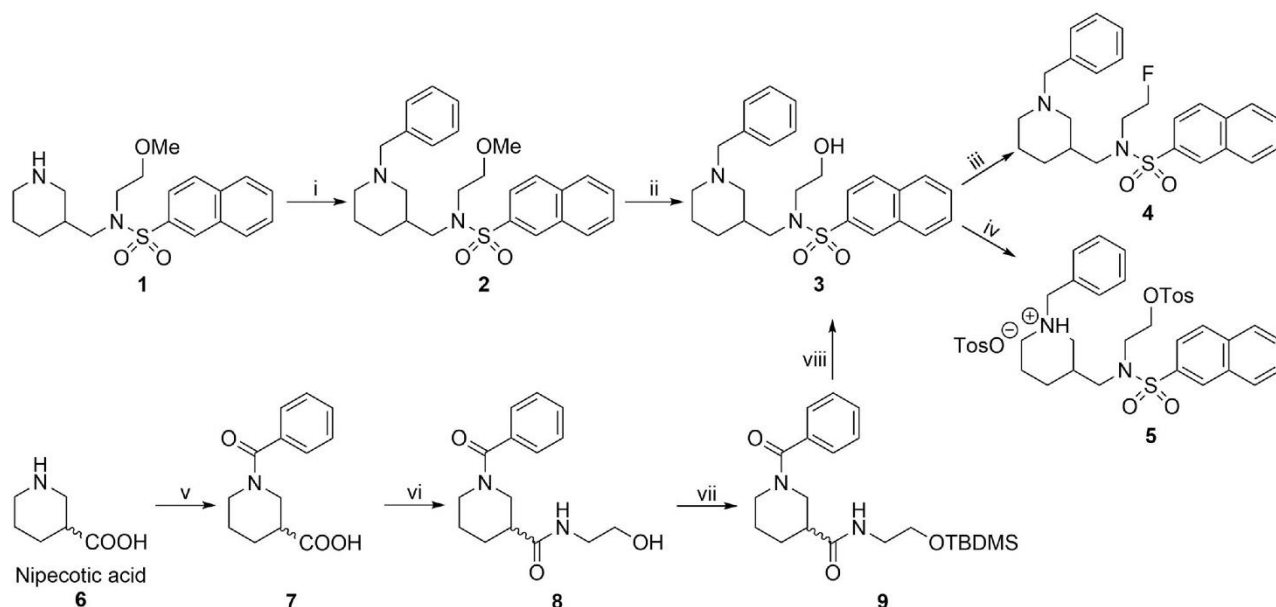


Fig. 2. Synthesis of precursor **5** and cold, reversible inhibitor of *h*BChE **4**. Reaction conditions and yields: (i) benzaldehyde, formic acid, 6 h, 180 °C, 44 %; (ii) $\text{BF}_3 \cdot \text{Et}_2\text{O}$, propane-1-thiol, 50 °C, 60 h, 60 %; (iii) DAST, CH_2Cl_2 , -10 °C \rightarrow RT, 24 %; (iv) 1. TosCl, NEt_3 , CH_2Cl_2 , RT, 18 h, 98 %, 2. *p*-TosOH, MeOH; (v) benzoyl chloride, K_2CO_3 , THF/ H_2O , 0 °C – RT, 20 h, 88 %; (vi) ethanolamine, HBTU, NEt_3 , DMF, RT, 18 h, 88 %; (vii) TBDMS-Cl, imidazole, DMF, RT, 24 h, 69 %; (viii) 1. LiAlH_4 , THF, reflux, 1 h; 2. naphthalene-2-sulfonyl chloride, DIPEA, CH_2Cl_2 , 0 °C – RT, 54 % (two steps).

the alcohol **3**, which can also be obtained from commercially available nipecotic acid (Fig. 2) [38]. Cold compound **4** was obtained by fluorination of **3** with diethylaminosulfur trifluoride (DAST) [39]. For radiolabeling with $\text{K}[^{18}\text{F}]$, a tosylate-leaving group was chosen, which was introduced by reacting **3** with *p*-toluenesulfonyl chloride (TosCl). We chose this synthetic strategy to utilize the advantage of having one central building block for generating both the precursor **5** for radiolabeling and the cold reference compound **4**.

In Vitro Studies

The inhibitory potency of compound **4** (Fig. 2) on *h*BChE was determined in the colorimetric Ellman's assay [40]. The incubation time of the compound stock solution (100 % in dimethylsulfoxide, DMSO) with Ellman's reagent (5,5'-dithiobis-(2-nitrobenzoic acid), DTNB) and recombinant *h*BChE was 5 min. The final concentrations were 370 μM of DTNB and 1 nM of the enzyme in a 0.1-M phosphate buffer at pH = 8.0. Reactions were started by addition of butyrylthiocholine iodide (BTCI) in a concentration of 500 μM with a final DMSO content of 1 %. IC_{50} values were determined by plotting residual enzyme activities against seven respective inhibitor concentrations. Tacrine served as a positive control (*cf.* ESM for further experimental details).

Kinetic studies to measure dissociation constants K_1 and K_2 of inhibitor **4** for binding to the free and acylated enzyme

were performed by measuring progress curves of product formation with ~50 μM BTCI as substrate. BTCI hydrolysis by *h*BChE was measured in the absence and presence of inhibitor **4** at three different concentrations (namely 40 nM, 80 nM, and 160 nM, respectively). The experiments were carried out at 25 °C in 25-mM phosphate buffer (pH = 7.0) according to the method of Ellman [40]. The concentration of purified *h*BChE, which was always the final addition to the assay probes, was approx. 1 nM. The hydrolysis of 46 μM BTCI was followed until completion in the presence of 1 mM DTNB (*cf.* ESM for further experimental details).

Radiochemistry

Radiofluorination of tosylate precursor **5** (Fig. 2) was performed in an established procedure. ^{18}F -Fluoride was separated from ^{18}O -water by an anion-exchange cartridge, which was eluted with 300 μl of 66-mM K_2CO_3 aqueous solution into a v-vial containing 15 mg of Kryptofix₂₂₂ in 500- μl acetonitrile. The mixture was dried azeotropically at 120 °C, which was repeated twice using dry acetonitrile (500 μl each time). Then, 1 mg of the precursor **5** (Fig. 2) in 400 μl of dry acetonitrile was added to the mixture and reacted for 10 min at 110 °C. After cooling to room temperature, the reaction mixture was neutralized by adding 5 % acetic acid (300 μl). The labeled compound was purified by semi-preparative, reversed phase HPLC (*cf.* ESM for further experimental details). Tracer identity and sufficient radiochemical purity were

confirmed by radio-thin layer chromatography (TLC). The radiotracer was diluted with saline to the required concentration for further investigation.

Preliminary Ex Vivo Tissue Binding Assay and In Vivo PET Imaging

Animal protocols were approved by the local Animal Care and Use Committee and conducted according to the Guide for the Care and Use of Laboratory Animals. One C57BL/6N mouse from Charles River was used for *ex vivo* tissue binding studies. Horizontal slices with 20- μ m thickness were made and separated into two series for either control or blocking group. The frozen mice brain slices were incubated in a buffer at pH = 8.0 (150-mM NaCl, 5-mM EDTA, 50-mM Na₂HPO₄) containing ¹⁸F-labeled compound **4** ($A = 1.44$ MBq) with or without ethopropazine hydrochloride (60 μ M) as blocking agent. After incubating for 30 min at 25 °C, the slices were rinsed five times in PBS buffer (1 min each time). After drying at room temperature, the slices were exposed to a phosphor imaging plate (Fuji SR-type image plate, Fujifilm Corporation, Tokyo, Japan). The images were obtained using a digital autoradiographic system (Typhoon FLA 7000). For *in vivo* PET imaging, a healthy male Wistar rat, which was anesthetized and maintained with isoflurane, was scanned using a micro-PET system (FOCUS, Siemens). Directly after the injection of tracer **4** (6.3 MBq), a 60-min dynamic imaging protocol was started. The obtained PET images were analyzed with the public domain tool AMIDE imaging software (A Medical Imaging Data Examiner, version 1.01) and used to generate time-activity curves of regions of interest.

Results

Chemistry

The fluorinated, reversible *h*BChE inhibitor **4** (Fig. 2) was synthesized in three steps with satisfying yields [36, 37, 39]. We applied the DAST fluorination method for alcohol **3** due to the short reaction times, mild conditions, and uncomplicated workup, despite lower yields (24 %). This compound was only required in minor amounts as reference during radiolabeling and for *in vitro* assays. The respective precursor for ¹⁸F-labeling was synthesized using the same building block, alcohol **3**, in almost quantitative yields. However, precursor **5** exhibited an instability problem, when present as free base. It was resolved by turning **5** into its tosylate salt. During purity control by liquid chromatography/mass spectrometry (LCMS), we found a slow side reaction due to intramolecular ring closure by nucleophilic attack of the piperidine nitrogen (Fig. 3). This can be explained with the excellent leaving group quality of tosylate, which is on the one hand required for a facile radiolabeling under preferably mild conditions, but makes the compound sensitive for this quaternization side

reaction on the other hand. Since building block **1** is not commercially available, we synthesized alcohol **3** additionally out of low cost and easy to handle nipecotic acid **6** (Fig. 2) [36, 37]. In the first step, the piperidine nitrogen was benzoylated in very good yields applying benzoyl chloride. Next, the carboxylic acid of compound **7** was activated with 3-[bis(dimethylamino)methylumyl]-3*H*-benzotriazol-1-oxide hexafluorophosphate (HBTU) and coupled to 2-aminoethanol in very good yields. Subsequently, compound **8** was protected at its hydroxyl group with *tert*-butyldimethylsilyl chloride (TBDMS-Cl) in good yields. Finally, both amide groups were reduced with lithium aluminum hydride and the crude product was used directly in a one-pot-two-steps manner to be coupled naphthalene-2-sulfonyl chloride at the reduced secondary amine function. It was found that the TBDMS group is cleaved under the applied conditions and alcohol **3** (Fig. 2) was obtained in satisfying yields.

In Vitro Studies

Subsequently, compound **4** was tested in an Ellman's assay for its inhibitory potency against *h*BChE [40]. We determined a low submicromolar value ($IC_{50} = 118.3 \pm 19.6$ nM), meaning a drop in inhibitory potency compared to the parent methoxy derivative (Fig. 1a, b; $IC_{50} = 4.9 \pm 0.3$ nM) [32]. This can be explained by means of the BChE crystal structure in complex with the inhibitor. Although the methoxy-ethylene moiety as a whole rather points out of the binding pocket, the missing methoxy-oxygen has been described to act as an additional H-bond acceptor with a structural water and Asn68 (Fig. 1b). This is still a good compromise, since the structure-activity relationships revealed that other positions to introduce fluorine in the molecule would presumably lead to a more drastic decline of activity (*cf.* Table 1). Still, this class of compounds exhibits high selectivity over *h*AChE, which had been described also for several derivatives thereof [32].

To gain in-depth insight into the binding potential of inhibitor **4**, the effects of different concentrations of the compound on *h*BChE activity were studied by measuring progressive curves of product formation at approximately 50 μ M of BTCl (Fig. 4a). The analysis of these progressive curves revealed good agreement between the experimental curves (Fig. 4a, in blue) and a theoretical model (Fig. 4a, in red) that defined a mixed reaction mechanism with binding of the inhibitor to both the free and the acylated enzyme (Fig. 4b). The dissociation constants revealed that the binding affinity of compound **4** to the acylated enzyme ($K_2 = 68.0$ nM) is lower than to the free enzyme ($K_1 = 32.9$ nM).

Radiochemistry

Next, precursor **5** (Fig. 2) was subjected to ¹⁸F-radio-labeling. We obtained [¹⁸F]-labeled tracer **4** in

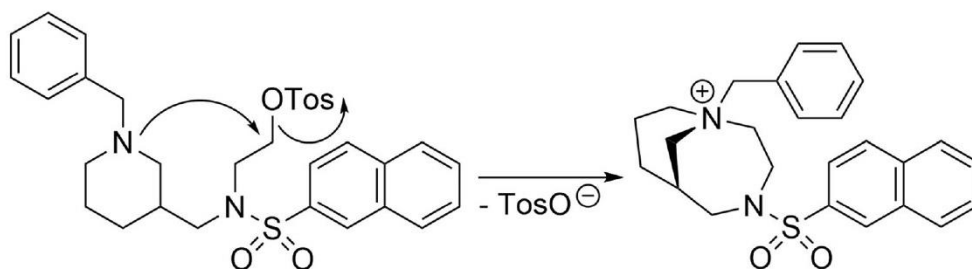


Fig. 3. Quaternization of precursor **5** when present as free base.

approximately 120 min with an average radiochemical yield of 20 ± 3 % (decay-corrected, $n=2$) without reaction condition optimization. The identity of the tracer and its radiochemical purity (≥ 95.3 %) were confirmed by TLC autoradiography. In a preceding ^{18}F radiolabeling approach of precursor **5** applying established conditions as described before (*cf.* “Materials and Methods”), we were able to verify tracer identity by its R_f value on radio-TLC. TLC autoradiography indicated a progress of fluorination by more than 33 % (Fig. 5c). Furthermore, the retention time of the radiotracer (γ detection, Fig. 5b) corresponded to that of the cold compound on HPLC (UV detection, Fig. 5a).

Preliminary Ex Vivo Tissue Binding and In Vivo PET Imaging

In the *ex vivo* autoradiography study, we found accumulation of high radioactivity in most of the brain area, especially high intensity at the cortex, where BChE activity is elevated even more during AD progression [41]. Ethopropazine hydrochloride, a selective and reversible inhibitor of BChE [42], successfully reduced tracer uptake, suggesting specific binding of the tracer to BChE in the brain tissue (Fig. 6a). Unfortunately, dynamic PET images in a healthy rat indicated low tracer retention in brain (Fig. 6b, c).

Table 1 Structures and inhibitory potencies of cold, reversible hBChE inhibitor **4** (Fig. 2) in contrast to respective derivatives with substituted benzyl group, naphthalene group, and altered alkyl chain length on sulfonamidic nitrogen [32]. ^aSEM standard error of means, ^bRA residual activity

R	R ¹	R ²	IC ₅₀ ± SEM ^a (nM) on hBChE	%RA ^b ± SEM at 10 μM on mAChE
	-(CH ₂) ₂ -F		118.3 ± 19.6	-
	-(CH ₂) ₂ -OMe		~ 53000	-
	-(CH ₂) ₃ -OMe		14.4 ± 0.8	95% ± 5%
	-(CH ₂) ₂ -OMe		156 ± 33	95% ± 7%

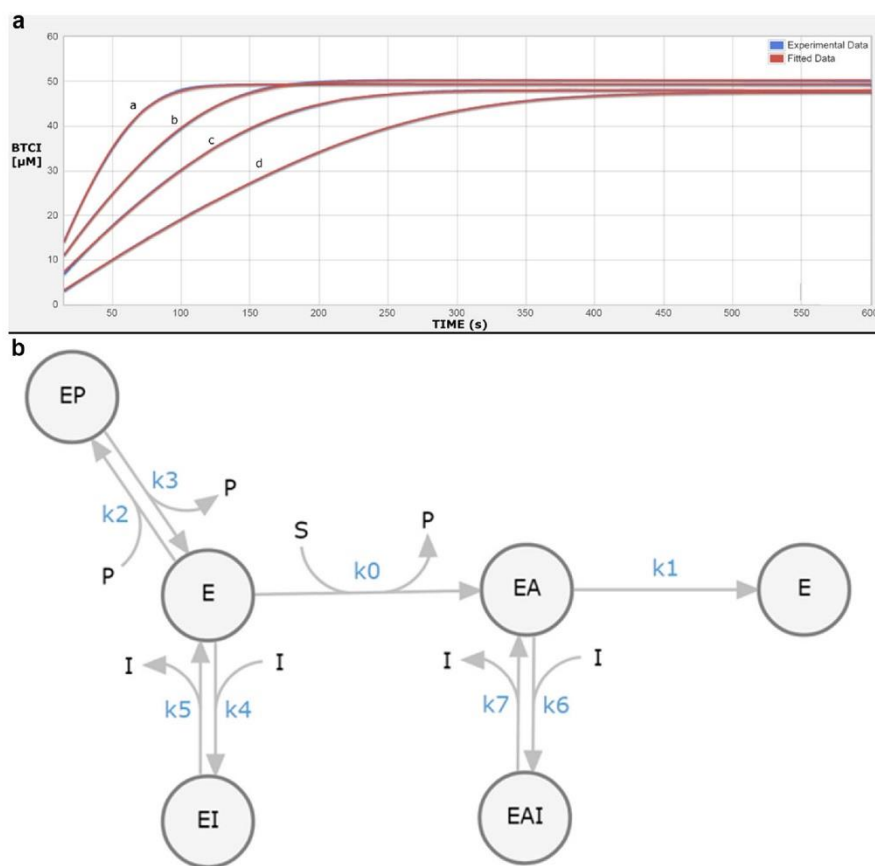


Fig. 4. **a** Time courses of product formation in the reactions between BTCl ($\sim 46 \mu\text{M}$) and purified *h*BChE (1 nM) in the absence (curve a) and presence of compound **4** (b, 40 nM; c, 80 nM; d, 160 nM). **b** Scheme for the inhibition of BTCl hydrolysis by *h*BChE in the presence of DTNB by compound **4**. E, free enzyme; EA, acylated intermediate; S, substrate (BTCl); P, all of the stoichiometrically released products (thiocholine-TNB, TNB⁻); and I, compound **4** (inhibitor). The symbols for the constants are k_{cat} (k_1), catalytic constant for BTCl turnover; K_m (k_0), Michaelis constant; $K_p = k_3/k_2$, inhibition constant for binding of the product thiocholine-TNB; $K_1 = k_5/k_4$ and $K_2 = k_7/k_6$, dissociation constants for binding of the compound to the free and acylated enzyme, respectively.

Discussion

In our synthetic approach towards cold, reversible *h*BChE inhibitor **4**, and the respective precursor **5** for ^{18}F labeling (Fig. 2), we were able to perform several optimizations of reaction conditions. Yields of the Leuckart-Wallach benzylation in the first step were significantly increased, when benzaldehyde was freshly distilled before the reaction to remove benzoic acid, which is formed due to slow oxidation of benzaldehyde in the presence of air [36, 43]. In the next step, we achieved demethylation of a methoxy group with boron trifluoride etherate in propane-1-thiol. However, at first, this step required long reaction times (6–7 days), even though it was described that increased amounts of $\text{BF}_3 \cdot \text{Et}_2\text{O}$ can accelerate conversion [37]. We found that slightly elevated temperatures (up to $50 \text{ }^\circ\text{C}$) significantly decreased reaction times (60 h). Fluorination of the alcohol **3** with DAST gave the desired product **4**; however, attempts to increase the yields failed. This is likely due to the side reactions that can appear when DAST is applied, namely

elimination or carbonium-ion type rearrangements [39]. Tosylation of alcohol **3** proceeded almost quantitatively under standard conditions [44]; however, the product has to be turned into its tosylate salt to prevent slow, but continuous quaternization (Fig. 3). In our additional synthetic approach towards central building block **3** (Fig. 2), we found that both amide groups of TBDMS-protected compound **9** can be reduced by lithium aluminum hydride and the crude product can directly be coupled to naphthalene-2-sulfonyl chloride to obtain deprotected alcohol **3**. This abbreviates the synthetic procedure by one additional TBDMS-deprotection step.

Next, we measured the inhibitory potency of our cold, reversible *h*BChE inhibitor in a colorimetric Ellman's assay and determined an IC_{50} value of $118.3 \pm 19.6 \text{ nM}$, meaning a significant drop of inhibitory activity compared to the parent compound (Fig. 1a, $\text{IC}_{50} = 4.9 \pm 0.3 \text{ nM}$). However, the structure-activity relationships for this class of compounds revealed that altering the *N*-alkyl moieties of the sulfonamide nitrogen led to the lowest changes in inhibitory

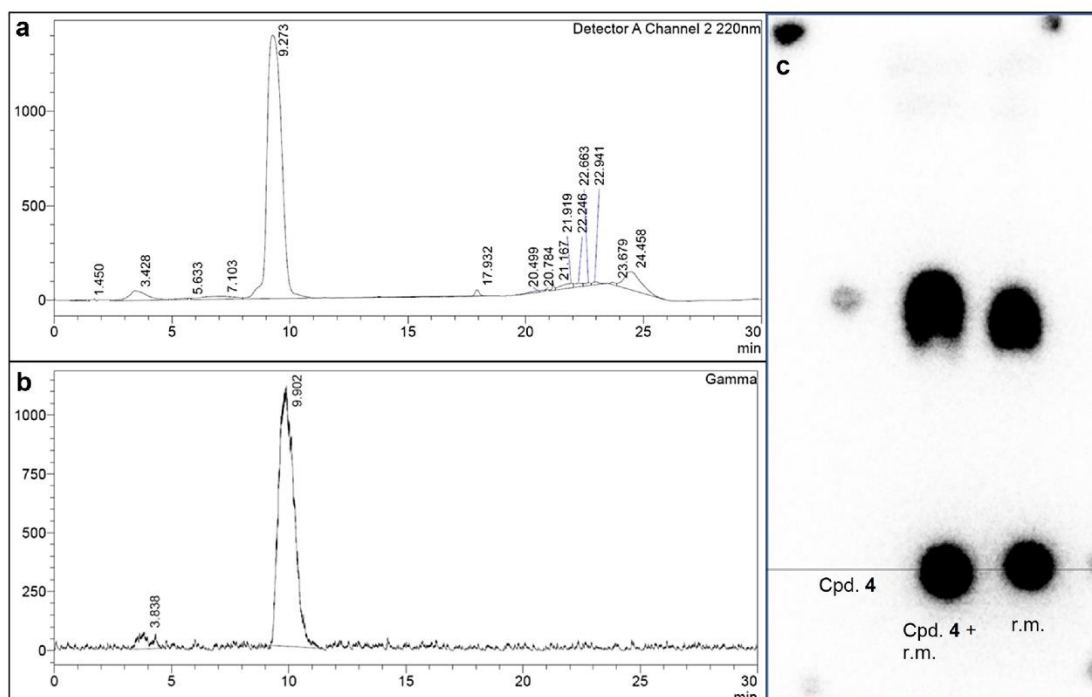


Fig. 5. HPLC – and radio-TLC analysis after first ^{18}F radiolabeling of precursor **5**. **a** HPLC chromatogram of reference compound **4**. The UV absorption at 220 nm was detected. **b** HPLC chromatogram of the purified radiotracer. γ -ray emission produced by the β^+ -(positron-) decay of ^{18}F and subsequent annihilation with electrons was detected. The retention time (Rt) is in good agreement with the reference (cold compound: Rt = 9.273 min; radiotracer: Rt = 9.902 min). **c** Radio-TLC analysis of labeling progress. The R_f values of cold compound (cpd. **4**) and the respective spot of the tracer in the reaction mixture (r. m.) are in good agreement. TLC autoradiography indicated a process of fluorination by more than 33 %.

potency, while substituted naphthalene or benzyl groups significantly decreased inhibitory potency (Table 1 and Fig. 1b) [32]. As an example, we synthesized a respective derivative with a fluoromethyl group in *para* position of the benzyl ring, which turned out to be almost inactive as *h*BChE inhibitor (Table 1). Even though replacement of the methoxy group with a fluorine atom reduced inhibitory potency more than expected considering the previously established structure-activity relationships, the submicromolar IC_{50} value in combination with the high selectivity ratio over AChE for this class of compounds still represent promising attributes for a suitable radiotracer [33]. Additionally, kinetic experiments revealed a good binding potential of compound **4** (Fig. 2) to *h*BChE. The dissociation constant K_1 , representing the binding affinity to the free enzyme, was generally lower than K_2 , the respective constant for binding to the acylated enzyme ($K_1 = 32.9$ nM, $K_2 = 68.0$ nM, *cf.* Fig. 4).

Subsequently, we performed ^{18}F -radiolabeling of the tosylate precursor **5** by nucleophilic substitution. Applying an established procedure with some variations on the technical details led to a reasonable radiochemical yield. Importantly, the whole process including labeling, tracer identification, and purification was feasible in approximately 120 min, considering the half-life of ^{18}F (1.8288 h) as a

limiting factor for time-consuming preparations of radiotracers [34]. In a precedent radiolabeling approach, we could already determine a facile progress of fluorination by TLC autoradiography. The tracer identity could be confirmed both by radio-TLC and HPLC retention times (Fig. 5). Since harsh radiolabeling conditions can lead to decomposition of unstable functional groups and unexpected side reactions of the respective precursor, our promising radiolabeling results motivated us to perform preliminary *ex vivo* and *in vivo* investigations.

The *ex vivo* autoradiography study demonstrated good binding of our tracer to BChE rich areas in mice brain tissues. We observed high intensities in cortex, which is in good agreement with the known BChE distribution in mice brain [45–47]. After preincubating the tissue with ethopropazine hydrochloride, a selective inhibitor of BChE [42], we found a significant decrease of binding (Fig. 6a). This finding met our expectations and provides further evidence of the pronounced selectivity over AChE for this compound. Nevertheless, a significant amount of tracer remains bound to the tissue despite blocking. Possible reasons are non-specific binding due to the lipophilicity of the tracer and/or potential off-target effects.

However, in our first approach to utilize the tracer for *in vivo* PET studies, we found only low brain uptake after

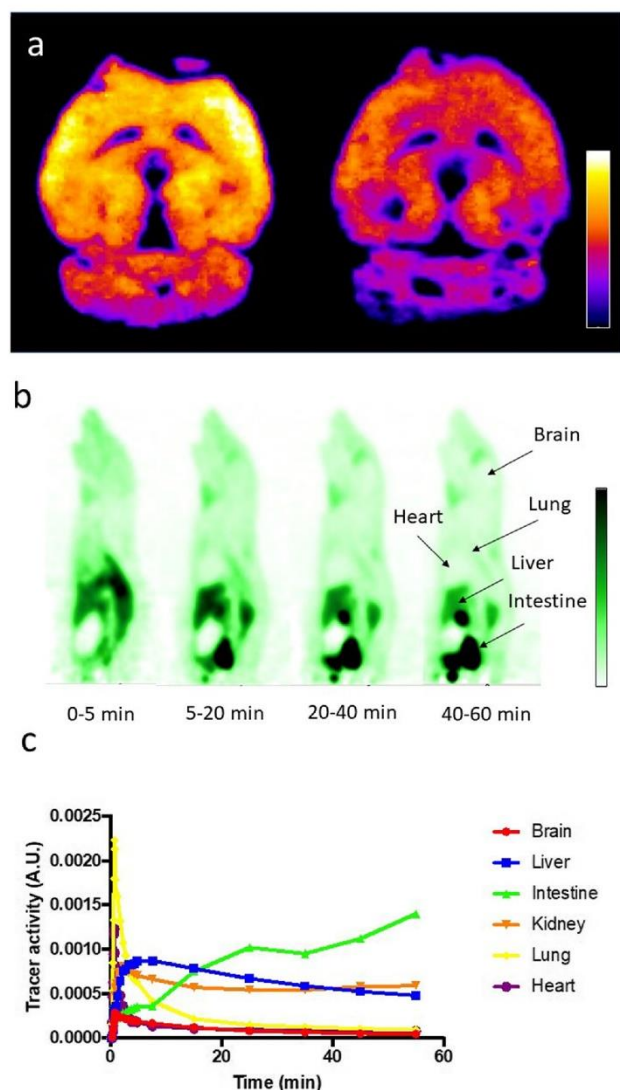


Fig. 6. **a** Autoradiographic image of tissue binding assay with healthy mice brain slices incubated with [^{18}F]-labeled BChE – tracer **4** without (left) and with (right) ethopropazine. Purple areas represent low binding; bright yellow areas represent high binding. **b** Dynamic PET images of sagittal sections after administration of radiotracer **4** in a healthy rat. Dark green areas represent high tracer accumulation; light green areas represent low accumulation. **c** Time-activity curves in each organ derived from the PET imaging.

administering the compound *via* tail vein to a male rat (Fig. 6b, c). This can reflect the compounds limited BBB permeability, since a moderate brain-to-plasma ratio (0.44 *vs.* Donepezil = 6.3) had already been described for the parent, methoxy compound (Fig. 1a) after *in vivo* blood plasma-brain distribution studies [32]. On the other hand, this compound had been investigated in permeability measurements using Caco-2 cells, where it exhibited neither low passive permeability nor active efflux by membrane transport proteins like P-glycoprotein or breast cancer resistance protein [32].

Conclusion

In our study, we present design and evaluation of a novel ^{18}F -PET radiotracer selectively targeting BChE with reversible mode of binding. Precursor and the respective cold compound are now synthetically easily accessible. Inhibitory potency of the cold compound was decreased compared to the parent compound. Therefore, future studies could additionally focus on ^{11}C labeling at the methoxy group to completely retain inhibitory potency of the radiotracer. Radiolabeling was achieved in a reasonable time frame and a good radiochemical yield applying a standard procedure. Preliminary *ex vivo* autoradiography on mice brain slices preincubated with the tracer revealed its good binding to brain tissue and blocking studies with ethopropazine hydrochloride demonstrated its selectivity towards BChE. However, future studies should focus on determining possible reasons for the significant compound retention despite blocking with respect to potential off-target effects and non-specific binding. Our preliminary *in vivo* PET study showed only limited brain uptake of the tracer after tail vein injection. After the initial blood pool circulation, the tracer was accumulated in liver and kidneys and excreted fast into intestine and urine. The tracer's ability to pass the BBB might be restricted. On the other hand, the parent compound, which served as design schedule for us, demonstrated neither low passive permeability nor active efflux. Due to these facts, the tracer will be applied in future studies towards its precise biodistribution to clarify the reason of its limited brain uptake.

Acknowledgments The authors are thankful to Dr. Jure Stojan (Medical faculty, University of Ljubljana, Slovenia) for helpful discussions regarding kinetic analysis and progress-curve analysis.

Funding Open Access funding enabled and organized by Projekt DEAL. This work was supported by the German Research Council (Deutsche Forschungsgemeinschaft DFG grants DE 1546/6-3 for M. Decker and HI 1789/3-3 Prof. T. Higuchi) and the Slovenian Research Agency (core financing P1-0208 and projects Z1-9195 granted to UK and NC-0009 to S. Gobec).

Compliance with Ethical Standards All applicable international, national, and/or institutional guidelines for the care and use of animals were followed. Animal protocols were approved by the local Animal Care and Use Committee and conducted according to the Guide for the Care and Use of Laboratory Animals.

Conflict of Interest

The authors declare that they have no conflict of interest.

Open Access This article is licensed under a Creative Commons Attribution 4.0 International License, which permits use, sharing, adaptation, distribution and reproduction in any medium or format, as long as you give appropriate credit to the original author(s) and the source, provide a link to the Creative Commons licence, and indicate if changes were made. The images or other third party material in this article are included in the article's Creative Commons licence, unless indicated otherwise in a credit line to the material. If material is not included in the article's Creative Commons licence and your intended use is not permitted by statutory regulation or

exceeds the permitted use, you will need to obtain permission directly from the copyright holder. To view a copy of this licence, visit <http://creativecommons.org/licenses/by/4.0/>.

References

- Masters CL, Bateman R, Blennow K, Rowe CC, Sperling RA, Cummings JL (2015) Alzheimer's disease. *Nat Rev Dis Primers* 1:15056
- Coyle J, Price D, DeLong M (1983) Alzheimer's disease: a disorder of cortical cholinergic innervation. *Science* 219:1184–1190
- Nichols E, Szoek CEI, Vollset SE, Abbasi N, Abd-Allah F, Abdela J, Aichour MTE, Akinyemi RO, Alahdab F, Asgedom SW, Awasthi A, Barker-Collo SL, Baune BT, Béjot Y, Belachew AB, Bennett DA, Biadgo B, Bijani A, Bin Sayeed MS, Brayne C, Carpenter DO, Carvalho F, Catalá-López F, Cerin E, Choi JYJ, Dang AK, Degefá MG, Djalalinia S, Dubey M, Duken EE, Edvardsson D, Endres M, Eskandarich S, Faro A, Farzadfar F, Fereshtehnejad SM, Fernandes E, Filip I, Fischer F, Gebre AK, Gercemew D, Ghasemi-Kasman M, Gnedovskaya EV, Gupta R, Hachinski V, Hagos TB, Hamidi S, Hankey GJ, Haro JM, Hay SI, Irvani SSN, Jha RP, Jonas JB, Kalani R, Karch A, Kasaeian A, Khader YS, Khalil IA, Khan EA, Khanna T, Khoja TAM, Khubchandani J, Kisa A, Kissimova-Skarbek K, Kivimäki M, Koyanagi A, Krohn KJ, Logroscino G, Lorkowski S, Majdan M, Malekzadeh R, März W, Massano J, Mengistu G, Meretoja A, Mohammadi M, Mohammadi-Khanaposhtani M, Mokdad AH, Mondello S, Moradi G, Nagel G, Naghavi M, Naik G, Nguyen LH, Nguyen TH, Nirayo YL, Nixon MR, Ofori-Asenso R, Ogbo FA, Olagunju AT, Owolabi MO, Panda-Jonas S, Passos VMA, Pereira DM, Pinilla-Monsalve GD, Piradov MA, Pond CD, Poustchi H, Qorbani M, Radfar A, Reiner RC Jr, Robinson SR, Roshandel G, Rostami A, Russ TC, Sachdev PS, Safari H, Safiri S, Sahathevan R, Salimi Y, Satpathy M, Sawhney M, Saylan M, Sepanlou SG, Shafieesabet A, Shaikh MA, Sahraian MA, Shigematsu M, Shiri R, Shiu I, Silva JP, Smith M, Sobhani S, Stein DJ, Tabarés-Seisdedos R, Tovani-Palone MR, Tran BX, Tran TT, Tsegay AT, Ullah I, Venketasubramanian N, Vlassov V, Wang YP, Weiss J, Westerman R, Wijeratne T, Wyper GMA, Yano Y, Yimer EM, Yonemoto N, Yousefifard M, Zaidi Z, Zare Z, Vos T, Feigin VL, Murray CJL (2019) Global, regional, and national burden of Alzheimer's disease and other dementias, 1990–2016: a systematic analysis for the Global Burden of Disease Study 2016. *Lancet Neurol* 18:88–106
- Villemagne VL, Burnham S, Bourgeat P, Brown B, Ellis KA, Salvado O, Szoek C, Macaulay SL, Martins R, Maruff P, Ames D, Rowe CC, Masters CL, Australian Imaging Biomarkers and Lifestyle (AIBL) Research Group (2013) Amyloid β deposition, neurodegeneration, and cognitive decline in sporadic Alzheimer's disease: a prospective cohort study. *Lancet Neurol* 12:357–367
- Jack CR Jr, Lowe VJ, Weigand SD et al (2009) Serial PIB and MRI in normal, mild cognitive impairment and Alzheimer's disease: implications for sequence of pathological events in Alzheimer's disease. *Brain* 132:1355–1365
- Braak H, Thal DR, Ghebremedhin E, Del Tredici K (2011) Stages of the pathologic process in Alzheimer disease: age categories from 1 to 100 years. *J Neuropathol Exp Neurol* 70:960–969
- Jack CR, Bennett DA, Blennow K et al (2018) NIA-AA research framework: toward a biological definition of Alzheimer's disease. *Alzheimers Dement* 14:535–562
- Rountree SD, Chan W, Pavlik VN, Darby EJ, Siddiqui S, Doody RS (2009) Persistent treatment with cholinesterase inhibitors and/or memantine slows clinical progression of Alzheimer disease. *Alzheimers Res Ther* 1:7. <https://doi.org/10.1186/alzrt7>
- Raina P, Santaguida P, Ismaila A, Patterson C, Cowan D, Levine M, Booker L, Oremus M (2008) Effectiveness of cholinesterase inhibitors and memantine for treating dementia: evidence review for a clinical practice guideline. *Ann Intern Med* 148:379–397
- Nordberg A, Ballard C, Bullock R, Darreh-Shori T, Somogyi M (2013) A review of butyrylcholinesterase as a therapeutic target in the treatment of Alzheimer's disease. *Prim Care Companion CNS Disord* 15. <https://doi.org/10.4088/PCC.12r01412>
- Lockridge O, Duysen E, Masson P (2011) Butyrylcholinesterase: overview, structure, and function. pp 25–41
- Arendt T, Brückner MK, Lange M, Bigl V (1992) Changes in acetylcholinesterase and butyrylcholinesterase in Alzheimer's disease resemble embryonic development—a study of molecular forms. *Neurochem Int* 21:381–396
- Giacobini E (2003) Cholinergic function and Alzheimer's disease. *Int J Geriatr Psychiatry* 18:1–5
- Greig NH, Utsuki T, Yu Q et al (2001) A new therapeutic target in Alzheimer's disease treatment: attention to butyrylcholinesterase. *Curr Med Res Opin* 17:159–165
- Darvesh S (2016) Butyrylcholinesterase as a diagnostic and therapeutic target for Alzheimer's disease. *Curr Alzheimer Res* 13:1–5
- DeBay DR, Reid GA, Pottier IR et al (2017) Targeting butyrylcholinesterase for preclinical single photon emission computed tomography (SPECT) imaging of Alzheimer's disease. *Alzheimers Dement (N Y)* 3:166–176
- Wang J, Gu BJ, Masters CL, Wang YJ (2017) A systemic view of Alzheimer disease - insights from amyloid- β metabolism beyond the brain. *Nat Rev Neurol* 13:612–623
- Koizumi K, Wang G, Park L (2016) Endothelial dysfunction and amyloid- β -induced neurovascular alterations. *Cell Mol Neurobiol* 36:155–165
- Katzman R, Terry R, DeTeresa R, Brown T, Davies P, Fuld P, Renbing X, Peck A (1988) Clinical, pathological, and neurochemical changes in dementia: a subgroup with preserved mental status and numerous neocortical plaques. *Ann Neurol* 23:138–144
- Reid GA, Darvesh S (2015) Butyrylcholinesterase-knockout reduces brain deposition of fibrillar β -amyloid in an Alzheimer mouse model. *Neuroscience* 298:424–435
- Macdonald IR, Maxwell SP, Reid GA, Cash MK, DeBay DR, Darvesh S (2017) Quantification of butyrylcholinesterase activity as a sensitive and specific biomarker of Alzheimer's disease. *J Alzheimers Dis* 58:491–505
- Vaquero JJ, Kinahan P (2015) Positron emission tomography: current challenges and opportunities for technological advances in clinical and preclinical imaging systems. *Annu Rev Biomed* 17:385–414
- Holland JP, Liang SH, Rotstein BH, Collier TL, Stephenson NA, Greguric I, Vasdev N (2014) Alternative approaches for PET radiotracer development in Alzheimer's disease: imaging beyond plaque. *J Labelled Compd Rad* 57:323–331
- Sawatzky E, Al-Momani E, Kobayashi R et al (2016) A novel way to radiolabel human butyrylcholinesterase for positron emission tomography through irreversible transfer of the radiolabeled moiety. *ChemMedChem* 11:1540–1550
- Logan J, Fowler JS, Ding Y-S, Franceschi D, Wang GJ, Volkow ND, Felder C, Alexoff D (2002) Strategy for the formation of parametric images under conditions of low injected radioactivity applied to PET studies with the irreversible monoamine oxidase tracers [^{11}C]clogyline and deuterium-substituted [^{11}C]clogyline. *J Cereb Blood Flow Metab* 22:1367–1376
- Fowler JS, Logan J, Volkow ND, Wang GJ, MacGregor R, Ding YS (2002) Monoamine oxidase: radiotracer development and human studies. *Methods* 27:263–277
- Roivainen A, Rinne J, Virta J, Järvenpää T, Salomäki S, Yu M, Nägren K (2004) Biodistribution and blood metabolism of 1- ^{11}C -methyl-4-piperidinyl n-butylate in humans: an imaging agent for in vivo assessment of butyrylcholinesterase activity with PET. *J Nucl Med* 45:2032–2039
- Kikuchi T, Zhang M-R, Ikota N, Fukushi K, Okamura T, Suzuki K, Arano Y, Irie T (2004) N-[^{18}F]fluoroethylpiperidin-4-ylmethyl butylate: a novel radiotracer for quantifying brain butyrylcholinesterase activity by positron emission tomography. *Bioorg Med Chem Lett* 14:1927–1930
- Macdonald IR, Reid GA, Pottier IR, Martin E, Darvesh S (2016) Synthesis and preliminary evaluation of phenyl 4-123I-iodophenylcarbamate for visualization of cholinesterases associated with Alzheimer disease pathology. *J Nucl Med* 57:297–302
- Thome MWD, Cash MK, Reid GA, Burley DE, Luke D, Pottier IR, Darvesh S (2020) Imaging butyrylcholinesterase in multiple sclerosis. *Mol Imaging Biol* 23:127–138. <https://doi.org/10.1007/s11307-020-01540-6>
- Hoffmann M, Stiller C, Endres E, Scheiner M, Gunesch S, Sottriffer C, Maurice T, Decker M (2019) Highly selective butyrylcholinesterase

- inhibitors with tunable duration of action by chemical modification of transferable carbamate units exhibit pronounced neuroprotective effect in an Alzheimer's disease mouse model. *J Med Chem* 62:9116–9140
32. Košak U, Brus B, Knez D, Šink R, Žakelj S, Trontelj J, Pišlar A, Šlenc J, Gobec M, Živin M, Tratnjek L, Perše M, Sašat K, Podkova A, Filipek B, Nachon F, Brazzolotto X, Więckowska A, Malawska B, Stojan J, Raščan IM, Kos J, Coquelle N, Colletier JP, Gobec S (2016) Development of an in-vivo active reversible butyrylcholinesterase inhibitor. *Sci Rep* 6:39495
 33. McCluskey SP, Plisson C, Rabiner EA, Howes O (2020) Advances in CNS PET: the state-of-the-art for new imaging targets for pathophysiology and drug development. *Eur J Nucl Med Mol Imaging* 47:451–489
 34. Sanchez-Crespo A (2013) Comparison of Gallium-68 and Fluorine-18 imaging characteristics in positron emission tomography. *Appl Radiat Isot* 76:55–62
 35. Kesch C, Kratochwil C, Mier W, Kopka K, Giesel FL (2017) (68)Ga or (18)F for prostate cancer imaging? *J Nucl Med* 58:687–688
 36. Ignatovich ZV, Gusak KN, Chernikhova TV, Kozlov NG, Koroleva EV (2007) Interaction of secondary amines with aromatic aldehydes-efficient method for synthesis of the functionalized heterocyclic amines. *Chem Heterocycl Compd* 43:1540–1543
 37. Node M, Hori H, Fujita E (1976) Demethylation of aliphatic methyl ethers with a thiol and boron trifluoride. *J. Chem. Soc. Perkin Trans. I*:2237–2240
 38. Košak U, Brus B, Gobec S (2014) Straightforward synthesis of orthogonally protected piperidin-3-ylmethanamine and piperidin-4-ylmethanamine derivatives. *Tetrahedron Lett* 55:2037–2039
 39. Middleton WJ (1975) New fluorinating reagents. Dialkylaminosulfur fluorides. *J Org Chem* 40:574–578
 40. Ellman GL, Courtney KD, Andres V, Featherstone RM (1961) A new and rapid colorimetric determination of acetylcholinesterase activity. *Biochem Pharmacol* 7:88–95
 41. Mesulam M, Geula C (1994) Butyrylcholinesterase reactivity differentiates the amyloid plaques of aging from those of dementia. *Ann Neurol* 36:722–727
 42. Meuling WJ, Jongen MJ, van Hemmen JJ (1992) An automated method for the determination of acetyl and pseudo cholinesterase in hemolyzed whole blood. *Am J Ind Med* 22:231–241
 43. Jorissen WP, van der Beek PAA (1930) The oxidation of benzaldehyde. *Recl Trav Chim Pays-Bas* 49:138–141
 44. Kabalka GW, Varma M, Varma RS, Srivastava PC, Knapp FF (1986) The tosylation of alcohols. *J Org Chem* 51:2386–2388
 45. Mesulam MM, Guillozet A, Shaw P, Levey A, Duysen EG, Lockridge O (2002) Acetylcholinesterase knockouts establish central cholinergic pathways and can use butyrylcholinesterase to hydrolyze acetylcholine. *Neuroscience* 110:627–639
 46. Reid GA, Chilukuri N, Darvesh S (2013) Butyrylcholinesterase and the cholinergic system. *Neuroscience* 234:53–68
 47. Geula C, Nagykerly N (2007) Butyrylcholinesterase activity in the rat forebrain and upper brainstem: postnatal development and adult distribution. *Exp Neurol* 204:640–657

Publisher's Note Springer Nature remains neutral with regard to jurisdictional claims in published maps and institutional affiliations.

Synthesis and Initial Characterization of a Selective, Pseudo-irreversible Inhibitor of Human Butyrylcholinesterase as PET Tracer

Christian Gentsch^{+, [a]} Matthias Hoffmann^{+, [a]} Yasuhiro Ohshima,^[c, d] Naoko Nose,^[e] Xinyu Chen,^[b, c, d] Takahiro Higuchi,^{*, [c, d, e]} and Michael Decker^{*, [a]}

The enzyme butyrylcholinesterase (BChE) represents a promising target for imaging probes to potentially enable early diagnosis of neurodegenerative diseases like Alzheimer's disease (AD) and to monitor disease progression in some forms of cancer. In this study, we present the design, facile synthesis, *in vitro* and preliminary *ex vivo* and *in vivo* evaluation of a morpholine-based, selective inhibitor of human BChE as a positron emission tomography (PET) tracer with a pseudo-

irreversible binding mode. We demonstrate a novel protecting group strategy for ¹⁸F radiolabeling of carbamate precursors and show that the inhibitory potency as well as kinetic properties of our unlabeled reference compound were retained in comparison to the parent compound. In particular, the prolonged duration of enzyme inhibition of such a morpholino-carbamate motivated us to design a PET tracer, possibly enabling a precise mapping of BChE distribution.

Introduction

Dementia and its most frequent form, Alzheimer's disease (AD), are increasingly challenging health-care systems all around the world. The number of affected people doubled from 1990 to 2016, meaning that there are up to 50 million patients right now. On the one hand, this can be correlated with a growing and aging world population, on the other hand, there is evidence that avoiding risk factors like high body mass index or

smoking can delay the onset and therefore contribute to a reduced future number of affected people, as there is still no chance to cure or even modify the progress of AD.^[1] Alzheimer published the first description of histological alterations,^[2] namely amyloid β deposits (A β plaques) and neurofibrillary tangles (NFTs), which occur during the progression of the disease named after him and are accompanied by memory deficits and cognitive decline.^[3] These pathological markers are still used to make a definite diagnosis of AD, which, however, can only take place *post mortem*.^[4] The fatal consequences of the disease can be ascribed to a proceeding loss of cholinergic neurons and a decline of the neurotransmitter acetylcholine, which is metabolized by the serine hydrolase acetylcholinesterase (AChE).^[5] Apart from the *N*-methyl-D-aspartate receptor antagonist memantine, all of the approved drugs on the market to combat AD are AChE inhibitors and can ameliorate symptoms in the early stage of the disease by preventing further degradation of acetylcholine through enzyme hydrolysis. This is far from any disease-modifying or curative treatment, and, in general, the complex pathologies of AD are yet too little understood.^[5a,6] However, there is evidence that butyrylcholinesterase (BChE) represents an attractive target for novel imaging probes in AD diagnostics and such imaging probes represent tool compounds to provide further insights into BChE's involvement in neuropathologies and consequently for more powerful drugs to combat the disease. It was shown that in late-stage AD, the level of AChE dramatically decreases by approximately 90%, while BChE activity remains unaffected or can be elevated by up to 30%.^[7] Furthermore, in the human brain large amounts of BChE can be found in regions associated with cognition and behavior, which are among the first areas affected by neurodegeneration.^[8] Last, there is evidence that BChE is involved in AD pathologies by generating harmful attributes of A β plaques.^[9] In up to 30% of cognitively normal older adults, A β plaques appear without being colocalized with

[a] C. Gentsch,[†] Dr. M. Hoffmann,[†] Prof. Dr. M. Decker
Pharmaceutical and Medicinal Chemistry
Institute of Pharmacy and Food Chemistry
Julius-Maximilians-University of Würzburg
Am Hubland, 97074 Würzburg (Germany)
E-mail: michael.decker@uni-wuerzburg.de

[b] Dr. X. Chen
Department of Nuclear Medicine
University Hospital of Augsburg
Stenglinstraße 2, 86156 Augsburg (Germany)

[c] Dr. Y. Ohshima, Dr. X. Chen, Prof. Dr. T. Higuchi
Comprehensive Heart Failure Center
University Hospital of Würzburg
Am Schwarzenberg 15, 97078 Würzburg (Germany)
E-mail: higuchi_t@ukw.de

[d] Dr. Y. Ohshima, Dr. X. Chen, Prof. Dr. T. Higuchi
Department of Nuclear Medicine
University Hospital of Würzburg
Oberdürrbacher Straße 6
97080 Würzburg (Germany)

[e] N. Nose, Prof. Dr. T. Higuchi
Graduate School of Medicine, Dentistry and Pharmaceutical Sciences
Okayama University
2-5-1 Shikata-cho, Kita-ku, Okayama (Japan)

[†] These authors contributed equally to this work.

Supporting information for this article is available on the WWW under <https://doi.org/10.1002/cmdc.202000942>

© 2021 The Authors. ChemMedChem published by Wiley-VCH GmbH. This is an open access article under the terms of the Creative Commons Attribution Non-Commercial NoDerivs License, which permits use and distribution in any medium, provided the original work is properly cited, the use is non-commercial and no modifications or adaptations are made.

BChE, which is the case in AD.^[10] Consequently, it has been shown in several studies that there is a positive, symptomatic effect on memory deficits and cognitive decline, when BChE is inactivated.^[11] Moreover, it is possible to reverse the effect of injected A β _{25–35} in an AD mouse model with highly selective BChE inhibitors exhibiting a pronounced neuroprotective profile, providing first hints that a disease-modifying treatment can potentially be achieved.^[12] Besides, BChE is known to play an important physiological role in serum metabolism by detoxifying xenobiotics or naturally occurring bioactive compounds with its ability to hydrolyze ester or carbamate functionalities. Therefore, the active site exhibits a low substrate specificity compared to AChE.^[13] Additionally, there is evidence that BChE contributes to other diseases, including cardiovascular pathologies, obesity or diabetes mellitus type 2.^[14] Interestingly, both ChEs are known to be involved in cellular proliferation and differentiation, which has raised attention to their potential role in tumorigenesis.^[15] For example, the malignancy grade of tumors in sporadic breast cancer is positively correlated with the total number of alterations in the BChE gene.^[16] Furthermore, a biphasic alteration of BChE level was observed in prostate cancer, meaning a downregulation in the early stage and a subsequent upregulation in the late-stage of the disease, which is additionally correlated with recurrence and reduction of disease-free survival.^[17] Consequently, there is the need for imaging probes selectively targeting BChE not only as potential AD diagnostics to support a diagnosis delimiting other forms of dementia, but also to shed new light on the pathologies of other diseases with related altered BChE activity, expression levels and occurrence. For this reason, positron emission tomography (PET) radiotracers have been developed to gain information about the spatial and temporal distribution of an injected, radiolabeled compound. Ideally, the tracer should address the target of choice with high affinity and selectivity.^[18] In case of BChE, one can design either an inhibitor- or substrate-based compound for radiolabeling, while the former can be classified in reversibly or irreversibly acting inhibitors. Even though substrate analogs as BChE PET tracers can usually pass the blood–brain barrier (BBB), their hydrolysis rate is often too high to achieve an accurate estimation of the actual enzyme distribution in the brain.^[6a,19] ¹¹C-Methyl-4-piperidinyl-*n*-butyrate (¹¹C-MP4B) and *N*-[¹⁸F] fluoroethylpiperidin-4-ylmethyl butyrate are examples of such tracers with a pronounced rate of hydrolysis in brain and plasma. The biodistribution of ¹¹C-MP4B in the brains of AD patients most widely represented the neuroanatomy of BChE known from post mortem studies of human brain, apart from a much higher uptake in the striatum than in the cortex. Further studies are required to fully characterize the diagnostic value of both tracers.^[6a,20] *N*-Methylpiperidin-4-yl 4-[¹²³I]iodobenzoate was consequently developed to overcome these problems and indeed it exhibited slower hydrolysis and retained capability of BBB penetration. It was possible to demonstrate increased brain retention in an AD mouse model compared to wild type and single-photon emission computed tomography (SPECT) studies revealed that radioactivity accumulated in cortical and sub-cortical brain areas in accordance with BChE activity known

from histochemistry.^[21] Thereby first preclinical evidence was provided that it is possible to distinguish healthy and AD mice by targeting BChE with imaging probes.

This approach was extended to an inhibitor-based, irreversibly acting ChE inhibitor, phenyl 4-[¹²³I]-iodophenylcarbamate (¹²³I-PIP). In *ex vivo* autoradiography studies using brain tissue of AD patients, cognitively normal, A β positive older adults and A β negative aged humans, this tracer could discriminate AD tissue from the other two.^[22] However, it is not selective towards BChE, *ex vivo* studies are preliminary due to a limited number of investigated brain tissues and the *in vivo* assessment of the tracer is still pending.^[22] Additionally, ¹²³I-PIP was investigated in a recent study for its potential ability to detect pathological changes in multiple sclerosis (MS). *In vitro* autoradiography revealed that the tracer can detect MS lesions in white matter by binding to BChE.^[23]

Other irreversible ChE inhibitors are organophosphates and a respective PET tracer was designed to target central nervous system AChE in rats, but these compounds are highly toxic nerve agents.^[24] However, due to the lack of results concerning irreversibly acting and selective BChE PET tracers as potential *in vivo* AD diagnostics, we continued our previous studies, in which we had investigated enzyme kinetics and binding, radiolabeling and preliminary *ex vivo* brain tissue binding of pseudo-irreversible, selective BChE inhibitors with high affinity.^[12,19,25] Starting point of our investigations was heptylcarbamate **1a** (Figure 1) bearing a tetracyclic carrier scaffold. Since this compound turned out to be a highly potent carbamate-based BChE inhibitor with pronounced selectivity over AChE, we performed kinetic studies to gain information about the complex binding mode of this class of BChE inhibitors (Figure 1). In the first binding step of a carbamate-based BChE inhibitor [C–X] to enzyme [E] the complex [EC–X] forms spontaneously, which may either dissociate or result in a transfer of the carbamate group C onto the enzyme E, which is subsequently inhibited by means of a covalent bond. Under the presumption that the formation of [EC–X], characterized by the kinetic rate constant k_1 , is considerably faster than the chemical reaction of carbamate transfer, the affinity of carbamate-based BChE inhibitors can be characterized by equilibrium constant K_c . Dissociation of [EC–X] is kinetically characterized by the rate constant k_2 . The carbamate transfer from the tetracyclic carrier scaffold [X] onto the enzyme [E] is a nucleophilic substitution reaction, in which the serine in the catalytically active site of BChE attacks the activated carbon of the carbamate group, while the carrier scaffold X is released as free alcohol. This chemical reaction is described by the kinetic rate constant k_3 and results in the formation of the carbamylated enzyme E–C, that is, the catalytic site in the enzyme is blocked by a covalent bond. Due to the inherent chemical instability of carbamate bonds, the enzyme is not inhibited in an irreversible fashion, but enzyme activity is reconstituted by hydrolysis of the carbamate, that is, a second chemical reaction characterized through rate constant k_4 and half-life $t_{1/2}$ of the carbamylated state.^[12,25–26] For the reason of their complex binding mode, carbamate-based PET tracers on the one hand need to be designed particularly carefully with respect to their kinetic

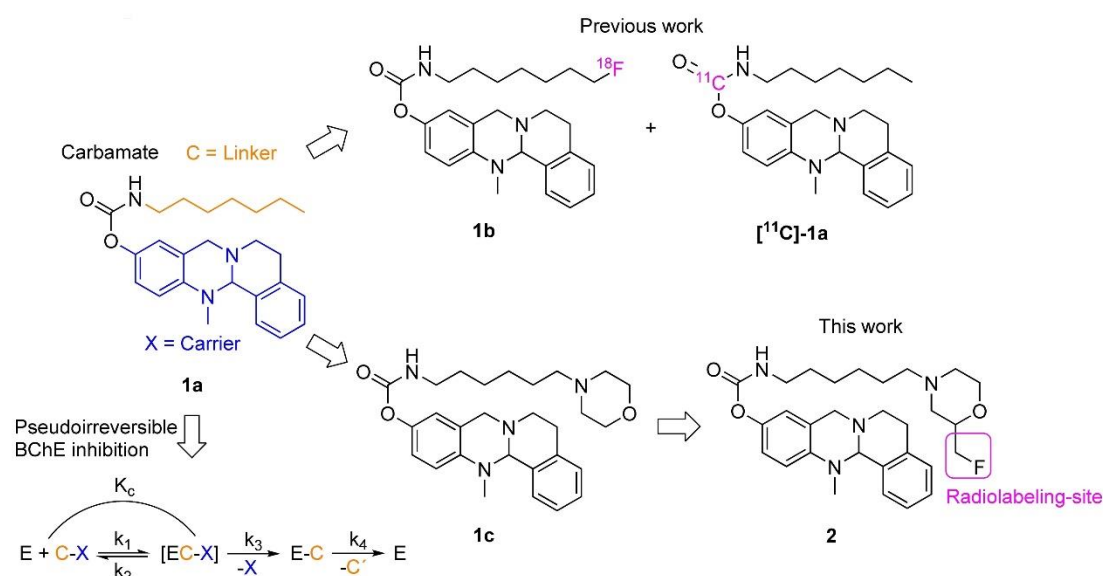


Figure 1. Design of radiotracer 2 based on potent, selective BChE inhibitors 1a, 1b and 1c with (pseudo-)irreversible binding mode. The mechanism of enzyme-inactivation is presented below.^[12,19]

behavior, but on the other hand offer great opportunities in their application. The first aspect to be considered is the speed of carbamylation (k_3), that is, the speed at which the enzyme is deactivated and is, hence, radiolabeled through transfer of a carbamate group comprising a positron emitting radionuclide. Nevertheless, the carbamylation rate requires precise tuning: If the rate is too high, the tracer may bind to BChE circulating in the blood immediately hampering the suitability for BChE imaging in the CNS. PET scans thus obtained only reflect the blood flow and highlight highly vascularized areas of the body, such as brain, liver, heart, kidneys, lung and the like, that is, high brain uptakes may be found although not reflecting true BChE distribution throughout the body. If the carbamylation rate is too slow, however, the tracer may be metabolized before binding to BChE occurs to a considerable extent, also rendering the tracer inappropriate. Only if the carbamylation speed is at an appropriate level, a molecular scan representing the true distribution of BChE throughout the body and CNS can be obtained. Once the enzyme is labeled with the radionuclide, however, slow hydrolysis and long half-life time of the carbamylated enzyme state result in a prolonged retention of radioactivity in the area of interest allowing for increased time of observation and highly flexible study design. Therefore, the ultimate aim for the successful design of a carbamate-based PET tracer for BChE imaging is the provision of a radiolabeled carbamate that is stably transferred to BChE to a considerable extent within a short period of time, such as 5 minutes, but remains bound to BChE for a preferably long time.

Due to the scarcity of highly selective and nanomolar BChE inhibitors, especially with pseudo-irreversible binding mode meeting the demanding requirements, we developed a first ^{18}F - or ^{11}C -labeled PET tracer by attaching fluorine at the end of the

heptyl chain (compound 1b, Figure 1) or introducing ^{11}C as the carbamate carbonyl group ([^{11}C]-1a, Figure 1).^[19]

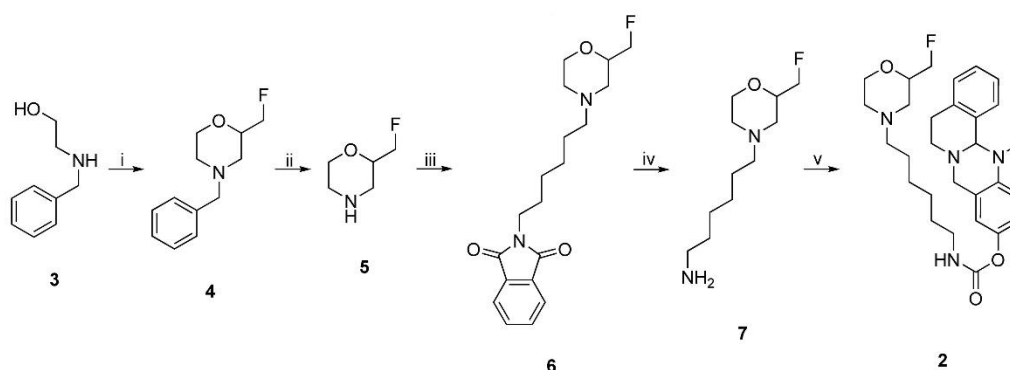
Even though the affinity of the fluorinated compound was not significantly altered, a harsh and complicated radiolabeling procedure of four steps and a short half-life of enzyme reactivation forced us to develop a new generation of carbamates with heterocyclic moieties at the end of alkylene chains of different lengths to examine their influence on inhibition times. Thus, we found out that a morpholine substitution at the end of a hexylene chain substantially increases the time of enzyme inactivation and beneficially increases water solubility of this highly lipophilic class of compounds.^[12] Consequently, in this study, we present a second generation BChE-selective ^{18}F -PET tracer with significantly prolonged duration of action, which most widely retains its inhibitory potency. Additionally, we demonstrate a new radiolabeling strategy for carbamates leading to improved radiochemical yields. Last, we show preliminary *ex vivo* and *in vivo* results of the tracer.

Results and Discussion

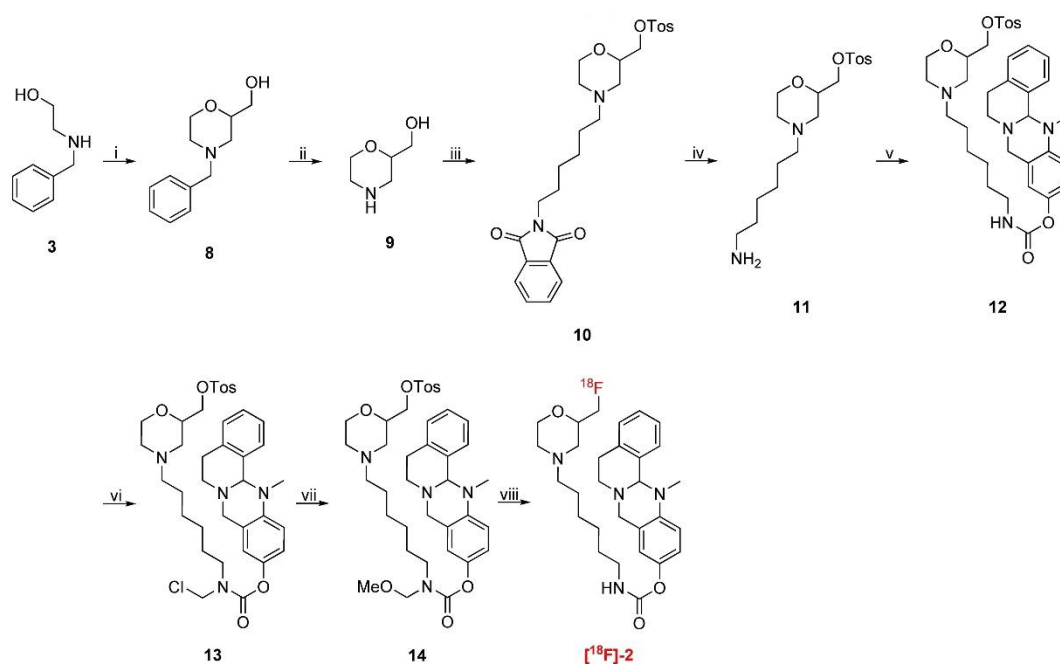
For the design of an advanced, pseudo-irreversible PET radiotracer, we chose highly selective and potent, carbamate-based BChE inhibitor 1c (Figure 1, $\text{IC}_{50} = 49.3$ nM, residual activity on hAChE at $10 \mu\text{M} = 26.1 \pm 1.0\%$) as scaffold, mainly due to its pronounced decelerated speed of enzyme regeneration (1c: $t_{1/2} = 16.50$ h, 1a: $t_{1/2} = 1.12$ h, 1b: $t_{1/2} = 0.86$ h).^[12,19] Our aim was to take advantage of a preferably long carbamoylated enzyme, since this would presumably result in representative, precise *in vivo* distribution of BChEs by PET imaging, when the radio-

nuclide is part of the transferred carbamate moiety (Figure 1). Previously described structure-activity relationships revealed that a hexylene-sized linker between the carbamate and morpholine is best for both retaining inhibitory potency and a prolonged duration of action.^[12] In contrast, the unsubstituted carbamate bearing a heptyl chain attached at the carbamate nitrogen exhibited a much shorter half-life of enzyme inhibition ($t_{1/2}=1.12$ h).^[25] This obvious influence of the morpholine moiety on the duration of enzyme inhibition has been well investigated using ChE inhibitors carrying either a morpholine or dimethylmorpholine moiety at the end of alkylene chain.^[27] The carrier X is responsible for generating selectivity over AChE and contributes to BChE binding.^[12] Considering the design of the radiotracer, we chose to introduce ^{18}F in the compound, because it has advantageous properties over other radioisotopes commonly used for nuclear imaging techniques like PET. These include a long half-life ($t_{1/2}=110$ min, $t_{1/2} (^{68}\text{Ga})=68$ min), high positron yields (96.86%, ^{68}Ga : 89.14%) and a good spatial resolution, which is a result of relatively low positron energies (0.65 MeV, ^{68}Ga : 1.90 MeV).^[28] Consequently, we aimed at the synthesis of the cold, fluorinated inhibitor **2** at first to investigate its binding properties and kinetics. Moreover, this compound was essential as reference during radiolabeling. Our first investigated radiotracer [^{18}F]-**1b** (Figure 1) required an inconvenient radiolabeling procedure of four steps and the respective cold reference had an even shorter half-life of enzyme reactivation ($t_{1/2}=0.86$ h) than heptyl carbamate **1a** ($t_{1/2}=1.12$ h). The synthetic procedure is shown in Scheme 1. The synthesis started from *N*-benzylaminoethanol **3**, which was reacted with epifluorohydrin and cyclized in an acid-mediated intramolecular ether formation to give 4-benzylated 2-fluoromethylmorpholine **4** in satisfying yield (Scheme 1).^[29] Subsequent deprotection of the benzylamine by catalytic hydrogenation,^[30] and Gabriel synthesis with 2-(6-bromohexyl)isoindoline-1,3-dione, were followed by a hydrazinolysis, which gave hexylamine **7** in very good yields. The resulting amine was activated with *p*-nitrophenyl chloroformate and subsequently transferred onto the 13-methyl-5,8,13,13a-tetrahydro-6*H*-isoquinolino[1,2-*b*]quinazolin-10-ol carrier scaffold to yield the non-radioactive compound **2** as a racemic mixture, which was used for *in vitro* evaluation of *h*AChE and *h*BChE binding properties and as a reference compound for analysis and purification after ^{18}F -labeling. Synthesis of the carrier scaffold has been described before in detail.^[31] Because radiolabeling with ^{18}F requires a precursor bearing a suitable leaving group to be replaced by the radionuclide, we developed a similar synthesis as presented in Scheme 1 leading to a respective tosylated compound **14** (Scheme 2). *N*-benzylaminoethanol **3** was reacted with epichlorohydrin, followed by an acid-mediated ether condensation giving 4-benzyl-2-(chloromethyl)morpholine in satisfying yield.^[29] After that, the chlorine atom was replaced by a hydroxy group in a nucleophilic substitution reaction with excellent yield,^[30] and the benzyl protecting group was subsequently removed by catalytic hydrogenation to yield morpholine-2-yl methanol **9** quantitatively (Scheme 2). Compound **9** was *N*-alkylated with 2-(6-bromohexyl)isoindoline-1,3-dione in satisfying yields for an upcoming hydrazinolysis (Gabriel synthesis). Then the hydroxy group on the morpholine moiety was activated by tosylation with 4-toluenesulfonyl chloride (TosCl) in good yield. The resulting tosylate **10** was subjected to a hydrazinolysis, and the amine **11** was subsequently activated with *p*-nitrophenyl chloroformate and transferred onto 13-methyl-5,8,13,13a-tetrahydro-6*H*-isoquinolino[1,2-*b*]quinazolin-10-ol to give the desired tosyl carbamate **12** as precursor again in excellent yields (Scheme 2). As carbamates can easily decompose under the harsh conditions of ^{18}F labeling, it is necessary to employ a protecting group strategy.^[19] We adopted a facile method by introducing a methoxymethyl ether (MOM) group at the carbamate nitrogen, without using highly cancerogenic methoxymethyl chloride.^[32] In the first step, a chloromethyl group was attached *in situ* at the carbamate yielding compound **13**. The reaction mixture was subsequently quenched with methanol to give the desired MOM-protected precursor in very good yields (Scheme 2). However, this inevitable modification of our precursor forced us to perform an additional deprotection step after radiolabeling, which might

nolino[1,2-*b*]quinazolin-10-ol carrier scaffold to yield the non-radioactive compound **2** as a racemic mixture, which was used for *in vitro* evaluation of *h*AChE and *h*BChE binding properties and as a reference compound for analysis and purification after ^{18}F -labeling. Synthesis of the carrier scaffold has been described before in detail.^[31] Because radiolabeling with ^{18}F requires a precursor bearing a suitable leaving group to be replaced by the radionuclide, we developed a similar synthesis as presented in Scheme 1 leading to a respective tosylated compound **14** (Scheme 2). *N*-benzylaminoethanol **3** was reacted with epichlorohydrin, followed by an acid-mediated ether condensation giving 4-benzyl-2-(chloromethyl)morpholine in satisfying yield.^[29] After that, the chlorine atom was replaced by a hydroxy group in a nucleophilic substitution reaction with excellent yield,^[30] and the benzyl protecting group was subsequently removed by catalytic hydrogenation to yield morpholine-2-yl methanol **9** quantitatively (Scheme 2). Compound **9** was *N*-alkylated with 2-(6-bromohexyl)isoindoline-1,3-dione in satisfying yields for an upcoming hydrazinolysis (Gabriel synthesis). Then the hydroxy group on the morpholine moiety was activated by tosylation with 4-toluenesulfonyl chloride (TosCl) in good yield. The resulting tosylate **10** was subjected to a hydrazinolysis, and the amine **11** was subsequently activated with *p*-nitrophenyl chloroformate and transferred onto 13-methyl-5,8,13,13a-tetrahydro-6*H*-isoquinolino[1,2-*b*]quinazolin-10-ol to give the desired tosyl carbamate **12** as precursor again in excellent yields (Scheme 2). As carbamates can easily decompose under the harsh conditions of ^{18}F labeling, it is necessary to employ a protecting group strategy.^[19] We adopted a facile method by introducing a methoxymethyl ether (MOM) group at the carbamate nitrogen, without using highly cancerogenic methoxymethyl chloride.^[32] In the first step, a chloromethyl group was attached *in situ* at the carbamate yielding compound **13**. The reaction mixture was subsequently quenched with methanol to give the desired MOM-protected precursor in very good yields (Scheme 2). However, this inevitable modification of our precursor forced us to perform an additional deprotection step after radiolabeling, which might



Scheme 1. Synthesis of nonradioactive compound **2** for *in vitro* ChE testing and as reference compound for HPLC purification after ^{18}F labeling. i) 1. epifluorohydrin, RT, 3 h; 2. H_2SO_4 , 140°C , 1 h, 67%; ii) H_2 , Pd/C, MeOH, RT, 1 h, quant.; iii) 2-(6-bromohexyl)isoindoline-1,3-dione, NEt_3 , DMF, 105°C , 4 h, 63%; iv) $\text{H}_4\text{N}_2\cdot\text{H}_2\text{O}$, EtOH, 85°C , 4 h, 77%; v) 1. *p*-nitrophenyl chloroformate, NEt_3 , CH_2Cl_2 , 2 h, RT, 67%; 2. 13-methyl-5,8,13,13a-tetrahydro-6*H*-isoquinolino[1,2-*b*]quinazolin-10-ol, NaH, CH_2Cl_2 , 1 h, RT, 75%.



Scheme 2. Synthesis of MOM-protected, tosylated precursor **14** for ^{18}F labeling to $[^{18}\text{F}]\text{-2}$. i) epichlorohydrine, RT, 3 h; 2. H_2SO_4 , 140°C , 1 h, 67% over two steps; 3. H_2O , CHONH_2 , 145°C , 20 h, 93%; ii) H_2 , Pd/C, MeOH, RT, 1 h, quant.; iii) 1. 2-(6-bromohexyl)isoindoline-1,3-dione, *N,N*-diisopropylethylamine (DIPEA), DMF, 100°C , 20 h, 66%; 2. TosCl, NEt_3 , CH_2Cl_2 , RT, 20 h, 71%; iv) $\text{H}_2\text{N}_2\cdot\text{H}_2\text{O}$, EtOH, 80°C , 1.5 h, 88%; v) 1. *p*-nitrophenyl chloroformate, NEt_3 , CH_2Cl_2 , 3 h, RT, 55%; 2. 13-methyl-5,8,13,13a-tetrahydro-6*H*-isoquinolino[1,2-*b*]quinazolin-10-ol, NaH, CH_2Cl_2 , 2 h, RT, 94%; vi) TMS-Cl, para-formaldehyde, CH_2Cl_2 , RT, 18 h; vii) MeOH, RT, 1 h, 85% (two steps); viii) 1. $[^{18}\text{F}]\text{KF}$, K_{222} , MeCN, 110°C , 10 min; 2. 6 M HCl_{aq} , 90°C , 5 min.

Table 1. Inhibitory potencies and kinetic parameters of heptylcarbamate **1a**, and cold reference compound **2**. K_c , k_3 and k_4 are presented with SEM (standard error of the mean) for triplicates of the respective experiments ($n=3$).

Cmpd.	IC_{50} (hBChE [nM])	IC_{50} (hAChE [nM])	$K_c \pm \text{SEM}$ (hBChE [nM])
1a	$6.4^{[12,19]}$	$3800^{[12,19]}$	$28.5 \pm 17.2^{[12,19]}$
1b	$5.2^{[19]}$	$3600^{[19]}$	$24.3 \pm 19.3^{[19]}$
1c	$49.3^{[12]}$	$> 100000^{[12]}$	$202 \pm 55^{[12]}$
2	66.6	> 100000	199.9 ± 160.4
	$k_3 \pm \text{SEM}$ (hBChE [min^{-1}])	$k_4 \pm \text{SEM}$ (hBChE [h^{-1}])	$t_{1/2}$ [h]
1a	$0.66 \pm 0.32^{[12,19]}$	$0.62 \pm 0.04^{[12,19]}$	$1.12^{[12,19]}$
1b	$0.78 \pm 0.48^{[19]}$	$0.81 \pm 0.04^{[19]}$	$0.86^{[19]}$
1c	$0.16 \pm 0.02^{[12]}$	$0.042 \pm 0.004^{[12]}$	$16.50^{[12]}$
2	0.42 ± 0.25	0.043 ± 0.003	16.13

be disadvantageous due to additional time investment for reaction and work-up. Even though the introduction of a fluoromethyl group might represent just a minor modification on the parent BChE inhibitor **1c** (Figure 1), we fully characterized cold reference compound **2** for its retained inhibitory potency in colorimetric Ellman's assay and performed an additional thorough kinetic study to compare the results.^[12,19,33] Thus, we have proven that both the binding properties and kinetic characteristics are in excellent accordance with the parent compound **1c** and greatly exceed the properties of heptylcarbamate **1a** (Table 1). The colorimetric assay (Ellman's assay) was performed by incubation of a solution of 5,5'-dithiobis-(2-nitrobenzoic acid) (DTNB) and the respective human ChE with the inhibitor. After 20 min, enzyme activity was

measured by adding the synthetic substrate of each ChE (acetylthiocholine for AChE and butyrylthiocholine for BChE). After reaction of the hydrolyzed thiols with DTNB and their photometric quantification, enzyme activity was calculated. The evaluation in kinetic studies revealed that the pseudo-irreversible binding of carbamate **2** is comparable to that of compound **1c**. K_c and k_3 representing kinetic values for the carbamylation step appear to be in the suitable range to allow for molecular scans reflecting the true BChE distribution among the whole body. The decarbamylation step is kinetically characterized by k_4 and the half-life of enzyme reactivation, $t_{1/2}$. Dilution experiments (Figure 2)^[12,19,34] revealed a time-dependent plot of enzyme activity characterized by a first-order

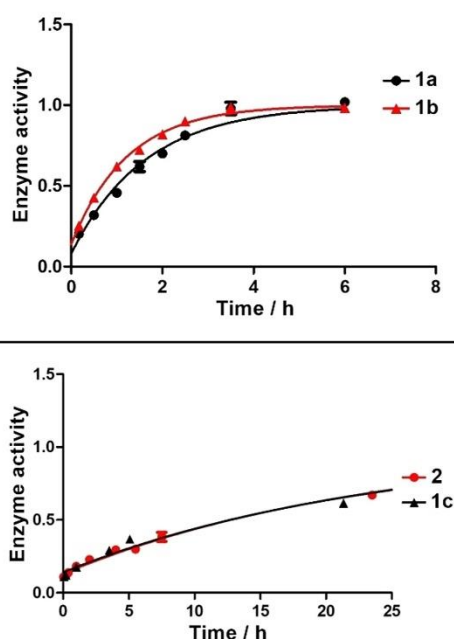


Figure 2. Recovery of *hBChE* activity after pseudo-irreversible inhibition with compounds **1a**, **1b**, **1c**, and **2** and subsequent dilution. Normalized enzyme activity (1 = full activity) was measured in triplicate for each time point (mean \pm SD).

exponential curve and the related Equation (1), out of which $t_{1/2}$ and k_4 were calculated (Figure 2).

$$A = (1 - e^{-k_4 t}) \cdot (1 - A_0) + A_0 \quad (1)$$

In summary, we found that our cold inhibitor **2** shows a very minor decrease in its inhibitory potency compared to parent compound **1c** (Table 1 and Figure 2), but still exhibits binding affinity in the two-digit nanomolar range. Importantly, it retains long duration of action considering the half-life ($t_{1/2} = 16.13$ h) and rate constant k_4 (Table 1, Figure 2), which met our expectations. Altogether, the pronounced selectivity over *hAChE*, the sufficiently fast transfer of the carbamate onto the enzyme and long binding represent promising attributes for a suitable *BChE* PET tracer. Consequently, we used precursor **14** (Scheme 2) for ^{18}F radiolabeling to generate the respective radiotracer. In the first step, we adopted an established procedure for ^{18}F labeling of tosylates by nucleophilic substitution. $[^{18}\text{F}]\text{KF}$ was reacted with the precursor at elevated temperatures in the presence of a [2.2.2]cryptand ($K_{2,2,2}$). Finally, the MOM group was deprotected with 6 M hydrochloric acid. Purification of the tracer was achieved by semi-preparative high-performance liquid chromatography (HPLC). Thus, we obtained the tracer in a time frame of 180 min and a radiochemical yield of 13% after decay correction (specific activity $a = 191$ GBq/mmol). Autoradiography of a thin-layer chromatogram (TLC) indicated sufficient purity (95.3%) of our tracer for subsequent preliminary *ex vivo* and *in vivo* experiments.

In the next step, we characterized the radiotracer's *in vitro* properties in protein binding assays on *hBChE*. First, the time course of binding was investigated by incubating a mixture of *hBChE* and radiotracer $[^{18}\text{F}]\text{-2}$ in PBS for 5, 10 and 20 min at 37 °C. A maximum of tracer-bound *hBChE* was reached after 20 min (Figure 3). This demonstrates the specificity of tracer binding to *hBChE* and the maximum after 20 min is in good agreement with previous kinetic studies of compounds **1a**, **1b** and **1c** (Figure 1), where equilibrium constant K_C and rate constant of carbamoylation k_3 were determined.^[12,19,25] Additionally, we studied the blocking of tracer binding *in vitro* by the known reversible *BChE*-selective inhibitor ethopropazine and nonselective, reversible *ChE* inhibitor tacrine.^[35] Therefore, a solution of *hBChE* in PBS was preincubated with ethopropazine hydrochloride (60 μM) or tacrine (1 μM), respectively. Subsequently, $[^{18}\text{F}]\text{-2}$ was added to each of the inhibitors and incubated for 20 min at 37 °C (cf. Figure S1 in the Supporting Information). Next, we investigated the binding properties of $[^{18}\text{F}]\text{-2}$ to mice brain tissue using autoradiography. After incubation of healthy mouse brain slices with the tracer, autoradiography images exhibited high accumulation of radioactivity in relevant brain areas (Figure 4), proving a good

binding of $[^{18}\text{F}]\text{-2}$ to brain tissue.^[36] In parallel, we performed blocking experiments on mice brain tissue preincubated with ethopropazine hydrochloride, a selective inhibitor of *BChE* that prevents binding of other *BChE* inhibitors and substrates due to its blocking of the active site.^[35a] Consequently, we found a significantly decreased binding of $[^{18}\text{F}]\text{-2}$ to the preincubated tissue, which demonstrates the specificity of the tracer towards *BChE* binding in areas with high *BChE* activity like white matter bundles, thalamus, upper brainstem and cerebral cortex.^[36] It has to be mentioned that a higher level of displaceable binding was observed in autoradiography experiments with $[^{18}\text{F}]\text{-1b}$, which is likely due to its higher binding affinity ($\text{IC}_{50} = 5.2$ nM).^[19] Nevertheless, the complicated radiolabeling procedure and unfavorable kinetic parameters of this tracer are disadvantageous compared to $[^{18}\text{F}]\text{-2}$. Due to the successful

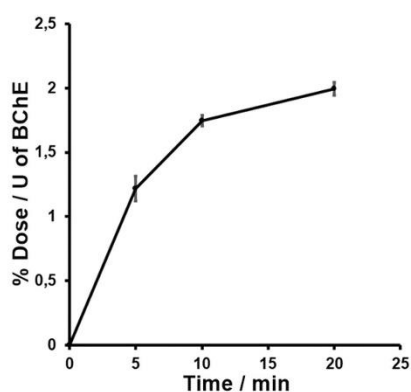


Figure 3. Time-dependent *in vitro* *hBChE* binding assay with radiotracer $[^{18}\text{F}]\text{-2}$. Enzyme-bound radioactivity was measured in triplicate after 5, 10 and 20 min (mean \pm SD). % Dose: the percentage of binding dose according to overall radioactivity used, U: the enzyme unit for *BChE* added in each vial.

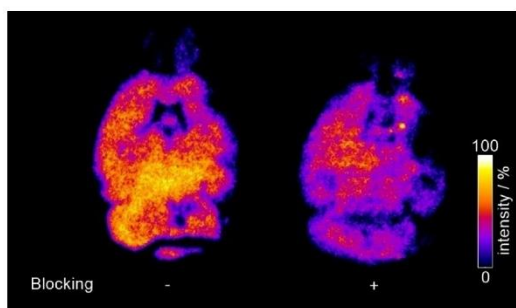


Figure 4. Autoradiography of mice brain slices incubated with radiotracer [^{18}F]-2. Left: without and right: with ethopropazine hydrochloride. Bright areas represent high binding of the tracer. Tracer intensity [arbitrary units] is shown as a percentage of the maximum tracer activity.

radiolabeling and promising *in vitro* and *ex vivo* results, we felt motivated to initially evaluate the radiotracers *in vivo* characteristics in PET studies. Therefore, a solution of the tracer (5% ethanol in saline) was injected via tail vein to a healthy male Wistar rat, which was directly scanned in a small animal PET system to obtain dynamic images and generate time-activity curves of regions of interest (Figure 5). From both dynamic images and time activity curves only limited brain uptake of the tracer could be observed, which could indicate limited BBB penetration. After initial blood-pool circulation and a rapid enrichment in heart and lung, the tracer accumulates in liver tissue. BChE occurs in the above-mentioned organs in an elevated manner.^[37] It is noteworthy that parent compound 1c (and closely related compounds) exhibited pronounced activity *in vivo*.^[12] Duration of action at hBChE *in vitro* ($t_{1/2}$) correlates well with neuroprotective effects *in vivo*. However, since the

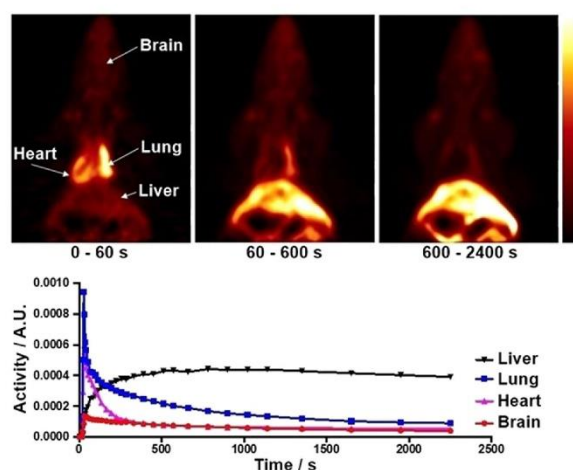


Figure 5. Preliminary *in vivo* evaluation of the tracer. Top: Dynamic coronal PET images after tail vein injection of a solution of [^{18}F]-2 to a male Wistar rat and subsequent microPET scanning over 40 min. Bottom: Time-activity curves of regions of interest obtained from the above images (A.U. = arbitrary unit).

tracer reaches heart, lung and liver with increased activity, a potential application is given in prognosis, diagnosis and monitoring disease state and progress or malignancy grade in certain types of cancer, which can be associated with down- and/or upregulation of BChE.^[38] In particular, BChE expression has been found to decrease significantly in large-cell- and squamous-cell lung carcinoma.^[39] Therefore, an application of the tracer in diseases monitoring and prognosis in lung cancer might be conceivable. Further studies in animal models are warranted based on the current initial evaluation to prove its feasibility.

Conclusion

In this study, we present design and synthesis of an ^{18}F -labeled radiotracer for PET imaging of BChE. A potent and selective BChE inhibitor with pseudo-irreversible binding mode served as parent compound due to its long duration of action. We modified the carbamate moiety by attaching a fluoromethyl group to the morpholine moiety, which is responsible for the prolonged enzyme inhibition. We present a facile synthesis of both cold reference compound and a MOM-protected tosylate precursor, which is very suitable for ^{18}F -radiolabeling in good radiochemical yields. Thus, we provide access to a new method to radiolabel sensitive carbamates. Colorimetric *in vitro* studies revealed that the compound widely retains the inhibitory potency of the parent compound, and kinetic investigations exhibited that the half-life of enzyme reactivation due to slow hydrolysis of the carbamate is in excellent accordance with the parent compound as well. Radiolabeling of the tosylate precursor was achieved in two steps through an established procedure with subsequent MOM deprotection in a reasonable time frame and good radiochemical yields. Subsequently, we investigated the tracer's properties in protein binding studies and found that the time course of binding was in accordance with our expectations. Consequently, we applied the radiotracer in preliminary *ex vivo* autoradiography studies on mice brain slices, where we could observe good binding to brain tissue. Additionally, we demonstrated the specificity of binding to BChE in blocking experiments with the selective BChE inhibitor ethopropazine. Finally, we present a preliminary *in vivo* PET study on a healthy male rat, where we found only limited brain uptake. The tracer rapidly addressed heart and lung, accompanied by long-term accumulation in liver tissue - organs with BChE expression. Future studies will build upon these results and elucidate the precise biodistribution of the tracer to clarify the remaining question of its limited brain uptake, which is likely due to the inability to penetrate the blood-brain-barrier efficiently or extrusion by P-glycoprotein. A potential application of this tracer in diagnosis and monitoring of diseases with altered BChE activity in the addressed organs, such as certain types of lung cancer, is conceivable.

Experimental Section

Chemistry

Reagents and solvents were obtained from commercial suppliers in reagent grade and were used without further purification unless stated otherwise. Dichloromethane as solvent was distilled from CaH₂ under argon. The reaction progress was controlled with analytical thin-layer chromatography (TLC) on precoated silica gel GF₂₅₄ plates (Macherey Nagel, Düren, Germany). Compounds were detected under UV light (254 and 366 nm) or through staining with iodine, KMnO₄, or Ehrlich's reagent. Crude products after work-up were purified by manual flash column chromatography. Silica gel (particle size of 40–63 μm; VWR chemicals, Leuven, Belgium) was used as the stationary phase and mixtures from petroleum ether/ethyl acetate or dichloromethane/methanol as eluent systems. The pure compounds were submitted for nuclear magnetic resonance spectra on a AV-400 NMR instrument (Bruker) in deuterated solvents (DMSO-d₆, CDCl₃, CD₂Cl₂, CD₃OD). Chemical shifts are expressed in ppm relative to DMSO-d₆, CDCl₃, CD₂Cl₂, or CD₃OD (2.50/7.26/5.32/3.31 for ¹H; 39.5/77.2/53.5/49.0 for ¹³C). Purity of compounds was controlled with analytical HPLC on a Shimadzu system equipped with a DGU-20A3R controller, LC20AB liquid chromatograph, and SPD-20 A UV/vis detector (Shimadzu): Stationary phase: Synergi 4U fusion RP (Synergi, Aschaffenburg, Germany) column; mobile phase: water + 0.1% formic acid (phase A) and methanol + 0.1% formic acid (phase B) with a flow of 1.0 mL/min. Method: conc. B, gradient 5→90% from 0 to 8 min, 90% isocratic from 8 to 13 min, gradient 90→5% from 13 to 15 min, 5% isocratic from 15 to 18 min. Compounds were detected at λ = 254 nm, and target compounds were ≥ 95% pure.

4-Benzyl-2-(fluoromethyl)morpholine (4): In a flask, 2-(benzylamino)ethan-1-ol (3; 1.866 mL, 1.988 g, 13.15 mmol, 1 equiv.) and epifluorohydrin (1 g, 13.15 mmol, 1 equiv.) were mixed together and stirred for 3 h at room temperature. Then concentrated H₂SO₄ (5 mL) was added carefully and the mixture was heated to 140 °C for 1 h. Afterwards, the reaction mixture was allowed to cool down to room temperature and was poured onto ice. The aqueous layer was basified with aqueous sodium hydroxide (10 M) and extracted with three portions of ethyl acetate. The combined organic layers were washed with water and brine, dried over sodium sulphate, filtered, and evaporated to dryness under reduced pressure. The residue was purified with flash column chromatography (petroleum ether/ethyl acetate 3:1, R_f=0.35) to yield 4-benzyl-2-(fluoroethyl)morpholine (4; 1.31 g, 6.26 mmol, 48%) as colorless oil. ¹H NMR (400 MHz, CDCl₃): δ = 7.29–7.14 (m, 5H), 4.41–4.31 (m, 1H), 4.29–4.21 (m, 1H), 3.89–3.58 (m, 3H), 3.53–3.35 (m, 2H), 2.74–2.55 (m, 2H), 2.14 (td, J = 11.4, 3.3 Hz, 1H), 2.04–1.86 ppm (m, 1H); ¹³C NMR (101 MHz, CDCl₃): δ = 137.7 (1 C), 129.3 (2 C), 128.5 (2 C), 127.4 (1 C), 85.0 (1 C), 83.3 (1 C), 74.5 (0.5 C), 74.3 (0.5 C), 66.9 (1 C), 63.5 (1 C), 53.9 (1 C), 53.8 (1 C), 53.0 ppm (1 C); MS (ESI): [M+H]⁺ calcd for C₁₂H₁₆NOF = 210.13, found 210.10.

2-(Fluoromethyl)morpholine hydroformiate (5): A solution of 4-benzyl-2-(fluoromethyl)morpholine (4; 1.3 g, 6.21 mmol, 1 equiv.) in MeOH (30 mL) was prepared and formic acid (0.5 mL) was added. No precipitation was observed. Then palladium on activated charcoal (10 wt%, 130 mg) was added and the atmosphere was replaced with hydrogen. The mixture was stirred for 1 h at room temperature. After that, the catalyst was filtered off by a pad of celite, which was washed with methanol. The filtrate was evaporated to dryness in vacuo to yield 2-(fluoromethyl)morpholine hydroformiate (5; 1.025 g, 6.21 mmol, quant.) as colorless oil. ¹H NMR (400 MHz, CD₃OD): δ = 8.37 (s, 1H), 4.57–4.49 (m, 1H), 4.44–4.37 (m, 1H), 4.15–4.06 (m, 1H), 4.04–3.90 (m, 1H), 3.90–3.80 (m, 1H), 3.39–3.32 (m, 1H), 3.29–3.26 (m, 1H), 3.25 (dt, J = 2.5, 1.3 Hz, 1H),

3.18–3.12 (m, 1H), 3.10–2.99 ppm (m, 1H); ¹³C NMR (101 MHz, CD₃OD): δ = 168.2 (1 C), 84.8 (1 C), 83.1 (1 C), 73.6 (0.5 C), 73.4 (0.5 C), 64.9 (1 C), 43.8 ppm (1 C); MS (ESI): [M+H]⁺ calcd for C₅H₁₀FNO = 120.08; found 120.15.

2-[6-[2-(Fluoromethyl)morpholino]hexyl]isoindoline-1,3-dione (6): 2-(Fluoromethyl)morpholine hydroformiate (5; 1001 mg, 6.06 mmol, 1 equiv.) was dissolved in dry dimethylformamide (10 mL) and triethylamine (3 mL) was added. Then 2-(6-bromohexyl)isoindoline-1,3-dione (2 g, 6.45 mmol, 1.06 equiv.) was added and the resulting solution was heated to 105 °C for 4 h. The mixture was allowed to cool down to room temperature and water was added. The aqueous layer was extracted with ethyl acetate (3x). Then the combined organic layers were washed with water and brine, dried over sodium sulphate, filtered, and the solvent was evaporated under reduced pressure. The residue was purified with flash column chromatography (CH₂Cl₂/MeOH 98:2, R_f=0.33) to yield 2-[6-[2-(fluoromethyl)morpholino]hexyl]isoindoline-1,3-dione (6; 1.334 g, 3.83 mmol, 63%) as colorless oil. ¹H NMR (400 MHz, CDCl₃): δ = 7.80–7.74 (m, 2H), 7.66–7.61 (m, 2H), 4.41–4.36 (m, 1H), 4.29–4.24 (m, 1H), 3.83 (ddd, J = 11.3, 3.3, 1.7 Hz, 1H), 3.66–3.50 (m, 4H), 2.74–2.67 (m, 1H), 2.61 (dd, J = 11.5, 1.9 Hz, 1H), 2.34–2.22 (m, 2H), 2.05 (td, J = 11.4, 3.3 Hz, 1H), 1.94–1.82 (m, 1H), 1.69–1.56 (m, 3H), 1.50–1.36 (m, 3H), 1.37–1.24 ppm (m, 4H); ¹³C NMR (101 MHz, CDCl₃): δ = 168.4 (1 C), 133.9 (2 C), 132.2 (1 C), 123.3 (2 C), 84.9 (1 C), 83.1 (1 C), 74.3 (0.5 C), 74.1 (0.5 C), 66.8 (1 C), 58.8 (1 C), 54.0 (1 C), 52.9 (1 C), 37.9 (1 C), 28.5 (1 C), 27.0 (1 C), 26.7 (1 C), 26.4 ppm (1 C); MS (ESI): [M+H]⁺ calcd for C₁₉H₂₆N₂O₄ = 349.19, found 349.15.

6-[2-(Fluoromethyl)morpholino]hexan-1-amine (7): To a solution of 2-[6-[2-(fluoromethyl)morpholino]hexyl]isoindoline-1,3-dione (6; 1.2 g, 3.44 mmol, 1 equiv.) in ethanol (50 mL), hydrazine hydrate (1 mL, >5 equiv.) was added. The solution was heated to 85 °C for 4 h. Then the mixture was allowed to cool down to room temperature and the precipitate was filtered off. The filtrate was evaporated to dryness under reduced pressure. The residue was triturated with CH₂Cl₂, filtered, and the filtrate was evaporated under reduced pressure to yield 6-[2-(fluoromethyl)morpholino]hexan-1-amine (7; 577 mg, 2.64 mmol, 77%) as colorless oil without further purification. ¹H NMR (400 MHz, CDCl₃): δ = 4.48–4.42 (m, 1H), 3.95–3.86 (m, 1H), 3.72–3.64 (m, 1H), 3.64–3.58 (m, 1H), 2.80–2.74 (m, 1H), 2.71–2.63 (m, 3H), 2.37–2.29 (m, 2H), 2.12 (td, J = 11.5, 3.4 Hz, 1H), 2.01–1.89 (m, 1H), 1.55–1.41 (m, 4H), 1.39–1.27 ppm (m, 4H); ¹³C NMR (101 MHz, CDCl₃): δ = 85.0 (1 C), 83.3 (1 C), 74.4 (0.5 C), 74.2 (0.5 C), 67.0 (1 C), 59.1 (1 C), 54.2 (1 C), 54.1 (1 C), 53.1 (1 C), 42.2 (1 C), 33.7 (1 C), 27.4 (1 C), 26.9 (1 C), 26.6 ppm (1 C); MS (ESI): [M+H]⁺ calcd for C₁₁H₂₃FN₂O = 219.19; found 219.20.

4-Nitrophenyl-[6-[2-(fluoromethyl)morpholino]hexyl]-carbamate: To a solution of 6-[2-(fluoromethyl)morpholino]hexan-1-amine (7; 500 mg, 2.29 mmol) in dry dichloromethane (10 mL), triethylamine (0.5 mL) and 4-nitrophenylchloroformate (508 mg, 2.52 mmol) were added. The resulting solution was stirred for 2 h at room temperature. Then the solvent was evaporated under reduced pressure and the residue was purified by flash column chromatography (CH₂Cl₂/MeOH 99:1, R_f=0.11) to yield 4-nitrophenyl [6-[2-(fluoromethyl)morpholino]hexyl]carbamate (588 mg, 1.53 mmol, 67%) as yellow oil. MS (ESI): [M+H]⁺ calcd for C₁₈H₂₆FN₃O₅ = 384.20, found 384.05.

Due to high instability of the title compound only LCMS data was measured, before directly reacting it in the next step.

13-Methyl-5,8,13,13a-tetrahydro-6H-isoquinolino[1,2-b]quinazolin-10-yl-[6-[2-(fluoromethyl)morpholino]hexyl]carbamate (2): To a solution of 4-nitrophenyl [6-[2-(fluoromethyl)morpholino]hexyl]carbamate (86 mg, 0.23 mmol, 1.2 equiv.) and 13-methyl-5,8,13,13a-tetrahydro-6H-isoquinolino[1,2-b]quinazolin-10-ol (50 mg,

0.19 mmol, 1 equiv.), sodium hydride (60% suspension in paraffin oil, 9 mg, 0.23 mmol, 1 equiv.) was added. The resulting mixture was stirred for 1 h at room temperature. Then water was added, and the aqueous layer was extracted with three portions of dichloromethane. The combined organic layers were washed with water, saturated aqueous sodium hydrogen carbonate solution and brine, dried over sodium sulphate, filtered, and evaporated to dryness under reduced pressure. The residue was purified by flash column chromatography (CH₂Cl₂/MeOH 98:2, *R_f*=0.14) to yield 13-methyl-5,8,13a-tetrahydro-6*H*-isoquinolino[1,2-*b*]quinazolin-10-yl {6-[2-(fluoromethyl)morpholino]hexyl}carbamate (**2**; 72 mg, 0.14 μmol, 75%) as colorless oil. ¹H NMR (400 MHz, CD₂Cl₂): δ = 7.38–7.32 (m, 1H), 7.22–7.15 (m, 2H), 7.14–7.09 (m, 1H), 6.89–6.81 (m, 2H), 6.74–6.68 (m, 1H), 4.77 (s, 1H), 4.42–4.35 (m, 1H), 4.30–4.22 (m, 1H), 3.94 (d, *J* = 15.6 Hz, 1H), 3.89–3.79 (m, 2H), 3.78–3.58 (m, 2H), 3.24–3.11 (m, 3H), 3.10–2.98 (m, 1H), 2.83–2.60 (m, 4H), 2.51 (s, 3H), 2.34–2.26 (m, 2H), 2.06 (td, *J* = 11.4, 3.3 Hz, 1H), 1.94–1.82 (m, 1H), 1.55–1.39 (m, 4H), 1.37–1.26 ppm (m, 4H); ¹³C NMR (101 MHz, CD₂Cl₂): δ = 155.5 (1 C), 146.3 (1 C), 144.9 (1 C), 136.7 (1 C), 134.5 (1 C), 129.1 (1 C), 128.9 (1 C), 127.7 (1 C), 126.1 (1 C), 120.7 (1 C), 120.5 (1 C), 120.0 (1 C), 85.5 (1 C), 83.8 (1 C), 76.8 (1 C), 74.8 (0.5 C), 74.6 (0.5 C), 67.0 (1 C), 56.5 (1 C), 54.38 (1 C), 54.33 (1 C), 54.26 (1 C), 53.8 (1 C), 53.4 (1 C), 48.3 (1 C), 41.5 (1 C), 38.2 (1 C), 30.2 (1 C), 29.0 (1 C), 27.4 (1 C), 27.0 (1 C), 26.8 ppm (1 C); MS (ESI): [*M*+*H*]⁺ calcd for C₂₉H₃₉N₄O₃ = 511.31, found 511.15; HPLC: *t_R* = 6.74 min, 97.5% purity.

Experimental procedures for the synthesis of MOM-protected precursor **14** (Scheme 2) are described in the Supporting Information.

Enzyme inhibition

*h*AChE (EC 3.1.1.7, from human erythrocytes), DTNB (Ellman's reagent), ATC and BTC iodides were purchased from Sigma-Aldrich. *h*BChE (E.C. 3.1.1.8) was kindly donated by Dr. Oksana Lockridge, Nebraska Medical Centre. For the assays, the inhibitors were dissolved in ethanol (absolute, reagent grade, Ph. Eur.) to give a concentration of 3.33 mM (100 μM in the assay) and stepwise diluted to 3.33 nM (0.1 nM in the assay). Buffer was prepared from 3.12 g of potassium dihydrogen phosphate in 500 mL of doubly distilled water. After the potassium dihydrogen phosphate was dissolved, the pH value was adjusted to pH 8.0 with 0.1 M sodium hydroxide solution. Both enzymes were dissolved in assay buffer and diluted to 2.5 units/mL. The solutions were stabilized with 1 mg/mL of bovine serum albumin (Sigma-Aldrich) and were stored at 7 °C until usage. DTNB was dissolved in buffer at 10 mM (0.3 mM in the assay). The substrates ATC and BTC were prepared with a concentration of 75 mM (452 μM in the assay) in assay buffer and kept frozen until usage. The absorbance of probes was measured with a Shimadzu UVmini-1240 spectrometer at 412 nm.

*I*_{C50} determination: The assay was carried out at room temperature (25 °C). Thereby, 900 μL of the buffer, 30 μL of DTNB solution (10 mM, 0.3 mM in the assay) and 30 μL of enzyme solution (*h*AChE or *h*BChE, 2.5 units/mL) were mixed in a cuvette. The incubation was started directly after the addition of 30 μL of inhibitor **2** (Scheme 1) solutions with different concentrations. The solutions were mixed well by manual stirring. After 20 min incubation, 6 μL of substrate solution (ATC or BTC; 75 mM, 452 μM in the assay) were added. The mixture was left for 2.5 min to allow substrate hydrolysis, and the absorbance was measured at λ = 412 nm, whereas enzyme activity was determined three times for every concentration with at least seven different concentrations. A blank value was determined by replacing the enzyme solution with buffer; the compound solution was replaced with ethanol. The maximum enzyme activity was determined with 30 μL of ethanol

instead of the compound solution. 10% of ethanol did not reduce enzyme activity. The enzyme activity in percent of maximum activity was plotted against the logarithmic inhibitor concentration, from which *I*_{C50} values were calculated with the software GraphPad Prism 5.

Kinetic studies: For determination of *K_c* and *k₃* values, the same general setup was used (900 μL of the assay buffer, 30 μL of DTNB solution (10 mM, 0.3 mM in the assay), and 30 μL of *h*BChE solution (2.5 units/mL) were mixed at room temperature). Then, 30 μL of inhibitor **2** (Scheme 1) solutions with different concentrations were added, but enzyme activity was determined after 1, 2, 4, 6, 10, 15, 20, 30, and 40 min of incubation by addition of 6 μL of BTC solution (75 mM, 452 μM in the assay). The absorbance at λ = 412 nm was measured after 2.5 min. All concentrations were measured three times, at least five different concentrations were measured for at least seven time points. The obtained enzyme activities in percent of maximum enzyme activity were plotted in a time-dependent manner and fitted to Equation (2) to determine the rate constant *k_{obs}* using the software GraphPad Prism 5.

$$A = A_0 \cdot e^{-k_{\text{obs}} \cdot t} + A_{\infty} \quad (2)$$

A: enzyme activity at time *t*, *A*₀: enzyme activity at time *t* = 0, 100%; *A*_∞: enzyme activity at infinite time.

The obtained inverse rate constants *k_{obs}* were plotted against the reciprocal concentration [I]⁻¹, and *k₃* was calculated from the y-intercept of the resulting curve, and *K_c* from the slope of the resulting linearization according to Equation (3) using the software GraphPad Prism 5.

$$\frac{1}{k_{\text{obs}}} = \frac{K_c}{k_3} \cdot \frac{1}{[I]} + \frac{1}{k_3} \quad (3)$$

[I]: concentration of BChE inhibitor **2** (Scheme 1).

For the measurement of decarbamylation kinetics, the enzyme was incubated with inhibitor **2** to carbamylate > 85% of the enzyme. After 1 h, the solution was diluted 1000-fold so that no enzyme was carbamylated anymore. The enzyme activity was measured at several (at least 8) time points, as described above. For the determination of full enzyme activity, a batch of the enzyme was treated with ethanol instead of inhibitor solution and diluted 1000-fold in the same manner. The enzyme activity in percent was plotted against time after dilution to give first-order rate constant *k_d* according to Equation (1) using the software GraphPad Prism 5. All experiments were carried out in triplicates.

Radiochemistry

Solvents and chemicals were purchased from Aldrich and directly used without further purification. [¹⁸F]F⁻ was produced by a cyclotron (GE Medical Systems, Uppsala) at the Department of Nuclear Medicine of the University Hospital of Würzburg. Enriched [¹⁸O]H₂O was irradiated with protons to produce [¹⁸F]F⁻ and radiofluorination was carried out manually. HPLC was used for purification and analyses of radioactive products (Shimadzu system equipped with UV detector, λ = 220 and 254 nm, and γ-detector). Purified radiotracer **2** (Scheme 1) was diluted with either PBS or saline to the corresponding concentration for further evaluation.

13-Methyl-5,8,13a-tetrahydro-6*H*-isoquinolino[1,2-*b*]quinazolin-10-yl-{6-[2-(¹⁸F)-fluoromethyl]morpholino}-hexyl}carbamate ([¹⁸F]-**2**): [¹⁸F]F⁻ was separated from [¹⁸O]H₂O by an anion exchange cartridge (Sep-Pak QMA Cartridge) and eluted with 0.5 mL of

25 mM potassium carbonate and 50 mM Kryptofix222 solution in MeCN/H₂O (6:2) into a V-vial. The solution was dried at 120 °C under a nitrogen flow, which was repeated twice with 500 µL of anhydrous MeCN. Labeling was carried out using 1.3 mg of precursor **14** (Scheme 2) dissolved in 0.4 mL of anhydrous MeCN at 110 °C for 20 min, followed by addition of 100 µL of 6 M hydrochloric acid with further 5 min heating at 90 °C. After addition of 500 µL of 1 M aqueous sodium hydrogencarbonate solution and 10 mL water to quench the reaction, the crude product was trapped on a Sep-Pak light C18, which was washed with 5 mL of water and eluted with 0.5 mL of ethanol. The crude radiotracer was purified via semi-preparative HPLC. Column: 10 × 100 mm C18 Phenomenex Onyx Monolithic, Mobile phase: Phase A: H₂O, Phase B: MeCN, 0–20 min, 20%→80% B, 20–26 min, 95% B, 28–30 min 20% B, Flow rate: 1.5 ml/min. The collected fraction was diluted with 10 mL water and trapped on a Sep-Pak light C18, which was dried with 5 mL air and eluted with 0.3 mL ethanol. The total radiolabeling procedure was feasible in 180 min in a radiochemical yield of 13% (corrected for decay). Sufficient radiochemical purity was measured by TLC autoradiography (95.3%).

Experimental procedures for protein binding assays with tracer [¹⁸F]-**2** (time course and blocking of binding) are described in the Supporting Information.

Tissue binding and in vivo PET imaging

Ex vivo tissue binding studies were carried out with one C57BL/6 N mouse from Charles River. Two series of horizontal brain slices with 20 µm thickness were prepared for either control or blocking group. A buffer (150 mM NaCl, 5 mM EDTA, 50 mM Na₂HPO₄, pH 8.0) containing [¹⁸F]-**2** (A = 1.44 MBq) with or without ethopropazine hydrochloride (60 µM) as blocking agent was prepared for incubation with the mice brain slices. Slices were incubated for 30 min at 25 °C and then rinsed five times in PBS buffer (1 min each time). The slices were dried at room temperature and exposed to a phosphor imaging plate (GE healthcare, BAS IP MS 2025 E, Munich, Germany). Images were produced with a digital autoradiographic system (Typhoon FLA 7000).

All applicable international, national, and/or institutional guidelines for the care and use of animals were followed. Animal protocols were approved by the local Animal Care and Use Committee (approval no. 15063) and conducted according to the Guide for the Care and Use of Laboratory Animals. A healthy, male Wistar rat was anaesthetized and maintained with isoflurane for *in vivo* PET imaging using a micro PET system (FOCUS, Siemens, Erlangen, Germany). A 60-min dynamic imaging protocol was started directly after the injection of a solution of [¹⁸F]-**2** (5% ethanol in saline, 6.3 MBq). Analysis of the obtained PET images was performed with the public domain tool AMIDE imaging software (A Medical Imaging Data Examiner, version 1.01) and time-activity curves of regions of interest were generated.

Acknowledgements

This work was supported by the German Research Council (Deutsche Forschungsgemeinschaft DFG; grants DE 1546/6-3 for M.D. and HI 1789/3-3 for T.H.). M.H. was supported by the German Academic Scholarship Foundation ("Studienstiftung des deutschen Volkes") with a PhD scholarship. C. G. and M. H. were supported by the MuTaLig COST Action (active participation at the 3rd Working Group Meeting, Paris). We gratefully acknowledge Professor Oksana Lockridge (University of Nebraska Medical

Center) for providing hBChE. Open access funding enabled and organized by Projekt DEAL.

Conflict of Interest

The authors declare no conflict of interest.

Keywords: carbamate · enzyme kinetics · fluorine-18 · positron emission tomography · radiotracers

- [1] a) E. Nichols, C. E. I. Szoeki, S. E. Vollset, N. Abbasi, F. Abd-Allah, et al., *Lancet Neurol.* **2019**, *18*, 88–106; b) M. Crous-Bou, C. Minguillón, N. Gramunt, J. Molinuevo, *Alzheimer's Res. Ther.* **2017**, *9*, 71; c) *Alzheimer's Dementia* **2019**, *15*, 321–387.
- [2] A. Alzheimer, *Neurologisches Centralblatt* **1906**, *25*, 1134.
- [3] R. Katzman, *Arch. Neurol.* **1976**, *33*, 217–218.
- [4] R. Sengoku, *Neuropathology* **2020**, *40*, 22–29.
- [5] a) P. Davies, A. J. F. Maloney, *Lancet* **1976**, *308*, 1403; b) E. Perry, R. Perry, G. Blessed, B. Tomlinson, *Lancet* **1977**, *309*, 189; c) J. Coyle, D. Price, M. DeLong, *Science* **1983**, *219*, 1184–1190; d) R. Bartus, R. Dean, B. Beer, A. Lippa, *Science* **1982**, *217*, 408–414.
- [6] a) S. Darvesh, *Curr. Alzheimer Res.* **2016**, *13*, 1–5; b) S. D. Rountree, W. Chan, V. N. Pavlik, E. J. Darby, S. Siddiqui, R. S. Doody, *Alzheimer's Res. Ther.* **2009**, *1*, 7.
- [7] N. H. Greig, T. Utsuki, Q. Yu, X. Zhu, H. W. Holloway, et al., *Curr. Med. Res. Opin.* **2001**, *17*, 159–165.
- [8] a) S. Darvesh, D. L. Grantham, D. A. Hopkins, *J. Comp. Neurol.* **1998**, *393*, 374–390; b) S. Darvesh, D. A. Hopkins, *J. Comp. Neurol.* **2003**, *463*, 25–43.
- [9] a) A. L. Guillozet, J. F. Smiley, D. C. Mash, M. M. Mesulam, *Ann. Neurol.* **1997**, *42*, 909–918; b) M. Mesulam, C. Geula, *Ann. Neurol.* **1994**, *36*, 722–727.
- [10] I. R. Macdonald, S. P. Maxwell, G. A. Reid, M. K. Cash, D. R. DeBay, et al., *J. Alzheimer's Dis.* **2017**, *58*, 491–505.
- [11] a) M. M. Mesulam, A. Guillozet, P. Shaw, A. Levey, E. G. Duysen, et al., *Neuroscience* **2002**, *110*, 627–639; b) J. Hartmann, C. Kiewert, E. G. Duysen, O. Lockridge, N. H. Greig, et al., *J. Neurochem.* **2007**, *100*, 1421–1429; c) Y. Furukawa-Hibi, T. Alkam, A. Nitta, A. Matsuyama, H. Mizoguchi, et al., *Behav. Brain Res.* **2011**, *225*, 222–229; d) N. H. Greig, T. Utsuki, D. K. Ingram, Y. Wang, G. Pepeu, et al., *Proc. Natl. Acad. Sci. USA* **2005**, *102*, 17213–17218; e) T. Maurice, M. Strehaiano, N. Siméon, C. Bertrand, A. Chatonnet, *Behav. Brain Res.* **2015**, *296*, 351–360; f) R. S. Naik, J. Hartmann, C. Kiewert, E. G. Duysen, O. Lockridge, et al., *J. Pharm. Pharm. Sci.* **2009**, *12*, 79–85; g) T. Darreh-Shori, S. Brimjoin, A. Kadir, O. Almkvist, A. Nordberg, *Neurobiol. Dis.* **2006**, *24*, 326–333.
- [12] M. Hoffmann, C. Stiller, E. Endres, M. Scheiner, S. Gunesch, et al., *J. Med. Chem.* **2019**, *62*, 9116–9140.
- [13] a) O. Lockridge, *Pharmacol. Ther.* **2015**, *148*, 34–46; b) Y. Ashani, *Drug Dev. Res.* **2000**, *50*, 298–308; c) B. Li, M. Sedlacek, I. Manoharan, R. Boopathy, E. G. Duysen, et al., *Biochem. Pharmacol.* **2005**, *70*, 1673–1684.
- [14] a) B. Li, E. G. Duysen, O. Lockridge, *Chem.-Biol. Interact.* **2008**, *175*, 88–91; b) T. Iwasaki, M. Yoneda, A. Nakajima, Y. Terauchi, *Intern. Med. J.* **2007**, *46*, 1633–1639; c) K. K. Sato, T. Hayashi, I. Maeda, H. Koh, N. Harita, et al., *Clin. Endocrinol. (Oxf)* **2014**, *80*, 362–367; d) M. Stojanov, A. Stefanović, G. Džingalašević, S. Mandić-Radić, M. Prostran, *Clin. Biochem.* **2011**, *44*, 623–626; e) V. M. Alcântara, E. A. Chautard-Freire-Maia, M. Scartezini, M. S. J. Cerci, K. Braun-Prado, et al., *Scand. J. Clin. Lab. Invest.* **2002**, *62*, 399–404.
- [15] a) P. G. Layer, *Cell. Mol. Neurobiol.* **1991**, *11*, 7–33; b) R. B. Aziz-Aloya, M. Sternfeld, H. Soreq, *Progress in Brain Research*, Vol. 98 (Ed.: A. C. Cuellar), Elsevier, **1993**, pp. 147–153; c) P. G. Layer, E. Willbold, *Prog. Histochem. Cytochem.* **1994**, *29*, III–92.
- [16] C. C. Bernardi, E. d. S. F. Ribeiro, I. J. Cavalli, E. A. Chautard-Freire-Maia, R. L. R. Souza, *Cancer Genet. Cytogenet.* **2010**, *197*, 158–165.
- [17] Y. Gu, M. J. Chow, A. Kapoor, W. Mei, Y. Jiang, et al., *Transl. Oncol.* **2018**, *11*, 1012–1022.
- [18] S. P. McCluskey, C. Plisson, E. A. Rabiner, O. Howes, *Eur. J. Nucl. Med. Mol. Imaging* **2020**, *47*, 451–489.

- [19] E. Sawatzky, E. Al-Momani, R. Kobayashi, T. Higuchi, S. Samnick, et al., *ChemMedChem* **2016**, *11*, 1540–1550.
- [20] a) A. Roivainen, J. Rinne, J. Virta, T. Järvenpää, S. Salomäki, et al., *J. Nucl. Med.* **2004**, *45*, 2032–2039; b) T. Kikuchi, M.-R. Zhang, N. Ikota, K. Fukushi, T. Okamura, et al., *Bioorg. Med. Chem. Lett.* **2004**, *14*, 1927–1930.
- [21] a) D. R. DeBay, G. A. Reid, I. R. Pottie, E. Martin, C. V. Bowen, et al., *Alzheimers Dement. (N Y)* **2017**, *3*, 166–176; b) I. R. Macdonald, G. A. Reid, E. E. Joy, I. R. Pottie, G. Matte, et al., *Mol. Imaging Biol.* **2011**, *13*, 1250–1261.
- [22] I. R. Macdonald, G. A. Reid, I. R. Pottie, E. Martin, S. Darvesh, *J. Nucl. Med.* **2016**, *57*, 297–302.
- [23] M. W. D. Thorne, M. K. Cash, G. A. Reid, D. E. Burley, D. Luke, I. R. Pottie, S. Darvesh, *Mol. Imaging Biol.* **2021**, *23*, 127–138.
- [24] S. L. James, S. K. Ahmed, S. Murphy, M. R. Braden, Y. Belabassi, et al., *ACS Chem. Neurosci.* **2014**, *5*, 519–524.
- [25] F. H. Darras, B. Kling, J. Heilmann, M. Decker, *ACS Med. Chem. Lett.* **2012**, *3*, 914–919.
- [26] a) E. Sawatzky, S. Wehle, B. Kling, J. Wendrich, G. Bringmann, et al., *J. Med. Chem.* **2016**, *59*, 2067–2082; b) G. Huang, B. Kling, F. H. Darras, J. Heilmann, M. Decker, *Eur. J. Med. Chem.* **2014**, *81*, 15–21.
- [27] a) C. Bartolucci, E. Perola, L. Cellai, M. Brufani, D. Lamba, *Biochemistry* **1999**, *38*, 5714–5719; b) E. Perola, L. Cellai, D. Lamba, L. Filocamo, M. Brufani, *Biochim. Biophys. Acta Protein Struct. Mol. Enzymol.* **1997**, *1343*, 41–50; c) A. Rampa, L. Piazza, F. Belluti, S. Gobbi, A. Bisi, et al., *J. Med. Chem.* **2001**, *44*, 3810–3820; d) A. Rampa, M. Bartolini, A. Bisi, F. Belluti, S. Gobbi, et al., *ACS Med. Chem. Lett.* **2012**, *3*, 182–186.
- [28] a) A. Sanchez-Crespo, *Appl. Radiat. Isot.* **2013**, *76*, 55–62; b) C. Kesch, C. Kratochwil, W. Mier, K. Kopka, F. L. Giesel, *J. Nucl. Med.* **2017**, *58*, 687–688.
- [29] a) S. K. Fehler, S. Maschauer, S. B. Höfling, A. L. Bartschat, N. Tschammer, et al., *Chem. Eur. J.* **2014**, *20*, 370–375; b) S. Kato, T. Morie, K. Hino, T. Kon, S. Naruto, et al., *J. Med. Chem.* **1990**, *33*, 1406–1413.
- [30] J. A. H. Lainton, M. C. Allen, M. Burton, S. Cameron, T. R. G. Edwards, et al., *J. Comb. Chem.* **2003**, *5*, 400–407.
- [31] E. Sawatzky, J. Bukowczan, M. Decker, *Tetrahedron Lett.* **2014**, *55*, 2973–2976.
- [32] D. M. Barnes, J. Barkalow, D. J. Plata, *Org. Lett.* **2009**, *11*, 273–275.
- [33] G. L. Ellman, K. D. Courtney, V. Andres, R. M. Featherstone, *Biochem. Pharmacol.* **1961**, *7*, 88–95.
- [34] C. Bartolucci, J. Stojan, Q.-s. Yu, N. H. Greig, D. Lamba, *Biochem. J.* **2012**, *444*, 269–277.
- [35] a) W. J. Meuling, M. J. Jongen, J. J. van Hemmen, *Am. J. Ind. Med.* **1992**, *22*, 231–241; b) M. Ahmed, J. B. T. Rocha, M. Corrêa, C. M. Mazzanti, R. F. Zanin, et al., *Chem.-Biol. Interact.* **2006**, *162*, 165–171.
- [36] G. A. Reid, S. Darvesh, *Neuroscience* **2015**, *298*, 424–435.
- [37] M. Uhlén, L. Fagerberg, B. M. Hallström, C. Lindskog, P. Oksvold, et al., *Science* **2015**, *347*, 1260419 (<http://www.proteinatlas.org>).
- [38] L. Santaripa, I. Grandone, F. Contaldo, F. Pasanisi, *J. Cachexia Sarcopenia Muscle* **2013**, *4*, 31–39.
- [39] P. Martínez-Moreno, S. Nieto-Cerón, J. Torres-Lanzas, F. Ruiz-Espejo, I. Tovar-Zapata, et al., *Carcinogenesis* **2005**, *27*, 429–436.

Manuscript received: December 7, 2020
Revised manuscript received: January 19, 2021
Version of record online: ■■■, ■■■■

Acknowledgements

The present thesis was enabled by good supervision, the collaboration of several cooperation partners and not least by the exchange of propellent ideas between all involved people.

Therefore, I want to express my sincere gratitude to the following people:

- Prof. Dr. Michael Decker for the uptake in the working group and supervision of the PhD project
- Dr. Antonios Drakopoulos for the supervision of my Master project, which represented the basis of the subsequent work on fluorescent ligands for the MOP, and his willingness to provide further tips and ideas throughout this project
- Dr. Kerstin Seier, Dr. Marie-Lise Jobin, Dr. Yann Lanoiselée and Dr. Zsombor Koszegi from the working group of Prof. Dr. Davide Calebiro for performing and evaluating the fluorescence microscopy experiments to characterize wild-type MOPs and subsequently incorporating these essential results in the respective manuscript
- Dr. Damien Maurel, Dr. Rémy Sounier and Dr. Sébastien Granier for characterizing the MOP selectivity of the fluorescent ligands in a HTRF assay and providing the data for the manuscript
- Dr. Harald Hübner from the working group of Prof. Dr. Peter Gmeiner for measuring binding affinities and functional activities of the fluorescent ligands and heterodimer-selective ligands
- Dr. Xinyu Chen from the working group of Prof. Dr. Takahiro Higuchi for performing ^{18}F -radiolabeling and *ex vivo* / *in vivo* experiments with the help of Naoko Nose (Okayama University, Graduate School of Medicine, Dentistry and Pharmaceutical Sciences)
- Dr. Urban Košak and Assist. Prof. Dr. Damijan Knez (laboratory of Prof. Dr. Stanislav Gobec, University of Ljubljana, Faculty of Pharmacy) for providing synthetic building blocks and performing assays to characterize inhibitory potency and binding kinetics of the fluorinated reversible BChE inhibitor
- Philipp Spatz for performing additional *in vitro* assays to characterize inhibitory potency of the reversible, fluorinated BChE inhibitors
- Dr. Matthias Hoffmann for providing the synthetic and *in vitro* groundwork of the pseudo-irreversible fluorinated BChE inhibitor

- Dr. Yasuhiro Ohshima for performing *in vitro* protein binding studies with the pseudo-irreversible, carbamate-based radiotracer for BChE
- My practical students Leonie Fischer and Felix Stuckenbrok, who helped out with the synthetic work on the reversible, fluorinated BChE inhibitors
- The whole working group of Prof. Dr. Michael Decker from 2017 to 2021 for the comfortable work atmosphere and mutual helpfulness

Eidesstattliche Erklärung

Hiermit erkläre ich an Eides statt, dass ich die Dissertation mit dem Titel

„Molecular Imaging of Opioid Receptors and Butyrylcholinesterase with Selective, Tailored Probes Using Positron Emission Tomography and Fluorescence Microscopy“

selbständig angefertigt, übernommene Inhalte eindeutig gekennzeichnet und die Regeln der Universität Würzburg über gute wissenschaftliche Praxis eingehalten habe.

Ich erkläre außerdem, dass ich die Gelegenheit zum Promotionsvorhaben nicht kommerziell vermittelt bekommen und insbesondere nicht eine Person oder Organisation eingeschaltet habe, die gegen Entgelt Betreuerinnen bzw. Betreuer für die Anfertigung von Dissertationen sucht.

Ich habe früher außer den mit dem Promotionsgesuch urkundlich vorgelegten Graden keine weiteren akademischen Grade erworben oder zu erwerben versucht.

Die eingereichte und oben genannte Dissertation habe ich weder vollständig noch teilweise schon einmal einer anderen Fakultät mit dem Ziel einen akademischen Grad zu erwerben vorgelegt.

Würzburg, den 16.06.2021

(Christian Gentsch)